Cryogenic Energy Storage Systems: An Exergy-based Evaluation and Optimization

vorgelegt von
M.Sc.
Sarah Hamdy

ORCID: 0000-0002-7577-9595

von der Fakultät III – Prozesswissenschaften
der Technischen Universität Berlin
zur Erlangung des akademischen Grades

Doktorin der Ingenieurwissenschaften
-Dr.-Ing.-

genehmigte Dissertation

Promotionsausschuss

Vorsitzender: Prof. Dr.-Ing. Felix Ziegler
Gutachterin: Prof. Dr.-Ing. Tetyana Morozyuk
Gutachter: Prof. Dr.-Ing. Aaron Praktiknjo
Gutachter: Prof. Dr.-Ing. George Tsatsaronis

Tag der wissenschaftlichen Aussprache: 12.07.2019

Berlin 2019

Acknowledgment

First and foremost, I would like to express my sincere gratitude to my supervisor Prof. Tetyana Morozyuk, for her immense engagement, trust, guidance, and continuous support not only with regards to scientific research but also concerning administrative, managerial and other academic assignments. I would also like to thank Prof. George Tsatsaronis for his inspiring lectures and research on exergy-based methods, his valuable feedback, and his encouragement. My genuine thanks to Prof. Aaron Praktiknjo for his willingness to be the external evaluator of this thesis, his invaluable advice, and always sympathetic ear. Without the remarkable assistance, patience, and reinforcement of my advisors, I would not have been able to complete this thesis in parallel to fulfill my role as a study coordinator. Successfully managing this challenge with the help and support of my advisors has greatly benefitted both my professional and personal growth. My gratitude also goes to Prof. Felix Ziegler, not only for chairing my PhD defense but also for the enriching discussions and his inspiration as a teacher.

This work was conducted during my period as a research associate at the Department of Energy Engineering of the Zentralinstitut El Gouna at the Technische Universität Berlin. My position in the Transnational Education (TNB) Project (ID 57128418) was supported by the German Academic Exchange Service (DAAD) with funds from the Federal Ministry of Education and Research (BMBF). I am deeply grateful for having had the opportunity to teach, coordinate, and shape two Master degree programs at the TU Berlin Campus El Gouna. I appreciated the opportunities given and the challenges faced in the project. Enabling a unique journey for very inspiring students has been a truly enriching experience. Therefore, I would like to express the deepest appreciation to those who made this exceptional academic environment possible.

Moreover, I offer my gratitude to all the colleagues from the department, and both chairs *Exergy-based methods of refrigeration systems* and *Energy Engineering and Environmental Protection*. In particular, my sincere thanks to Stefanie Tesch, Timo Blumberg, Johannes Wellmann, Sara AlAhmed, Mohamed Noaman, Saeed Sayadi, Sebastian Spieker, Jing Luo and Elisa Papadis for the knowledge exchange, the great motivation, and the fruitful scientific discussions.

My special thanks also to Dr. Daniel Wolf, who initiated the idea of my master and later PhD research together with Prof. Morozyuk, as well as Dr. Martin Robinius for his honest feedback, and encouragement. I would also like to thank the students who assisted in my work and research: Tala Rifka, Jimena Incer Valverde, Bianca Astorga, Francisco Moser, and Bahaa Alhaddad.

I as well owe very important debt to my friends and family for their tremendous spiritual support. In particular, I am grateful to my husband Louay, for the precious commitment, patience, and proofreading as well as my parents and my brother Ibrahim for the endless support. Moreover, I am deeply thankful for the patience and strength that God rewarded me to pursue this goal.

Abstract

Grid-scale energy storage systems are capable of providing the needed flexibility to the power grid operators in order to ensure a secure power supply with increasing shares of highly intermittent electricity generation from renewable energy sources. Cryogenic energy storage (CES) is a grid-scale energy storage concept in which electricity is stored in the form of liquefied gas enabling a remarkably higher exergy density than competing technologies such as pumped hydro storage and compressed air energy storage and frees the technology of common geographical restrictions. CES has recently received much attention in research and application due to its advantageous characteristics, e.g., the long cycle life, low storage losses, and being composed of mature components.

The present work aims to identify and apply measures for thermodynamic performance enhancement and cost reduction of CES systems with the aid of exergy-based methods. Various system configurations were designed and simulated in Aspen Plus® and evaluated with energetic, exergetic, economic, and exergoeconomic analysis. Moreover, iterative exergoeconomic optimization was performed. Six liquefaction systems (charging process) with and without "cold" (low-temperature exergy) storage were assessed. Based on the cost-optimal and the most efficient liquefaction process, two adiabatic CES systems (base cases) with an installed discharge power/energy capacity of 100 MW/400 MWh were evaluated and optimized. The cost-optimized system (optimized case) was subjected to the integration of external heat sources and sinks (integrated systems) to analyze the effect of system integration on the thermodynamic and the economic performance of CES systems.

The results showed that the addition of cold storage increases the roundtrip efficiency by 60-80 % and reduces the specific costs of the liquefaction (charging) process by 50 %. The selection of the liquefaction process was also revealed to be of significance. The liquefaction process causes the majority of the bare module costs and more than 60 % of the exergy destruction in the base case systems. In the exergoeconomic optimization, the levelized cost of discharged electricity was reduced from 267 €/MWh to 195 €/MWh at the expense of a reduction in the roundtrip efficiency from 47 to 40 %. The specific investment cost of the cost-optimal adiabatic CES system reached 1,200 €/kW, similar to competing technologies but relatively high concerning the low roundtrip efficiencies. The integration of waste heat, combustion and/or the regasification of LNG to CES is a viable option reaching roundtrip efficiencies higher than 70 % and further reducing the levelized cost of discharged electricity to 130-170 €/MWh.

Apart from the costs; the operation hours and the response time were identified as the constraint to the economic feasibility. Potential energy storage applications suitable for CES were identified accordingly. However, the monetary value of the identified applications is too low to recover the revenue required of the CES systems. As a result, CES is only economically viable if further revenue streams are identified and financial incentives for the investment in ES are provided, or the CES costs are reduced significantly.

Zusammenfassung

Mittels leistungsstarker Energiespeichersysteme kann die notwendige Flexibilität bereitgestellt werden, um eine sichere Stromversorgung bei steigender Einspeisung hoch fluktuierender Stromerzeugung aus erneuerbaren Energiequellen zu gewährleisten. In dieser Arbeit werden kryogene Energiespeichersysteme (CES) untersucht, welche große Mengen an Überschussstrom in Form eines Flüssiggases zwischen speichern können. Dies ermöglicht eine deutlich höhere Exergiedichte, welche im Verhältnis zu anderen Netzspeicheranlagen, wie Pumpspeicherkraftwerken oder Druckluftspeichern, eine gleichzeitige Unabhängigkeit von geografischen Einschränkungen erlaubt. Aufgrund seiner vorteilhaften Eigenschaften, wie z.B. einer langen Lebensdauer, geringen Speicherverlusten und der Zusammensetzung aus ausgereiften Komponenten, hat das Interesse an CES-Systemen in den vergangenen Jahren in der Industrie und der Forschung stark zugenommen.

Die vorliegende Arbeit befasst sich mit der thermodynamischen Leistungssteigerung und der Kostensenkung kryogener Energiespeichersysteme mit Hilfe exergiebasierter Methoden. In diesem Zusammenhang wurden verschiedene Systemkonfigurationen mit der Simulationssoftware Aspen Plus® entworfen, simuliert und mittels energetischer, exergetischer, wirtschaftlicher und exergoökonomischer Analysemethoden bewertet. Darüber hinaus, wurde eine iterative exergoökonomische Optimierung durchgeführt. Sechs Luftverflüssigungsprozesse (Einspeicherung) mit und ohne "Kältespeicher" (Niedertemperaturspeicher) wurden betrachtet. Auf Grundlage des kostengünstigsten und des effizientesten Verflüssigungsprozesses wurden zwei adiabate CES-Systeme (base cases) mit einer installierten Ausspeicherleistung/Speicherkapazität von jeweils 100 MW/400 MWh entwickelt, bewertet und optimiert. Das optimierte System (optimized case) wurde anschließend mit verschiedenen Konzepten der Integration externer Wärmequellen und - senken erweitert (integrated systems) um die Auswirkungen der Systemintegration auf die thermodynamische und wirtschaftliche Leistungssteigerung von CES-Systemen zu untersuchen.

Die Auswertung der Ergebnisse zeigt, dass die Integration des Kältespeichers eine Effizienzsteigerung um 60-80 % ermöglicht und gleichzeitig die Kosten des Verflüssigungs- bzw. Ladeprozesses um die Hälfte reduziert. Hierbei ist auch die Wahl des Verflüssigungsprozesses von Bedeutung. Der Verflüssigungsprozess verursacht den Großteil der Anlageninvestitionskosten und der Exergievernichtung in den Base-Case-Systemen. Die exergoökonomische Optimierung ermöglicht die Minderung der Stromgestehungskosten der Entladung von 267 €/MWh auf 195 €/MWh, welche eine Reduzierung des Gesamtwirkungsgrades von 47 auf 40 % nach sich zieht. Das kostenoptimale adiabate CES-System erreicht spezifische Investitionskosten von 1.200 €/kW, was im Vergleich zu anderen Netzspeichertechnologien konkurrenzfähig ist. In Anbetracht des niedrigen Gesamtwirkungsgrad fallen die spezifischen Investitionskosten jedoch relativ hoch aus.

Die Integration von industrieller Abwärme, von Verbrennungsprozessen und/oder von der Wiedervergasung von Flüssigerdgas (LNG) erhöht den Gesamtwirkungsgrad auf über 70 % und senkt die Stromgestehungskosten der Entladung weiter auf 130-170 €/MWh. Neben den reinen Investitionskosten wurden auch die Betriebsstunden und die Reaktionszeiten des CES als Hindernisse für eine wirtschaftliche Umsetzung deutlich. Darauf basierend wurden potentielle Anwendungen für CES-Systeme hervorgehoben. Die mit den Energiespeicheranwendungen verbundenen potentiellen Einnahmen, ermöglichen jedoch nicht die Rückzahlung der gesamten Investitionskosten der dargelegten CES-Systeme. Daher sind CES-Systeme nur dann wirtschaftlich, wenn weitere Einnahmequellen identifiziert, finanzielle Anreize für die Investition in Energiespeichersysteme gegeben oder die Investitionskosten deutlich reduziert werden.

Nomenclature

Symbol	Explanation	Unit
A	area	m^2
c	specific cost of power	€/kW
C	cost	€
$\dot{C}$	cost rate	€/s, €/cycle
e	specific exergy	J/kg
E	exergy	J
$\dot{E}$	exergy rate	MWh/cycle, W
f	factor, exergoeconomic factor	-
h	specific enthalpy	J/kg
H	enthalpy	J
$\dot{H}$	enthalpy rate	W
k	overall heat transfer coefficient	W/m^2K
m	mass	kg
$\dot{m}$	mass flow rate	kg/s
n	economic life	years
p	pressure	bar
$\dot{Q}$	heat transfer rate	MWh/cycle, W
r	(splitting) ratio, relative cost difference (exergoeconomic analysis)	-
s	specific entropy	J/kgK
T	temperature	°C, K
$\dot{W}$	power	W
X	equipment cost	€
$\dot{Z}$	cost rate	€/s, €/cycle

Greek symbols

α	scaling component	-
γ	rate, ratio, yield	-, %
Δ	difference	-
ε	exergetic efficiency	%
η	energetic (or thermal) efficiency	%
η_s	isentropic efficiency	%
τ	duration	h

Superscripts

CH	chemical
KN	kinetic
M	mechanical
PH	physical
PT	potential
T	thermal

Subscripts

0	ambient, restricted dead state, reference
A	state point at T_0 and p
char	charge
CC	combustion chamber
CI	capital investment
CP	cryogenic pump
CS	cold storage
cs	carbon steel
CM	compressor/compression
el	electricity
D	destruction
d	design
dis	discharge
EX	expander/expansion
F	fuel
HE	heat exchanger
HS	heat storage
i, j	running index
inst	installed
k	k-th component
L	loss (exergetic analysis), levelized (economic analysis)
l	liquid
m	material
ma	metal alloys
Mix	mixer
OM	operation and maintenance
P	product
p	pressure
PE	purchased equipment
Q	associated with heat transfer
RH	reheater
SP	splitter
ss	stainless steel
ST	storage tank
sys	system
T	turbine
tot	total

Abbreviations

ASU	air separation unit
BMC	bare module cost
CAES	compressed air energy storage
CAPEX	capital expenditure
CC	carrying charges
CELF	constant escalation levelization factor
CEPCI	chemical engineering plant cost index
CES	cryogenic energy storage
CRF	capital-recovery factor
EES	engineering equation solver
ES	energy storage
FC	fuel cost
FCI	fixed capital investment
FES	flywheel energy storage
FLH	full load hours
FT	flash tank
IC	Intercooler
LA	lead acid battery
LAES	liquid air energy storage
LCOE	levelized cost of electricity
LMTD	log mean temperature difference
LNG	liquefied natural gas
Li-Ion	lithium ion battery
MHE	main heat exchanger
NaS	sodium sulfur battery
NA	not available
OMC	operation and maintenance costs
OPEX	operational expenditure
ORC	organic Rankine cycle
PBCS	packed-bed cold storage
PHS	pumped hydro storage
RE	renewable energy
RTE	roundtrip efficiency
SNG	synthetic natural gas
SOFC	solid oxide fuel cell
SPECO	specific exergy costing
TCI	total capital investment
TIT	turbine inlet temperature
TRL	technology readiness level
TRR	total revenue requirement
TV	throttling valve
T&D	transmission and distribution
UPS	uninterruptible power supply
VRB	vanadium redox flow battery
WH	waste heat

Contents

Acknowledgment III

Abstract V

Zusammenfassung VII

Nomenclature IX

Chapter 1: Introduction 21

Chapter 2: State of the art 23

2.1. Historical development of cryogenic energy storage 23

2.2. Adiabatic cryogenic energy storage systems 26

2.2.1. Principle of operation 26

2.2.2. System parameters 27

2.2.3. Charging processes 28

2.2.4. Discharging processes 30

2.3. System integration: waste heat, waste cold, and combustion 31

2.4. Classification, characteristics and benchmarking 33

2.4.1. Classification and competing technologies 33

2.4.2. Characteristics and benchmarking 34

2.5. Potential application and economic benefit 39

2.5.1. Applications suitable for CES systems 39

2.5.2. Economic benefits and value propositions 41

2.6. Summary of the literature review 45

Chapter 3: Methodology 47

3.1. Energetic analysis 47

3.2. Exergetic analysis 48

3.3. Economic analysis 51

3.3.1. Cost estimation 51

3.3.2. Assumptions made 53

3.3.3. TRR method 54

3.3.4. Economic sensitivity analysis 55

3.3.5. Determination of cost rates 56

3.4. Exergoeconomic analysis and optimization 57

3.4.1. Exergy costing 58

3.4.2. Exergoeconomic optimization 59

3.5. Summary of the methodology 60

Chapter 4: Design and simulation 61
4.1. Simulation and data management software 62
4.2. General assumptions made in the simulation 62
4.3. Adiabatic cryogenic energy storage systems 64
4.3.1. Charging unit 65
4.3.2. Storage unit 70
4.3.3. Discharging unit 72
4.4. Integrated systems 75
4.4.1. Waste heat integration 77
4.4.2. Diabatic CES with combustion 77
4.4.3. Integration of LNG low-temperature exergy 78
4.5. Summary of the design and simulation 80
Chapter 5: Results and discussion 81
5.1. Evaluation of different charging processes for adiabatic CES 81
5.1.1. Energetic and exergetic evaluation of the liquefaction processes 81
5.1.2. Economic evaluation of the Claude-based liquefaction processes 85
5.2. Analysis and optimization of two adiabatic CES systems 86
5.2.1. Exergetic analysis 86
5.2.2. Economic analysis 90
5.2.3. Exergoeconomic analysis and optimization 91
5.3. Exergy-based evaluation of CES system integration 100
5.3.1. Comparative energetic and exergetic analysis 100
5.3.2. Comparative economic analysis 102
5.4. Economic viability of CES systems 107
5.4.1. Economic sensitivity analysis of the a-CES system 107
5.4.2. Economic sensitivity analysis of the integrated CES systems 109
5.4.3. Validation and assessment of results 112
5.5. Summary of the results and discussion 116
Chapter 6: Conclusion and outlook 119
6.1. Summary of the main results 120
6.2. Scope of the present work 121
6.3. Limitations 123
6.4. Summary of potential future work 123
References 125
Appendix A 137
Appendix B 141
Appendix C 155
Appendix D 163

List of figures

Figure 2.1: Historical development of cryogenic energy storage. 23
Figure 2.2: Country of origin of reviewed articles and patents on CES. 24
Figure 2.3: Principle of operation of adiabatic CES. 26
Figure 2.4: Integration of internal/external heat and ”cold” sources to a CES system. 31
Figure 2.5: Rated power, energy capacity and discharge duration of ES technologies. 33
Figure 2.6: Comparison of selected weighted characteristics of CES, CAES, and PHS. 35
Figure 2.7: CES specific costs per kW installed capacity reported in the literature. 36
Figure 2.8: CAPEX and specific costs over CES system capacity. 37
Figure 2.9: Discharge period and power rating of various energy storage applications. 39
Figure 2.10: “Life cycle” value proposition of ES applications. 42
Figure 2.11: Potential primary (“anchor”) and secondary services of CES. 43
Figure 2.12: Value proposition for stacked benefits suitable for CES. 44

Figure 3.1: The exergy transfer rate associated with the heat transfer over the temperature difference. 50
Figure 3.2: Logic flowchart for the exergoeconomic optimization applied in this work. 57

Figure 4.1: Schematic of the system configurations considered for this work. 61
Figure 4.2: Flowsheet of the stand-alone adiabatic CES system (Base Cases A and B). 64
Figure 4.3: Flowsheet of the gas cleaning and purification unit 65
Figure 4.4: Minimum specific work and the maximum liquid yield over the pressure. 66
Figure 4.5: Flowsheets of the Linde-based liquefaction processes with cold recycle. 68
Figure 4.6: Flowsheets of the Claude-based liquefaction processes with cold recycle. 69
Figure 4.7: T, $\Delta\dot{H}$-diagram of the main heat exchanger in the discharge process. 72
Figure 4.8: RTE over pumping pressures for Base Case B. 73
Figure 4.9: Specific discharge work per kg of liquid air, RTE, and η over the TIT. 74
Figure 4.10: Flowsheets of the integrated systems. 75
Figure 4.11: RTE and exergetic efficiency over the specific mass flow of LNG. 79

Figure 5.1: Results of the energetic and exergetic evaluation for the liquefaction processes with/without integrated cold storage. 82
Figure 5.2: Sensitivity analysis results for the Claude-based liquefaction processes. 83
Figure 5.3: Minimum specific work and maximum liquid yield over the splitting ratio. 84
Figure 5.4: Exergetic efficiency of selected components of the two base case systems. 86
Figure 5.5: Grassmann diagram of the exergy flow in the Base Case A. 87
Figure 5.6: Grassmann diagram of the exergy flow in the Base Case B. 88
Figure 5.7: Breakdown of the exergy destruction of the overall systems. 89
Figure 5.8: Cost breakdown of the $LCOE_{dis}$ for the two base case systems 90
Figure 5.9: Bare module costs of the Base Cases A and B. 91
Figure 5.10: Exergoeconomic analysis results for the five components with the highest total cost rate. 92

Figure 5.11: Component cost rates of selected components of the Base Case B. 95
Figure 5.12: RTE over $LCOE_{dis}$ for the optimization steps for the Base Case A. 96
Figure 5.13: RTE over $LCOE_{dis}$ for the optimization steps for the Base Case B. 96
Figure 5.14: Normalized capital investment cost over the relative exergetic efficiency.. 97
Figure 5.15: Exergoeconomic analysis results for the base cases and optimized cases. .. 98
Figure 5.16: Exergetic analysis results for the integrated CES system configurations. . 100
Figure 5.17: Bare module costs of the components of the integrated systems. 102
Figure 5.18: Specific investment costs over RTE of the ten CES systems..... 104
Figure 5.19: Specific investment costs and $LCOE_{dis}$ over the spec. mass flow of LNG. 105
Figure 5.20: The levelized cost of electricity of the ten CES system configurations. 106
Figure 5.21: Economic sensitivity analysis results of the a-CES system. 107
Figure 5.22: $LCOE_{dis}$ over the FLH_{dis} for the ten considered systems. 109
Figure 5.23: $LCOE_{dis}$ over the price of electricity for selected CES systems..... 111
Figure 5.24: $LCOE_{dis}$ of PHS, d-CAES, a-CAES, and selected CES systems. 112
Figure 5.25: Box-plot diagram of the specific costs of PHS, CAES, and CES. 113
Figure 5.26: $LCOE_{dis}$ of selected CES systems compared to values from the literature. 114

Figure A.1: Patents and research articles published from 2013 to 2017. 138
Figure A.2: Compatibility of occasional and frequent use ES application..... 140

Figure B.1: Day-ahead market clearing price over the hours in the year in Germany. .. 144
Figure B.2: Historical development of the annual average value of the CEPCI. 144
Figure B.3: Historical data for the conversion rate of €/USD and €/GBP..... 145
Figure B.4: Printed circuit heat exchanger by Heatric used by Highview Ltd. [161] 148

Figure C.1: Sensitivity analysis results for the isentropic efficiency of the expander.... 157
Figure C.2: Flowsheet of the cold storage integration into the CES system. 160
Figure C.3: RTE and exergetic efficiency over mass flow rate of the fuel for the d-CES system 161

Figure D.1: T, $\Delta\dot{H}$-diagrams of the MHE1 in the Claude-based liquefaction processes. 163
Figure D.2: Comparison of the composite curves of the MHE1 for the Claude and the Kapitza process. 164
Figure D.3: Max. exergetic efficiency and min. specific work required for liquefaction over the liquefaction pressures for the Claude process and the Heylandt process. 165
Figure D.4: Maximum liquid yield and liquefaction pressure over the splitting ratio. . 165
Figure D.5: Exergy destruction ratio of selected components for the base cases. 167
Figure D.6: Effect of the increased mass flow rate of the heat storage media on the RTE over the $LCOE_{dis}$ for the base cases. 168
Figure D.7: Specific exergy destruction and losses over the cost of the final product for the optimized cases after parametric changes on Base Cases A and B. 168

Figure D.8: $LCOE_{dis}$ over the mass flow of LNG in the integrated systems. 169
Figure D.9: $LCOE_{dis}$ over the mass flow of fuel supplied to the d-CES system 169
Figure D.10: $LCOE_{dis}$ over FLH for all considered systems with consideration of CO_2 emission prices. 170
Figure D.11: Box-plot diagram of the spec. costs of different bulk ES technologies. ... 172
Figure D.12: Box-plot diagram of the $LCOE_{dis}$ of PHS, CAES, and CES. 172

List of tables

Table 2.1: Parameters of CES systems presented in literature. 27

Table 3.1: Cost functions developed for the estimation of the BMC of the CES system. 53
Table 3.2: Assumptions made in the economic analysis. 54

Table 4.1: Isentropic efficiencies presumed for the turbomachinery. 62
Table 4.2: General assumptions and design parameter for the heat exchangers. 63
Table 4.3: Refrigerant properties compared to air [37, 56]. 71
Table 4.4: Energy densities and efficiencies reported in the literature. 74
Table 4.5: Power and heat capacities in MW for indicated work and heat flows..... 76

Table 5.1: Design parameters for the three Claude-based CES systems compared. 85
Table 5.2: Results of the economic analysis for the Claude-based liquefaction units..... 85
Table 5.3: Results obtained from the exergetic evaluation of the two base case systems. 86
Table 5.4: Results obtained in exergoeconomic analysis for the two base case systems. 92
Table 5.5: Decision variables for exergoeconomic optimization. 93
Table 5.6: Parameters and results of the optimization steps for the Case A..... 94
Table 5.7: Parameters and results of the optimization steps for the Case B.. 94
Table 5.8: RTE, energetic and exergetic efficiency of the ten considered systems..... 101
Table 5.9: Results of economic analysis for the ten CES system configurations. 103

Table A.1: Comparison of CES characteristics to other bulk ES technologies 137
Table A.2: Bulk energy applications compatible with CES characteristics 138
Table A.3: Ancillary services compatible with CES characteristics 139
Table A.4: Frequency regulation services compatible with CES characteristics 139
Table A.5: Renewable energy integration applications compatible with CES 139
Table A.6: T&D support applications compatible with CES characteristics..... 139
Table A.7: Results of the literature review on the economic value of potential CES applications. 140

Table B.1: Definition of the exergetic and energetic efficiencies for CES systems..... 141
Table B.2: Definition of exergy of fuel and exergy of product of selected components 142
Table B.3: Definition of exergy of fuel and exergy of product of pumps and turbines for different cases of the entering and the exiting temperature. 141

Table C.1: Stream values of the Base Case A. 155
Table C.2: Stream values of the Base Case B..... 156
Table C.3: Stream values for the states indicated in the flowsheets in Figure 4.6 158
Table C.4: Stream values for the states indicated in the flowsheets in Figure 4.5 159
Table C.5: Stream values for the adiabatic CES systems with waste heat integration... 160
Table C.6: Stream values for the CES systems with single and double combustion..... 161
Table C.7: Stream values for for the CES systems with/without integration of LNG.... 162

Table D.1: Exergy analysis results on component level for Base Case A. 166
Table D.2: Exergy analysis results on component level for Base Case B. 167
Table D.3: Economic analysis results for Base Cases A and B. 168

Chapter 1: Introduction

There is no doubt that the challenges in the power sector are nowadays of greater importance than earlier, resulting in major political, social, economic, and ecological consequences [1, 2]. The rapid development towards a higher penetration of electricity generation from renewable energy sources introduces new challenges to the electricity grids [2]. The highly fluctuating generation pattern, as well as the low power capacity factor of renewable energy generators, offer a weak prediction for power availability; leave power grid operators with little means to sustain the supply-demand equilibrium and secure uninterrupted power supply [3]. Especially wind and solar power generation, which are subject to strong intermittency, have recently faced a significant boost globally [2, 3, 4]. The power supply should be able to cover the demand at any point in time. The infrastructure and services of the existing electricity grid are not optimized to sustain reliable function while accommodating a high amount of electricity from renewable energy sources [5, 6, 7].

So far, grid operators avoid system failures, which would cause power cutbacks and would harm equipment, during a possible mismatch between demand and generation, by introducing flexibility to the grid [8]. Energy storage (ES) and particularly grid-scale electricity storage is widely regarded to be the most valuable option to advance power grid flexibility while facing extensive renewable energy incorporation [6, 9, 10, 11]. Mid and long-term electricity storage provide flexibility on multiple layers by (a) leveling the high penetration of renewable energies and capturing surplus electricity at low demand; (b) providing peak shaving, and (c) reducing necessary reserve capacity [12]. Grid-scale energy storage technologies vary in their energy capacities, power capacities, discharge periods, roundtrip efficiencies (AC/AC efficiency), response times, and capital costs [6]. Grid balancing services entail a storage device with reasonable efficiency (> 50 %) but low costs at a significant scale. These requirements are consistent with the concept of cryogenic energy storage [13, 14].

The working principle of *Cryogenics-based energy storage* (CES) is classified as thermal or thermo-electric energy storage (ES). CES charges excess electricity in an energy-intense air liquefaction process. The liquefied gas is stored at ambient pressure and a cryogenic temperature in an insulated storage vessel. During discharge; the liquid air is pumped to high pressures, evaporated, superheated, and finally expanded partially recovering the electricity charged. CES is the only grid-scale ES technology without geographical constraints, a remarkably higher volumetric energy density, very low storage losses, and a long cycle life. CES integration with other processes such as the recovery of “waste heat” or “waste cold” increase the technologies attractiveness as well as the efficiency [15]. CES consists of components with well-known industrial-scale applications [2], allowing great scale-up excessing present supply infrastructure [16, 17, 18]. Hence, CES is expected comparatively fast progress towards commercialization [19]. Being a pre-commercial, technology CES still has to prove its favorable characteristics [3].

The reduction of the energy requirement in the liquefaction process and the increase of the specific power output of the discharge process were identified as two main research and development objectives, that need to be met to prepare CES technology for the market [20]. Apart from the enhancement of the roundtrip efficiency, the reduction in costs is a major milestone to be accomplished for the technology to reach maturity.

With this background, the present work on cryogenic energy storage aims to

- evaluate the **potentials of the technology and the associated challenges** reviewing and validating CES characteristics stated in literature (e.g., exergy density, roundtrip efficiency, specific costs), drawing a comparison to its competing technologies and evaluating its potential application.
- quantify the impact of the different charge, storage and discharge process configurations on the **thermodynamic** and **economic** performance of adiabatic CES systems.
- reveal the relation of **thermodynamic inefficiencies** and costs in the CES system and identify a measure for **cost reduction**.
- identify the **cost-optimal system design** of adiabatic CES systems.
- evaluate the **performance enhancement through the integration** of liquid natural gas (LNG), internal combustion and waste heat to CES systems.
- evaluate CES **economic viability** using sensitivity analysis: identifying the limiting factor and revealing potential revenue streams.

These objectives are achieved with the application of exergy-based methods after the design and simulation of several CES configurations in Aspen Plus® based on an intense literature review.

In *Chapter 2* of this thesis, the background to the CES principle of operation, history, and maturity is given. CES core characteristics are reviewed and benchmarked towards competing energy storage technologies. Moreover, potential energy storage applications for CES are identified along with potential revenue streams. The assumptions made and methods applied in the analysis are subject to *Chapter 3*. In *Chapter 4*, the considered CES system configurations are presented, the design decisions made for the system configurations are justified, and the assumptions made in the simulation are elaborated. The results from the analysis of the different system configurations, their sensitivity, validation, and discussion are presented in *Chapter 5*. While *Chapter 6*, places the main findings in a holistic context. The conclusions are stated, and the limitations to the present work are assessed with the prospect for future work.

Chapter 2: State of the art

In this chapter, cryogenic energy storage history, principle of operation, most significant system parameters and system configurations are introduced. In particular, different charge and discharge unit configurations are reviewed, and the potential for system integration with external heat sources and sinks is discussed. Further, the CES is addressed in a broader context. ES technologies are classified, and competing technologies are identified. Further CES characteristics are compared to those of competing technology. Finally, the potential applications for CES and their economic benefit are outlayed.

2.1. Historical development of cryogenic energy storage

The concept of storing electricity in the form of liquefied air has been firstly published by Smith et al. [21] from the University of Newcastle in 1977. The storage concept was claimed to enable roundtrip efficiencies (RTE), see equation (3.5), up to 72 % through adiabatic compression and expansion [21]. The associated patents were obtained by several research groups in France, Japan, and Germany (1981-1983) [15]. In particular, Hitachi Ltd [22, 23, 24, 25] and Mitsubishi Hitachi Power Systems Ltd [26, 27, 28] engaged in the technology's further development. [3]

The first pilot plant was built in 1995 (Mitsubishi Hitachi Power Systems Ltd, [27]) by extending an existing air liquefaction plant with a 2.6 MW cryogenic power recovery unit (discharge unit). The pilot plant was argued to confirm the system viability [27] despite a very low RTE [29]. The technology's historical advancement is shown in Figure 2.1.

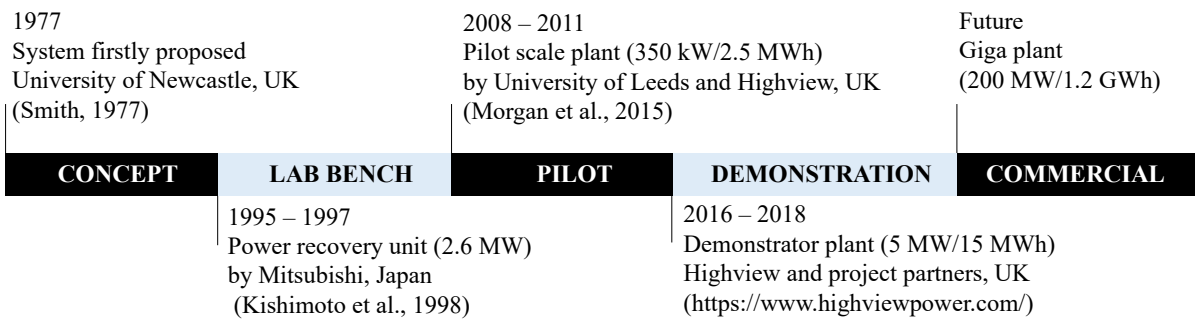

Figure 2.1: Historical development of cryogenic energy storage [3] adopted from [30].

The first integrated pilot CES plant (350 kW/2.5 MWh) was the result of a joint research project of the University of Leeds and Highview Power Storage Ltd. (further "Highview Ltd."), a privately owned company [31]. The discharge unit was built in 2009. The pilot plant was collocated to a biomass-fired power plant providing waste heat to the system in Slough, UK. In 2010, the system was connected to the electricity grid. Only in 2011, the recovery unit was extended with an air liquefier. First results from this pilot plant were published in 2015 by Morgan et al. [16][1]. The system reached a RTE of 7-11 % [32]. Provision of grid balancing services such as load follow was found technically realizable. The technologies efficiency and costs were predicted as competitive once the system would reach commercial scale. The plant was later moved to the University of Birmingham for further testing [29].

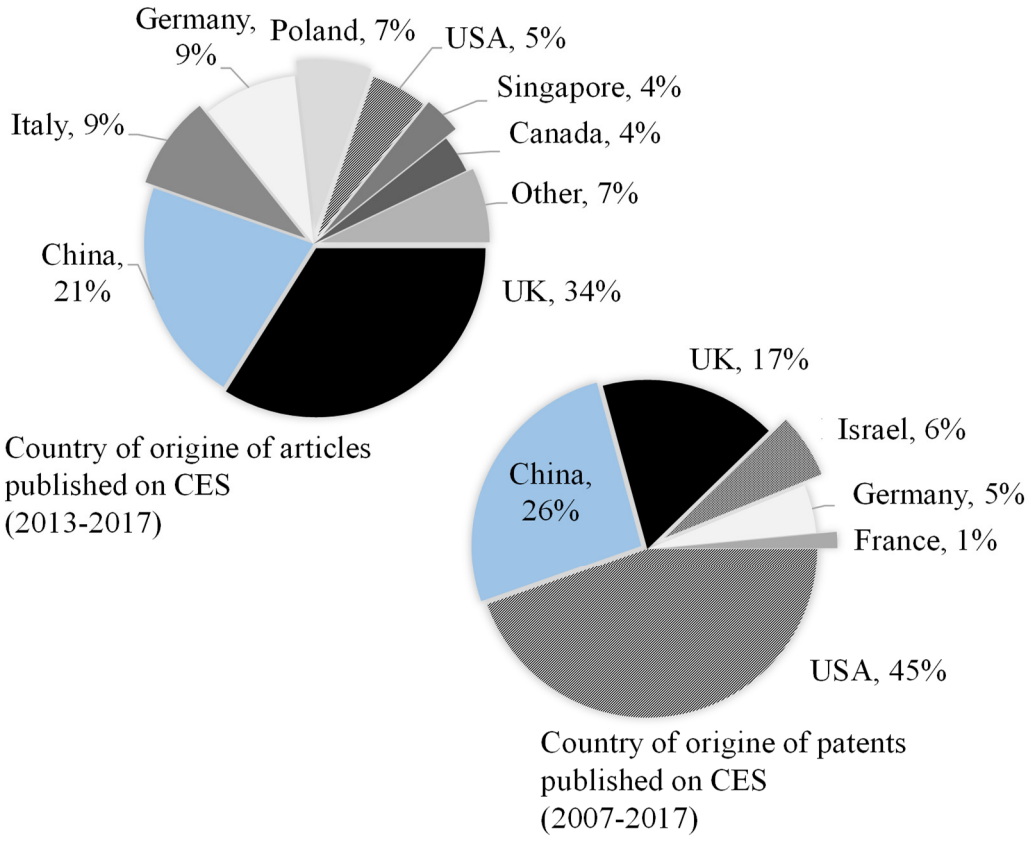

Figure 2.2: Country of origin of reviewed articles and patents on CES [3].

In 2014, funding of approximately € 9 Million by the UK Department of Energy and Climate Change was granted to Highview Ltd. and project partners for the construction of the demonstration plant (5 MW/15 MWh). In April 2018, the demonstration plant started operation next to a landfill facility in Bury, Greater Manchester. The plant provides selected balancing services such as peak shaving and short term operating reserve [31]. The "Giga plant" developed by Highview Ltd. is planned to be located in Dallas, Texas, USA, at a total cost of € 230 Million and reach a RTE of 60 %. [3]

[1] In this work, the names of the authors are only given for key publications.

In 2013, the Liquid Air Energy Network (LAEN) was formed as a result of a joint research project between UK universities and the Centre for Low Carbon Futures [8]. The LAEN aims to investigate the potential role of liquid air as an energy vector in the future energy and transportation sectors [30]. The number of publications and patents on cryogenics-based or liquid-air energy storage increased since 2013 (the number of publications can be extracted from Figure A.1 in Appendix A). Figure 2.2 shows the origin of reviewed papers and patents on cryogenic and liquid air energy storage. Leading companies in the field of industrial gases, e.g., Air Liquide, and Linde AG obtained patents in 2012 and 2014, respectively. The largest number of patents and articles came from Chinese and UK experts. [3] The large majority of UK patents relate to the activities of Highview Ltd. [31].

Maturity of the technology

CES consists of mature components with well-known industrial-scale applications in the field of industrial gases and chemical processes as well as power generation; allowing scale-up excessing present supply infrastructure [15, 16, 17, 18]. For the same reason, developers expect comparatively fast progress towards commercialization [19]. According to several case studies, e.g. [20], CES is expected to reach maturity in less than five years. The European Association for Storage of Energy evaluated CES in 2017 with a Technology Readiness Level (TRL) of approximately TRL 8 (TRL 9 denoting a mature technology) [33]. The TRL 8 refers to the system being in the end phase of the development for the majority of components. CES commercial design has been completed and the technology was proven in testing and demonstration [34, 35].

For example, the charging system of CES is in parts similar to conventional air separation units (ASU). Commercial air liquefaction plants are about ten times smaller than the liquefaction capacities needed for grid-scale CES. Thus a technological gap still exists [15] while it could be adapted from commercial-scale natural gas liquefaction. Available industrial cryogen storage vessels based on liquefied natural gas (LNG) technology enable capacities of 200,000 m³, which would enable 17-23 GWh of storage capacity [18]. The discharge unit is also assembled of components common in the power and process sector (e.g., turbines, compressors, pumps, and electric motors). Potential vendors and supply chains for CES key components were evaluated by Strahan et al. [8]. Limitations to the scale of the systems were identified by Brett and Barnett [18]. Scales comparable with a plant size of up to 100 MW are currently achievable [12, 16, 18]. Being a pre-commercial technology, CES still has to prove its expected advantageous characteristics [3], e.g., its specific cost and its efficiency (section 2.4.2). The operation and design of CES systems are subject to the following subsection 2.2 and 2.3.

2.2. Adiabatic cryogenic energy storage systems

2.2.1. Principle of operation

In CES systems, large quantities of electricity are stored in the form of liquefied gas at cryogenic temperature (< - 150 °C). CES is frequently named *liquid air energy storage* (LAES) as air, or air constituents are commonly utilized as the working and storage media. The integrated methods of operation (charging, storage, and discharging) of an adiabatic CES system are displayed in Figure 2.3.

An energy-intensive liquefaction process forms the *charging process* of CES. In the liquefaction process, the gas is pre-treated, compressed, cooled and expanded until it reaches its due point. The liquefied gas (cryogen) is stored in a site-independent thermally insulated storage vessel at approximately ambient pressure and very low temperatures (e.g., - 194 °C). The compression process of the liquefaction is presented separately, as in the adiabatic CES the heat of compression is recovered and stored to be used in the discharge process.

In the *discharge process,* the liquefied gas is pumped to supercritical pressure (e.g., 150 bar) in a cryogenic pump, evaporated and superheated. The thermal energy supplied to the gas in the superheating process can be provided by the environment (e.g., 15 °C), the internal heat storage (e.g., 200 °C), a combustion process (e.g., > 800 °C) or a waste heat source (e.g., 350 °C). The high-temperature high-pressure gas is supplied to a series of expanders regaining a part of the electricity charged to the system.

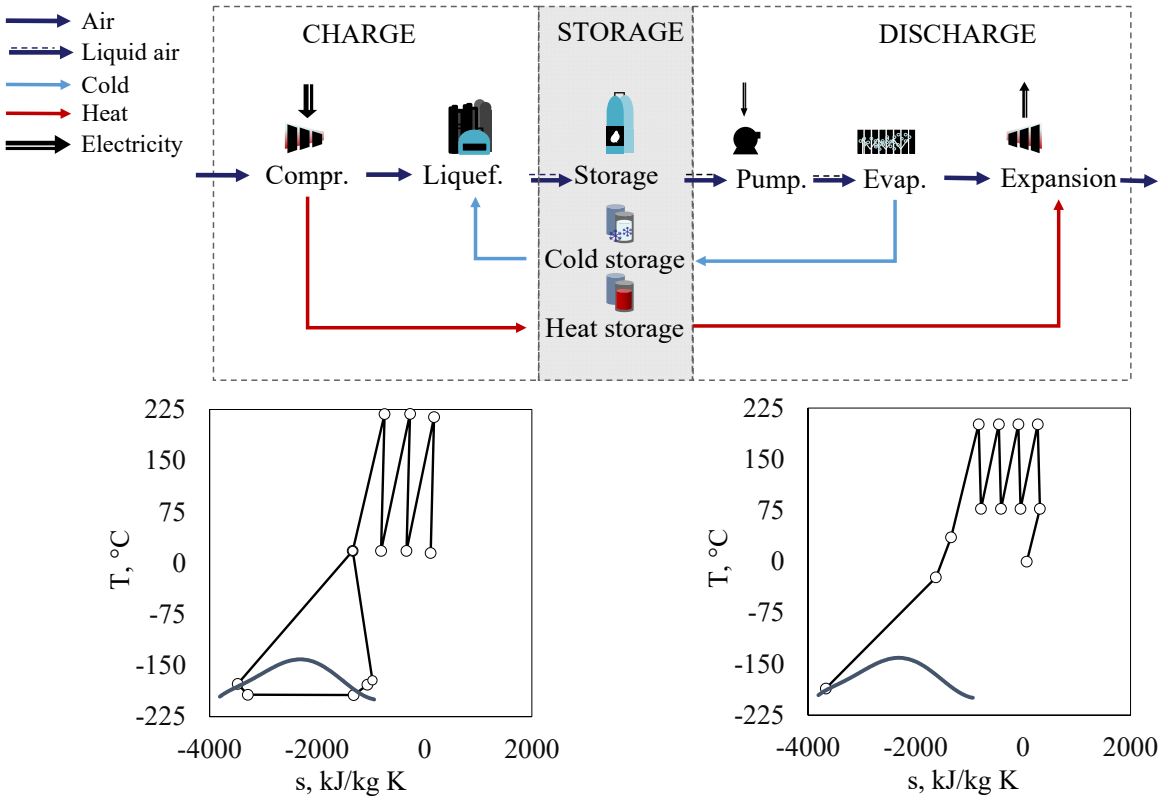

Figure 2.3: Principle of operation of adiabatic CES systems. T,s-diagram for the charging and the discharging process [36].

The low-temperature exergy (or "cold") rejected during the evaporation process can be recovered and stored. When additional low-temperature exergy is supplied to the liquefaction process (charging), the amount of air that is liquefied is increased. Without cold storage and recovery, CES systems would reach roundtrip efficiencies of less than 30 %. Stand-alone adiabatic CES systems reach a roundtrip efficiency of 40-50 % [37, 38]. The integration of thermal energy through external heat and cold sources can significantly increase the RTE to above 70 %. The potential for system integration is reviewed in section 2.3.

The state of the art of different parameters, charging and discharging configurations of adiabatic CES systems are discussed in the following subsections 2.2.2 to 2.2.4. The system design and simulation of the CES systems evaluated in this work are discussed in greater detail in chapter 4.

2.2.2. System parameters

Recently, several publications have discussed the thermodynamic performance of CES. A number of adiabatic CES system configurations have been proposed. The different liquefaction processes, charge and discharge pressures (p_{char}, p_{dis}), liquid yields (γ), cold storage configurations and roundtrip efficiencies (RTE) of the adiabatic CES systems discussed in selected literature are given in Table 2.1. The selected system parameters varied significantly; the liquefaction pressures range from 20 to 180 bar and discharge pressures vary between 50 and 150 bar.

Table 2.1: Parameters of CES systems presented in the literature.

Ref.	Liquefaction process	p_{char}, bar	γ, -	Cold storage configuration	p_{dis}, bar	RTE, %
[39]	Linde-Hampson	~130	0.44-0.74	fluid tanks (CH_4O, R218)	112-120	28-37
	Expander cycle	NA	NA	fluid tanks (CH_4O, R218)	NA	40-46
[10]	Linde-Hampson	20	0.70	direct integration (ideal)	100	20-50
[40]	Linde-Hampson	120	0.83	fluid tanks (CH_4O, C_3H_8)	50	50-60
[41]	Integr. Linde-Hampson	90	0.60	fluid tanks (CH_4O, C_3H_8)	120	60
[42]	modified Claude	180	0.86	packed bed gravel (air)	75	48.5
[14]	4 turbine Claude	56.8	0.551	packed bed gravel (air)	190	> 50
[16]	2 turbine Claude/Collins	54	NA	packed bed gravel (air)	150	47
[2]	Heylandt	180	0.61	fluid tanks (CH_4O, R218)	150	41
[43]	Linde-Hampson	180	0.842	fluid tanks (CH_4O, C_3H_8)	65	50
[44]	Linde-Hampson	140	NA	NA	70	47.2

The liquid yield γ refers to the ratio of the mass flow of the air liquefied in the liquefaction process to the mass flow of the compressed air, equation (3.4). The liquid yield is an indication of the charging-unit performance. The values for the liquid yield vary strongly (0.44-0.86),

while the *RTE* are within the same range mostly between 40 % and 55 %. Therefore, no optimal CES design configuration could be identified [3]. Different assumptions were made in simulation, e.g., ideal dry air was assumed, heat and pressure losses in most components as well as heat losses in the cold recovery and the associated heat exchangers were neglected [40], or assumed lower than 8 % [14].

Moreover, the reviewed publications rarely used exergy-based methods on the component level. Neither the "fuel and product approach" nor the "splitting of physical exergy" was taken into consideration. The origin and margin of thermodynamic inefficiencies in the system have thus not thoroughly been identified. The role of cold storage and heat recovery was emphasized in all papers. Nevertheless, the effect of heat and cold recovery and storage was not quantified in terms of exergy. A comparison of the simulation and analysis results while neglecting the various assumptions would result in misleading conclusions. In order to identify an optimal system design, the different parameters and configurations must be analyzed under common assumptions. In this work, a cost-optimal system design of adiabatic CES systems is identified with the aid of exergy-based methods. In the following subsections the different air liquefaction processes, cold storage configurations and potential discharge processes are assessed in the context of CES.

2.2.3. Charging processes

The significance of the liquefaction process to the CES's performance was addressed in [39] as "the key part" of the system as the discharge unit is relatively simple and efficient. Despite air liquefaction being commercial since the 1940s [45], the charging process of CES systems still has room for improvement [46]. When additional low-temperature exergy is available, e.g. through cold storage, the performance of the liquefaction process is considerably improved [2, 15]. One of the vital findings from the testing of the first pilot plant was the increase of system efficiency though cold recovery and storage [14]. Thus, the choice of the liquefaction process for CES influences the thermodynamic and economic performance of the overall system. This work aims to quantify this improvement and identify the most suitable liquefaction process with cold storage and recovery.

(a) Liquefaction processes

Nowadays, various liquefaction processes are in operation. The first-industrialized and simplest configuration is the Linde process. The purified air is thereby compressed, cooled and fed to a throttling valve to undergo an isenthalpic expansion, bringing the air to its due point [47]. Gas liquefaction is at the present time achieved in more complex processes [10]. The Claude process and its modifications are the most commonly applied in commercial air liquefaction plants due to their elevated efficiency [48].

In the Claude process, the compressed air is cooled by a cold recycle stream – a share of the pressurized air that underwent an isentropic expansion in one or more cold turbines [14]. The Heylandt process implied the elimination of the first heat exchanger in the Claude system [48] and the Kapitza process dates back to 1939 when the inventor suggested the use of centrifugal expansion turbines in the Claude process [47]. Most modern liquefiers use expansion turbines proposed by Kapitza [49] and most high-pressure air liquefaction plant operate with the Heylandt process. [46]

A comparative evaluation of air liquefaction processes in the context of CES systems was presented by Li et al. [39], Borri et al. [50] and Abdo et al. [51]:

Borri et al. [50] compared three air liquefaction processes for application in a micro-scale CES: the Linde-Hampson, the Claude, and the Collins process. The Claude process was identified as the most suitable air liquefaction process for application in CES. The Linde-Hampson process operating with a Joule-Thomson valve was claimed to be inferior. Also, a second cold expander used in the Collins process was found not economically feasible. Borri et al. [50] thereby did not take into account the effect of the integration of cold recovery and storage on the performance of the liquefaction processes.

Li [39] only considered the integration of a cold expander instead of a throttling valve in the Linde process apart from an "expander process" which employs a refrigeration process with Helium as working fluid. Li [39] came to the same conclusion than Borri et al. [50], that the throttle-valve-based Linde-Hampson process is not applicable for CES.

Abdo et al. [51] compared a CES system design (patented by Chen et al. [52]) based on a simple Linde-Hampson process to two alternative systems: the Collins and the Claude process. The heat of compression was accounted for in the analysis, but the cold storage was not considered. The Claude and Collins process showed similar thermodynamic performance and reached greater *RTE* than the Linde-based process. The more efficient Claude-based system was evaluated as the best option, although the Linde-Hampson achieved the lowest specific costs [51].

None of the three comparative analyses reviewed assessed the impact of cold storage on the selection and performance of the liquefaction despite discussing specifically the application in CES systems. The present work aims to compare several air liquefaction processes with integrated cold storage to identify the most efficient and economic liquefaction process for implementation in CES systems. The different liquefaction processes that were considered are described in section 4.3.1. The results from the comparative energetic, exergetic, and economic evaluation are presented in section 5.1.

(b) Cold storage

Without cold recovery and storage, adiabatic CES efficiency would drop below 35 % [15]. The temperature in the cold storage cyclically varies between cryogenic temperature (discharging process) and environmental temperature (charging process) [53]. For the effective recovery and storage of the low-temperature exergy from the discharging process, the characteristics of the storage medium play a vital role [42]. From the literature reviewed (Table 2.1), two kinds of a cold storage configuration can be extracted:

1) quartzite gravel based packed bed storage with dry air as the secondary working fluid, and
2) two-tank fluid storage with methanol and propane (or R218) as secondary working fluids and storage media on two different temperature levels.

The latter cold storage configuration (2) dates back to 1997 when Hitachi, Ltd. developed and patented the first concept for cold recovery and storage [22]. The concept was afterward adopted for a solid-packed-bed of pebbles by Highview Power Storage Ltd. [52]. The high density and specific heat capacity of the pebbles in packed bed cold storage (PBCS) enables higher energy density. The PBCS can be designed with a wide range of storage materials. Hd-

polyethylene and polypropylene were evaluated suitable for application in PBCS while metals were found unfitting by [53]. The dynamic performance evaluation of PBCS revealed that the dynamic cycling between the charging and the discharging process increases the work required for the liquefaction process by an undesired 25 % in comparison to steady-state analysis [42].

Due to a large amount of low-temperature exergy to be stored, safe (non-toxic and non-flammable) and inexpensive cold storage media are preferable [39, 22]. The cold storage configuration was the subject of many publications. The cold storage performance (e.g., temperature, the minimum pinch temperature and the pressure drop in the CS) has a high impact on the *RTE* of the overall system independent of the storage material [43, 52, 22]. On a system level, the recovery rate of the low-temperature exergy and the cold storage costs are of importance. Thus, the cold storage configuration itself is not analyzed in this work. Solely, one CES configuration was considered (a pair of thermal fluids). The considered CS design is explained in more detail in section 4.3.2.

2.2.4. Discharging processes

Power cycles are driven by the temperature gradient between two thermal reservoirs: the heat sink and the heat source [2]. The electricity "charged" to a cryogen (liquid gas) while liquefaction may be partially regained in a cold power generation cycle where the cryogen acts as the heat sink. Diverse heat sources can be utilized: ambient heat, low/high-grade waste heat or heat of combustion [45, 54]. Various methods for extracting low-temperature exergy stored in a cryogen have been published in China, USA, and Belgium [10, 17, 37, 55, 56, 57]. Altogether three different methods for power generation and their combination can be identified [2]:

1) The *'Direct Expansion'* refers to power generation while expanding the beforehand pressurized, vaporized and superheated cryogen, in a direct manner [8, 45, 55]. The cryogen thereby serves as the only working fluid of the Rankine cycle.

2) Methods for extracting cold exergy from a cryogen employing a second working fluid in addition to the cryogen are referred to as 'indirect':

    a. The *'Indirect Rankine'* cycle is the most commonly considered indirect cold power generation method [10, 37, 45, 58]. The cryogenic fluid thereby acts as the heat sink of the cycle, while the heat for evaporation of the working fluid is provided by the ambient or another heat source.

    b. Within the *'Indirect Brayton'* cycle the cryogen cools down a gas to decrease compression work, the dense gas is further heated and expanded generating shaft work in a gas turbine [54, 58].

3) Combinations of the three methods can be referred to as *'Combined Methods'* [45, 54].

Methods for extracting cold exergy in power cycles is most commonly discussed in the context of the regasification of LNG. The low-temperature exergy vented in the LNG regasification usually serves no further purpose. The cold exergy released in the evaporation process in CES systems, in contrast, could be stored and supplied for the subsequent charging process. For CES the indirect methods (2.-3.) are thus in direct competition with the *cold recovery and storage* within the system. For CES only the direct expansion of the liquid air was considered.

2.3. System integration: waste heat, waste cold, and combustion

Cryogenic energy storage *RTE* can be increased by 40-75 % when internal and/or external heat sources or heat sinks ("cold" sources) are integrated. Examples for the integration of external heat and cold sources to an adiabatic CES system are shown in Figure 2.4. Four different system configurations can be differentiated [59]:

- the adiabatic system,
- waste heat recovery,
- LNG waste cold recovery, and
- the integration of internal combustion.

In adiabatic systems, the heat of compression in the charging process can be recovered and stored in the heat storage subsystem. The heat storage is commonly realized with pressurized water or thermal oil. The stored thermal energy is later used to increase the turbine inlet temperature (TIT) and power output of the discharge process. The specific power output of the discharge unit increases linearly with the increase in TIT [2]. The temperature of the captured thermal energy increases with fewer compression stages and higher pressures.

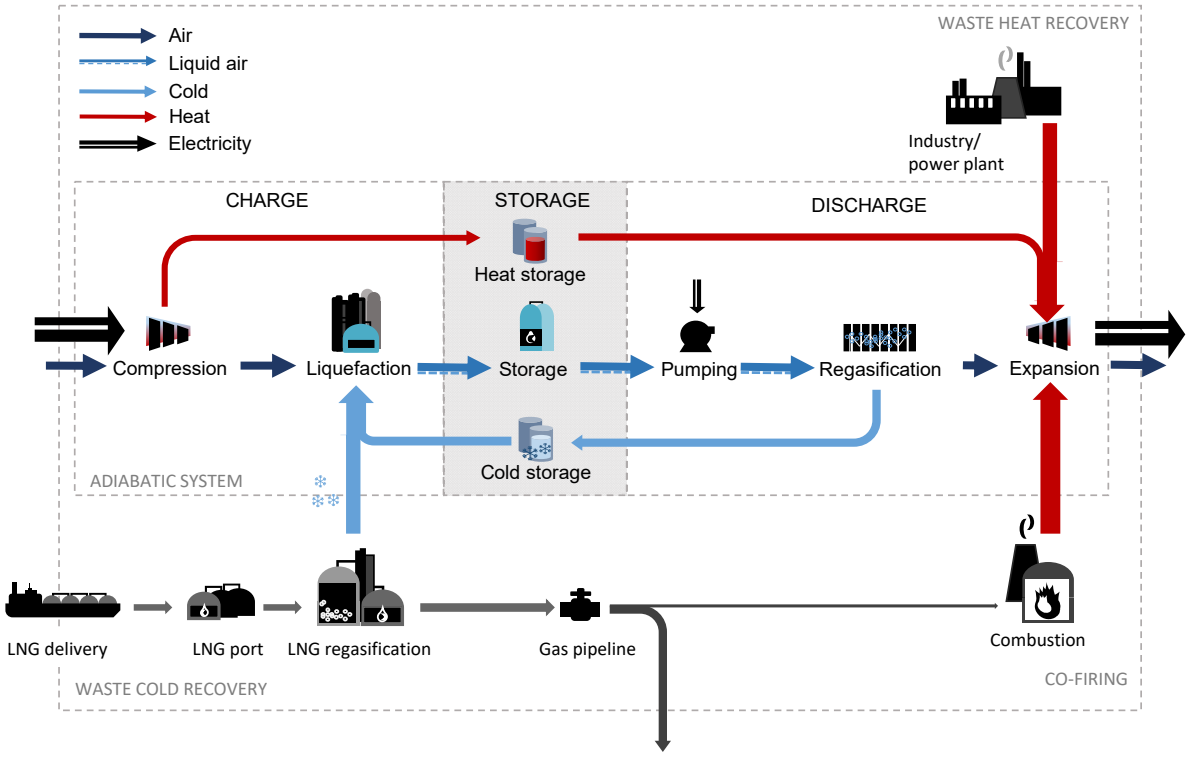

Figure 2.4: Integration of internal and external heat and "cold" sources to a CES system [59].

The recovery of "waste heat" is seen as one of the main potentials of CES [10, 8, 16, 37]. *Waste heat* refers to heat transfer streams from energy and manufacturing processes that serve no further purpose and may occur at different temperature levels [60]. For waste-heat recovery in

cryogenic energy storage, only high-temperature (> 300 °C) waste heat is of interest. The heat of compression recovered in adiabatic CES systems easily reaches temperatures of 200 °C. Waste heat recovery would necessitate colocation of the storage to an existing waste heat source setting up geographical limitations. As an alternative, a CES can contain a *combustion process* in which fuel, e.g., natural gas, is burned to supply additional thermal energy, which increases the temperature of the high-pressure gas before expansion. Natural-gas-fired systems may reach *RTE*s of 55-60 % [15, 43].

In the discharge process of adiabatic CES systems, the pressurized liquid gas is evaporated in heat exchange to the cold storage media to recover and store the low-temperature exergy. When the low-temperature exergy is supplied to the subsequent liquefaction process, a higher share of compressed air is liquefied, and the efficiency of the charging process significantly increases [2], section 2.2.3.

Low-temperature exergy may also be supplied from *LNG regasification* plants or industrial processes, e.g., air separation units [61]. Low-temperature exergy that would else be released to the environment is often referred to as “waste cold”. The waste cold can either be integrated instead of or in addition to the cold storage. Especially in the context of environmental impact, as well as energy and cost savings waste cold recovery from the LNG re-gasification processes has attracted great interest in the past decade. LNG integrated CES systems were reported to reach *RTE*s of 63-70 % [8, 62, 63]. Exergetic efficiencies for LNG integrated systems presented by [62], [63] and [64] reached 33-43 %. Integrating both LNG cold recuperation and combustion, the system may reach energetic efficiencies above 70 % [43] and exergetic efficiencies of 60-70 % [64].

Other CES system integrations have been suggested, e.g. into gas-fired power plants [8, 39], with a secondary organic Rankine cycle (ORC) driven by the heat of compression [41, 63], with an absorption refrigeration machine [65], or with a pumped thermal energy storage operating as a topping cycle [66].

Several sources mention the favourable integration of CES with other processes. The influence of system integration on cost was rarely discussed in the reviewed literature. Different system configurations were not compared on common ground (neither thermodynamically nor economically) to quantify the performance enhancement of integrating different heat sources and sinks. The only comparison of CES *RTE*s was given by Stöver et al. [15]. Stöver et al. emphasized the unavailability of reliable data and presented only rough estimates for *RTE*s of different system configurations [15]. For this reason, the integration of CES in this work aims to quantify the effect of system integration on CES thermodynamic performance and economics, see section 4.3 and 5.3.

2.4. Classification, characteristics and benchmarking

2.4.1. Classification and competing technologies

Great interest in energy storage systems has emerged in recent years [67], and a large number of energy storage (ES) technologies exist. ES technologies can be classified according to:

- the principle of operation or type of energy stored (mechanical, chemical electromagnetic/electrical, thermal);
- the rated power,
- the energy capacity, and
- the frequency and duration of discharge [3].

The working principle of CES systems is classified as thermal (or thermo-electric) ES [7]. The rated power, energy capacity and discharge duration of most common ES technologies are shown in Figure 2.5. When classifying ES technologies according to the rated power of the discharge unit, small (≤ 1 MW), medium (10-100 MW) and large-scale (≥ 100 MW) ES systems are differentiated [68].

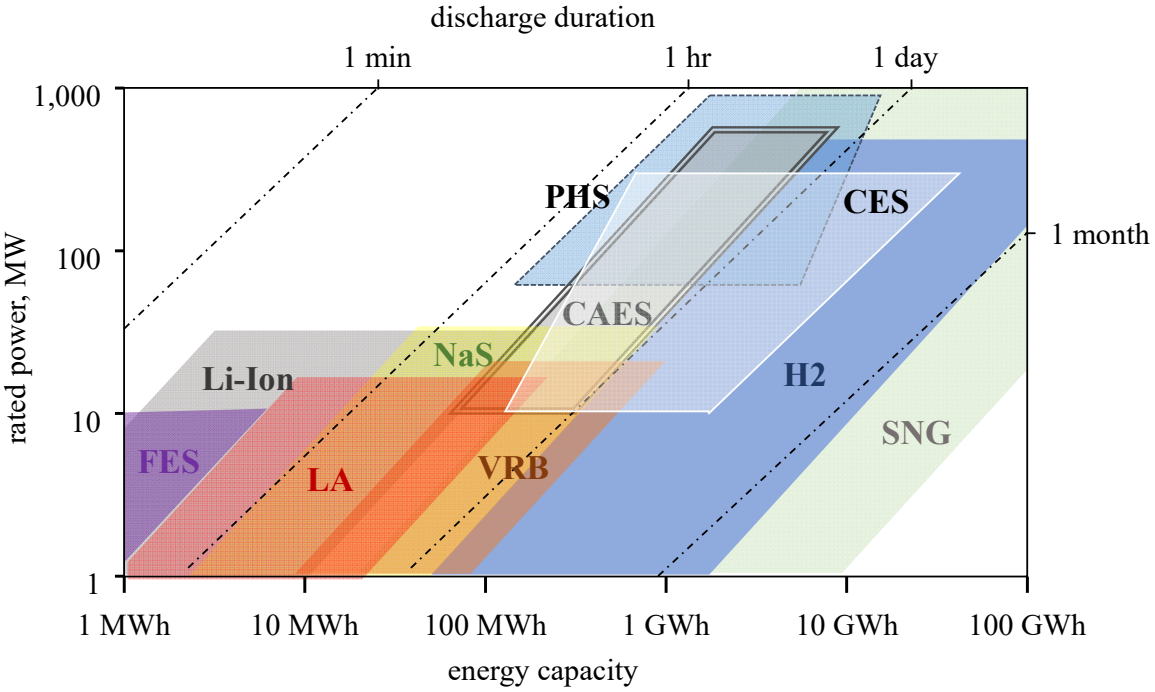

CES	cryogenic energy storage	Li-Ion	Li-Ion battery
CAES	compressed air energy storage	NaS	sodium sulphur battery
FES	flywheel energy storage	PHS	pumped hydro
H2	hydrogen storage	SNG	Synthetic natural gas
LA	lead acid battery	VRB	vanadium redox flow battery

Figure 2.5: Rated power, energy capacity and discharge duration of ES technologies [3] based on Guney and Tepe [69] and Yoon et al. [70].

Being anticipated to achieve hundreds of MW in power rating and energy capacities larger than 10 GWh, CES is categorized as grid-scale energy storage. As an alternative, energy storage can be classified according to the application [3]. Technologies with similar characteristics compete for the same services (or applications) that can be provided to various stakeholders in the power system (e.g., transmission or distribution system operators) [71]. The services an ES technology can provide are dependent on a number of characteristics. The power and energy capacity, as well as the response time, are of particular importance. In the following section, a comparison is drawn between the characteristics of CES and the characteristics of the competing technologies. Potential ES applications suitable for CES storage are assessed in section 2.5.

Being characterized by high power ratings and energy capacity along with response times of up to several minutes CES competes with other bulk ES technologies for *energy management* applications [7, 37, 72]. Cryogenics-based energy storage is in direct competition with other grid-scale ES technologies such as pumped hydro storage (PHS) and compressed-air energy storage (CAES), as well as selected battery-based and hydrogen-based ES technologies [3].

2.4.2. Characteristics and benchmarking

In order to identify suitable ES applications, it is necessary to evaluate the characteristics of the respective ES technology. In particular, the *rated power*, the *energy capacity*, the *RTE*, the *response time*, and the *discharge time* influence the technologies viability for various applications. The characteristics of CES and competing technologies are reviewed in this section. The gathered data are given in Table A.1 in Appendix A.

The capacity of the charge and the discharge unit of CES systems can be sized independently, contrary to other bulk ES technologies. The *power rating* of CES systems commonly refers to the installed capacity of the discharge unit. CES *power ratings* of 10 to 500+ MW are economically and ecologically difficult to achieve by hydrogen-based and battery-based energy storage [7, 16, 17, 29, 72]. The volume of the storage tank and the specific work output of the discharge unit determine the *energy capacity* of CES systems. Energy capacities larger than 25 GWh [39] are realizable with available industrial cryogen tanks, enabling storage losses below 0.2 $\%_{Vol}$ per day, and come at low associated costs (approximately 160 €/kW_{dis} [18]) [12, 16]. Selected characteristics of bulk-energy technologies (PHS, CAES, and CES) are compared on a weighted scale in Figure 2.6. Energy capacities of multiple hundreds of MWh and power ratings of 50-200 MW are expected to be achieved by CES systems in the near future [8].

One of the greatest advantages of CES systems is the high *volumetric energy density*. CES energy density may reach values of 90 Wh/l [18, 73], or even 160-200 Wh/l [10, 17, 37], while, other bulk energy storage technologies such as PHS (0.5-1.5 Wh/l) and CAES (3-6 Wh/l) reach by the order of two magnitudes smaller energy densities [8, 15, 16, 29, 37]. The high volumetric density enables CES "site-free" or site-independent storage. Only hydrogen-based energy storage achieves a higher volumetric energy density than cryogens, regardless of the storage form [74]. The storage of hydrogen, however, entails potential safety hazards due to extreme flammability at high pressures [29, 74]. Liquid air can be stored with low technical requirements at ambient pressure [3].

For a daily cycling CES system, the start-up of the liquefaction process takes up to 20 minutes. While ramp up after a day at standby may take one hour [18]. The *response time* of the discharge

unit of the pilot plant of fewer than 150 seconds was reported by Alyami and Williams [75]. For comparison, CAES systems take 10-15 minutes to start operation [76].

The *discharge duration* is solely limited by the charge-to-discharge ratio and the storage tank size and may be adjusted according to the aimed application of the storage. The charge-to-discharge ratio of CES systems is usually anticipated between two and seven [18, 31, 77]. Several minutes to days [7], and even longer discharge durations e.g. seasonable storage are technically realizable. The standing losses of CES systems are rather low and are comparable to that of battery-based ES technologies [18]. A discharge duration of multiple hours at daily operation is most commonly reported [7, 11, 37]. Regarding the response time of the charging process (< 20 min [18]), charging time should exceed 2-4 hours.

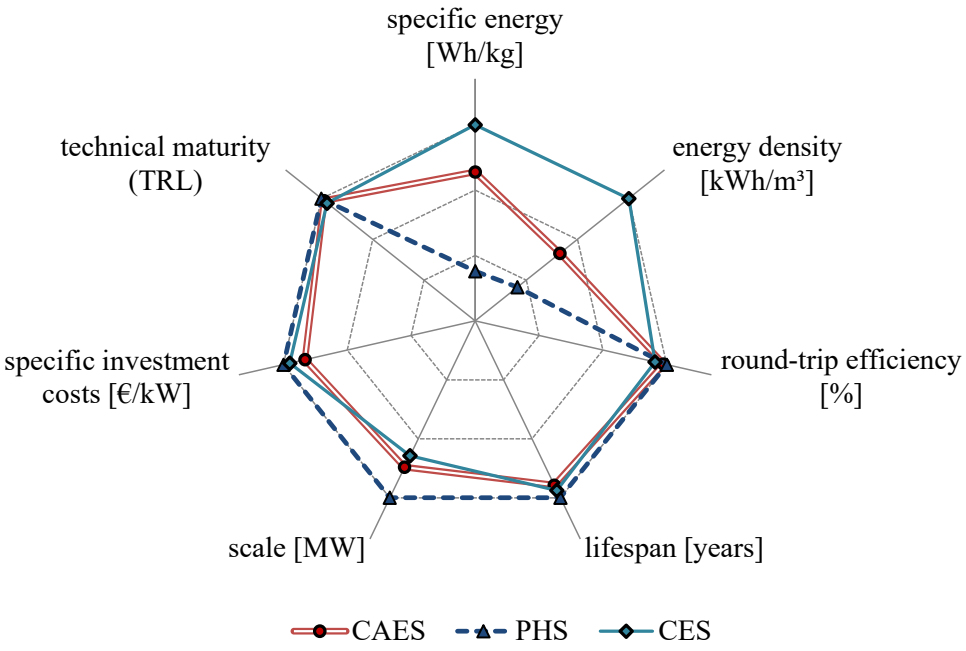

Figure 2.6: Comparison of weighted characteristics of CES, CAES, and PHS [36] adopted from [68], based on data extracted from literature (see Table A.1).

The *roundtrip efficiency* of stand-alone CES is reported to reach 40-50 % [37, 38]. The specific power output of the discharge unit can be increased by the recovery of waste heat e.g., from industrial processes [10, 16]. The *RTE* may reach values of up to 55 % with the integration of waste heat [12]. The integration of "waste cold" (low-temperature exergy) provided by e.g., re-gasifying LNG can also increase the *RTE* of CES systems. The significant reduction in the energy demand for liquefaction process may increase the *RTE* of CES systems to 63-70 % according to [8, 62, 63]. The integration of CES systems with external heat/cold sources is discussed in section 2.3 and section 4.4.

PHS has currently the highest installed energy storage capacity globally. As a mature technology, the *RTE*s typically range from 70 to 85 % [33, 78, 79, 80]. The performance of CAES systems depend on the respective system configuration. CAES systems in operation achieve *RTE*s of 40-54 % [33] and are expected to increase to 60 % [76, 81]. Adiabatic CAES systems with heat storage as well as isothermal small-scale CAES systems are expected to reach

*RTE*s of 70 % and higher [33]. These efficiencies are only approachable for CES systems with the integration of waste cold or a combustion process.

Cryogens (liquid air and nitrogen) were compared to hydrogen as an energy carrier and storage media by Ding et al. [74]. The *RTE*s of both ES technologies were found comparable, while CES was evaluated and regarded to be more environmentally friendly. A number of charging and discharging technologies are possible for hydrogen-based ES. For the generation of hydrogen, water electrolysis is the most common process, reaching efficiencies of up to 70 %. The discharge process e.g. fuel cells reaches an efficiency of 40-70 %. Hence, hydrogen-based ES reach *RTE*s as low as 30-50 % [74, 82].

The *RTE* of CES systems does not decrease during the lifecycle, unlike battery-based ES. The *lifetime* of CES system components is expected to be more than 25 years and up to 60 years [29, 37, 38], which is multiple times higher than for the components of batteries or hydrogen-based ES systems (5-15 years [37], < 30 years [83, 84]) [29, 82]. In contrast to a limited cycle life of batteries, the cycle frequency has little effect on CES system performance. The low-temperature energy supplied by the cold storage is limited, which is why the cold storage performance limits the "depth of discharge" of CES systems. The performance of industrial air liquefaction plants strongly increases with the size (installed capacity) [74]. Hence, the scale of the CES system also determines the achievable *RTE* [3].

Due to the low *RTE*, the *specific investment cost* of CES is of great importance to CES applicability, section 2.5.1, in particular, due to the rather low *RTE*. The specific capital cost (per kW of installed capacity) for CES systems reported in the literature vary strongly, Figure 2.7. CES technologies specific costs reduce with size, according to the "economy of scale", Figure 2.8. The specific costs of CES are expected to decrease by 24.2 % when the power capacity is doubled [32]. The large variation in the considered CES power capacity may justify the large cost range reported in the literature [3].

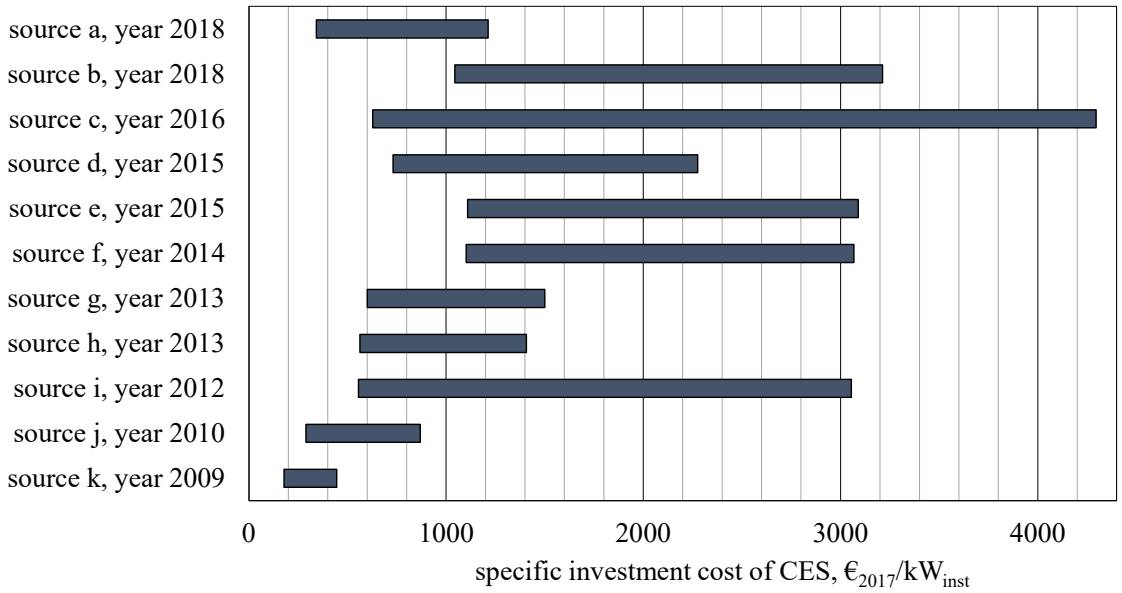

Figure 2.7: CES specific cost per kW installed capacity reported in literature (a: [85], b: [64], c: [33], d: [72], e: [16], f: [18], g: [15], h: [8], i: [32], j: [38] and k: [37]).

High capital investment costs also characterize competing technologies: Compressed air energy storage has a capital cost per kW installed of 500 €/kW to 2,200 €/kW [33]. The investment cost for PHS can be lower, about 350 to 1,500 €/kW [33], but may reach values up to 4,300 €/kW [86] depending on the site. In the industrialized countries, economically feasible sites for PHS are widely diminished. The specific capital cost of CES systems is reported to reach 500-2,400 €/kW and be comparable with CAES, PHS, and flow batteries [29]. When CES technology reaches maturity, costs are expected to decrease further [3].

Hydrogen-based ES lower investment cost limit is approximately 2,000 €/kW, accounting 520 €/kW for hydrogen storage in salt caverns, 500 €/kW for the electrolyzer, and 920 €/kW or 1500 €/kW for polymer electrolyte membrane fuel cells (PEMS) or solid oxide fuel cell (SOFC), respectively. The specific investment costs of hydrogen are thus significantly higher than that of CES, as well as other bulk energy storage technologies CAES, and PHS [87].

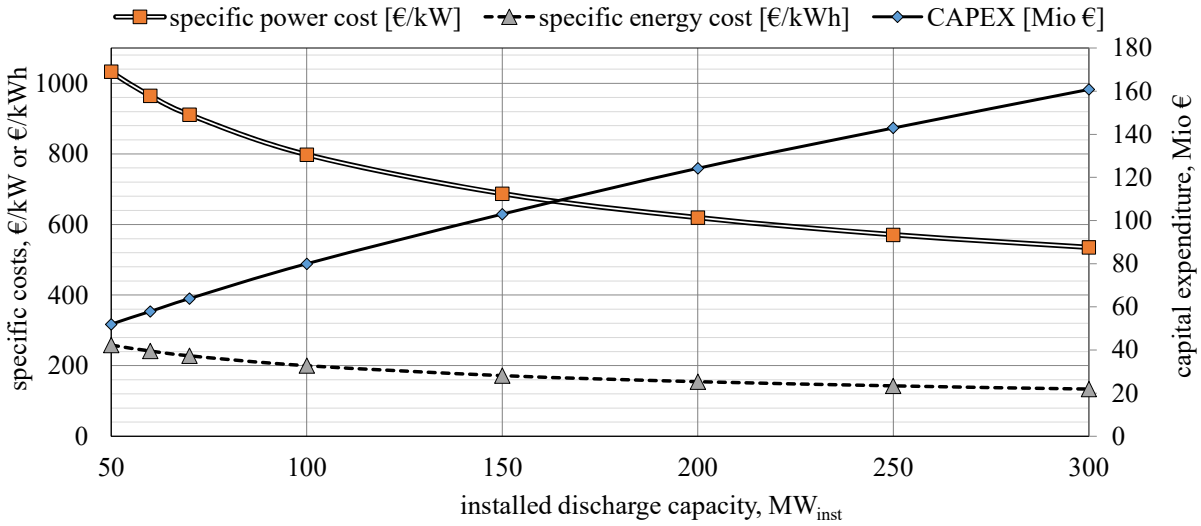

Figure 2.8: Capital expenditure (CAPEX), specific costs (per unit of power and unit of energy stored) over CES system capacity based on cost estimations published by Highview Ltd. [88].

Another base for the comparison of ES technologies can be the specific *cost of storage* (per kWh of installed energy capacity). In particular, battery-based ES technologies are commonly compared based on the specific capital *cost of storage*. Yet, for grid-scale ES technologies, the comparison based on the cost per unit of installed energy capacity can be misleading due to the dissimilar specific cost of the storage unit. Large-scale reservoirs necessary for PHS and CAES make up for a significant share of the overall investment costs, whereas, cryogenic tanks have low specific costs in comparison to other CES equipment. The values reported for PHS for example range from 5-100 €/kWh [37], 250-430 €/kWh [86] or 10-20 €/kWh [83] according to different sources, Table A.1.

The construction lead-time of CES projects is expected to be only one or two years, which is vastly faster than for CAES and PHS projects (5-10 years) [15, 76]. Fast commissioning paired with an extensive economic life (25-60 years [20, 29, 37, 38]) is in favor of CES economic performance.

The *environmental impact* of ES technologies is as well regarded as an important decision criterion. The major negative impacts of ES technologies are, e.g. the occupation of large areas for PHS [37], the use of scarce and toxic chemical materials in batteries [72], the air pollution by exhaust gases of diabatic CAES. In adiabatic CES systems, no chemical reactions take place. Thus, CES is often classified as "low-carbon" or environmentally friendly technology [45]. The recovery of energy that else would have been vented to the environment as well as the gas cleaning process in CES systems can be viewed as a positive environmental impact [74].

The site-independent installation of the systems frees CES projects of geological risks that occur in PHS and CAES projects. Also, the high-pressure storage of hydrogen imposes *potential safety hazards* [45]. High-pressure CAES systems in cavities face challenges, e.g., uplift failure [89] or gas enrichment and ignition of residual hydrocarbons [90]. The storage of cryogens implies fewer safety issues. CES implies common health hazards alike in cryogenic ASUs or power plants, which may be avoided by protective measures, e.g., clothing and equipment [18, 91].

2.5. Potential application and economic benefit

2.5.1. Applications suitable for CES systems

Energy storage systems are capable of supplying both positive (supply-side) and negative (consumption-side) control power to the grid. Therefore, ES technologies have a broad range of applications. ES applications can be classified according to multiple criteria. In Figure 2.9 the classification according to the capacity and discharge duration of ES systems is given. Three types of applications can be differentiated: *uninterruptible power supply* (UPS), *grid support*, and *energy management* applications.

- To provide *power quality applications* or *UPS*, the ES system needs to be capable to supply one-fourth of its power capacity (less than 1 MW) within milliseconds.
- To ensure *grid support*, which is also referred to as *bridging power* or *ride-through capability*, the rated power is required to exceed 100 kW and the response time of the storage system may be up to one second.
- For *energy management* application a slower response of several minutes is acceptable but capacities above 100 MW are necessary [3, 72].

Due to the slow start-up time, CES systems are not suitable to supply *UPS* or *ride-through capability* applications. *Energy management* is, therefore, the only category of applications, which is suitable for CES systems [7, 37].

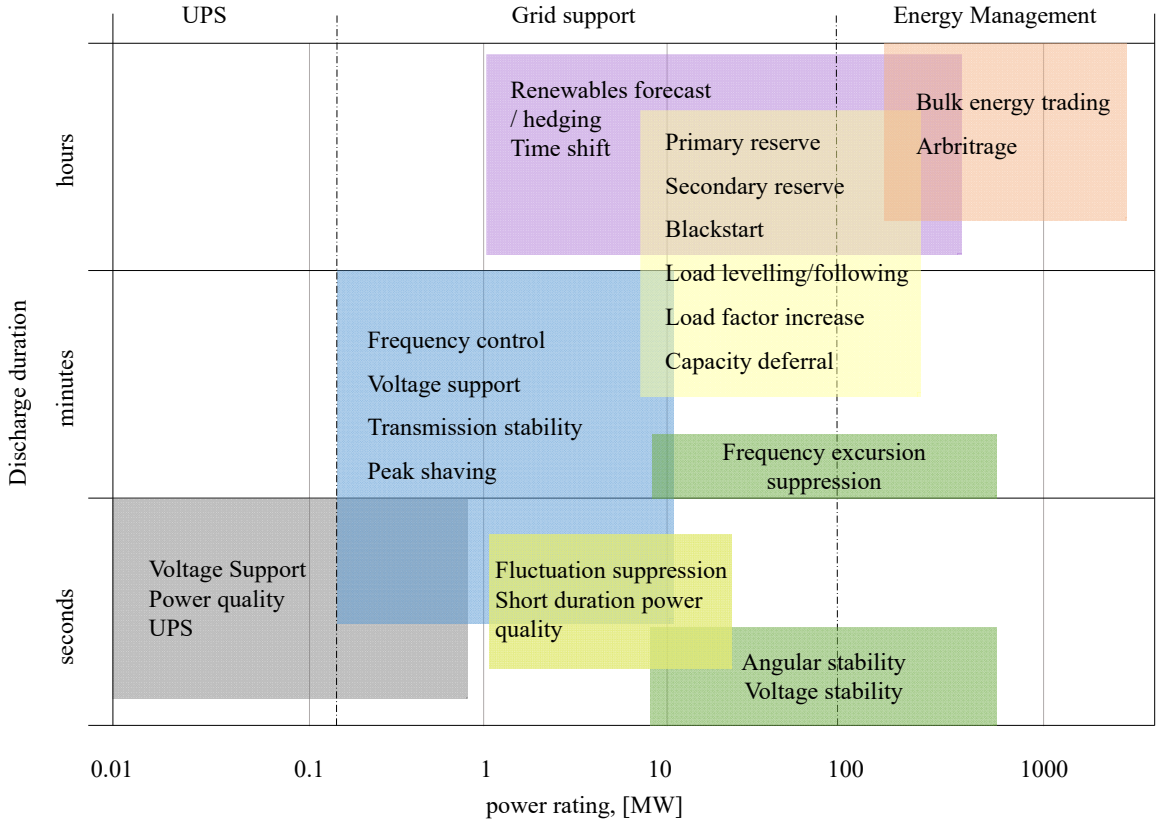

Figure 2.9: Discharge period and power rating of various energy storage applications [3] based on [72, 92, 93, 94].

The characteristics of the selected ES applications suitable for CES are given in Table A.2 through Table A.5 in Appendix A. *Bulk energy applications*, selected *ancillary services*, *transmission and distribution support* as well as facilitating the *integration of renewable energy (RE) sources* are among the energy management applications relevant for CES.

Bulk energy application refers to the applications that make use of the electricity price difference (trading) by electricity time shifting between the low-priced electricity charged and the discharge during high-price hours [95]. Both *peak shaving* and *energy arbitrage* are bulk energy applications suitable for the response time of CES systems (> 100 seconds). *Peak shaving* is commonly installed at the consumer end, whereas*, energy arbitrage* rather takes place at the supply side. The principle of *energy arbitrage* application is characterized by the economic benefit of electricity time shifting [3]. The main goal of *peak shaving* is to supply energy during peak load hours by leveling out the typical fluctuation of the demand curve [78]. Peak shaving thereby does not have a primary economic target but improves the outlay of the overall power system by reducing the required nominal installed capacity [92].

Ancillary services, also referred to as "grid operational support", enable the maintenance of the power reliability and quality by facilitating the smooth operation of the power grid as well as reducing efficiency losses [93]. CES has the potential to supply; *reserve generating capacity, load following, tertiary frequency regulation,* and *black start* [3].

The presence of *reserve generating capacity* in the power system is indispensable to compensate for sudden changes in the load curve or loss of operating generators. Reserve generating capacity accounts as installed capacity but is not used in normal operation [92]. For reserve generating capacity; "spinning" reserves – immediately accessible, and "non-spinning" reserves – available within 10-30 minutes [96] are differentiated. Only the non-spinning reserve application is suitable for CES systems. For non-spinning reserve application, the CES systems must enable discharge periods larger than one hour in order to bridge the power generation until the nominal output is reinitiated, e.g. ,by the backup power system [3, 92].

Load following assists in the maintenance of the real-time balance between electricity supply and demand, also called *regulation control*. Preventing a supply-demand mismatch at all times brings along noteworthy technical and economic benefits [93]. The capability of load follow was a key finding of the first integrated CES pilot plant [16].

The frequency of the power grid is required to be continually preserved within the tolerated limit (e.g., 0.1 Hz or 0.2 Hz, North or Middle Europe [92]). ES systems can operate as frequency regulators by amending any deviation and keep the frequency within the regulatory range of operation [71]. CES is appropriate for tertiary frequency control application [3], which is manually controlled by the system operator within 15 minutes (or hours) subsequent to a frequency disruptive incident [71, 92].

When power is injected to a power system that suffered a blackout, it is referred to as *black start capacity*. Black start capacity facilitates the start-up of large power plants or re-energizes the distribution lines [96]. CES response time and capacity range are suitable to provide this application, yet the storage unit is required to be capable to start operation autonomously. During the discharge process of CES systems, pumping power is required before electricity can be discharged. To provide black start capacity, CES systems need to be extended, e.g., with battery storage [3, 92].

The integration of highly fluctuating RE generation to the grid is associated with technical issues such as frequency and voltage irregularities [1]. The successful integration of intermittent electricity generation from RE sources embodies the greatest potential of ES systems [95]. The application of ES in firming, shifting, and smoothing the electricity generation from RE sources may enable a higher share of RE generators in the power system without endangering the supply security [96]. *Renewable energy capacity firming* application, in essence, aims to smooth both the voltage and the power output of RE generators. This increases the capacity credit of the overall power system, which allows a higher penetration of RE generators and avoids the cost of additional backup power [92, 95]. [3]

The delay and at times entire avoidance of investment in upgrades of the transmission and distribution system is referred to as *transmission and distribution (T&D) support* [97]. Such upgrades include, e.g., congestion relief, infrastructural upgrades, and avoided load-shedding due to access generation that cannot be incorporated by the infrastructure of the T&D system [3, 93].

To ensure a secure and reliable power system operation, *congestion management* is of great importance [71]. T&D capacity extensions are widely unable to keep pace with the rapid increase in peak demand. By either lowering the peak demand or excess electricity generation, ES systems facilitate the reduction, postponing or even waiving of congestion-related costs, e.g., additional transmission capacity (*transmission curtailment* or *upgrade deferral*) [96, 97]. Moreover, this application prevents congested transmission lines and substations and avoids the undesirable shut down of excess RE generation [78]. In *congestion management* application, the ES unit is required to enable a discharge duration of multiple hours. CAES has been identified to be compatible with *congestion management* application. CES is expected to be suitable as well, as the systems operate very similarly [3, 78].

The objective of *load shifting* application is the avoidance of a number of technical operation problems of the T&D system that occur in case of a demand-supply mismatch and entail economic drawbacks [1]. In operation, this application is very similar to *peak shaving*, *energy arbitrage,* and *renewable time shift*. The key difference is that the services are provided to different stakeholders. Thus, the economic value of similar applications vary, and must be distinguished [3].

2.5.2. Economic benefits and value propositions

The applications that CES may potentially supply have diverse monetary compensations. The monetary compensation for providing a specific service is referred to as “benefit” or “value proposition”. The benefit of a particular application is either determined by the market rate (e.g., ancillary service or electricity market clearing price) or the cost of the alternative solution (e.g., grid extension). The economic benefits presented in this section are based on the US (and Canada) market due to the availability of data [3].

In Figure 2.10, the potential “life cycle” value propositions of multiple applications is shown with the corresponding discharge duration. The life cycle value proposition of the services that a specific ES system can provide is the key driver for investment in the technology, system or project [97]. The applications within the discharge time range of CES (2-6 hours) enable the highest potential economic benefit.

The specific value proposition (in €/kW) of the applications suitable for CES are given in Table A.7 in Appendix A [3]. The potential value and the value propositions are calculated over an ES lifetime of 10 years. Various services are traded in markets and are acknowledged as products, whereas the monetary value of other applications is harder to assess. Therefore, the value propositions in the literature vary [98], Table A.7. The largest uncertainty in the value proposition is associated with transmission curtailment and distribution upgrade deferral. Reason for this is that the monetary value of the application is determined by the avoided investment and may reach values of up to 1000 €/kW. Reserve capacity reaches a rather low value proposition of less than 200 €/kW. RE integration (time shift and capacity firming), as well as peak shaving and energy arbitrage, are more consistent and economically viable applications for CES.

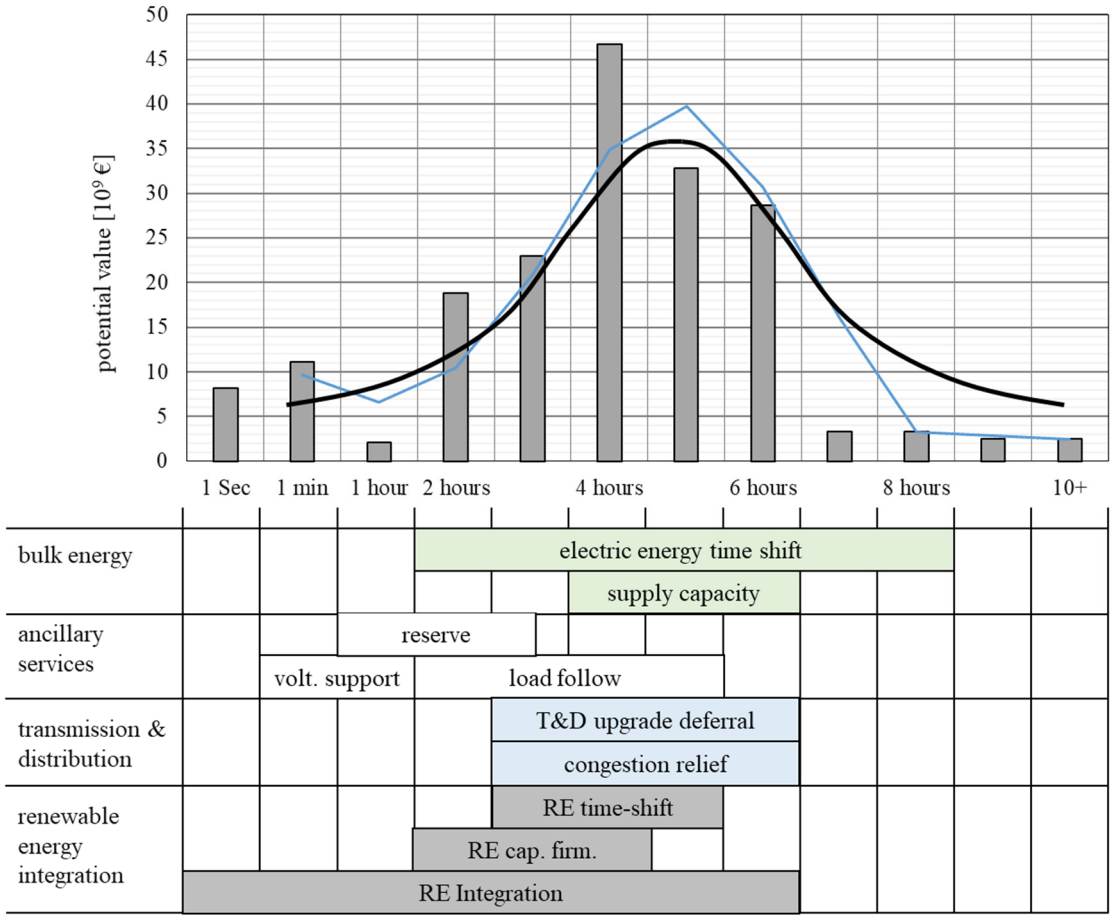

Figure 2.10: "Life cycle" value proposition of ES applications for various discharge durations [3] adapted from [99] based on [97].

The investment in an ES system is only favorable if the value proposition of the potential applications exceeds the cost associated with the ES system by a significant margin. In order to maximize the market value of an ES technology, a number of services that can be provided simultaneously or successively are to be identified. The aim of increasing the value proposition

of an ES by bundling multiple applications is referred to as “benefit aggregation” or “value stacking” [100, 101].

The compatibility of different ES applications is shown in Figure A.2 in Appendix A. CES potentially low specific cost per unit of energy and high energy density make the technology most suitable for energy applications. *Frequent* energy applications, e.g., supply capacity, RE time shift or energy arbitrage, as well as *infrequent* energy applications such as T&D support, are easily coupled with other applications. For stacking benefits, the main application is referred to as the “anchor service” (or “anchor application”). The primary service should have a value proposition at least as high as 25-50 % of the costs associated with the ES [102]. Potential anchor and secondary services suitable for CES are shown in Figure 2.11 [3].

When an ES supplies a specific service, e.g., with positive reactive power, for an extended amount of time, not sufficient ES capacity is available for further discharge to supply another application. ES applications that require unlimited availability of the storage capacity for sudden discharge, e.g., spinning reserve and black start, are, therefore, hard to combine with other applications. While a number of other services can easily be provided simultaneously. To evaluate the compatibility of different ES applications energy system modeling is necessary to account for the time series and state of charge required for different applications [3]. Moreover, the combination of potentially appropriate applications is required to be modeled to identify the stacked value proposition [103].

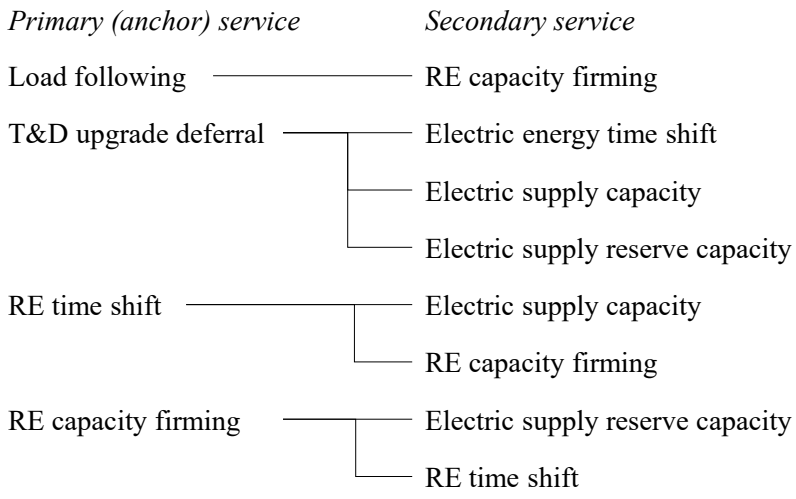

Figure 2.11: Potential primary (“anchor”) and secondary services of CES [3] based on reviewed literature [37, 72, 78, 84, 92, 93, 102, 103, 104, 105]

The value propositions (Table A.7) are not additive. The aggregation of benefits is difficult as there is not sufficient experience with *value stacking* [3]. There are various reasons for *benefit aggregation* not being common practice: technical and operational conflicts, the lack of engineering standards and regulatory framework, unproven and new technology, weak or missing price signals, and multiple stakeholders that must to be coordinated [3, 97].

Disregarding the still unfavorable market situation, potential value ranges for stacked value propositions of selected ES applications are approximated and shown in Figure 2.12 based on

Table A.7 in the Appendix A. To determine the exact stacked value proposition an energy system model is necessary [103]. As compatible applications have nearly additive stacked value, Figure 2.12 shows the additive value propositions for selected CES applications.

With the exception of renewable energy time shifting application combined with either peak shaving or energy arbitrage, the additive value of the value propositions of most of the potential anchor and secondary services for CES systems are higher than 1,000 €/kW reaching values of up to 1,600 €/kW.

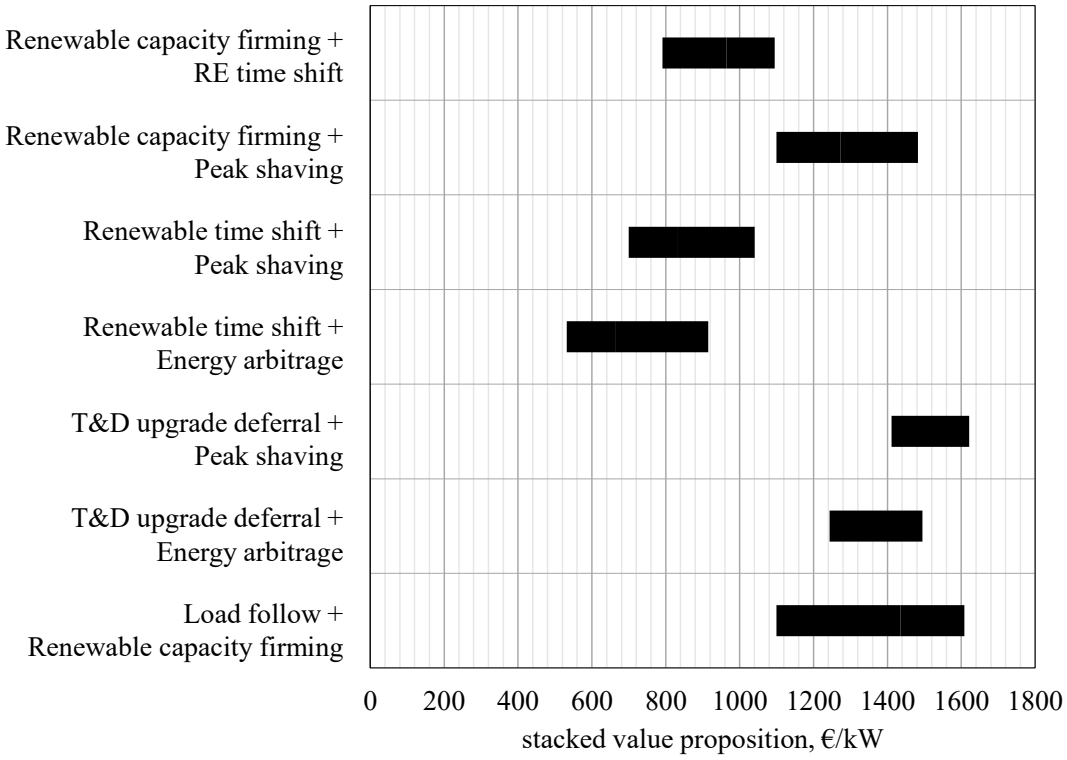

Figure 2.12: Value proposition for stacked benefits suitable for CES based on data presented in reviewed literature [97, 106, 107, 108, 109]

The application-specific value propositions indicate that CES costs should be lower than the potential stacked value proposition. When reducing CES costs below the equivalent of 1,000 €/kW (10 years), CES could cover its investment by providing the proposed services. The limiting factors to CES economic viability is thus, not only the comparatively low *RTE* and the long response time but also the relatively high specific costs.

2.6. Summary of the literature review

Cryogenic energy storage is a thermal bulk-electricity storage technology that has attracted great interest in research and application since the installation of the first integrated pilot-scale plant in 2011. CES is composed of mature components with well-known application in power generation, industrial gases, and LNG value chain. Thus rapid commercialization of CES is expected.

The *thermodynamic performance* of CES systems has been subject to many publications in the past three years; an optimal CES system configuration could not be derived. The charging process of CES is an inverse thermodynamic cycle in which a gas, e.g., air, is liquefied. A number of *air liquefaction processes* are in commercial operation, and different liquefaction processes have been considered for implementation in CES systems. Despite, the cold storage being the key component of the charging system, the impact of cold storage integration on the selection and performance of the liquefaction process has not been subject to thorough analysis.

The *cold storage design* and in particular safe and low-cost storage material that allows high energy recovery is subject to several research projects, especially in joint research with industry. For the overall system, only the low-temperature exergy recovered, and the costs of the cold storage are of relevance. For the *discharge process*, thus far, only the direct expansion method – a liquid air Rankine cycle has been considered for CES systems in literature and application. Alternatives of using a secondary working fluid or combined methods are possible, similar to the low-temperature exergy recovery from re-gasifying LNG.

The *integration of external heat sources and sinks* (e.g., industrial waste heat, low-temperature exergy from re-gasifying LNG or combustion) into CES systems was frequently suggested, but no comparative analysis quantifying and comparing the effect on CES thermodynamic and economic performance was presented.

Due to its high power ratings and energy capacities (> 100 MW/10 GWh), CES is suitable for energy management applications and primarily competes with compressed air energy storage (CAES), pumped hydro storage (PHS) and hydrogen-based ES. CES most significant advantages are its high volumetric energy density, site-free storage, low storage losses, and long lifetime. The specific investment costs of CES are comparable with PHS and CAES (500 – 2,400 €/kW) but are high concerning the rather low *RTE* of only 40-60 %. The slow response time of CES limits its application to energy arbitrage and peak shaving, selected ancillary and T&D support services. A single application cannot cover CES projected investment costs. Providing the proposed combined applications, e.g., load follow and RE capacity firming or T&D upgrade deferral and peak shaving, a revenue of up to 1,600 €/kW can be returned over 10 years.

Chapter 3: Methodology

This section aims to introduce the methods applied to achieve the objectives presented in *Chapter 1*. Different CES system configurations have been evaluated and enhanced in the present work. The design and simulation of the analyzed systems are discussed in *Chapter 4*. The methods applied for evaluation are energetic and exergetic analysis, economic analysis, exergoeconomic analysis, and optimization.

3.1. Energetic analysis

For energetic analysis, the *principle of energy and mass conservation* is applied. For an open system (control-volume), the global mass and energy balance are given in equation (3.1) and (3.2). Only stationary processes are evaluated, and the changes in kinetic and potential energy of the system are neglected.

$$\sum \dot{m}_{in,i} = \sum \dot{m}_{out,j} \tag{3.1}$$

$$0 = \dot{Q} + \dot{W} + \sum \dot{m}_{in,i} \cdot h_{in,i} - \sum \dot{m}_{out,j} \cdot h_{out,j} \tag{3.2}$$

The net rate of energy transported by mass (enthalpy flowrates) over the system boundaries is equivalent to the net rate at which energy is transferred by heat transfer $\dot{Q}$ and by power $\dot{W}$ [110]. For the air liquefaction process in CES systems, the liquid yield γ is a measure of performance [48]. The liquid yield refers to the ratio of the mass flow that is liquefied $\dot{m}_{liquid\ air}$ relative to the mass flow entering the high-pressure compressor in the liquefaction unit $\dot{m}_{CM}$.

$$\dot{m}_{CM} = \underbrace{\dot{m}_{liquid\ air}}_{\gamma \cdot \dot{m}_{CM}} + \underbrace{\dot{m}_{gaseous\ air}}_{(1-\gamma) \cdot \dot{m}_{CM}} \tag{3.3}$$

$$\gamma = \frac{\dot{m}_{liquid\ air}}{\dot{m}_{CM}} \tag{3.4}$$

The overall performance of an energy conversion system is defined by the ratio of the positive effect (in terms of energy, $\dot{W}$ or $\dot{Q}$) over the driving energy. For simple electricity storage, both the positive effect and the driving energy are electricity. In more complex ES configurations, the supplied fuel or thermal energy needs to be accounted as part of the driving energy. In Table B.1 in Appendix B, the energetic efficiencies are defined for the different CES systems evaluated in this work.

The overall performance of an energy (electricity) storage system can be evaluated with its roundtrip efficiency (*RTE)*. The *RTE* is defined as the ratio between the electricity charged to the system and the electricity discharged by the system:

$$RTE = \frac{\dot{W}_{dis}}{\dot{W}_{char} \cdot {}^{\tau_{char}}/_{\tau_{dis}}} \tag{3.5}$$

The charging duration τ_{char} and the discharge duration τ_{dis} need to be accounted for as the charge-to-discharge ratio (${}^{\tau_{char}}/_{\tau_{dis}}$) may be unequal to one.

3.2. Exergetic analysis

Exergy is a measurement for the quantity and quality or "true thermodynamic value" of *energy* [111, 112]. Exergy is defined as the maximum useful work that would theoretically be obtained when a given thermodynamic system would be brought into complete thermodynamic equilibrium with the environment with sole interaction with the environment [113]. Maximum theoretical useful work is, for example, shaft work or electrical work, while the heat has a lower exergy content. When comparing systems operating at different temperatures and integrating different energy sources (e.g., fuel, heat or low-temperature energy), *exergy* is of greater economic value as well as the best ground for analysis, optimization, and comparison of energy conversion systems [112].

The total exergy of a system consists of four components when magnetic, nuclear, surface tension, and electrical effects are absent or negligible. The overall exergy of a system E_{sys} can be described as the sum of the chemical exergy E^{CH}, the physical exergy E^{PH}_{sys}, the potential exergy E^{PT}, and the kinetic exergy E^{KN}.

$$E_{sys} = E^{CH} + E^{PH}_{sys} + E^{PT} + E^{KN} \tag{3.6}$$

The specific exergy on a mass basis is expressed with a lower case e:

$$e_{sys} = E_{sys}/m_{sys} = e^{CH} + e^{PH}_{sys} + e^{PT} + e^{KN} \tag{3.7}$$

The assumption of the system being at rest in relation to the environment ($e^{PT} = e^{KN} = 0$) is applicable for many engineering applications [112]. In this work, the changes in kinetic and potential exergy are not considered.

The physical exergy of a system or stream is defined by the systems deviation to the *restricted dead state*, when the temperature and pressure are equivalent to those of the environment ($T = T_0, p = p_0$). At a given state j, the specific physical exergy can be expressed by:

$$e^{PH}_j = \left(h_j - h_0\right) - T_0 \cdot \left(s_j - s_0\right) \tag{3.8}$$

Where h, T, and s denote, respectively, the enthalpy, temperature and entropy of the system. The subscript 0 denotes the properties when the system is at the restricted dead state [112].

The physical exergy of a material stream can further be split into the thermal exergy e^T(its temperature related part) and the mechanical exergy e^M(its pressure related part) [112]:

$$e_j^{PH} = \underbrace{\left[\left(h_j - h_{j,A}\right) - T_0 \cdot \left(s_j - s_{j,A}\right)\right]_{p=const}}_{e^T} + \underbrace{\left[\left(h_{j,A} - h_0\right) - T_0 \cdot \left(s_{j,A} - s_0\right)\right]_{T=const}}_{e^M} \tag{3.9}$$

Thermal and mechanical exergies are calculated through consideration of an additional stream at state A. State A has the same pressure as the j-th material stream but ambient temperature T_0 [114]. As systems analyzed in this work partially operate below (or crossing) the temperature of the environment, a distinction between pressure related and temperature related physical exergy becomes valuable.

The chemical exergy is defined by the deviation of the chemical composition of the material stream or system from that of the thermodynamic environment [113]. In other words, the chemical exergy is the maximum useful work that can be obtained when a system that is already at thermal equilibrium ($T = T_0, p = p_0$) is brought into chemical equilibrium with the environment [111]. The chemical composition of the thermodynamic environment needs to be defined (exergy-reference environment) [112]. The chemical exergies in this work are based on Szargut's standard model for chemical exergies [115].

The exergetic analysis applied in this work is based on Bejan et al. [112] and follows the "fuel and product" approach. Exergetic analysis aims to identify the cause, the magnitude and the location of thermodynamic inefficiencies in a thermodynamic system [111]. In contrast to energy analysis, exergy is not conserved but can be destroyed [112]. *Exergy destruction* refers to the true thermodynamic inefficiency that occurs within a system due to irreversibilities [111].

Under steady-state condition ($dE_{cv}/dt = 0$), the exergy balance for a controlled volume (open system) is expressed as:

$$0 = \sum \dot{E}_{q,j} + \dot{W}_{cv} + \sum \dot{m}_{in} \cdot e_{in} - \sum \dot{m}_{out} \cdot e_{out} - \dot{E}_D \tag{3.10}$$

The rate at which exergy is destroyed in the system (or controlled volume) $\dot{E}_D$ due to irreversibilities is the difference between the rate at which exergy is transferred into and the rate at which exergy is transferred out of the system. Exergy can be transferred over the system boundaries by matter, heat $\dot{E}_{q,j}$ or work $\dot{W}_{cv}$ (other than flow work) [112]. The exergy associated with heat transfer is given by

$$\dot{E}_{q,a} = (1 - T_0/T_a) \cdot \dot{Q}_a \tag{3.11}$$

The temperature T_a is the thermodynamic average temperature at which the heat is supplied. The exergy transfer rate associated with the heat transfer ($\dot{E}_{\mathrm{q,a}}/\dot{Q}_{\mathrm{a}}$) is displayed as a function of the temperature difference $T_a - T_0$ in Figure 3.1.

At the same temperature difference to ambient temperature $|T_a - T_0|$, the exergy transfer rate associated with the heat transfer ($\dot{E}_{\mathrm{q,a}}/\dot{Q}_{\mathrm{a}}$) is higher at a thermodynamic mean temperature below the environmental temperature ($T_a < T_0$) than above the environment ($T_a > T_0$). Hence, the exergy content of thermal energy stored below the ambient temperature is higher than above the environmental temperature at the same ΔT.

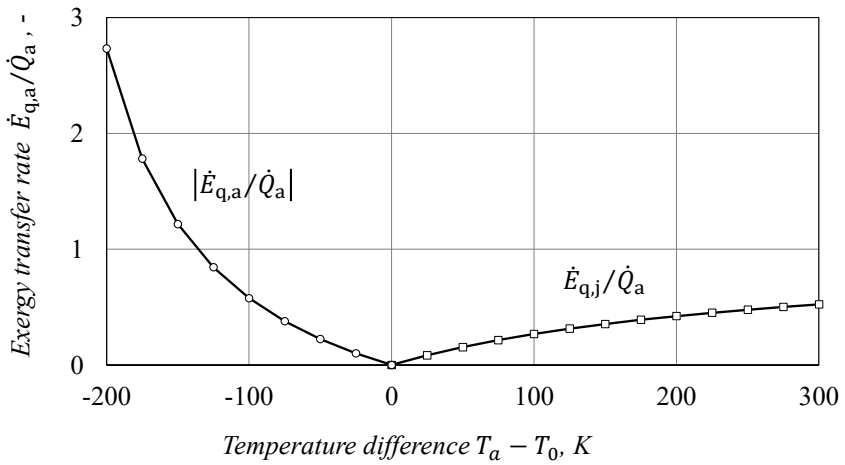

Figure 3.1: The exergy transfer rate associated with the heat transfer ($\dot{E}_{q,a}/\dot{Q}_a$) over the temperature difference $T_a - T_0$, based on [112] adopted from [39]

The thermodynamic performance of any given energy conversion system or system component can be evaluated with the exergetic efficiency ε. The definition of the exergetic efficiency ε necessitates the definition of the *fuel* (expended resources) and the *product* (the desired effect) of the respective system (or component) expressed in terms of exergy [112].

$$\varepsilon = \frac{\dot{E}_P}{\dot{E}_F} \tag{3.12}$$

The overall performance of the CES system is evaluated with the *RTE*, the energetic efficiency η and the exergetic efficiency ε, in order to assess values given for the CES efficiency in the literature. The definition of ε_{tot} of the analyzed systems are given in Table B.1. The definitions for the exergetic efficiency on the component level can be derived from Table B.3.

The summation of the exergy destruction $\dot{E}_D$, the exergy of the product $\dot{E}_P$ and the exergy loss $\dot{E}_L$ amount to the exergy of fuel $\dot{E}_F$ of the system. The definition of fuel and product is further discussed in section 3.4 and definitions on the component level are given in Table B.2 to Table B.3 in Appendix B.

$$\dot{E}_F = \dot{E}_P + \dot{E}_D + \dot{E}_L \tag{3.13}$$

The exergy loss $\dot{E}_L$ refers to the exergy transfer to the environment [111, 112]. For exergetic analysis on the component level, the component boundaries are set to environmental conditions, the exergy loss $\dot{E}_{L,k}$ of the k-th component thus amounts to zero. To identify the components with greater significance to the overall system enhancement, the exergy destruction ratio $\gamma_{D,k}$ and the exergy destruction rate $\gamma^*_{D,k}$can be calculated.

$$\gamma_{D,k} = \frac{\dot{E}_{D,k}}{\dot{E}_{F,sys}} \tag{3.14}$$

$$\gamma^*_{D,k} = \frac{\dot{E}_{D,k}}{\dot{E}_{D,sys}} \tag{3.15}$$

3.3. Economic analysis

The economic analysis of an energy conversion system in the design phase serves three main purposes: the evaluation and improvement of the overall project profitability, the evaluation of various design options and the optimization of the system parameters [116].

The economic analysis presented in this work was performed according to the Total Revenue Requirement (TRR) method [111, 112]. The TRR method originated from procedures adopted by the Electric Power Research Institute [117]. For the cost evaluation and optimization of an energy conversion system the levelized annual values for the capital expenditures, the fuel costs and the operation and maintenance need to be computed and compared.

The TRR method consists of three main steps:

- the estimation of the total capital investment (section 3.3.1),
- the determination of parameters necessary for the detailed cost calculation (section 3.3.2),
- the calculation of the total revenue required and the levelized cost of the final product (section 3.3.3).

An additional step is necessary to provide the input value to exergoeconomic analysis, the calculation of the component cost rates (section 3.3.5). In order to evaluate and compare the results gained in economic analysis, the parameters set in section 3.3.3 are varied in sensitivity analysis to determine the cost range of the levelized cost of the final product (section 3.3.4).

3.3.1. Cost estimation

For the estimation of the total capital investment, the system design, parameters, and components need to be known first. With the help of the system design parameters, the *bare module costs* (*BMC)* of the components can be estimated.

Estimation of bare module costs can be based on the following options: vendors quotations, past purchase orders, cost estimating charts, or cost estimating equations. The optimal estimate of BMC can be acquired through quotations from vendors [111, 112]. As cryogenics-based energy storage is composed of mature components with well-known industrial-scale applications in the LNG, industrial gas and power sector [15, 16, 17, 18], several sources can be accessed for estimation of the BMC [2]. Cost estimating charts for process and chemical engineering such as [118, 119], cost estimating equations and capital cost correlations [39, 112, 116], as well as past purchase orders for CES [14, 32, 120], were considered.

Potential supply chains for CES key components were evaluated in [8]. Despite being based on mature and commercially available technology [15] limits to the scale of single components were identified [18]. Key components for CES systems of up to 100 MW are available from power and process industry supply chains [16]. Consequently, the base case system size was kept to 100 MW_{dis}. The scale was an important factor for deciding the method of BMC estimation for each component type. When available, preference was given to past purchase orders.

In order to estimate the component costs based on the known costs of a similar component of different size [112], the effect of size of equipment on costs can be accounted for with the following equation

$$C_{PE,new} = C_{PE,0} \cdot \left(\frac{\mathrm{X}_{new}}{\mathrm{X}_0}\right)^{\alpha} \tag{3.16}$$

where $C_{PE,0}$ is the known cost of the equipment of the size X_0 extracted from literature and $C_{PE,new}$ is the desired BMC at the respective size X_{new}. The equipment "size" X is thereby a primary design variable dependent on the equipment type. For heat exchangers, the primary design variable is the heat exchanger area A_{HE} in m², while for turbomachinery it is typically the power capacity $\dot{W}_T$ in kW [118].

The scaling factor α, is also dependent on the size and type of the equipment. For very small sized equipment α is close to zero while at large scale when transport and assembly of the component become very costly, the scaling factor α approaches one [111]. As for equipment types, the BMC of heat exchangers increases rather linearly ($\alpha \approx 0.16…0.66$) while turbomachinery (e.g., compressors, turbines) follow the economy-of-scale ($\alpha \approx 0.60…0.95$) [112]. The average value for α across the chemical industry is about 0.6 [121], which implies a cost reduction of 24.2 % at twice the size. The same value was recommended to be used in the absence of other values for α [112] and was used by Highview Power Storage Ltd. [32] for estimating the component costs for the demonstration plant.

In cost estimating charts purchased-equipment base costs are typically plotted versus the equipment size on a graph that uses logarithmic scales on both axes (log-log plot) [111, 118, 119] and is based on equations similar to equation (3.16). Apart from the scale, the pressure and temperature ranges were also taken into account, with the choice of the material (e.g., stainless steel or aluminum) and equipment type (e.g., cryogenic pump, fin plate heat exchangers).

For consistent comparability of the economic analysis, cost functions were developed to estimate the BMC of the components in the evaluated CES systems. The cost functions, design variables, assumptions, and references are given for the most important component types in Table 3.1. The detailed information on the component design, range of operation, construction material, potential supply chain, and limitations considered for the cost estimation are given in detail in Appendix B.

The reference cost data is extracted from a variety of sources with different reference years and currencies. By using cost indices, the data can be brought to a common basis with the following equation.

$$C_{PE,new} = C_{PE,\mathrm{ref}} \cdot \frac{\mathrm{Index}_{new}}{\mathrm{Index}_{\mathrm{ref}}} \tag{3.17}$$

The Chemical Engineering Plant Cost Index CEPCI was used, being particularly suitable for the type of equipment incorporated in CES systems [116]. The Chemical Engineering Magazine regularly publishes the annual and monthly cost index [111]. The costs in this work are given in € and are adjusted to the CEPCI of the year 2017. The historical development of the CEPCI is shown in Figure B.2 in Appendix B. The conversion rates used for the conversion of the currencies are given in Figure B.3 in Appendix B.

Table 3.1: Cost functions developed for the estimation of the BMC of the CES system components.

Component	Design variable	Cost function $['000\ €_{2017}]$	Assumptions	Adopted from
Compressors	capacity, $\dot{W}_{CM}$[MW]	$795 \cdot \left(\frac{\dot{W}_{CM}}{8\ MW}\right)^{0.60}$	Centrifugal	[32], [119]
Expander	capacity, $\dot{W}_{EX}$[MW]	$f_m \cdot 1{,}795 \cdot \left(\frac{\dot{W}_{EX}}{0.001\ \text{MW}}\right)^{0.70}$	$f_{m,ss}$= 5.0, $f_{m,cs}$= 3.0	[118]
Turbines	capacity, $\dot{W}_T$[MW] max 45 MW [8]	$f_m \cdot 3{,}945 \cdot \left(\frac{\dot{W}_T}{0.0001}\right)^{0.588}$	$f_{m,cs}$= 3.5, $f_{m,ss}$= 6.0, $f_{m,ma}$= 8.0, axial	[118]
Combustion chambers	Outlet temperature, T_{CC}[K], mass flow, $\dot{m}_{air}$[kg/s]	$\left(\frac{67.49}{0.995 - \frac{p_{ex}}{p_{in}}}\right) \cdot \dot{m}_{air} \cdot \left(1 + e^{(0.018 \cdot T_{CC} - 26.4)}\right)$		[112]
Cryopumps	capacity, $\dot{m}_{CP}$[kg/s] max 50 kg/s	$644 \cdot \left(\frac{\dot{m}_{CP}}{23\ \text{kg/s}}\right)^{0.6}$	reciprocating pump	[32]
Storage tanks	capacity, V_{ST}[m³] 50,000 m³	$f_d \cdot f_m \cdot (0.0458 \cdot V_{ST} + 117.80)$	$f_{m,ss}$ = 2.0…3.0, $f_{m,cs}$ = 1.0	[119]
Intercoolers, Reheaters	HE area, A_{HE}[m²]	$\left(f_p \cdot 1.3 + 1.88\right) \cdot 57.64 \cdot \frac{A_{HE}}{1{,}000}$	f_p= 1…1.3, shell/tube, cs/cs	[118]
Cryogenic heat exchangers (MHE)	MHE area, A_{MHE}[m²]	$\left(91.28 + 45.64\left(f_m + f_p\right)\right) \cdot \frac{A_{MHE}}{2{,}000}$	plate-fin, $f_{m,ss}$ =2.3, f_p= 1.2…1.3	[118]

cs carbon steel, ss stainless steel

3.3.2. Assumptions made

For the detailed cost calculation, the economic parameters need to be determined first. The assumptions made for economic analysis are summarized in Table 3.2. CES industrial projects are expected to have a relatively fast construction lead-time of only one or two years [76]. The economic life of CES projects is expected to be higher than that of other energy projects. CES economic life is expected to reach more than 25 years and up to 60 years [29, 37, 38]. Both faster commissioning and a long economic life favor the economic performance of CES systems.

All systems analyzed are daily cycling units, designed to supply electricity for up to four hours of peak demand at a charge-to-discharge ratio of 2/1 and 1460 annual hours at full load discharge operation. The operation and maintenance costs (OMC) are accounted for as 4 % of the fixed capital investment (FCI) per annum. The company Air Products and Chemicals, Inc. rates the CES OPEX at approximately 105 €/MW [20] annually, while [8] estimated OMC at 1.5 % to 3 % of the purchase costs of CES and the company Expansion Energy claimed CES OMC lower than those of natural gas-fired power plants [20]. The system is assumed to operate at low electricity prices.

The price of electricity of 20 €/MWh at the beginning of the first year of operation was set based on the assumption that the CES system charges at average day-ahead market price in

Germany for the 2,920 lowest priced hours in the year 2016-2018, see Figure B.1. In this work, ES systems are assumed to be exempted from the taxes on electricity, RE act levy (EEG Umlage) as well as distribution and grid charges. The plant operation is scheduled for 01.01.2021, and the construction and commissioning time is two years. The changes in the prices, e.g., electricity and fuel, were accounted for in elevated charges for the contingency of 15 % of BMC. Contingencies refer to the additional costs added to the project budget taking into account the potential variation from the initial cost estimate, as all cost estimates are uncertain. As CES system parameters and associated costs are still to be proven, a higher value was assumed [121].

Table 3.2: Assumptions made in the economic analysis.

Parameter	Assumption
Effective interest rate	10 %
Plant economic life	40 years
Average general inflation rate	2.5 %
Daily charging/discharging duration, τ_{char}/τ_{dis}	8 h/4 h
Annual full-load discharging operation, τ_{dis}	1,460 h/a
Base electricity price, $c_{el,0}$	20 €/MWh
Natural gas price, $c_{NG,0}$	262 €/ton
Service facilities and architectural work	30 % of BMC
Contingencies	15 % of BMC
Annual OMC	4 % of FCI

3.3.3. Total revenue requirement method

The sum of sales of products in a year needs to cover the annual expenditures. This annual revenue requirement (TRR) of a system consists of carrying charges and expenses. The *carrying charges* CC represent the indebtedness associated with the initial capital investment, accounting for the capital recovery (capital lent from investors), the return on investment (debt, stock, and equity) as well as taxes and insurances.

$$TRR_L = CC_L + FC_L + OMC_L \tag{3.18}$$

The *fuel costs* FC and the *operation and maintenance costs OMC* are the most prominent examples of expenditures that also need to be estimated over the economic life of the system [111]. The series of annual expenditures (FC and OMC) and costs associated with carrying charges CC is not uniform. All costs are thus levelized to constant annuities over the systems economic life, e.g., with the help of the capital recovery factor (CRF).

$$CC_L = TCI \cdot CRF \tag{3.19}$$

The total capital investment (TCI) is gained from the fixed capital investment (FCI), which represents the direct and indirect cost associated with the design, construction, and installation of the plant and the alterations needed for the preparation of the plant site [121]. The direct costs are on- and offsite costs associated with the permanent expenditures such as the BMC,

the installation of equipment, the land, and other resources and labor costs required for the system. The indirect costs refer to the costs associated with the design and construction phase, e.g., engineering and supervision, construction costs, and contingencies. The TCI is the sum of the FCI, and other outlays such as the allowance for the funds needed during construction time, the working capital, the licensing costs, and the start-up costs.

The expenditures (FC and OMC) are escalated under the assumption of a constant escalation levelization factor *CELF*.

$$FC_L = FC_0 \cdot CELF = FC_0 \cdot CRF \cdot \frac{k_{FC}(1 - k_{k_{FC}}^n)}{(1 - k_{FC})} \tag{3.20}$$

The fuel cost at the beginning of the first year FC_0 is converted into constant annuities accounting for both the cost of money and the constant escalation. The OMC are escalated and levelized in the same manner.

Finally, when the TRR is determined, the product costs can be calculated, and the feasibility of the investment can be evaluated.

3.3.4. Economic sensitivity analysis

The final product of the CES systems is the electricity generated in the discharge process and fed back into the grid or supplied to a customer. The levelized cost of electricity discharged $LCOE_{dis}$ can directly be calculated from the annual TRR and the annually generated electricity E_n.

$$LCOE_{dis} = \frac{TRR}{E_n} = \frac{CC_L + FC_L + OMC_L}{E_n} \tag{3.21}$$

An economic sensitivity analysis was conducted to evaluate the economic parameters stated in literature and identify the dependency of economic viability on economic parameters independent of the system design.

For the economic sensitivity analysis, the most significant parameters were identified and varied. The economic life, the discharge capacity, the *RTE*, the FLH of the discharge unit, the OMC as share of the TCI, the interest rate, and the BMC were varied in a range of 20-60 years, 25-200 MW, 31.5-46.5 %, 720-2920 h/a, 1-8 % TCI, 5-15 % and € 60-130 million, respectively. In order to compare the weighted effect of parametric changes on the overall economic viability measured by the $LCOE_{dis}$, the parametric changes are normalized to the initial value of the respective base case parameter. Finally, the $LCOE_{dis}$ is compared to $LCOE_{dis}$ of other bulk ES technologies reported in the literature under similar assumptions for the economic parameters.

3.3.5. Determination of cost rates

When the economic analysis is conducted as part of an exergoeconomic analysis, the levelized cost rate $\dot{Z}_k$ of each component k and the specific cost per unit of exergy of the fuel c_F need to be determined. The component cost rate considers the contribution of each respective component to the costs associated with the capital investment and the operation and maintenance costs. The component cost rate is calculated as

$$\dot{Z}_k = \dot{Z}_k^{CI} + \dot{Z}_k^{OM} = \frac{BMC_k}{\sum BMC_k} \cdot \frac{(CC_L + OMC_L)}{\tau_k} \tag{3.22}$$

τ_k refers to the annual operation time of the k-th component, BMC_k to the components investment costs and $\sum BMC_k$ to the sum of the bare module costs of all components in the systems. The component cost rate associated with the initial capital investment $\dot{Z}_k^{CI}$ is calculated over the levelized carrying charges CC_L. The component cost rate associated with the operation and maintenance costs $\dot{Z}_k^{OM}$, respectively, over the OMC_L.

The specific costs of all streams entering the system need to be identified for the exergoeconomic analysis. The specific costs associated with the exergy rate of the fuel to the system are given by:

$$\dot{C}_F = \frac{FC_L}{\tau} \tag{3.23}$$

3.4. Exergoeconomic analysis and optimization

In this work, exergoeconomic optimization is applied to determine the effect of parametric and conceptional changes on the cost-effectiveness of CES systems to minimize the cost of the final product. Exergoeconomic optimization follows the approach of Bejan et al. [112]. The logic flowchart for the methodology followed is shown in Figure 3.2. The optimization is performed in several iterations.

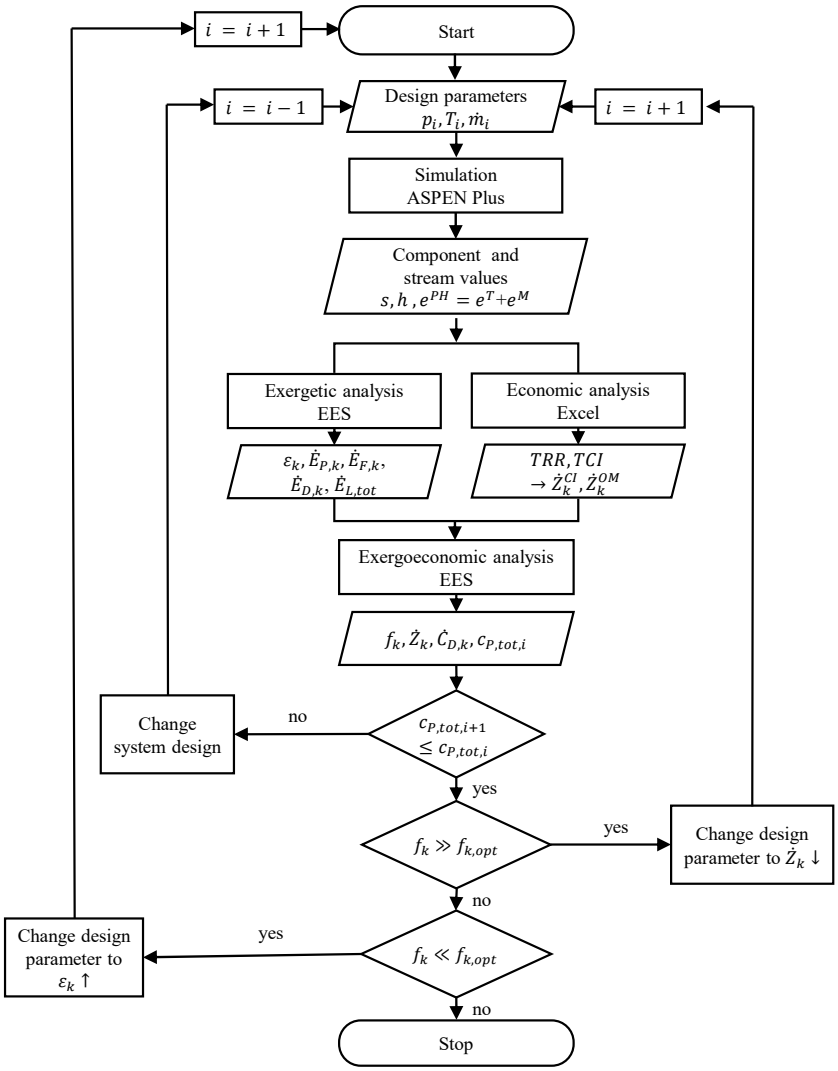

Figure 3.2: Logic flowchart for the exergoeconomic optimization applied in this work [36].

After the definition of the initial design parameters of the base case system, the system is simulated in Aspen Plus®. In the simulation, the mass and energy balances are fulfilled, and the enthalpy and the entropy values at all given states are calculated. The exergy values are calculated with the help of an integrated Fortran routine.

For exergetic analysis, the exergy of the fuel $\dot{E}_{F,k}$, the exergy of the product $\dot{E}_{P,k}$, the exergy destruction $\dot{E}_{D,k}$ and the exergetic efficiency ε_k are determined on the component and the system level. The exergy of the losses $\dot{E}_{L,tot}$ of the overall system are calculated.

The cost rate of the components $\dot{Z}_k$ are determined in economic analysis. Exergoeconomic analysis corresponds to the combination of the exergetic and cost analysis and discloses the costs associated with thermodynamic inefficiencies (exergy destruction) $\dot{C}_{D,k}$. The exergoeconomic factor f_k is the decision variable used to determine whether to adjust the design parameters to:

- increase the exergetic efficiency ε_k (reduce the exergy destruction $\dot{E}_{D,k}$), or
- decrease the investment cost $\dot{Z}_k$ of the respective component.

After each change in the design parameters, a new iteration (simulation, exergetic, economic, and exergoeconomic analysis) is conducted. As long as the cost of the final product is reduced, the changes are continued ($c_{P,tot,\,i+1} < c_{P,tot,\,i}$). When parametric changes do not reduce the cost of the final product any further, changes in the system design are applied. If changes in system design do reduce the cost further and the exergoeconomic factor of the components is close to the optimum, the optimization is discontinued. The final product of the CES systems $c_{P,tot}$ is the discharged electricity. As a result, the terms *average cost of the final product* $c_{P,tot}$ and *levelized cost of discharged electricity* $LCOE_{dis}$ are used interchangeably in this work.

3.4.1. Exergy costing

The exergoeconomic analysis aims to determine; the costs associated with thermodynamic inefficiencies, the main contributing components to the costs of the overall system, the cost-effectiveness of a system, and the potential for reduction in costs. This correlation between thermodynamic performance and costs is achieved by applying *exergy costing* [112].

In exergy costing, each stream with an associated exergy transfer rate $\dot{E}_n$, e.g., matter, work or heat, is denoted an average cost per unit of exergy c_n, e.g.

$$c_n = \frac{\dot{C}_n}{\dot{E}_n} \tag{3.24}$$

$$c_w = \frac{\dot{C}_w}{\dot{W}} \tag{3.25}$$

$$c_q = \frac{\dot{C}_q}{\dot{E}_q} \tag{3.26}$$

The specific costs are determined in *cost balances*. For each component k, the difference of the sum of the cost rates $\dot{C}_k$ (associated with the m exiting and n entering streams of the matter) is equal to the sum of the cost rates associated with the heat supplied to the component $\dot{C}_{k,q}$ and the work done by the component ($\dot{C}_{k,w}$) as well as the cost rate of the respective component $\dot{Z}_k$.

$$\sum_{1}^{m} \dot{C}_{out,k} - \sum_{1}^{n} \dot{C}_{in,k} = \dot{C}_{k,q} + \dot{C}_{k,w} + \dot{Z}_k \tag{3.27}$$

All costs associated with the streams entering the systems need to be known. Auxiliary equations are necessary when more than one stream exits the component. For the definition of fuel and product, the SPECO approach [122] was followed. Following the “fuel and product”

approach the cost balance can also be expressed with the cost rate associated with the fuel $\dot{C}_{F,k}$ and the product $\dot{C}_{P,k}$ of the component.

$$\dot{C}_{P,k} = \dot{C}_{F,k} + \dot{Z}_k, \text{ and} \tag{3.28a}$$

$$\dot{C}_{P,tot} = \dot{C}_{F,tot} - \dot{C}_{L,tot} + \sum_k \dot{Z}_k \tag{3.28b)(3.28a}$$

The cost balances for the components in the evaluated systems are given in Appendix B. On system level the cost rate associated with the exergy losses $\dot{C}_{L,tot}$ needs to be considered as well. The costs associated with the exergy destruction in the k-th component are determined by the average cost per unit of exergy of the fuel $c_{F,k}$:

$$\dot{C}_{D,k} = c_{F,k} \cdot \dot{E}_{D,k} \tag{3.29}$$

The cost rate associated with the exergy losses $\dot{C}_{L,tot}$ is calculated similar to equation (3.29). The exergoeconomic factor f_k and the relative cost difference r_k should be used for evaluation of the cost-effectiveness of the k-th component:

$$f_k = \frac{\dot{Z}_k}{\dot{Z}_k + \dot{C}_{D,k}} \tag{3.30}$$

$$r_k = \frac{c_{P,k} - c_{F,k}}{c_{F,k}} \tag{3.31}$$

3.4.2. Exergoeconomic optimization

After the exergoeconomic analysis is performed on the *Base Case* system, the first iteration of the exergoeconomic optimization is conducted based on [112]. Aim of the exergoeconomic optimization is the significant reduction of the *average cost of exergy of the product* $c_{P,tot}$. The exergoeconomic optimization does not intend to identify a single mathematical optimum but operates with a knowledge-based iterative approach to limit system complexity and account for availability and safety. The optimization can be broken down in three main steps:

1. Identify the components with the highest cost importance ($\dot{Z}_k + \dot{C}_{D,k}$)
2. Identify the potential source of the high costs in the respective components by reviewing:
    a. the relative cost difference r_k,
    b. the exergoeconomic factor f_k and
    c. system design.
3. Apply changes to the system design:
    a. conceptional changes or
    b. parametric changes.

By ranking the components according to the sum of costs associated with the initial investment of the component $\dot{Z}_k$ and the costs associated with the exergy destruction $\dot{C}_{D,k}$ priority is given to the components with the highest contribution to the cost of the exergy of the product of the system.

The cause of the high costs caused by a component or component group can be identified by reviewing the exergoeconomic parameters (r_k, f_k) of the component(s) and the overall system design. The relative cost difference r_k indicates whether the component is the origin of the high costs associated with the exergy destruction $\dot{C}_{D,k}$ or whether the average cost of the exergy of the fuel to the component $c_{F,k}$ is relatively high. If the $c_{F,k}$ is relatively high, the components prior to this component and the system design should be inspected first. Reviewing the exergoeconomic factor f_k two recommendations can be drawn:

- when f_k is elevated, the costs associated with the initial investment of the component $\dot{Z}_k$ dominate and should be reduced despite a potential reduction in efficiency ε_k, and
- when f_k is low, the costs associated with the exergy destruction $\dot{C}_{D,k}$ dominate and the exergetic efficiency ε_k should be increased (exergy destruction $E_{D,k}$ ↓).

In general, the initial investment of the component $\dot{Z}_k$ and the costs associated with the exergy destruction $\dot{C}_{D,k}$ should be in the same magnitude ($f_k \rightarrow 0.5$). However, the "optimal" value for the exergoeconomic factor ($f_{k,opt}$ in Figure 3.2) differs according to the type of component. For turbomachinery for instance an elevated exergoeconomic factor is characteristic, e.g., f_k= 0.6-0.7. Apart from identifying parametric changes on component level, changes in system design should also be considered. If the effect of the parametric change is positive, it can be continued until no effect can be identified.

3.5. Summary of the methodology

For the evaluation of cryogenic energy storage systems presented in this work, exergy-based methods based on Bejan et al. [112] were applied. The "fuel and product" approach was used, and the physical exergy was split into its pressure related (mechanical exergy e^M) and temperature related (thermal exergy e^T) part. These methods were applied for several reasons:

- CES systems partially operate below the environmental temperature.
- For the analysis of the integrated CES systems, the quantity and quality of different energy sources need to be considered.
- The relationship between thermodynamics and costs should be analyzed, and a cost-optimal CES system design should be identified.

The economic analysis follows the Total Revenue Requirement (TRR) method [111, 112]. Cost estimation is based on past purchase orders from previous CES projects and potential supply chains from LNG, industrial gas, and power industry. Limitations for commercial availability of components were acknowledged. For this reason, the design size of the evaluated CES systems was kept to 100 MW of discharge capacity. The exergoeconomic optimization presented in this work operates with a knowledge-based iterative approach to limit system complexity and account for availability and safety.

Chapter 4: Design and simulation

The methods described in *Chapter 3* were applied to different CES system configurations. A number of design configurations are possible for the charge, the storage, and the discharge unit of a cryogenic energy storage system. Moreover, CES systems have great potential for system integration with internal and external heat sources and sinks ("cold sources"). In this section, the assumptions made in simulation, the process design, the selection of components, working fluids, and parameters are described. The design options that were considered and applied for the *pre-design*, the *base cases,* and the *integrated systems* are shown in Figure 4.1.

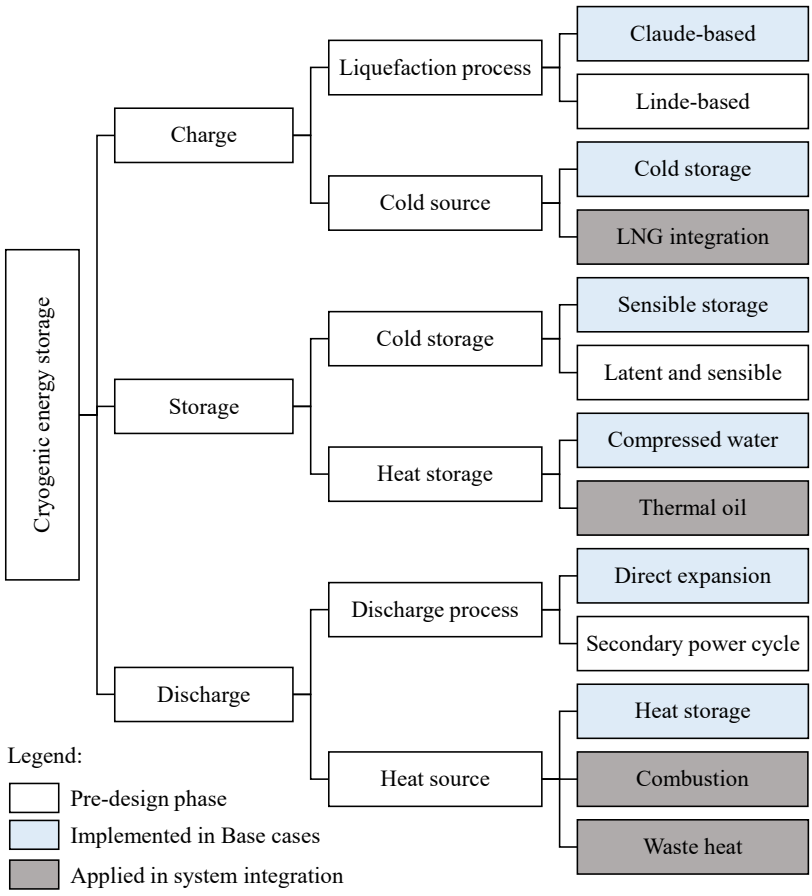

Figure 4.1: Schematic of the system configurations considered for this work.

In the pre-design phase, different design options were reviewed and compared in simulation. The design options that are indicated in white color in Figure 4.1 were considered in the pre-design phase but were finally not implemented in the Base Case systems for various reasons,

e.g., the systems thermodynamic performance, or economic feasibility. The design of the charge, the storage, and the discharge unit of the stand-alone adiabatic CES are described in section 4.3.1, 4.3.2 and 4.3.3, respectively.

The integrated systems are based on the adiabatic CES system design but were extended with external heat sources and sinks. For system integration, waste heat and internal combustion were considered as external heat sources. LNG as well as cold storage were considered as heat sinks. The design of the integrated systems is discussed in section 4.4.

4.1. Simulation and data management software

Aspen Plus® [123] was chosen as a suitable software for process simulation. Aspen Plus software is characterized by several advantages amongst other its years of experience and close cooperation with the chemical industry, its practical user interface with appropriate computational basis, an extensive model library, and the possibility for integration of user-specific modules, e.g., in FORTRAN, Excel or VBA. With the aid of the simulation software, all mass and energy balances are fulfilled, and the specific enthalpy and entropy values of all streams and substances are calculated. The *Peng-Robinson equation of state* was selected, and the simulation was performed under steady-state conditions. FORTRAN-based user property subroutines[2] were integrated with Aspen Plus to calculate exergy values as input for the exergetic analysis. For the execution of exergy-based analysis, the Engineering Equation Solver (EES) [124] was used. The core benefit of the software package EES is its built-in, extensive, and accurate thermodynamic database.

4.2. General assumptions made in the simulation

The ambient temperature is assumed at 15 °C and ambient pressure at 1.01325 bar according to the International Standard Atmosphere [125]. Both liquid nitrogen and liquid air are widely considered as working fluid in CES systems as their thermo-physical properties are similar [8, 37]. The inlet air to the compression process is modeled with a molar fraction of 0.79 for nitrogen and 0.21 for oxygen. The real operation of the turbomachinery was assumed with isentropic efficiencies; the values were chosen according to the literature reviewed, see Table 4.1.

Table 4.1: Isentropic efficiencies presumed for the turbomachinery.

Isentropic efficiencies	Value	Ref.
Compressors	0.85	[42]
Cold expander	0.84	[57, 126]
Cryogenic pump	0.75	[57]
Turbines	0.90	[39]

The isentropic efficiency of the cold expander in the liquefaction process was reported to have efficiencies as low as 0.60-0.78 [126], while recent enhancement in the design of cryogenic

[2] Developed and revised in the Chair for Energy and Environmental Protection at Technische Universität Berlin

turbines enabled isentropic efficiencies as high as 0.88 in testing [57]. Sensitivity analysis showed that varying the isentropic efficiency $\eta_{is,EX}$ between 0.78 and 0.88 has no significant effect on the performance of the system. While when $\eta_{is,EX}$ is reduced further, the roundtrip efficiency (*RTE*) is reduced significantly, Figure C.1 in Appendix C.

The heat exchangers in the systems can be divided into two types of heat exchangers:

- the cryogenic multi-stream heat exchangers – the main heat exchangers (MHE1, MHE2) of the charge and the discharge unit, and
- two-stream heat exchangers, e.g., intercoolers and reheaters that operate above T_0.

The assumptions made for the pinch temperature difference ΔT_{pinch}, the pressure drop Δp and the design parameters for the heat exchangers are given in Table 4.2. Two Cases are differentiated: the *Base Case* and the *Optimized Case*. The Base Case refers to the initial design parameters of the two system configurations for the stand-alone adiabatic CES: the Base Case A and the Base Case B. After performing exergoeconomic optimization on the two base case systems, the Optimized Case was derived. The integrated systems are based on the design parameters of the Optimized Case.

Table 4.2: General assumptions and design parameter for the heat exchangers.

Component	Unit	Base Case	Optimized Case
Intercoolers			
Hot end exit temperature, $T_{IC,exit}$	°C	18	18
Pinch temperature difference, $\Delta T_{IC,pinch}$	K	2	3
Relative pressure drop (liquid/gas), Δp_{IC}	%/K	0.02	0.02
Reheaters			
Hot end temperature approach, $\Delta T_{IC,exit}$	K	2	6
Pinch temp difference, $\Delta T_{RH,pinch}$	K	2	6
Pressure drop (liquid/gas), Δp_{RH}	%/K	0.02	0.02
Main heat exchanger 1			
Hot end exit temperature, T_{11}	°C	- 177	- 177
Pinch temperature difference, $\Delta T_{MHE1,pinch}$	K	1	3
Pressure drop (evaporation/liquefaction), Δp_{MHE}	%/K	0.04	0.04
Main heat exchanger 2			
Pinch temperature difference, $\Delta T_{MHE2,pinch}$	K	1.3	4
Pressure drop (evaporation/liquefaction), Δp_{MHE}	%/K	0.04	0.04

For the cryogenic heat-exchangers, a minimum approach temperature $\Delta T_{pinch,min}$ of 1 K is realizable. In the MHE1 and the MHE2 of the base case systems, the $\Delta T_{pinch,min}$ was approached. The pressure drop in a given system is affected by various factors, in particular, the type of flow (e.g., laminar or turbulent), the density of the working fluid, and the geometry of the section in heat exchangers. The pressure drop assumed in the heat exchangers accounts for the type of heat exchanger (two-stream or multi-stream) and whether phase-changed occurs, adopted from [127].

4.3. Adiabatic cryogenic energy storage systems

In this section, the design and simulation of the overall stand-alone adiabatic CES systems are discussed. The schematic flowsheet of the adiabatic CES (a-CES) system is shown in Figure 4.2; the different process steps are denoted with (a) to (g). The decisions made in the pre-design phase for the simulation of the charge, the storage, and the discharge unit are specified in the subsections 4.3.1 to 4.3.3. The properties of the streams displayed in Figure 4.2 are given in Table C.1, and Table C.2 in the Appendix C. The a-CES systems are designed for a power capacity of the discharge unit of 100 MW_{el} and an energy capacity of the storage unit of 400 MWh_{el}. The systems are daily cycling units, enabling four hours of daily discharge at full load capacity during peak demand at a charge-to-discharge ratio of two (8h/4h).

The charging process is a conventional air liquefaction process consisting of the gas cleaning and purification unit, the compression and the final expansion and liquefaction process *(a)-(c)* in Figure 4.2. In the charging process, the pre-treated air is compressed in three compression steps with inter-stage cooling – *(b) compression process*. The liquefaction process is based on the Kapitza process for Base Case A (stream 7a-13 in Figure 4.2) and the Heylandt process for Base Case B (stream 7b-13) with one cold expander – *(c) liquefaction process*. The heat rejected in the intercoolers is recovered and stored to enhance the performance of the discharge unit – *(f) heat recovery and storage*.

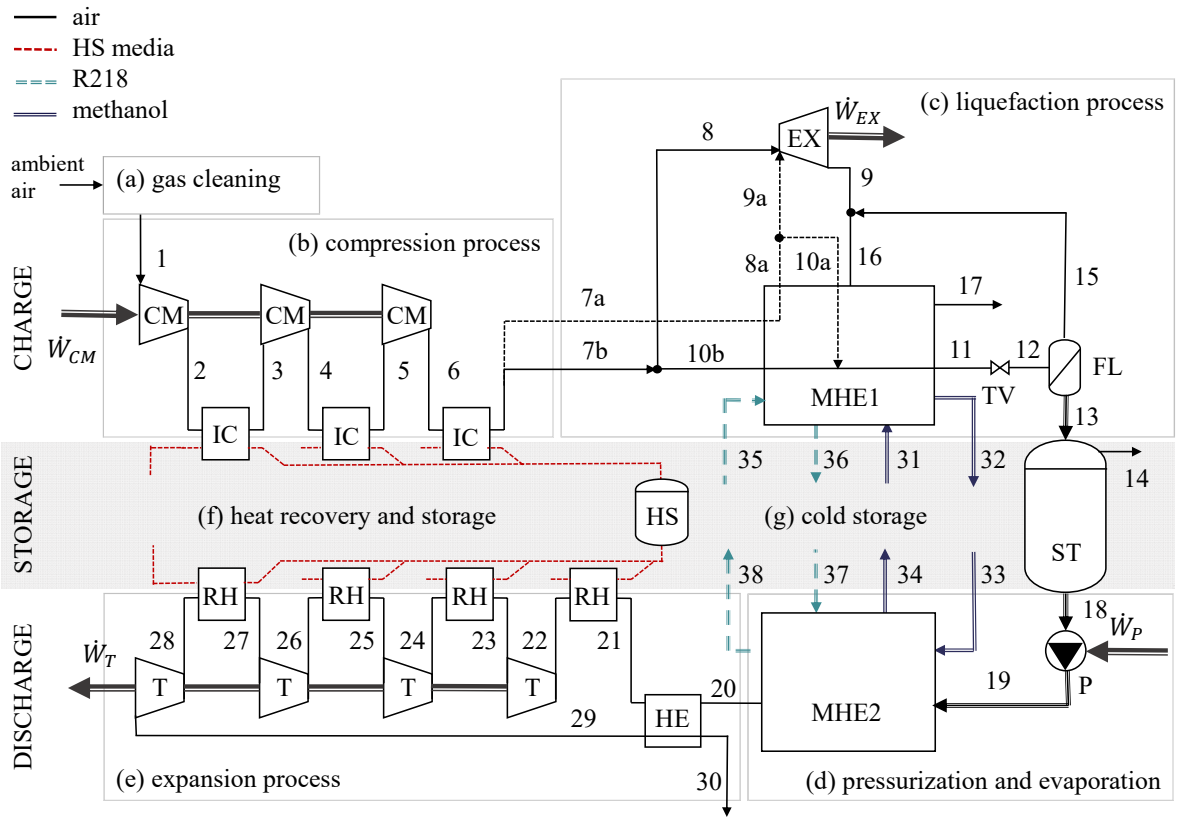

Figure 4.2: Flowsheet of the stand-alone adiabatic CES system (Base Cases A and B).

In the discharge process, the exergy stored in the liquid air is recovered in a simple direct Rankine cycle. The liquid air is pumped to supercritical pressure and supplied to the second main heat exchanger (MHE2). In the MHE2 the liquid air is evaporated and heated in heat exchange with the cold storage media – *(d) pressurization and evaporation*. The low-temperature exergy released during evaporation of the pressurized liquid air is recovered in the cold storage. The cold storage is realized through two circulating working fluids in liquid state – *(g) cold storage*. The recovered cold is supplied to the first main heat exchanger (MHE1) to increase the share of liquefied air in the liquefaction process of the subsequent charging process.

The slightly subcooled liquid air is stored in a simple insulated storage vessel at near ambient pressure (1.1 bar) and a temperature of - 194 °C. The mass flow in the discharge process is twice as large ($\dot{m}_{19} = 2 \cdot \dot{m}_{18}$) as in the charging process. The high-pressure air is superheated and expanded in four gas turbine stages with reheating – *(e) expansion block*. The different process steps (a) to (g) are described in more detail in the following subsections.

In a comparative analysis, the systems were evaluated with uniform design parameters. Either,

- the compression pressure and mass flow rate $\dot{m}_1$ in the compressors ($\dot{W}_{CM}$= const.) or
- the discharge power $\dot{W}_{dis}$ ($\dot{W}_T - \dot{W}_P$) and the energy stored E_{stored} ($\dot{W}_{dis} \cdot \tau_{dis}$)

were kept consistent for all systems in comparative analysis.

4.3.1. Charging unit

Gas cleaning and purification unit (block (a) in Figure 4.2)

Prior to compression and liquefaction, any contaminants and unwanted components of the inlet air, e.g., hydrocarbons and elements which may disrupt the liquefaction process, such as freezing water and CO_2, are removed in the gas cleaning and purification process (Figure 4.3) [18, 75]. In cryogenic air separation units, this is commonly realized by feeding filtered ambient air at slightly elevated pressure (e.g., 1.03 bar) to a direct contact cooler and a vessel with a fixed bed of adsorbent, e.g., molecular sieve unit [128] or activated alumina [91]. After all trace contaminants have been removed the purified air is fed to the compressors.

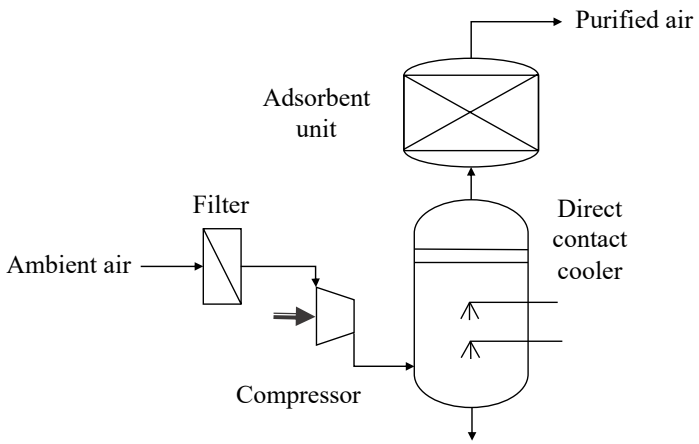

Figure 4.3: Flowsheet of the gas cleaning and purification unit adopted from [128].

The air purification contributes to the energy requirement of the liquefaction unit. The thermal energy required for the regeneration of the absorbent used to remove the undesirable components contributes about 10 % of the energy requirement in the air liquefaction process [129]. This process step cannot be avoided. The air purification process does not need to be simulated for the different system configuration, but the energy consumption and costs need to be accounted. The air exiting the gas cleaning and purification process is estimated with a molar fraction of 0.79 for nitrogen and 0.21 for oxygen at ambient temperature and pressure.

Compression process (block (b) in Figure 4.2)

In the liquefaction process, the air is compressed to high pressure, cooled and expanded to achieve low temperatures (< - 192 °C) and reach the due-point. The compression process is considered separately from the liquefaction process in this thesis due to its role in heat recovery and storage. In adiabatic CES systems, the heat of compression that is rejected in the intercoolers (IC) is recovered and stored to be supplied to the discharging process, superheating the air at the inlet of the turbines. The lower the number of compression-steps and the higher the compression-pressure (p_{CM}), the higher the temperature recovered in the IC as well as the higher the turbine inlet temperature (TIT) in the discharging process.

For the base cases, a three-stage compression process with intercooling was selected. After each compression step, the air is cooled to 18 °C. An isentropic efficiency of $\eta_{is,CM}$ = 85 % [42] was selected for the compressors. Lower values for $\eta_{is,CM}$ increase the temperature at the compressor outlet. The compression pressure was selected according to conducted sensitivity analysis of the maximum liquid yield γ achieved and the minimum specific work required for the liquefaction process for different charging pressures (70 – 140 bar), Figure 4.4.

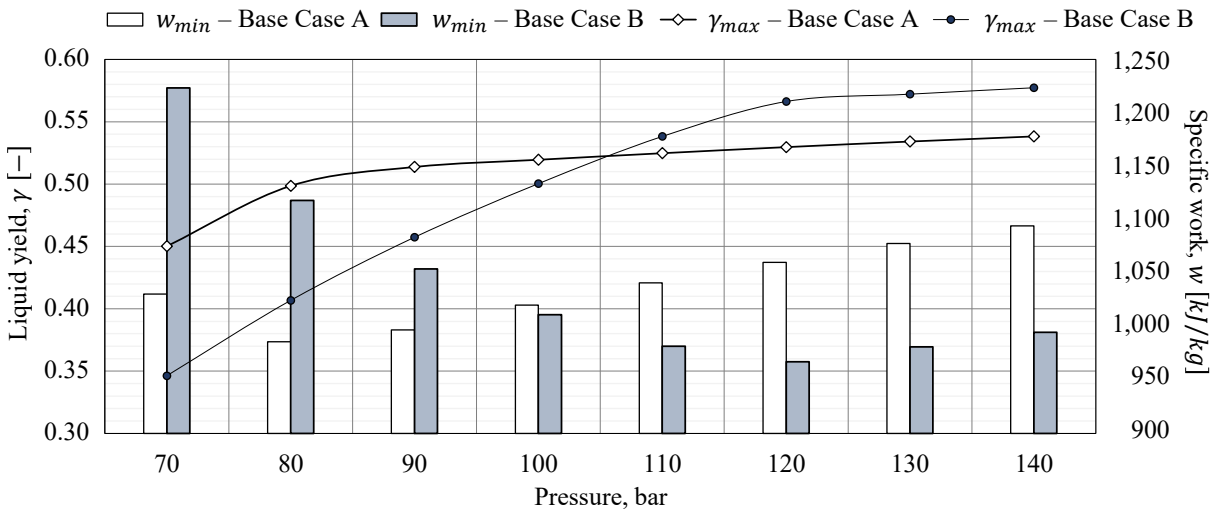

Figure 4.4: Minimum specific work requirement w_{min} and maximum liquid yield γ of the charging process over the compression pressure p_{CM} for the Base Cases A and B.

The specific work requirement refers to the work required to liquefy one kg of air w_{char}. The liquid yield γ is defined as the ratio between the mass flow of the air liquefied and the mass

flow exiting the last compression step $\dot{m}_{CM}$ (Eq. (3.4)). Both the specific work w_{char} and the liquid yield γ are indicators for the performance of the liquefaction process. The two base cases use different liquefaction processes and thus achieve their best performance (w_{min}, γ_{max}) at different pressures. The operation pressures were chosen at 85 bar and 120 bar, for the Base Cases A and B, respectively, when the specific work required to liquefy a kg of air reaches its minimum w_{min}.

Liquefaction processes (block (c) in Figure 4.2)

The performance of the liquefaction process has a significant influence on the overall performance and cost-effectiveness of the CES system. Hence, a number of air liquefaction processes were considered and evaluated for application in adiabatic CES systems.

Most commercial air liquefaction plants operate with the Claude process and its modifications due to their high efficiency [48], section 2.2.3 (a). The leading CES developer, Highview Ltd., base their charging station on the Claude process, relying on the maturity of the process and the trouble-free scale-up [18].

Despite Claude-based systems leading in industrial air liquefaction, other liquefaction processes are of interest for implementation in adiabatic CES systems. The Linde process, for example, has often been proposed for CES, see Table 2.1 in Chapter 2.

In the comparative exergy-based analysis, three liquefaction process based on the Linde process, and three Claude-based processes were evaluated:

- the simple Linde process,
- the precooled Linde process,
- the dual-pressure Linde process,
- the simple Claude process,
- the Kapitza process, and
- the Heylandt process.

The simulated systems are shown in Figure 4.5 and Figure 4.6, the stream values are reported in Table C.3 and Table C.4 in Appendix C. A second bypass turbine was found to be redundant regarding *RTE*, liquid yield and costs in a previous study. The Collins process was, therefore, not further investigated in this work [51].

At first, the liquefaction processes were manually optimized and later modified to accommodate the cold storage. The operation pressures for the different liquefaction processes deviate [48]. For comparison, the liquefaction pressure was kept to $p_{max,CM}$ = 200 bar [48] first and later $p_{max,CM}$ was varied in a sensitivity analysis (80-200 bar). The systems were simulated with and without cold storage. The modeling and assumption for the cold storage and recovery are described in section 4.3.2.

Linde-Hampson

Consisting of only four sets of components: the compressor(s), the main heat exchanger (MHE), the throttling valve (TV) and the flash tank (FT), the Linde-Hampson process is the most straightforward of all liquefaction processes. In the Linde process, Figure 4.5 (a), purified compressed air is cooled (1-2) and undergoes isenthalpic expansion (2-3) in a throttling valve, being brought to its dew point by the Joule-Thomson effect [47]. The temperature of the high-pressure air is reduced to a value below - 100 °C in heat exchange with the recurring stream (5-6). The recurring stream is the gaseous air that exits the flash tank after being separated from the liquefied air (3-4-5).

Precooled Linde

The temperature of the air at the inlet of the throttling valve (2) strongly influences the efficiency of the Linde-Hampson process. By reducing this temperature with the help of a secondary refrigeration cycle, the *precooled Linde* process (Figure 4.5 (b)) aims to achieve higher liquid yields. Carbon dioxide, ammonia, or Freon compounds are commonly used for the compression refrigeration process [48]. In this work, R32 (Difluormethane) was used.

Dual-pressure Linde

By introducing a second pressure level, the heat transfer in the MHE1 is improved. In the *dual-pressure Linde* process, the air is compressed to an intermediate-pressure before entering the liquefaction process (1). Further, the pressure of the air is elevated to the high-pressure level (2-3) after being mixed with the recurring gaseous stream exiting the intermediate-pressure flash tank (1-12-2). The air is cooled in the MHE1 before undergoing isenthalpic expansion to the intermediate-pressure level (4-5). The liquefied air exiting the intermediate-pressure tank is fed to the second pressure-stage (6-8). In the *dual-pressure Linde* process, the specific work required to liquefy the air is reduced at the expense of the liquid yield, with respect to the simple Linde process.

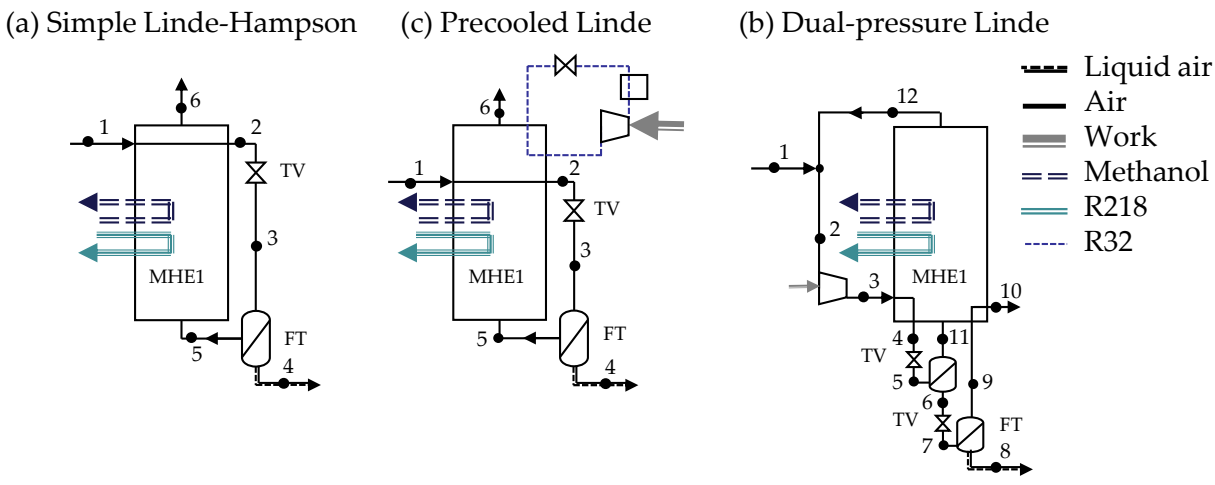

Figure 4.5: Flowsheets of the Linde-based air liquefaction processes with cold recycle [46].

Simple Claude

The Claude process was developed to reduce the liquefaction pressure. The Claude process proposes a solution with two expansion mechanisms, a throttling valve, and a cold expander. The cold expander is located along a bypass [51]. The pressurized air that underwent the isentropic expansion in the cold expander is used to provide a low-temperature cold recycle stream ($\dot{m}_{10}$) to further reduce the temperature before the throttling process [14]. The expander thus does not replace the throttling valve (4-5) before the flash tank. The addition of a cold expander avoids part of the exergy destruction in the throttling process and reduces the required power for liquefaction by the power output of the expander ($\dot{W}_{Char} = \sum \dot{W}_{CM} - \dot{W}_{EX}$) while allowing lower working pressures than in the Linde process.

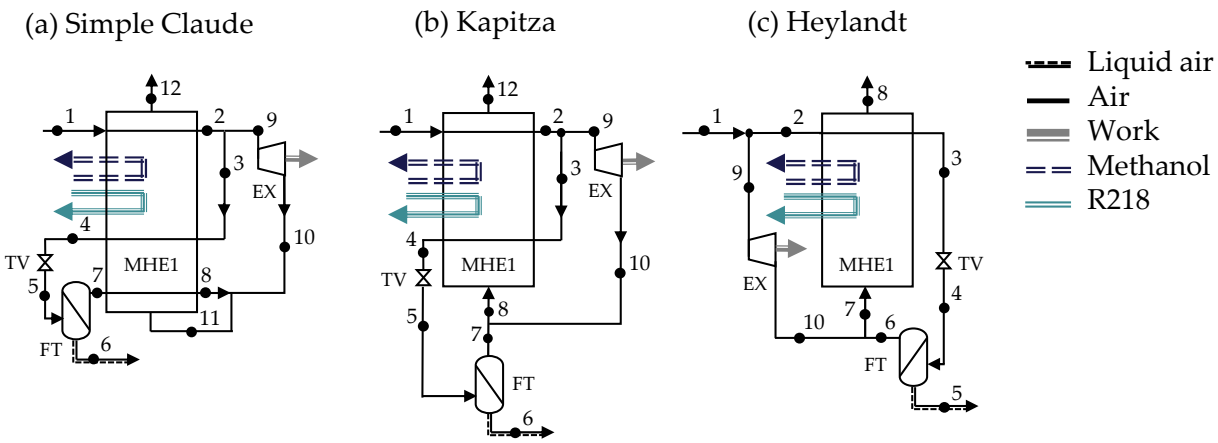

Figure 4.6: Flowsheets of the Claude-based air liquefaction processes with cold recycle [46].

Kapitza

The Kapitza process is adopted from the Claude process, yet, the low-temperature heat exchanger is eliminated. In other words, stream 7 is not fed back to the MHE1 before being mixed with stream 10, avoiding the third partition of the MHE1. The difference in the performance of the Claude and the Kapitza process is commonly little, due to the rather small temperature difference of the two mixing streams (7 and 10).

Heylandt

The Heylandt process can either be seen as analogous to the Claude process or as a variation of the precooled Linde-Hampson process using air as a refrigerant. In the Heylandt process, the first partition of the MHE1 in the Claude system is eliminated. A partition of the air is fed to the cold expander directly (at ambient temperature) instead of being fed to the MHE1 first to be precooled. The splitting of the compressed air before entering the MHE1 improves the heat transfer process in the MHE1 [48].

Splitting ratio r for Claude-based systems

The performance of the Claude-based processes is dependent on the splitting ratio r. The splitting ratio is defined as the mass flow through the expander $\dot{m}_{EX}$ over the mass flow exiting the compression process $\dot{m}_{CM}$.

$$r = \frac{\dot{m}_{EX}}{\dot{m}_{CM}} \tag{4.1}$$

The splitting ratio, therefore, influences the share of air liquefied in the liquefaction process. When a smaller share of air bypasses the MHE1 and is fed to the expander, the temperature difference in the MHE1 is decreased, and a larger share of air is fed to the throttling process and liquefied. The splitting ratio is constrained by the minimum pinch temperature of the MHE1 ($\Delta T_{MHE1,min} \rightarrow 1$ K). When the splitting ratio is reduced to its minimum, the liquid yield is maximized (γ_{max}) and the specific liquefaction work is minimized (w_{min}).

4.3.2. Storage unit

Heat storage (block (f) in Figure 4.2)

Aim of the recovery and storage of the compression heat is to supply additional thermal energy to the discharge process – increasing the TIT and the power generated in the expansion process. The heat rejected in the intercooling process is recovered with a single heat transfer and storage medium [18]. Pressurized water or thermal oil can be employed as working media [12].

In the simulation, pressurized water (25 bar) was utilized as heat transfer, and storage media for low-medium temperatures (T ≤ 200 °C) and thermal oil (6 bar, Dowth-01) was used for medium-high temperatures (200 °C < T ≤ 500 °C). The heat losses in the heat storage were accounted for with 5 K/cycle. The mass flow of the heat transfer fluid is adapted to reduce the temperature after each compression step to 18 °C. Accordingly, the mass flow of the fluid is determined by the compression pressure p_{CM} and the mass flow rate of the air $\dot{m}_1$.

Cold storage (block (g) in Figure 4.2)

The "cold" (low-temperature exergy) rejected in the evaporation process of the liquid air Rankine cycle (discharge process) can be recovered and stored. Supplying this low-temperature exergy to the liquefaction process significantly decreases the specific work required for liquefaction and increases the *RTE*.

Two different storage configurations have been discussed in the context of CES. Either, gravel-based packed bed storage (PBCS) or fluid storage with methanol and propane (or R218) were considered, see Table 2.1. The cold storage of the Base Case CES systems was modeled with two fluid tanks, as suggested in [39, 40, 41, 43].

Reason for this is that the cold storage (CS) media are kept in a liquid state in contrast to dry air being the secondary working fluid in the PBCS. The work required in the cold storage is expected to be much lower when pumping the liquid working fluids in comparison to the work necessary to overcome the pressure drop in the PBCS configuration. Moreover, the use of dry

gas, e.g., nitrogen would require gas storage, which would decrease the volumetric energy density of the storage – the main advantage towards competing technologies, see section 2.4.2.

Several refrigerants were reviewed and evaluated concerning: their boiling and freezing temperatures, their toxicity and flammability and commercial use, Table 4.3. Being neither toxic nor flammable, R218 was found to be more suitable to recover the high-grade cold as Propane. Propane was suggested by [22, 39, 43]. For recuperating the low-grade cold Methanol is more appropriate as its boiling point is higher than the ambient temperature. The same conclusion was derived by [39]. The cold recovery is thus realized with these working fluids circulating on two temperature levels:

- Perfluoropropane C_3F_8 (R218), between -180 to -61°C, 2 bar
- Methanol (CH_3OH), between -21 to -59 °C, 5 bar

The pressure of the cold storage media is slightly elevated to avoid air leakage and ensure improved heat exchange. The amount of low-temperature energy recovered is determined by the amount of air liquefied in the liquefaction process. The mass flow rates of the cold storage media are therefore determined by a share of the mass flow rate of the liquefied air $\dot{m}_{liquid\ air}$:

$$\dot{m}_{R218} = 2.29 \cdot \dot{m}_{liquid\ air} \tag{4.2}$$

$$\dot{m}_{methanol} = 0.46 \cdot \dot{m}_{liquid\ air} \tag{4.3}$$

The ratio is adjusted to the optimal heat transfer between the evaporating liquid air and the cold storage media. According to [14] the efficiency of the cold storage may reach values of ε_{CS} = 95 % [14]. Stöver et al. [12] estimated the CS efficiencies at 85-95 %. Thermal losses in the cold storage were accounted for with 4 K/cycle and 2 $\%_{mass}$ of boil-off losses. The integration of the cold storage with the two main heat exchangers is displayed in Figure C.2.

The T, $\Delta\dot{H}$-diagram of the evaporating liquid air and the cumulative curve of the CS media in the MHE2 is displayed in Figure 4.7. The pressure of the liquid air was varied from subcritical pressures of 20-30 bar to supercritical pressures of 40-150 bar. Air reaches the critical point at - 140.5 °C and 37.4 bar.

Table 4.3: Refrigerant properties compared to air [39, 58].

Refrigerant no.	Name	Chemical formula	Boiling point at 1 bar	Freezing point at 1 bar
R-218	Octafluoropropane	C_3F_8	- 38	- 183
R-290	Propane	C_3H_8	- 42	- 190
-	Methanol	CH_3OH	65	- 97
R-729	Air	-	- 196	- 210
R-732	Oxygen	O_2	- 196	- 216
R-728	Nitrogen	N_2	- 183	- 218

Liquid air storage

The liquefied air is stored in a simple insulated storage tank as standard for bulk storage in the industrial gas and the LNG industry (e.g. double-wall flat-bottom tank) [15]. At a size larger than 1,000 tons, liquid gases are stored at about ambient pressure [32]. Storage vessels for LNG can contain more than 5,000 tons of liquid air [15]. According to reported values, boil-off losses in low-pressure tanks range from 0.05 % up to 0.2 % by volume per day decreasing with tank size [12, 16, 18, 39, 130].

The storage vessel simulated has a pressure of 1.1 bar and temperature of - 192 °C with boil-off losses of 0.2 $\%_{Vol}$ per cycle. Being physically independent, the charge and the discharge unit may be sized independently [75]. The storage tank size is dependent on the amount of air liquefied in the charging process ($\dot{m}_{liquid} \cdot \tau_{char}$). With an estimated charging duration of 8 hours, the tank size amounts to approximately 3,000 tons for all considered systems.

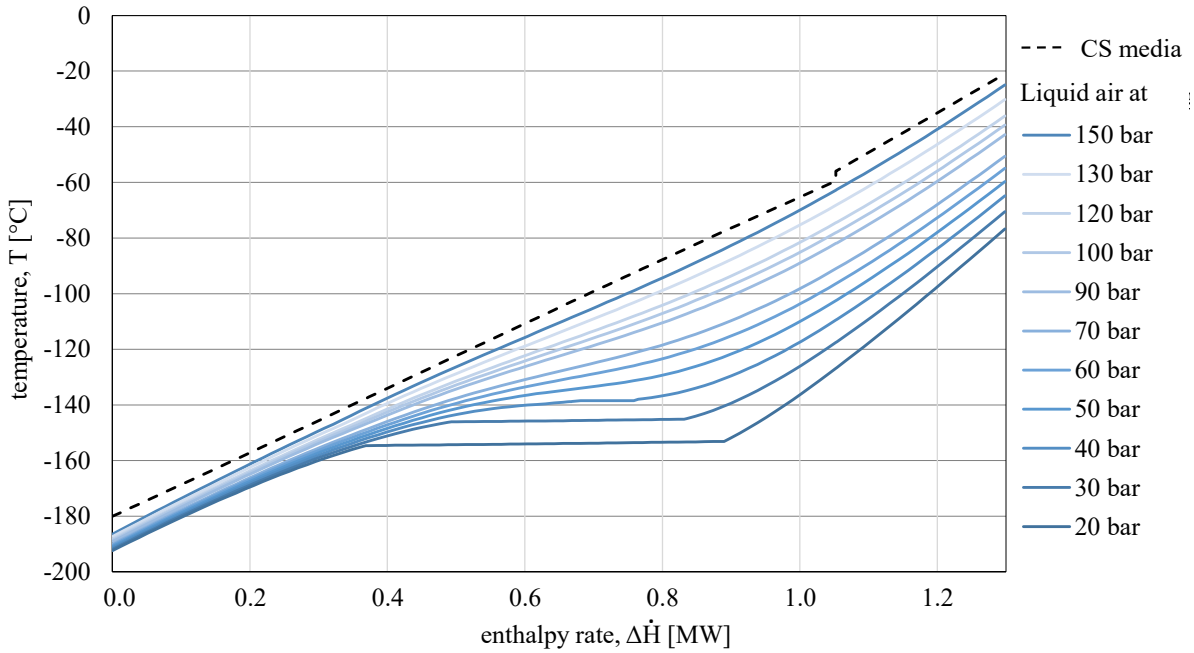

Figure 4.7: T, ΔḢ-diagram of the main heat exchanger in the discharge process (MHE2) for different pressures of the liquid air evaporating in heat exchange to the cold storage media (cumulative curve).

4.3.3. Discharging unit

Pressurizing and evaporation (block (d) in Figure 4.2)

During discharge, the liquid air undergoes a Rankine cycle. At first, the subcooled liquid air is brought to high pressures in a cryogenic pump before being evaporated, superheated, and expanded for electricity generation. In the simulation, the liquid air enters the cryopump slightly subcooled (1.1 bar, -192 °C) to avoid cavitation.

A cryopump is a vacuum pump that seizes liquid gas by surfaces cooled to cryogenic temperatures (< 120 K) [131]. Both centrifugal and positive displacement pumps may operate as cryogenic compression pumps, and at large-scale, high-pressure positive displacement

pumps operate at pressures higher than 200 bar [47]. A multi-stage centrifugal pump out of aluminum and stainless steel with copper windings in the motor was suggested for commercial-scale CES systems to enable discharge pressures of up to 200 bar and mass flowrates of up to 300 kg/s [8]. Brett and Barnett [18] stated that 200 bar and mass flow rates necessary for commercial size are the long-term targets for CES further development, while a single cryogenic pump can already achieve flowrates greater than necessary for 20 MW (50 kg/s) discharge capacity and pressures > 100 bar, e.g., applied in LNG regasification terminals.

The power output of the discharge unit $\dot{W}_{dis}$ increases with the pumping pressure p_{CP} until a threshold is reached above which the additional power generated in the turbines $\sum \Delta \dot{W}_T$ counterparts the additional pumping power necessary to increase the pressure $\Delta \dot{W}_P$. The threshold depends on the discharge configuration. Additionally, the amount of cold recycled in the evaporation process reduces with increasing pressure, reducing the effectiveness of the charging process [16], Figure 4.7. In Figure 4.8, the roundtrip efficiency is displayed over the pumping pressure (< 200 bar).

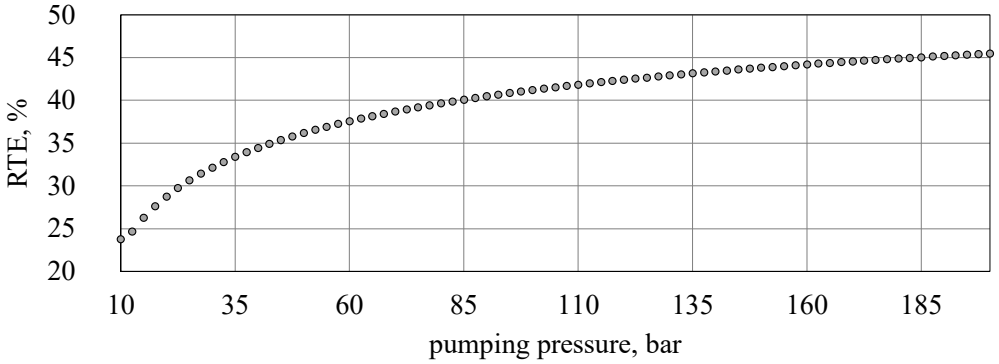

Figure 4.8: RTE over pumping pressures for Base Case B.

Ameel et al. [10] stated that the enhancement in power output for pressure increase between 100 and 500 bar is insignificant. Morgan et al. [16] identified the threshold between 150-200 bar. Several other feed pressures were suggested in the literature, Table 2.1. In the evaluated system, this power threshold is reached at a pressure above 200 bars. The feed pressure of the Base Case was set to 150 bar, and the isentropic efficiency is assumed with 0.75 [57]. The isentropic efficiency was estimated low in comparison to values suggested in the literature (0.75-0.80 [16, 42, 39, 51]) based on a recommendation from the industry.

The pressurized liquid air is subsequently fed to the second main heat exchanger (MHE2) and re-gasified. The heat exchange in the MHE2 is shown in Figure 4.7 for different pumping pressures. The air is further heated in heat exchange with the stream exiting the expansion line (HE4) and superheated in heat exchange with the heat storage media (HE5), Figure 4.2.

Expansion process (block (e) in Figure 4.2)

The high-pressure high-temperature gas is expanded in four gas turbine stages with reheating. The superheating occurs with the aid of the heat supplied by the heat storage. The isentropic efficiency of the turbines is estimated at 90 %. Values proposed in the literature on CES systems reached 90-92 % [14, 57]. The specific energy generated per kg of liquid air increases linearly with the turbine inlet temperature (TIT), Figure 4.9.

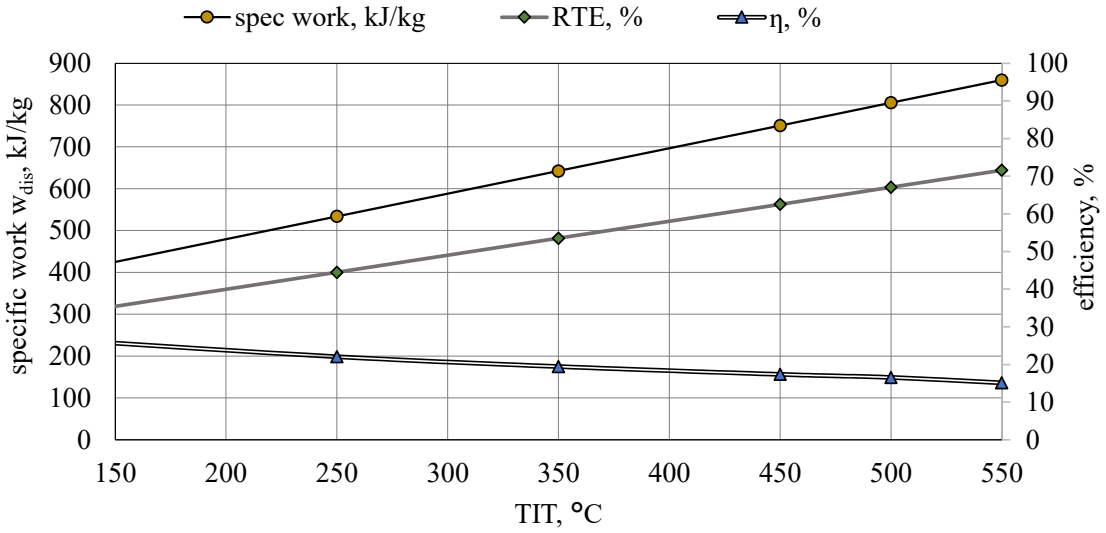

Figure 4.9: Specific work of the discharge unit per kg of liquid air, RTE, and η over the TIT based on the assumptions made for the integrated systems (section 4.4, w_{char} = 1,200 kJ/kg).

For an adiabatic system with heat recovery and storage (TIT ≈ 200 °C), the specific energy is approximately 475 kJ/kg while with the integration of waste heat at 350-450 °C values of 650-750 kJ/kg are reached. The integration of heat sources and sinks is further discussed in section 4.4.1. Energy densities and efficiencies reported in the literature are given in Table 4.4. The values range from 360 to 900 kJ/kg, which are realizable with waste heat integration and TIT of 175-600°C. The *RTE* accordingly would range from 37 to 70 %, [17] and [18] claim to reach even higher values. In order to reach higher *RTE* at energy densities that are similar to those achieved in adiabatic CES systems or with waste heat integration are only realizable with integrated systems, e.g., with LNG waste cold. Integrated systems are subject to the following section 4.4.

Table 4.4: CES energy densities and efficiencies reported in the literature.

Energy density [kJ/kg]	Efficiency [%]	Source
540-900	40-60	[37]
360-720	70 +	[17]
360-515	60, 70+	[18]
540	47-57	[16]

4.4. Integrated systems

The reduction of the energy requirement in the liquefaction process and the increase of the specific power output of the discharge process were identified as two primary research and development objectives, that need to be met to prepare CES technology for the market [20]. The integration of CES systems with internal/external thermal energy sources aims for such enhancement in performance. Aim of the exergy-based evaluation of the "integrated systems" is to identify the potential of integrated CES systems concerning thermodynamic and economic performance.

In this section, the design and simulation of the systems with the integration of different heat sources and sinks is discussed. A total of ten system configurations were assessed in this work (Figure 4.10). Waste heat (TIT 350-450°C) and internal combustion are considered an alternative to heat storage in the a-CES system. The integration of LNG waste cold instead of or in combination with cold storage is also considered. Two adiabatic CES systems, one without cold storage (a-CES w/o CS) and one with CS (a-CES). The a-CES systems were compared to two systems with waste heat integration at 350 °C and 450 °C, four systems with LNG waste cold integration and two diabatic CES systems with combustion.

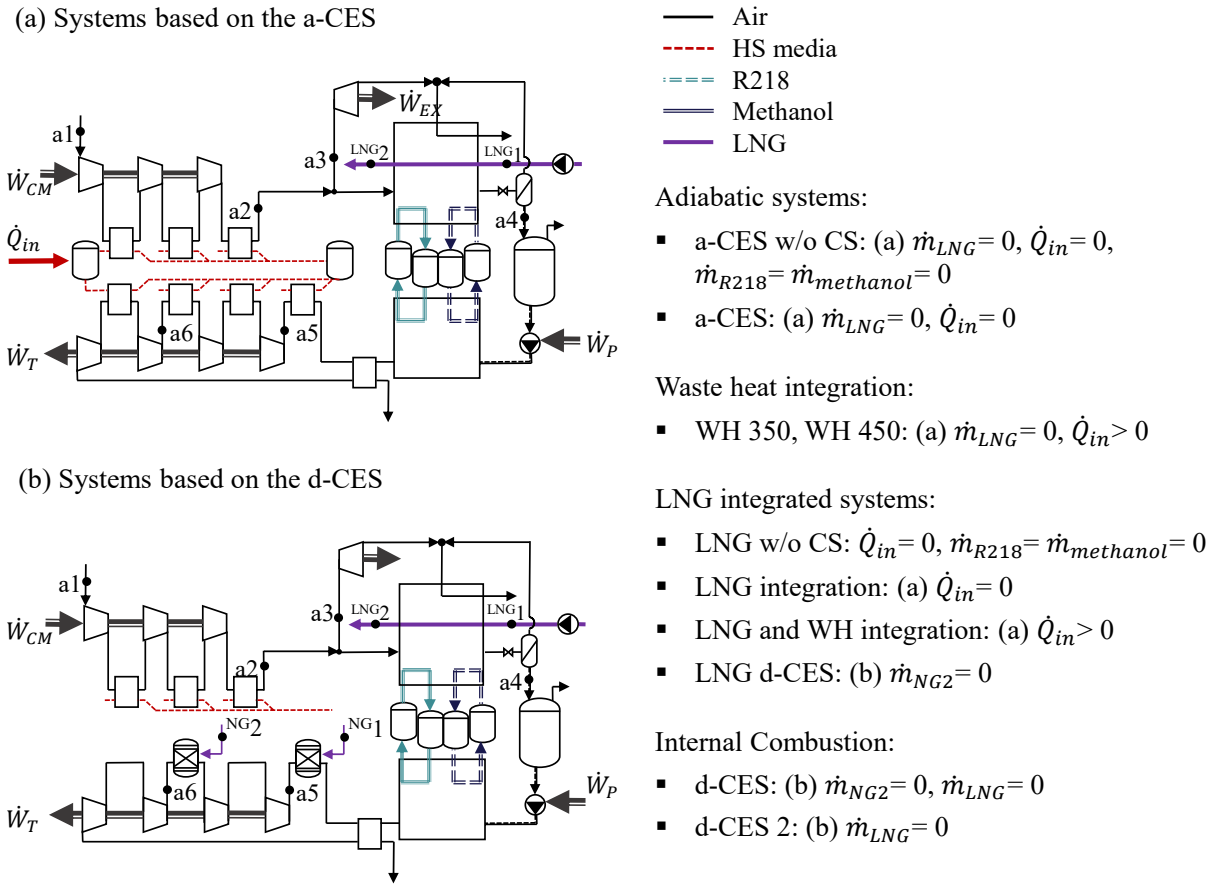

Figure 4.10: Flowsheets of the integrated systems (a) based on the adiabatic CES system and (b) based on the diabatic CES system.

For exergetic analysis the compression pressure and mass flow rate $\dot{m}_{a1}$ in the compressors (compression work $\dot{W}_{CM}$) were kept uniform for all system configurations. In economic analysis, the results for

a) a common mass flow rate $\dot{m}_{air}$= 200 kg/s, and

b) a common discharge capacity of $\dot{W}_{dis}$= 100 MW,

were compared. All considered systems are based on the design parameters of the Optimized Case (Table 4.2) and the general assumptions made for the isentropic efficiencies of the turbomachinery (Table 4.1).

The stream values of the systems presented in Figure 4.10 are given in Table C.5 and Table C.6 in Appendix C. The power and heat capacities of the work and heat flows indicated in the Figure 4.10 are given in Table 4.5. The systems are described in detail in the following subsections.

Table 4.5: Power and heat capacities in MW for all work and heat flows indicated in Figure 4.10 for the ten systems considered in comparative analysis.

System	Abbrev.	$\sum \dot{W}_{CM.i}$	$\dot{W}_{EX}$	$\dot{\boldsymbol{W}}_{\boldsymbol{char}}$	$\dot{Q}_{in}$	$\sum \dot{W}_{T.i}$	$\dot{W}_{CP}$	$\dot{\boldsymbol{W}}_{\boldsymbol{dis}}$
Adiabatic CES systems								
without cold storage	a-CES w/o CS	138.2	21.2	117.0	-	59.1	2.9	56.1
with cold storage	a-CES	138.2	11.2	127.0	-	105.2	5.2	100.0
Waste heat integration								
with TIT of 350 °C	WH 350	138.2	11.2	127.0	222.1	141.0	5.2	135.8
with TIT of 450 °C	WH 450	138.2	11.2	127.0	329.7	164.0	5.2	158.8
LNG integration								
without cold storage	LNG w/o CS	138.2	20.1	118.0	-	64.6	3.2	61.4
with cold storage	LNG	138.2	2.8	135.4	-	144.1	7.1	137.0
with waste heat	LNG + WH	138.2	2.8	135.4	290.0	224.7	7.1	217.6
with combustion	LNG d-CES	138.2	2.8	135.4	-	297.4	4.1	293.4
Diabatic CES systems								
with single combustion	d-CES	138.2	11.2	127.0	-	217.4	3.0	214.4
with double combustion	d-CES 2	138.2	11.2	127.0	-	188.7	3.0	185.8

4.4.1. Waste heat integration

Recovery of "waste heat" was identified as one of the core potentials of CES (section 2.3) [8, 10, 14, 37]. As the heat of compression recovered in a-CES systems, may exceed TIT of 200 °C and waste heat (WH) integration entails the colocation to the waste heat source, only high-temperature WH higher than 300 °C is considerable for CES systems.

The sources for high-temperature waste heat are limited. The quality of waste heat from electricity production was found insufficient in terms of exergy content and temperature level (< 100 °C). The European annual waste heat potential in the temperature range of 200–500 °C was estimated higher than 75 TWh [60]. In the industry and transportation sectors, high-quality waste heat (> 300 °C) is disposed of [132]. For application in CES, only industrial waste heat is of potential. Apart from the quality of the waste heat, the thermal carrier of the waste heat is also of importance. The heat rejected from industrial processes is contained in various thermal carriers, e.g., exhaust gases, low-quality steam, hot oil, cooling water, or commodities such as hot steel [60]. Among the numerous industrial processes and sectors, the quantity of waste heat varies strongly [133]. The industrial sectors with the highest potential of high-grade waste heat (200-500 °C) are iron and steel, non-metallic mineral, and chemical industry [60]. In Germany alone, the high-grade waste heat potential of iron and steel industry is estimated larger than 45 TWh annually [60].

In the simulation, high-grade waste heat necessary to elevate the TIT to 350-450 °C was taken into consideration. The power output of the discharge unit increases linearly with increased TIT, Figure 4.9. The flowsheet for CES with waste heat is similar to that of the adiabatic CES system except for an additional heat rate $\dot{Q}_{in}$, that is supplied to the heat storage, Figure 4.10 (a). Reason for the waste heat being supplied to the heat storage is that the waste heat is disposed of continuous industrial processes, which have operation hours independent from that of the discharge process of the CES system. Due to the high temperatures, the heat transfer and storage media of the system with waste heat integration is thermal oil (Dowth-01) at a pressure of 6 bar. The power and heat capacities of the systems with waste heat integration (WH 350, WH 450) are compared to the adiabatic CES system in Table 4.5. The stream values indicated in Figure 4.10 (a) are given in Table C.5 in Appendix C.

4.4.2. Diabatic CES with combustion

As an alternative, a CES can contain a combustion process in which fuel is burned to supply additional heat, increasing the temperature of the high-pressure gas before the expansion process [12, 134]. The combustion of natural gas (NG) causes the least specific GHG emissions and pollution. Being the relatively "cleanest" conventional fuel, NG is used in the combustion of the evaluated d-CES systems. The NG was simulated with CH_4 and a lower heating value of 50 MJ/kg.

Two diabatic CES systems were considered in the analysis: d-CES, with a single combustion chamber, and d-CES 2, with two combustion chambers. The flowsheet of the diabatic CES systems are shown in Figure 4.10 (b), the corresponding stream values are given in Table C.6 in Appendix C. The pressure drop in the combustion chamber (CC) is estimated with 4-8 % of the inlet pressure adopted from [127], depending on the size of the CC.

In the CES systems that employ combustion, heat storage can be avoided. As a result, a higher mass flow rate of pressurized water at ambient temperature is used as a cooling medium in the intercoolers.

With increasing mass flow of the fuel, the *RTE* and the exergetic efficiency of the d-CES system rise, Figure C.3. The mass flow rate of the fuel was adjusted to the maximum operating temperature of the construction material of the turbines (metal alloys, < 1100 °C [118]) to avoid excessively expensive equipment. The total mass flow of the fuel for both systems was kept consistent for comparison of the systems performance and cost-effectiveness. With a mass flow rate of $\dot{m}_{NG}$= 4.5 kg/s the temperature at the inlet of the subsequent turbine is augmented to 1,100 °C in the d-CES 1 system. In the d-CES 2 system, the TIT of the two turbines is 720 °C and 730 °C. The reason for introducing a second combustion chamber is to use cheaper materials for the turbines while achieving comparable power capacity of the discharge unit.

The power and heat capacities of the d-CES systems (for $\dot{m}_{air}$= 200 kg/s) are compared to the a-CES system in Table 4.5. The liquid air is pumped to 80 bar instead of 150 bar in the d-CES systems, reducing the energy requirement of the cryogenic pump. The d-CES systems achieve approximately twice the power capacity and *RTE* than the a-CES. The performance of the d-CES 2 system is by 13.4 % lower.

4.4.3. Integration of LNG low-temperature exergy

The most prominent waste cold source is the regasification process of LNG. Natural gas is globally transported by ship in the form of LNG in cryogenic storage vessels at about atmospheric pressure and a temperature of approximately - 160°C [135]. The NG is fed back to the transmission grid at pressures between 30-70 bar [136]. For the transmission grid, a pressure of 70 bar is required, while local distribution requires lower pressures. The mass flowrates in LNG terminals may exceed values of 150 kg/s [137].

In the considered systems, the LNG is fed to the MHE1 of the liquefaction process with a pressure of 32 bar and a temperature of - 158 °C. Four different systems were simulated and evaluated in this work. LNG regasification was integrated into:

- an a-CES system without cold storage (LNG w/o CS),
- an a-CES system with cold storage (LNG),
- a CES system with waste heat integration at 450 °C (LNG + WH), and
- a d-CES system with NG combustion (LNG d-CES), see Figure 4.1(a) and (b).

The effect of integrating LNG to the adiabatic CES system is depicted in Figure 4.11. With a higher mass flow of LNG fed to the system, the splitting ratio can be reduced, and a higher share of the air mass flow is fed to the MHE1 and liquefied. The splitting ratio and liquid yield are limited by the minimum temperature difference in the MHE1, section 4.3.1(c). The *RTE* and the exergetic efficiency of the system ε_{tot} increase linearly at first. When the mass flow of the LNG reaches approximately 9 % of the mass flow of the compressed air, the maximum value for the *RTE* and the ε_{tot} is reached.

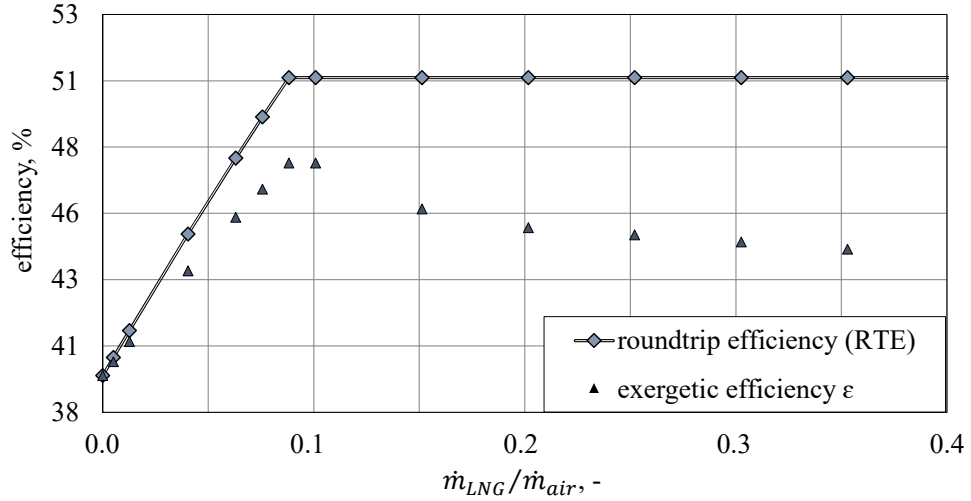

Figure 4.11: RTE and exergetic efficiency over the specific mass flow of LNG.

With the further supply of LNG, the *RTE* stays constant. The exergetic efficiency declines with higher mass flows $\dot{m}_{LNG}$, as the exergy of fuel–the low-temperature exergy supplied by the LNG fed to the system–increases further, while the exergy of the product stays constant. For the LNG systems, the mass flow of the LNG was set to 8.8 % of the mass flow of the air to achieve maximum exergetic efficiency for all systems with the exception of the system without cold storage (LNG w/o CS). For the LNG w/o CS system, the minimum splitting ratio and maximum efficiency is achieved at a mass flow ratio ($\dot{m}_{LNG}/\dot{m}_{air}$) of 2.8 %.

The stream values for the states indicated in Figure 4.10 are given for the LNG integrated systems in Table C.7. The LNG leaves the MHE at a temperature of – 4 °C and a pressure of 30 bar, to be fed to the local distribution grid [136]. The share of the liquefied air is increased by 10 % (w/o CS) and by 40 % in respect to the a-CES systems after the integration of LNG waste cold. The results of the comparative analysis of the integrated CES systems are discussed in Chapter 5.3.

4.5. Summary of the design and simulation

Several design options exist for the charge, storage, and discharge process of CES systems. In the pre-design phase, different design options were assessed and are discussed in this chapter. Two types of systems can be differentiated:

- the adiabatic stand-alone CES systems, and
- the integrated CES systems.

Two sets of assumptions are presented for the *Base Case(s)* and the *Optimized Case(s)*. The Base cases refer to the two stand-alone adiabatic CES systems that are undertaken comparative exergetic and economic analysis followed by exergoeconomic analysis and optimization. The integrated systems are adopted from the final design of the Optimized Case configuration and are extended with external heat sources and sinks. Waste heat and internal combustion were integrated as heat sources. As heat sink, the integration of LNG instead of or in combination with cold storage was considered.

For correct comparability, the capacities were kept consistent in the comparative analysis. Either the compression work $\dot{W}_{CM}$, or the discharge power $\dot{W}_{dis}$ were kept constant as common ground. The processes simulation was undertaken in Aspen Plus® software, while the evaluation was commenced in the Engineering Equation Solver (EES).

Chapter 5: Results and discussion

5.1. Evaluation of different charging processes for adiabatic CES

This section presents the results from the evaluation of different charging process configurations in adiabatic CES systems with exergy-based methods. At first, the performance of six different liquefaction processes is compared using energetic and exergetic analysis with and without the integration of cold storage. Subsequently, the effect of cold storage on different system parameters of the liquefaction processes is quantified. Concerning the three liquefaction processes with the highest exergetic efficiency, further sensitivity analyses are undertaken to identify the optimal system pressure. The three systems are compared, applying an economic analysis at optimal system pressure.

5.1.1. Energetic and exergetic evaluation of the liquefaction processes

The results of the energetic and exergetic analyses of the six analyzed liquefaction configuration before and after the integration of cold storage are presented in Figure 5.1. The integration of cold storage significantly increases the liquid yield γ (Figure 5.1 (a)). The liquid yield of the simple Linde and the dual-pressure Linde is tripled. The liquid yield in the Claude-based systems is increased by 80-90 %. The exergy of the product increases correspondingly.

With an increase in the mass flow rate of the liquefied air $\dot{m}_{liquid\ air}$, the low-temperature exergy supplied to the liquefaction process by the cold storage $\dot{E}_{cold}$ increases proportionally. With the addition of cold storage, also a substantial reduction of the specific work required to produce one kg of liquid air (w_{char}), by 30 to 70 %, is observed for all processes. Thus, the cold storage augments the exergetic efficiency considerably by up to 200 %, as shown in Figure 5.1 (b) and (c).

Despite the more significant reduction in the specific work requirement in the Linde-based configurations, their overall performance cannot compete with that of the Claude-based configurations. The simple Claude process, the Heylandt process, and the Kapitza process reach the highest exergetic efficiencies (69-72 %), have the lowest specific work requirement (1,435-1,533 kJ/kg) and reach the highest liquid yields (0.566-0.601).

For the most efficient liquefaction configurations – the Claude-based processes – a sensitivity analysis was conducted. The compression (liquefaction) pressure was varied (p_{CM} = 70-140 bar), and the splitting ratio r was reduced to its absolute minimum value. The effect of these variations on the exergetic efficiency ε can be seen in Figure 5.2. The exergetic efficiencies for the respective liquefaction pressure are given over the splitting ratio for (a) the Claude and the Kapitza process and (b) the Heylandt process.

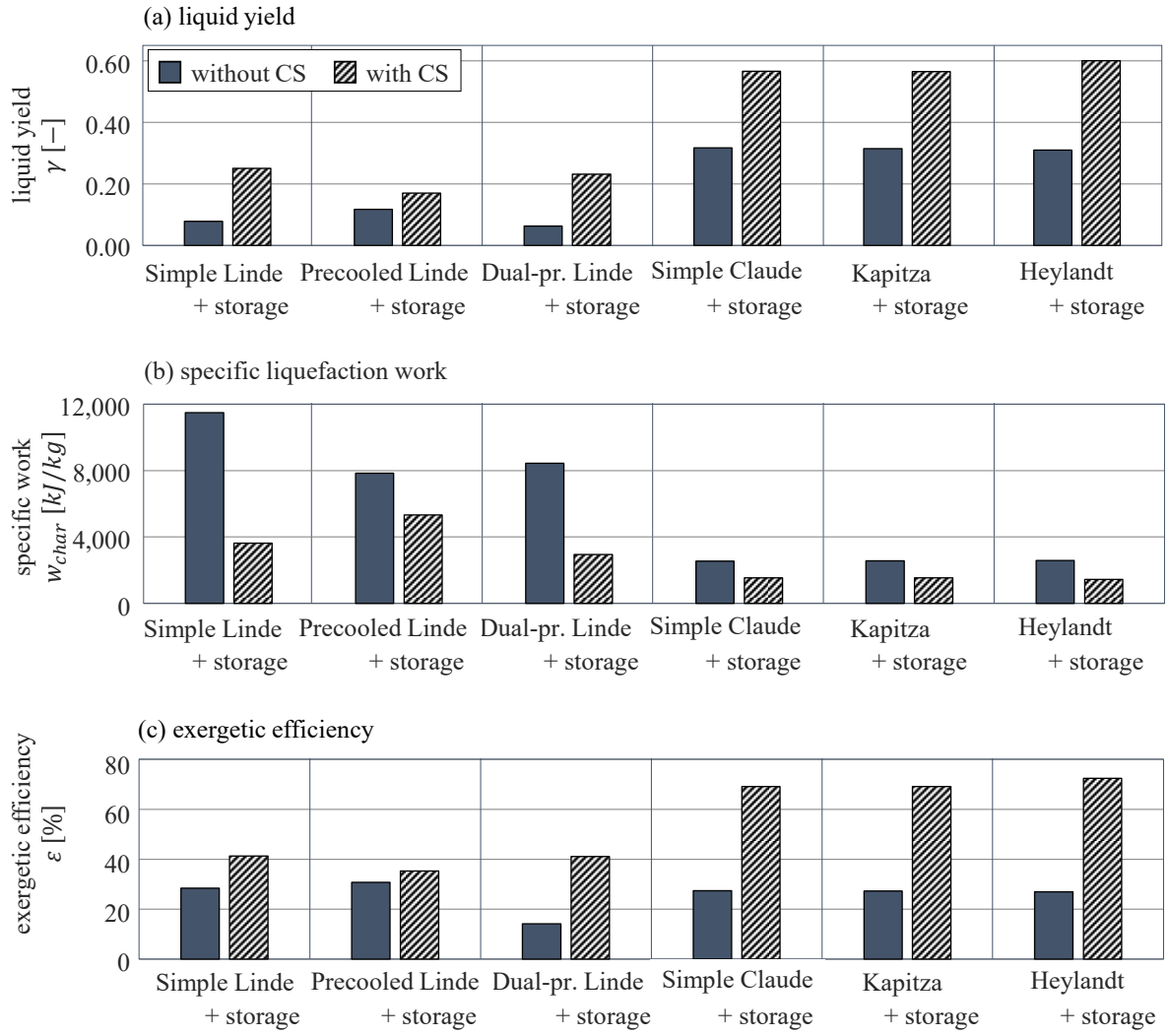

Figure 5.1: Results of the energetic and exergetic evaluation for the liquefaction processes with/without integrated cold storage (CS).

With increasing liquefaction pressure, lower splitting ratios are achievable (Figure 5.2). The share of air liquefied in the process increases with a reduction in the value of the splitting ratio ($r = \dot{m}_{EX}/\dot{m}_{CM}$), as a greater mass flow enters the MHE1 and the throttling process. The temperature difference in the MHE1 decreases with a reduction in "cold feed" ($\dot{m}_{EX}$) and a simultaneous increase in "hot feed" ($\dot{m}_{CM} - \dot{m}_{EX}$). The minimum splitting ratio is therefore restricted by the minimum pinch temperature ($\Delta T_{MHE1,min} \rightarrow 1$ K).

By minimizing the splitting ratio the maximum liquid yield γ_{max}, the maximum efficiency ε_{max}, and the minimum specific liquefaction work w_{min} are obtained for the respective pressure. The maximum exergetic efficiency curves are indicated in Figure 5.2 with a solid black line. The thermodynamic performances of the Claude and Kapitza processes are non-differentiable. Reason for this is the temperature difference of only 2 K of the two mixing streams (Figure 4.6) and that the minimum pinch temperature in the MHE1 was set to 1 K for all processes. The T, ΔḢ-diagrams of the MHE1 for all processes are given in Figure D.1 and Figure D.2 in Appendix D.

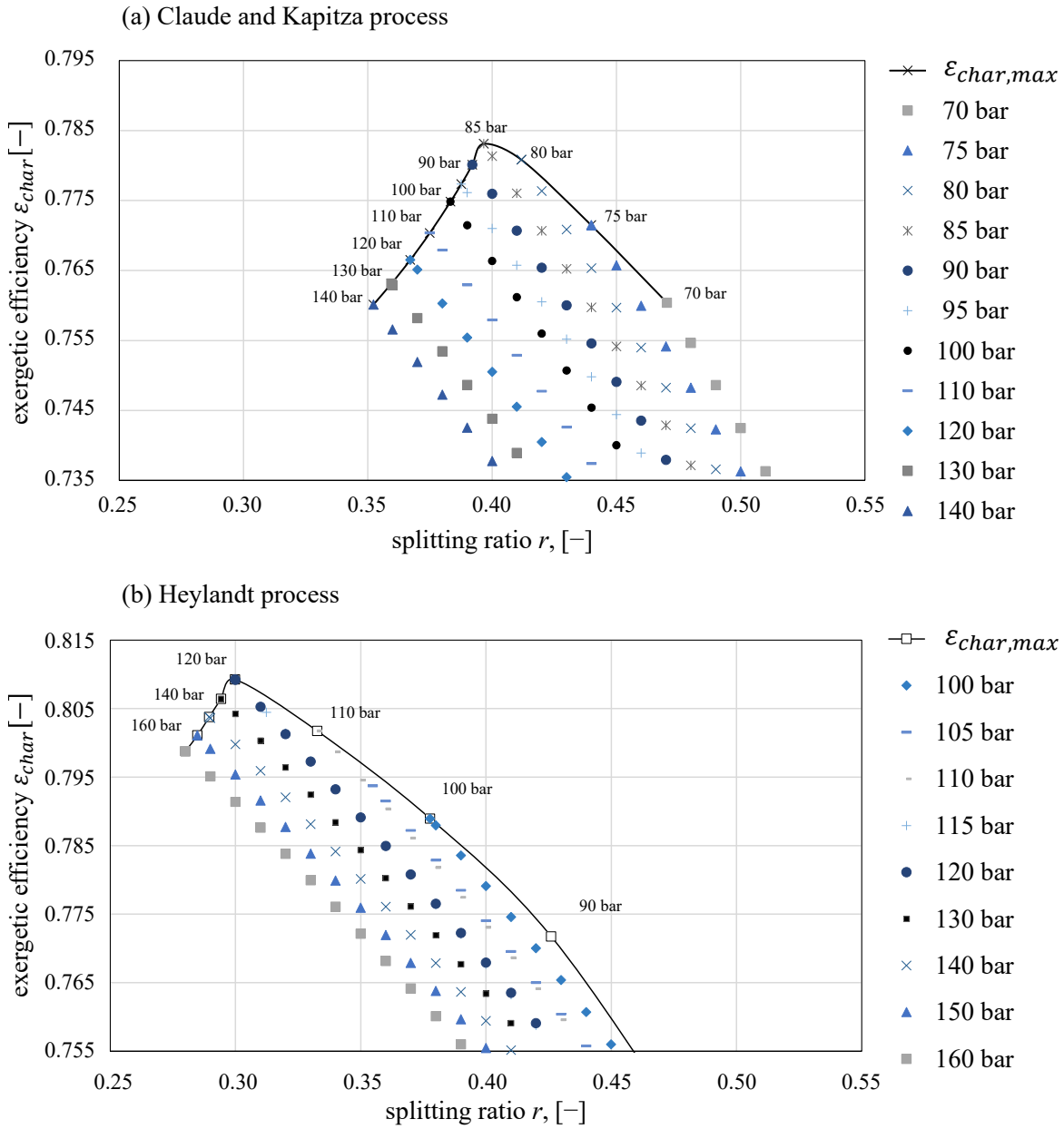

Figure 5.2: Sensitivity analysis results for (a) the Claude and the Kapitza process and b) the Heylandt process: the exergetic efficiency ε over splitting ratio r, for various liquefaction pressures.

The Heylandt process reaches lower splitting ratios (< 0.3) and higher exergetic efficiencies (> 80.5 %) than the Claude and the Kapitza process (r > 0.35, ε_{max}< 78.5 %), Figure 5.2. The processes reach their maximum exergetic efficiency ε at different splitting ratios and pressures. This confirms that comparing the systems at a single pressure level is not sufficient. The Heylandt process reaches its maximum exergetic efficiency ε_{max} of 80.9 % at a splitting ratio of 0.3 and a pressure of 120 bar while the Claude and the Kapitza process reach ε_{max} = 78.3 % at a splitting ratio of 0.397 and a pressure of 85 bar. In Figure 5.3, the change in the minimal specific work required for liquefaction w_{min} and the maximum liquid yield γ_{max} are given over the splitting ratio r for the Claude and the Heylandt process.

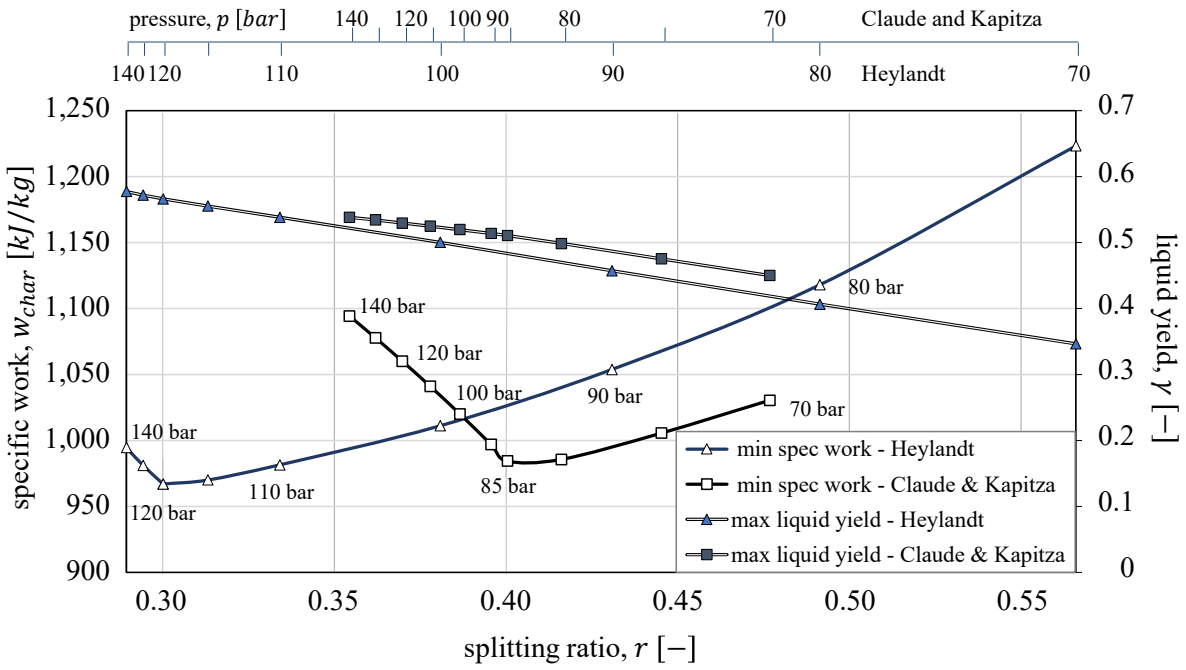

Figure 5.3: Minimum specific work required for liquefaction w_{char} and maximum liquid yield γ over the splitting ratio r of the Claude/Kapitza process and the Heylandt process.

In Figure 5.3, the liquefaction pressures are indicated with a secondary x-axis. The reduction in the splitting ratio r at higher pressures is less significant. The maximum liquid yield γ_{max} increases linearly with the reduction in the splitting ratio r. Thus, at higher pressures the increase in the maximum liquid yield γ_{max} is less substantial. As a result, the minimal specific work required for liquefaction w_{min} increases at higher pressures as the additional compression power outweighs the increase in air liquefied (γ_{max}). The minimal specific liquefaction work w_{min} thus reaches a minimum at 85 bar for the Claude/Kapitza process and at 120 bar for the Heylandt process. The process parameters at the minimum work requirement are consistent with that of the maximum efficiency ε_{max}.

The minimum work required to liquefy one kg of air in the Heylandt process amounts to 967 kJ/kg (120 bar). The Claude/Kapitza process requires more specific liquefaction work w_{min}= 984 kJ/kg (85 bar). For liquefaction pressures lower than 95 bar, the Claude/Kapitza process reaches lower values for w_{min} and higher values for γ_{max} and ε_{max} than the Heylandt process. While, for variable and higher pressures, the application of the Heylandt process in CES systems is preferable in terms of thermodynamic performance, Figure D.3 in Appendix D.

5.1.2. Economic evaluation of the Claude-based liquefaction processes

The economic analysis was conducted for the optimal design of each of the three Claude-based liquefaction units. The design parameters are given in Table 5.1. The liquefaction capacity of all processes was adjusted to supply a 100 MW/400 MWh a-CES system. The results of the economic analysis are presented in Table 5.2. Except for the higher charging pressure p_{CM} of the Heylandt system, all design parameters of the Claude and the Kapitza process-based systems are similar. The liquid yields γ and specific work requirement of the liquefaction processes correspond to a *RTE* of approximately 44.4-46.8 %, which is within the expected range of 40-60 % for stand-alone CES systems [37, 38].

The results of the economic analysis for the Claude and the Kapitza process differ despite their identical design parameters and similar performance in the energetic and the exergetic analysis. The small difference in the size of the MHE1 results in a notable difference in component costs. The specific investment costs and the production costs per kg of liquid air are lowest for the Kapitza liquefaction process, Table 5.2.

When comparing the results of energetic and economic analysis of the liquefaction processes with integration of cold storage to values for stand-alone air liquefaction plants, the effect of cold storage becomes even more apparent. The work required to produce one ton of liquid air is reduced to the half (~ 290 kWh/ton), the values reported in literature range from 520 to 760 kWh/ton [8, 50]. The production costs of liquid air are also significantly reduced, amounting to only 14-17 €/ton instead of 37-48 €/ton [8] without cold storage. The specific costs associated with the initial investment for the liquefaction unit are also reduced by half, compared to values reported in the literature for the Claude process of 1.640 €/kW [51].

Table 5.1: Design parameters for the three Claude-based CES systems compared in economic analysis.

Parameter	Unit	Claude process	Heylandt process	Kapitza process
Liquefaction pressure	bar	85	120	85
Charging capacity	MW	112	107	113
Liquefaction capacity	tons/day	9,256	8,985	9,256
Liquid yield	-	0.503	0.559	0.501

Table 5.2: Results of the economic analysis performed on the three Claude-based liquefaction units.

Parameter	Unit	Claude process	Heylandt process	Kapitza process
Specific investment costs	€/kW	807	959	803
Specific work requirement w_{char}	kWh/ton	291	286	292
Production costs of liquid air	€/ton	13.8	16.4	13.7

The TRR of the liquefaction units amounts to € 21.9, € 22.8 and € 20.8 million for the Claude, the Heylandt and the Kapitza process respectively. The most cost-efficient system is based on the Kapitza process with a specific production cost of the liquid air of $c_{liquid\ air}$ = 13.7 €/ton. The highest-efficiency system, which is based on the Heylandt process performed less well in economic analysis and reached by 20 % higher specific product costs of $c_{liquid\ air}$ = 16.4 €/ton.

5.2. Analysis and optimization of two adiabatic CES systems

In this section, two complete adiabatic CES systems based on the cost-optimal and the highest-efficiency liquefaction process are evaluated and optimized with exergy-based methods. The system employing the Kapitza process is henceforth referred to as *Base Case A* and the Heylandt-based system as *Base Case B*. The two system configurations are compared in the exergetic, economic, and exergoeconomic analysis. The base case systems are further optimized in iterative exergoeconomic analysis, and an optimal system configuration is identified.

5.2.1. Exergetic analysis

Both base case systems compared in this section were designed for the same exergy of the product $\dot{E}_{P,tot}$ – a discharge capacity of 100 MW. The results of the exergetic analysis on the system level: the exergy of the fuel $\dot{E}_{F,tot}$ the exergy destruction $\dot{E}_{D,tot}$, the exergy losses $\dot{E}_{L,tot}$ as well as the exergetic efficiency ε_{tot} are given in Table 5.3. The exergy values are given in MWh per cycle, to avoid misleading results caused by the different operating hours of the charge, storage and discharge unit. Each daily cycle entails eight charging hours and four discharging hours at full capacity. The exergetic efficiencies of selected components are given in Figure 5.4. Further results of the exergetic analysis on the component level are given in Table D.1 and Table D.2 in Appendix D.

Table 5.3: Results obtained from the exergetic evaluation of the two base case systems.

	$\dot{E}_{F,tot}$ [MWh/cycle]	$\dot{E}_{P,tot}$ [MWh/cycle]	$\dot{E}_{D,tot}$ [MWh/cycle]	$\dot{E}_{L,tot}$ [MWh/cycle]	ε_{tot} [-]
Base Case A	900.9	400.0	439.7	61.1	0.444
Base Case B	855.2	400.0	393.9	61.3	0.468

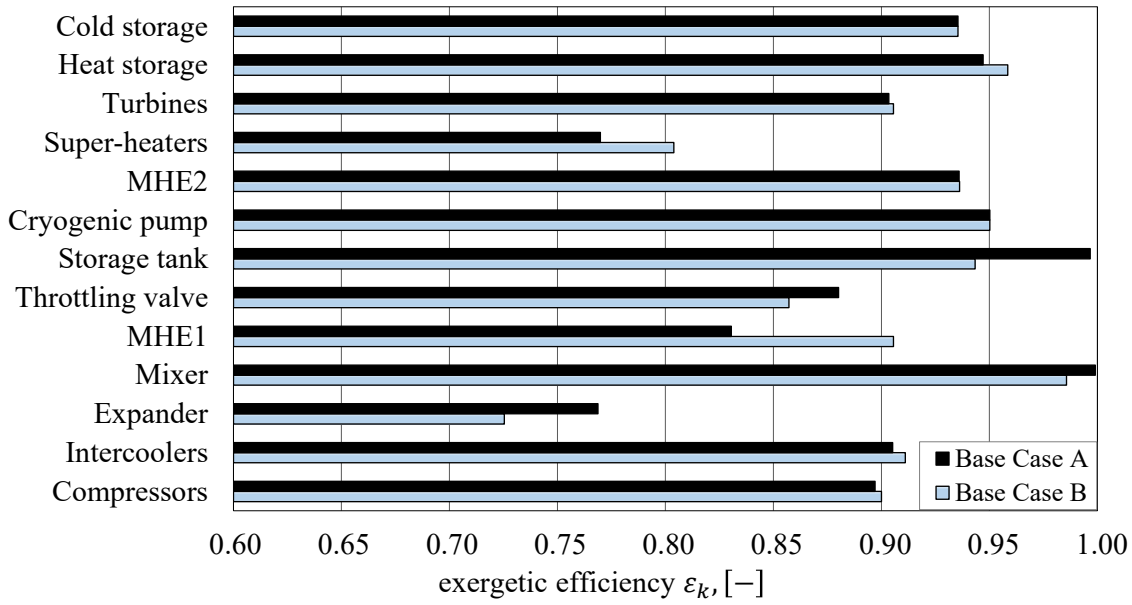

Figure 5.4: Exergetic efficiency ε_k of selected components of the two CES base case systems.

The exergy of the fuel $\dot{E}_{F,tot}$ to the Base Case A is 45 MWh higher than that of the Base Case B, due to the lower exergetic efficiency of 44.5 % in contrast to 46.8 %, Table 5.3. The exergy losses $\dot{E}_{L,tot}$ in both systems are relatively low (7 % $\dot{E}_{F,tot}$). All exiting streams and the heat vented from the heat storage after discharge are accounted as losses, while heat losses and leakages on component level, e.g., in the cold storage, are considered as exergy destruction. The exergy flow through the base case systems over the period of one cycle is presented Grassmann diagrams for the Base Case A and the Base Case B, in Figure 5.5 and Figure 5.6, respectively.

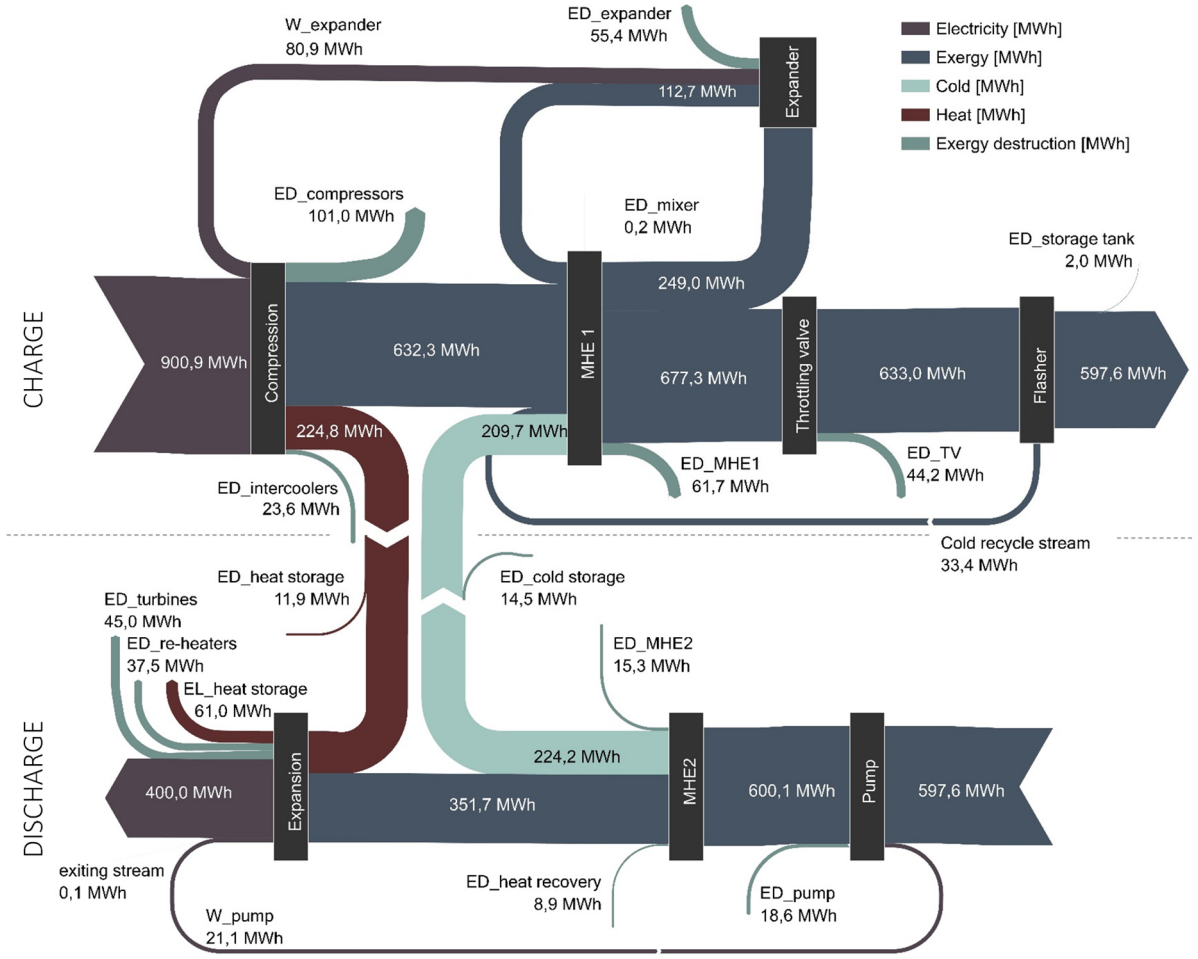

Figure 5.5: Grassmann diagram of the exergy flow in the Base Case A system throughout one cycle.

The Base Case B system shows higher exergetic efficiencies in most components except the expander, the throttling valve, and the mixer in the liquefaction process, Figure 5.4. The higher compression pressure of the Base Case B not only improves the thermodynamic performance of the compressors and the heat exchangers in the charging unit (MHE1, IC) but also increases the TIT and thermodynamic performance of the turbines and the superheaters in the discharge unit and the heat storage.

The high exergetic efficiency in the MHE1 in the Base Case B results from the lower logarithmic mean temperature difference (LMTD), Figure D.1. In the Base Case A, the high-

pressure air is fed to the MHE1 to reduce the temperature to approximately - 40 °C before a fraction of the mass flow is fed to the expander. In the Base Case B, the air is split before passing the MHE1, and the air enters the expander at about ambient temperature resulting in the lower exergetic efficiency of the expander. The stream exiting the expander is mixed with the recurring gas stream from the flash tank to be fed back to the MHE1. In the Base Case A, the air exits the expander at approximately the same temperature than the recurring stream (- 191°C), almost completely avoiding exergy destruction in the mixing process ($\varepsilon_{mix,A}$ = 99.9 %). In the expansion process of the Base Case B, the air is cooled down to only - 171°C causing avoidable exergy destruction in the mixing process caused by the temperature difference of the two mixing streams.

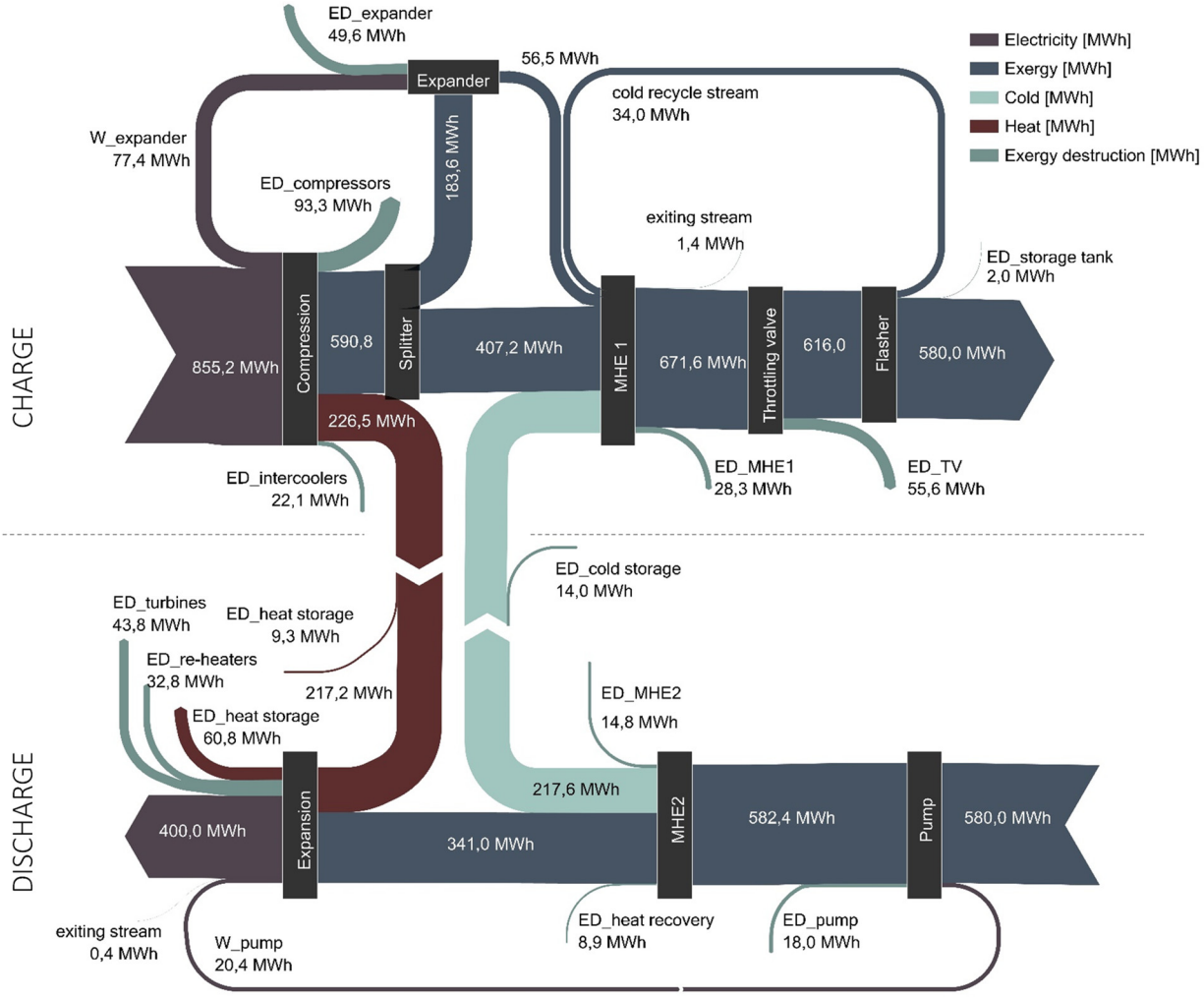

Figure 5.6: Grassmann diagram of the exergy flow in the Base Case B system throughout one cycle [36].

The cold expander serves two purposes in the liquefaction process. On the one hand, additional low-temperature exergy is supplied to the MHE1. On the other hand, the exergy of the fuel to the system $\dot{E}_{F,tot}$ is reduced by the electricity generated in the expansion process. In both cases, the expander supplies approximately 8 % of the $\dot{E}_{F,tot}$ despite the by 4.4 percentage points lower exergetic efficiency of the expander in the Base Case B ($\varepsilon_{EX,B}$ = 72.5 %).

The low-temperature exergy recovered from the evaporating liquid air in the MHE2 (discharge process) and supplied to the liquefaction process amounts to a significant share of the exergy of the liquid air of approximately 35 % (Figure 5.5 and Figure 5.6). The effect of the heat recovery is also of magnitude to the performance of the overall system, amounting to 37-39 % of the exergy the final product of the system $\dot{E}_{P,tot}$.

The major contributor to the exergy losses are the 61 MWh/cycle of thermal exergy vented from the heat storage to the environment after the discharge process. Reason for this is that the heat storage medium must be supplied to the intercoolers at ambient temperature to reduce the work requirement in the compression process. The thermal exergy could be utilized in an additional ORC, as reported in [41].

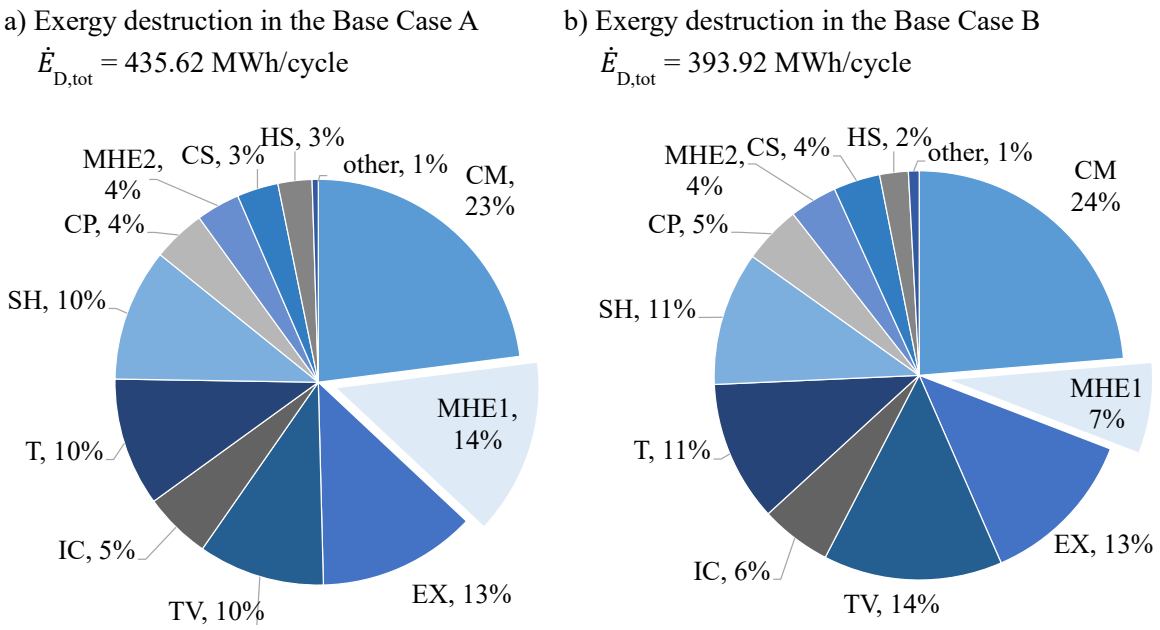

Charge unit		Discharge unit		Storage unit	
CM	the compressors	T	the turbines	CS	the cold storage
MHE1	the main heat exchanger 1	SH	the superheaters	HS	the heat storage
EX	the expander	CP	the cryogenic pump		
TV	the throttling valve	MHE2	the main heat exchanger 2		
IC	the intercoolers				

Figure 5.7: Breakdown of the exergy destruction of the overall system $\dot{E}_{D,tot}$ shown by the exergy destruction rates $\gamma^*_{D,k} = \frac{E_{D,k}}{E_{D,tot}}$ for Base Cases A and B.

The exergy destruction breakdown into the exergy destruction rates $\gamma^*_{D,k}$ of selected components of the base cases are depicted in Figure 5.7. In both base cases, the compressors cause the highest share of the total exergy destruction in the system, approximately 23-24 %, despite high exergetic efficiency (ε_{CM} = 90 %). Reason for this is the large exergy of the fuel entering the compression process of 850-900 MWh/cycle. For the Base Case A, the second highest contribution to the exergy destruction originates from the MHE1 (14 % $\dot{E}_{D,tot}$) followed by the expander (13 % $\dot{E}_{D,tot}$) and the throttling valve (10 % $\dot{E}_{D,tot}$). In the Base Case B, the exergy

destruction in the MHE1 is less dominant (7 % $\dot{E}_{D,tot}$), while the exergy destruction in the throttling valve (14 % $\dot{E}_{D,tot}$) is more significant.

The higher exergy destruction in the TV of the Base Case B is a result of the lower exergetic efficiency of 85.7 % ($\varepsilon_{TV,A}$ = 88.0 %) and the lower $\dot{E}_{D,tot}$. The absolute values of the exergy destruction in the components of the discharge unit (e.g., the turbines, the superheaters, the cryogenic pump, the MHE2) are smaller in the Base Case B despite the higher exergy destruction ratio $\gamma_{D,k}$, Figure D.5 in the Appendix D.

In both Base Cases A and B, the highest share of exergy destruction is caused in the charging process (64-66 %) while the exergy destruction in the discharge system amounts to only 28-30 % of the exergy destruction in the overall system. The high exergy destruction in the charging process underlines the importance of the selection of the liquefaction process to the overall exergetic efficiency. The share of the exergy destruction in the storage unit amounts to only 6 % of $\dot{E}_{D,tot}$, indicating that CES systems allow long storage durations at low losses. Further results of the exergetic analysis on the component level are given in Table D.1, Table D.2 and Figure D.5, in Appendix D.

5.2.2. Economic analysis

Results of the economic analysis revealed that similar to the economic analysis on the charging systems the TRR of the Base Case A is lower than that of the Base Case B. The TRR for the base cases amount to 37.3·10^6 € and 39.0·10^6 €, respectively. Moreover, despite the lower exergetic efficiency and *RTE* of the Base Case A, a lower $LCOE_{dis}$ of 255 €/MWh was achieved, compared to 267 €/MWh in the Base Case B. In Figure 5.8, the $LCOE_{dis}$ of both base cases is broken down into the cost associated with the levelized carrying charges of the charging, storage and discharging units as well as the levelized O&M costs and the levelized fuel costs.

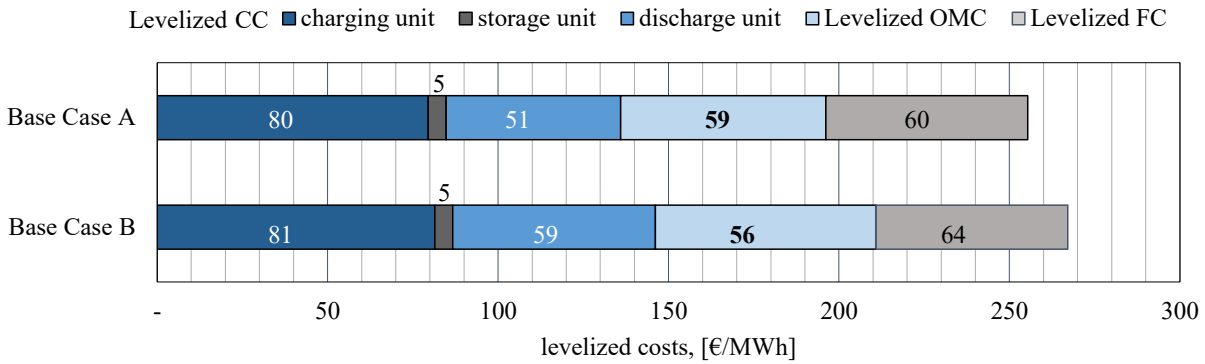

Figure 5.8: Cost breakdown of the $LCOE_{dis}$ into levelized carrying charges (CC), levelized fuel costs (FC) and levelized operation and maintenance costs (OMC) for the two base case systems.

Figure 5.8 shows that the levelized CC represent around 53.3 % and 54.3 % of the $LCOE_{dis}$ of the Base Cases A and B. The costs of the components in the charging system dominate in both base case systems, while the costs associated with the storage unit are rather insignificant.

The fuel to the systems refers to the electricity charged during the liquefaction process. Varying the price of electricity in sensitivity analysis showed that the $LCOE_{dis}$ of the Base Case A is smaller than that of the Base Case B for electricity prices smaller than 100 €/MWh. For higher electricity prices, the Base Case B becomes more economically feasible than the Base Case A.

The distribution of the bare module costs (BMC) of the main system components is shown in Figure 5.9. The heat exchangers are responsible for 62-64 % of the investment costs in both Base Case systems. In the Base Case B, the two main heat exchangers alone make up for 51 % of the total component costs. The MHE 1 is the major reason for the cost difference between both systems being twice as expensive in the Base Case B than in the Base Case A. The intercoolers, in contrast, are less costly in the Base Case B. The costs of all other components are similar for both base case systems. The specific investment costs amount to 2,089 €/kW and 1,942 €/kW of installed discharge capacity which is within the range for cost estimates suggested by [16, 18, 33, 64, 72].

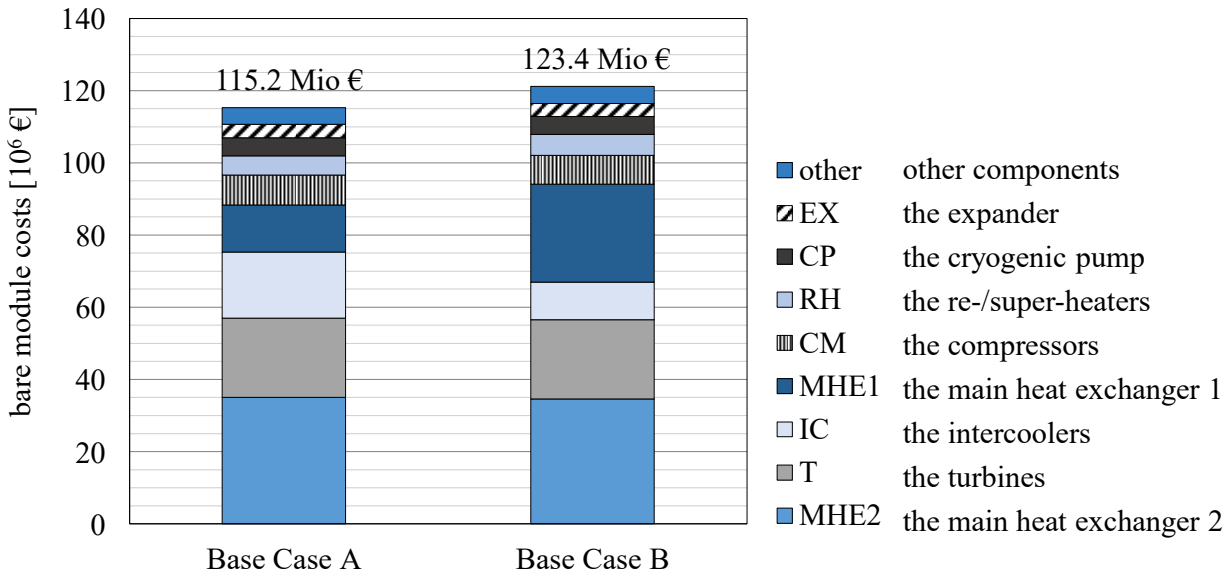

Figure 5.9: Bare module costs of the Base Cases A and B with indicated cost shares of selected components.

5.2.3. Exergoeconomic analysis and optimization

In the exergoeconomic analysis, the cost rate associated with the exergy of the fuel $\dot{C}_{F,tot}$, the exergy of the product $\dot{C}_{P,tot}$ and the thermodynamic inefficiencies – the exergy destruction $\dot{C}_{D,tot}$, and the exergy losses $\dot{C}_{L,tot}$ – are obtained. The results of the exergoeconomic analysis of the two base case systems are given in Table 5.4. The relative cost difference r_{tot} between the specific costs per unit of exergy of the product and the exergy of the fuel is large. The cost per exergy unit of the product of the system ($LCOE_{dis}$) is approximately ten times as high as the cost per exergy unit of the fuel to the system. The exergoeconomic factor f_{tot} is elevated ($\gg 0.5$) which indicates that the cost rate associated with the initial investment and the OMC outsizes the costs associated with the exergy destruction in the system.

Table 5.4: Results obtained in exergoeconomic analysis for the two base case systems.

	$\dot{Z}_{tot}$ [€/cycle]	$\dot{C}_{F,tot}$ [€/cycle]	$\dot{C}_{P,tot}$ [€/cycle]	$\dot{C}_{D,tot}$ [€/cycle]	$\dot{C}_{L,tot}$ [€/cycle]	$c_{P,tot}$ [€/MWh]	r_{tot} [-]	f_{tot} [-]
Base Case A	78.513	23,422	102,197	11,433	1,590	255	8.8	0.814
Base Case B	84.317	22,235	106,803	10,242	1,593	267	9.3	0.828

With the aim of identifying means to reduce the cost of the final product, the components with the highest associated total cost rate $\dot{Z}_k + \dot{C}_{D,k}$ are prioritized in exergoeconomic analysis and optimization. Five sets of components: *the main heat exchangers*, *the turbines*, *the intercoolers*, *the compressors* and *the reheater*s, make up more than 80 % of the sum of component cost rates in both base case systems.

In Figure 5.10, the component cost rates of the five prioritized components are displayed. For the majority of the components, the costs associated with the initial investment and OMC $\dot{Z}_k$ dominate, which is also indicated in an elevated exergoeconomic factor f_k.

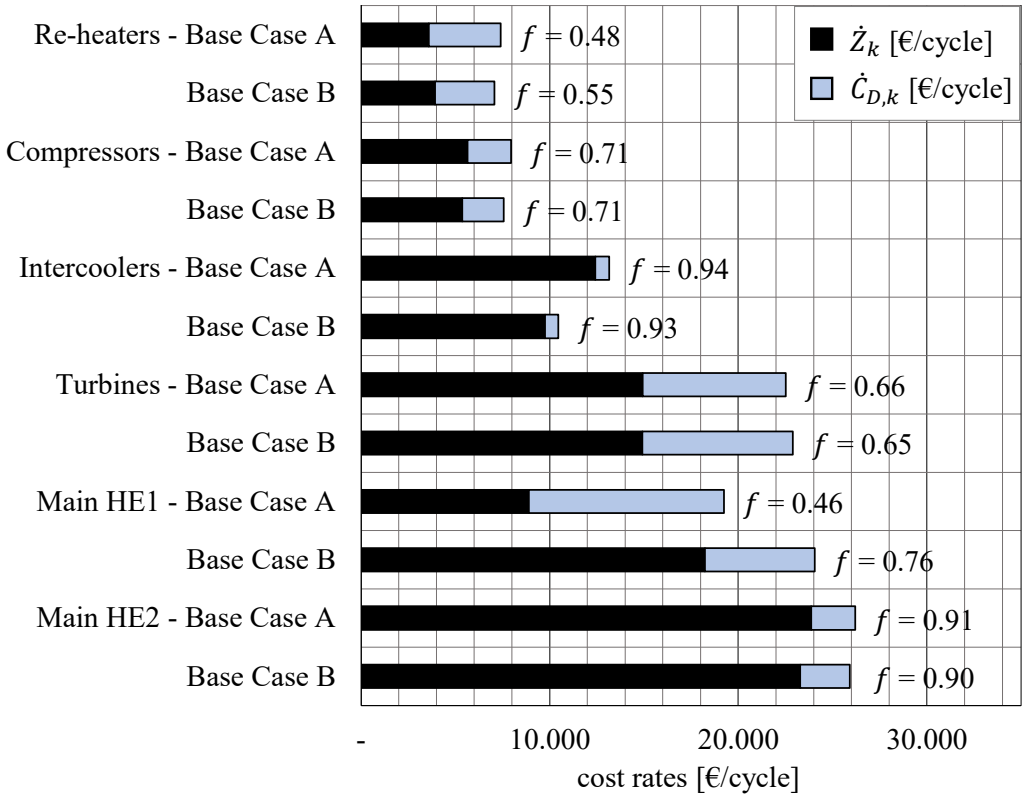

Figure 5.10: Exergoeconomic analysis results for the five components with the highest total cost rate $\dot{Z}_k + \dot{C}_{D,k}$.

Only in the MHE1 and the reheaters of the Base Case A the costs associated with the exergy destruction in the components $\dot{C}_{D,k}$ cause more than 50 % of the total cost rate of the respective component. For turbomachinery such as the turbines and the compressors an elevated exergoeconomic factor e.g., 0.6-0.8 is to be expected, while in heat exchangers the costs associated with the exergy destruction commonly takes over ($f_{HE} < 0.5$).

The objective for the prioritized components is to decrease the component cost rate $\dot{Z}_k$ while accepting a lower thermodynamic performance of the respective component in order to reduce the $LCOE_{dis}$. The decision variables that were selected to reduce the initial investment cost of the respective component are given in Table 5.5.

With the exception of the MHE1 in the Base Case A, the same changes to the selected decision variables were applied to both systems. The iteration in which the parameters were changed is given for both systems. The turbines and the compressors were not listed despite being the third and 5th most cost-intense components. Reason for this is that the reduction in component costs through parametric changes is not applicable. The investment costs of the turbomachinery are determined by the power capacity. The isentropic efficiency of the purchased machinery is fixed. Reducing costs at the expense of performance is therefore practically not possible in that sense unless components are purchased secondhand. For the compressors, the component cost rate can only be reduced when the *RTE* is increased, and less compression capacity is required. The capacity of the turbines is fixed by the boundary conditions of a fixed discharge capacity for all systems of 100 MW.

Table 5.5: Decision variables for exergoeconomic optimization of selected components.

Component	Decision variable	Parametric change	Base Case A	Base Case B
MHE1	$LMTD_{MHE1} \uparrow$	$p_{CM} \uparrow$	-	1st iteration
MHE2	$LMTD_{MHE2} \uparrow$	$\dot{m}_{R218}, \dot{m}_{methanol} \downarrow$	2nd iteration	2nd iteration
Intercoolers	$LMTD_{IC} \uparrow$	$\dot{m}_{HS} \uparrow$	3rd iteration	3rd iteration
Reheaters	$LMTD_{RH} \uparrow$	$T_{out,RH} \downarrow$	4th iteration	4th iteration

The investment costs of the heat exchangers are a function of the heat exchanger design, working fluid properties (e.g., pressure, temperature, heat capacity), materials and heat exchanger area A_{HE}. For cost reduction in the heat exchangers, the A_{HE} can be reduced by increasing the LMTD. Four distinct iterations were applied:

1st iteration: To reduce the costs and increase the LMTD between the cumulative curves of the MHE1 of the Base Case B, the compression pressure was gradually increased. The splitting ratio was kept to its minimum.

2nd iteration: The LMTD in the MHE2 is increased by reducing the mass flow of the cold storage media ($\dot{m}_{R218} \downarrow$, $\dot{m}_{\mathrm{CH3OH}} \downarrow$).

3rd iteration: By increasing the mass flow of the heat storage media $\dot{m}_{\mathrm{HS}}$ the LMTD of the intercoolers is increased, decreasing the heat exchanger area A_{IC} and $\dot{Z}_{IC}$.

4th iteration: For cost reduction in the reheaters, a lower exit temperature $T_{out,RH}$ (or TIT) is accepted to increase the logarithmic mean temperature difference.

The parametric change and the effect of all performed optimization steps on the TRR, the $LCOE_{dis,}$ and the exergetic efficiency are given in Table 5.6 and Table 5.7. The effect of the parametric changes on the *RTE* and $LCOE_{dis}$ are indicated in Figure 5.12 and Figure 5.13 for the Base Cases A and B, respectively.

Table 5.6: Parameters and results of the optimization steps for the Case A.

Parameter	Unit	Base Case A	1st	2nd	3rd iteration
p_{CM}	bar	85	85	85	85
$\dot{m}_{R218}/\dot{m}_{liquid}$	-	2.280	2.083	2.083	2.083
$\dot{m}_{methanol}/\dot{m}_{liquid}$	-	0.450	0.414	0.414	0.414
ΔT_{IC}	K	2	2	3	3
ΔT_{RH}	K	2	2	2	7
TRR	10^6 €	37.3	32.3	30.7	30.4
$LCOE_{dis}$	€/MWh	255	221	210	208
RTE	-	0.444	0.397	0.386	0.381

Table 5.7: Parameters and results of the optimization steps for the Case B.

Parameter	Unit	Base Case B	1st	2nd	3rd	4th iteration
p_{CM}	bar	120	180	180	180	180
$\dot{m}_{R218}/\dot{m}_{liquid}$	-	2.280	2.280	2.000	2.000	2.000
$\dot{m}_{methanol}/\dot{m}_{liquid}$	-	0.450	0.450	0.400	0.400	0.400
ΔT_{IC}	K	2	2	2	3	3
ΔT_{RH}	K	2	2	2	2	6
TRR	10^6 €	39.0	33.6	28.8	28.6	28.5
$LCOE_{dis}$	€/MWh	267	230	197	196	195
RTE	-	0.468	0.449	0.415	0.399	0.394

In the 1st *iteration* of the exergoeconomic optimization the pressure p_{CM} of the compression ratio of the compressors in the Base Case B, was gradually increased to reach a higher absolute pressure in the liquefaction process. The component cost rates of the Base Case B (120 bar) and the cases with increased pressure are shown in Figure 5.11. The aimed reduction in the investment costs of the MHE1 and the intercoolers was achieved while the component cost rate of the MHE2 only decreased slightly. The iteration was stopped at 180 bar to avoid more costly equipment and materials of subsequent components.

The cost of the MHE1 was reduced by almost 70 % and the exergoeconomic factor of previously 0.75 was reduced to 0.42, due to the increase in LMTD from 3 K to 9 K. The increased compression ratio also leads to a 60 K higher temperature at the outlet of the compressors T_{CM} that can be recovered in heat storage. The turbine inlet temperature TIT increases, improving the exergetic efficiency ε_T and reducing the cost rate associated with the exergy destruction in the turbines $\dot{C}_{D,T}$. The temperature level in the reheaters rises, which at constant mass flow would decrease their heat exchanger area. However, at increased p_{CM} the *RTE* drops and a higher mass flow in the discharge unit becomes necessary, retaining the cost rate of the reheaters. By increasing p_{CM} to 180 bar, the $LCOE_{dis}$ of the Base Case B was significantly reduced from 267 €/MWh to 230 €/MWh.

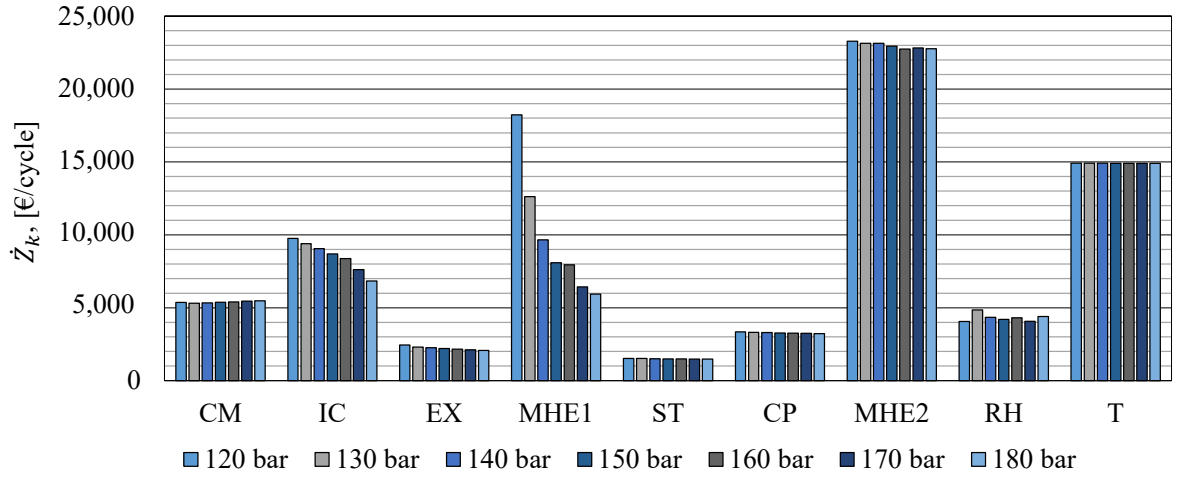

CM	the compressors	MHE1	the main HE 1	MHE2	the main HE 2
IC	the intercoolers	ST	the storage tank	RH	the reheaters
EX	the expander	CP	the cryogenic pump	T	the turbines

Figure 5.11: Component cost rates $\dot{Z}_k$ of selected components of the Base Case B (with increased compression pressure from 120 to 180 bar).

The 2nd iteration that is applied to both base case systems entails the reduction of $\dot{Z}_{MHE2}$. The reduction of the mass flow rate of the cold storage working fluid reduces the amount of low-temperature exergy that is supplied to the MHE1. At a constant splitting ratio, this leads to a reduction in the LMTD and increases costs of the MHE1. Therefore, the splitting ratio r needs to be increased to meet the minimum temperature difference $\Delta T_{min,MHE1}$ = 1 K and avoid a rise in the investment costs of the MHE1. When the splitting ratio r is increased, the liquid yield γ is reduced and the exergetic efficiency ε of the liquefaction process and the overall system is reduced.

The mass flow rates $\dot{m}_{R218}$ and $\dot{m}_{\mathrm{CH3OH}}$ are reduced until the exergetic efficiency of the charging systems drops so low, that the additional investment in larger equipment in the charging unit exceeds the cost reduction in the MHE2. For the Base Case A system, the $LCOE_{dis}$ was minimized at $\dot{m}_{R218}/\dot{m}_{liquid\ air}$= 2.083 and $\dot{m}_{methanol}/\dot{m}_{liquid\ air}$ = 0.414. The ratios reached lower values in Base Case B, Table 5.7. The $LCOE_{dis}$ of both systems is reduced by 13-14 % to 221 €/MWh and 197 €/MWh. As the splitting ratio needed to be increased from 0.39 to 0.46 (0.31 to 0.33), the liquid yield of the system decreases from 0.501 to 0.445 (0.559 to 0.533) in the Base Case A (B) and the exergetic efficiency ε_{tot} (*RTE*) drops accordingly, Figure 5.12 and Figure 5.13. The reduction in performance in the Base Case A is more significant (10.6 %) than in the Base Case B (7.6 %).

By increasing the mass flow of the heat storage media $\dot{m}_{HS}$ in the *3rd iteration*, the temperature difference within the intercoolers ΔT_{IC} is increased to a maximum of 3 K. Increasing the $\dot{m}_{HS}$ further increases the LMTD while reducing the $LCOE_{dis}$ further. With an increased mass flow of the heat transfer media, the TIT decreases, reducing the exergetic efficiency of the turbine and the reheaters and accordingly, the specific power output of the discharge unit. Consequently, a minimum $LCOE_{dis}$ is reached when the additional investment in larger equipment and fuel costs outweighs the cost reduction in the intercoolers. The $LCOE_{dis}$ is minimized at a LMTD of the intercoolers of approximately 7 K (9 K) for Base Case A (B).

The effect of cost reduction when increasing $\dot{m}_{HS}$ is more significant in the Base Case A. Nevertheless, Base Case B achieves a lower $LCOE_{dis}$ at considerably higher *RTE*, Figure D.6 in Appendix D.

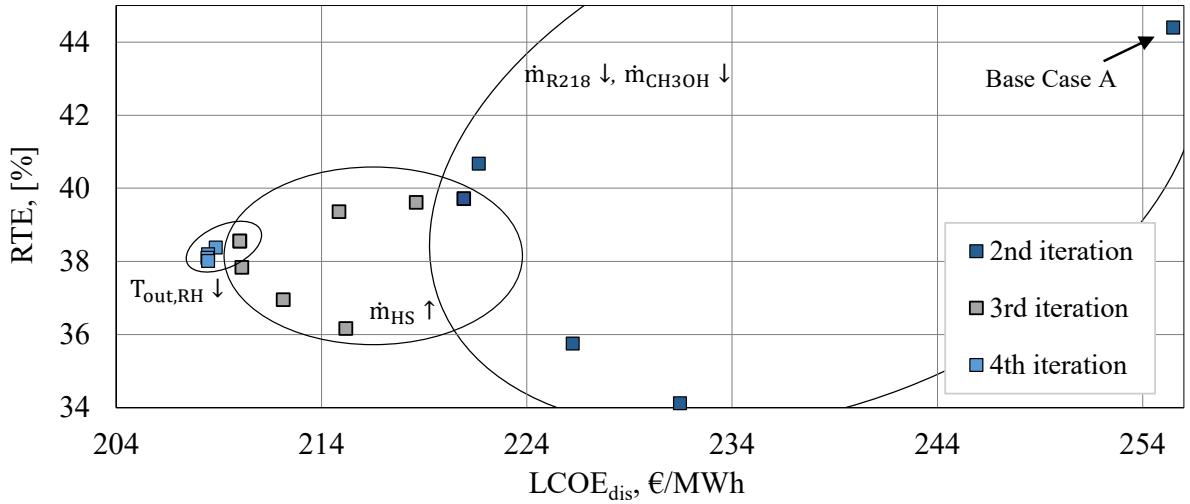

Figure 5.12: RTE over $LCOE_{dis}$ for the optimization steps performed on the Base Case A with an indication of the changes applied to the decision variables in the respective iteration.

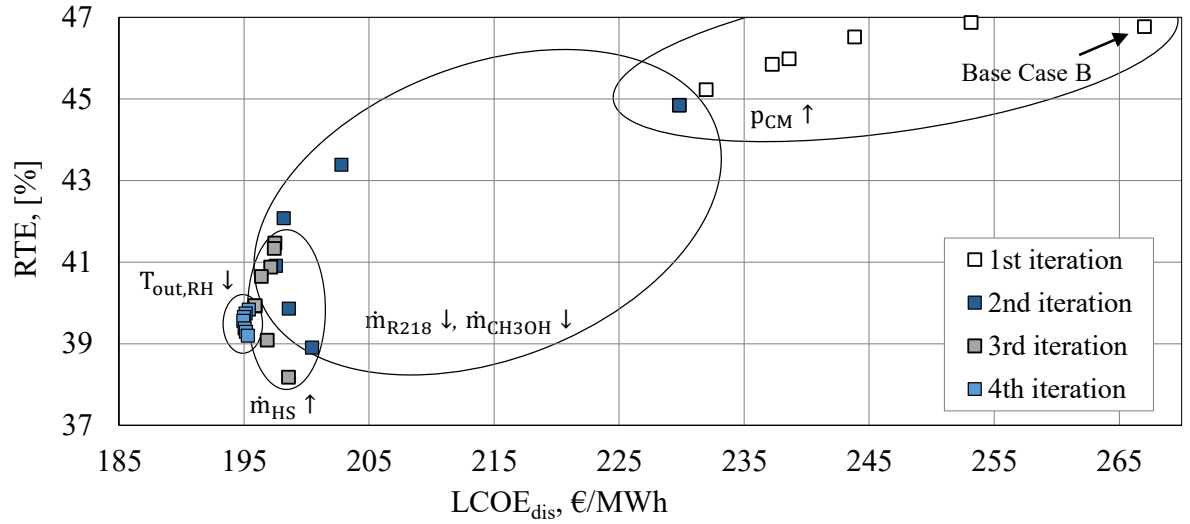

Figure 5.13: RTE over $LCOE_{dis}$ for the optimization steps performed on the Base Case B with an indication of the changes applied to the decision variables in the respective iteration.

In the *final iteration* performed on both systems, the outlet temperature of the reheaters was reduced resulting in a higher temperature difference ΔT_{RH} between the heat storage media and the TIT (2 K → 10 K). The minimum $LCOE_{dis}$ of the base cases was achieved at 6-7 K, Table 5.6 and Table 5.7 – 4th iteration. The reduction in *RTE* in both cases is comparable, 14.1 % and 15.4 % for the Optimized Cases A and B, respectively. However, the cost reduction is much more drastic in the Optimized Case B.

The effect of the parametric changes in the iterative exergoeconomic optimization on the *RTE* and the $LCOE_{dis}$ is depicted in Figure 5.12 and Figure 5.13. In each of the iteration, a sensitivity analysis of the *RTE* and the $LCOE_{dis}$ while gradually changing the respective decision variable was conducted. The operation steps are performed successively. The parametric changes of the subsequent iteration were applied to the "best case" (lowest $LCOE_{dis}$) of the respective iteration.

The reduction of the cost of the final product in the system is more significant when adopting changes to the components with higher cost-importance (higher $\dot{Z}_k + \dot{C}_{D,k}$). When the liquefaction pressure or the mass flow of the cold storage medium is gradually changed to reduce the component cost rates of the MHE1 and MHE2, the reduction in the $LCOE_{dis}$ is much more noticeable than when changing the parameters of the less cost-intensive components such as the intercoolers and the reheaters. For this reason, the cost reduction when applying further changes is expected to be insignificant.

In Figure 5.14, the sum of the component cost rates normalized to the unit of product exergy ($\sum \dot{Z}_k / \dot{E}_{P,tot}$) is given over the sum of exergy destruction and exergy losses per unit of product exergy ($(\dot{E}_{D,\,tot} + \dot{E}_{L,\,tot})/\dot{E}_{P,tot} = (1 - \varepsilon_{tot})/\varepsilon_{tot}$) for the intermediate results of the exergoeconomic optimization steps performed on the base cases. For both cases, the levelized costs are reduced at the expense of a reduction in exergetic efficiency of the systems. Despite lower levelized investment costs and $LCOE_{dis}$ of the Base Case A, the Optimized Case B achieves lower levelized costs and the sum of exergy destruction and losses per unit of product exergy throughout the iterative optimization. This underlines again the importance of exergy-based methods when evaluating the systems in regards to cost-effectiveness.

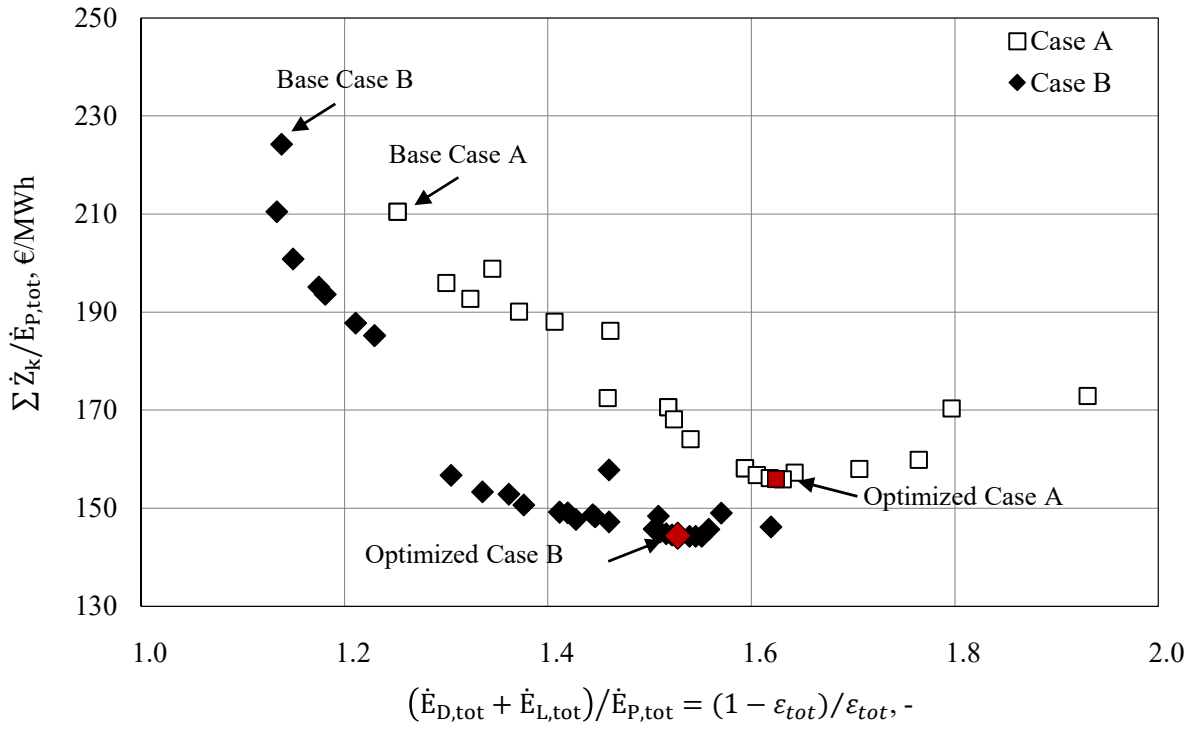

Figure 5.14: Normalized capital investment cost (per unit of exergy of product) for the Cases A and B during the iterative exergoeconomic optimization over the relative exergetic efficiency.

The exergoeconomic analysis results on the component level of the optimized cases are compared to those of the base cases in Figure 5.15. The objective of reducing the costs associated with the initial investment $\dot{Z}_k$ was achieved for all of the selected components. The met objective is indicated in the reduction of the exergoeconomic factor.

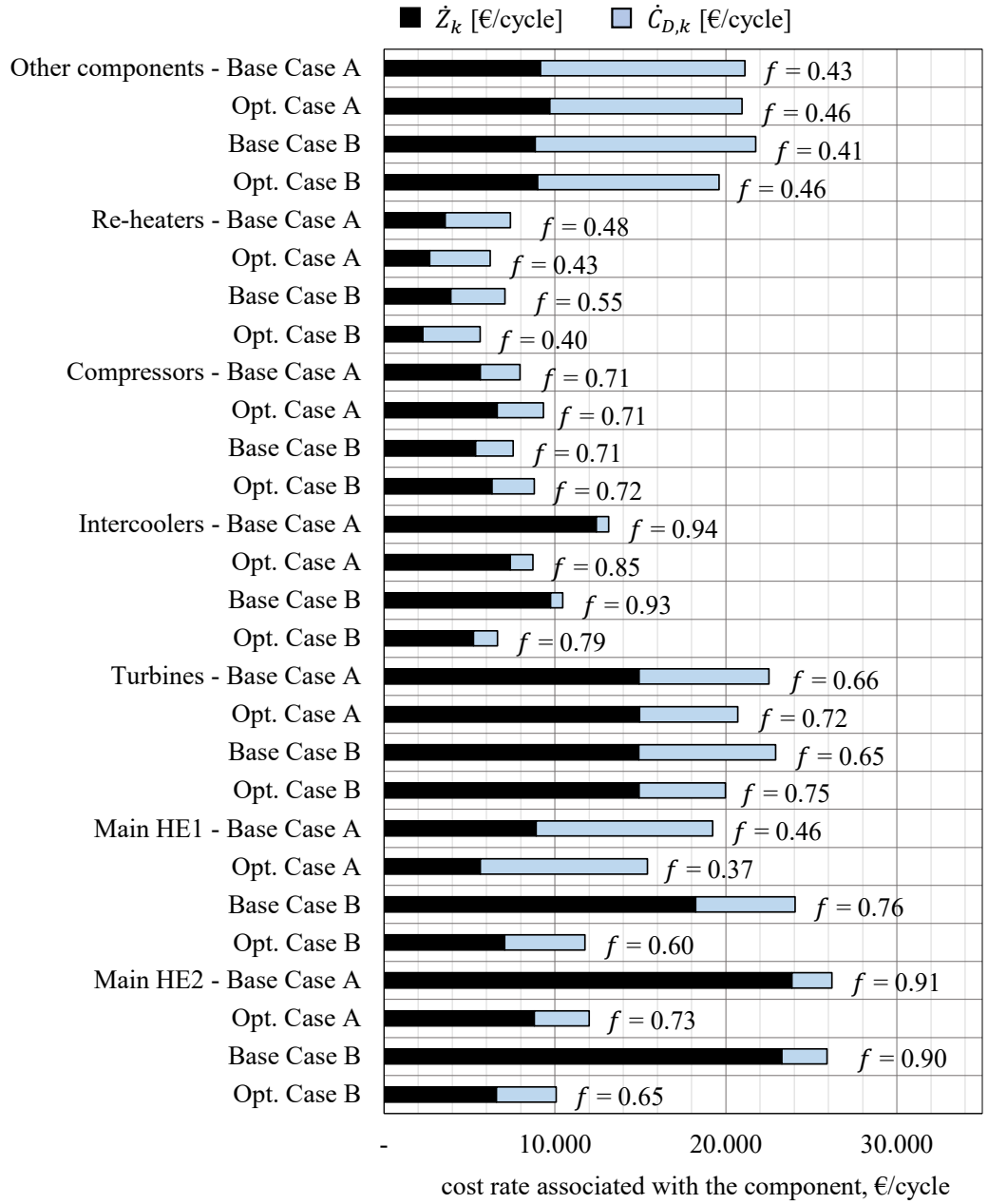

Figure 5.15: Exergoeconomic analysis results for the base cases and the optimized cases.

Due to the cost reduction in the overall system, the specific cost of the exergy of the fuel to the turbines c_F was reduced. Consequently, the costs associated with the exergy destruction in the turbines $\dot{C}_{D,T}$ were decreased. Nevertheless, after the exergoeconomic optimization is completed, the turbines become the components with the highest associated total cost rate.

In the optimized cases, the BMC of the turbines amount to approximately 30% of the BMC of the total systems. A cost reduction of the turbines could thus reduce the $LCOE_{dis}$ considerably.

To compensate for the reduction in *RTE* in the optimized cases, the compression power needs to be augmented, which results in an increased total cost rate of the compressors. The changes made to the parameters of the Base Case A, reduce the exergoeconomic factor of the MHE1 further.

In both systems, the interrelation of the components is very strong. An example of this is the intercoolers. Despite the exergoeconomic factor suggesting a further reduction in investment costs at the expense of exergetic efficiency, any further reduction in ε_{IC} would cause the cost of the final product to increase. Reason for this is, that in order to increase the LMTD in the IC, either the temperature at the outlet of the IC would need to be raised or the mass flow in the heat storage would need to be increased which would reduce the TIT. In both cases, the work requirement of the compression process would be augmented and the additional investment costs for larger compressors would outweigh the reduction in costs of the intercoolers.

The objective of cost reduction of the costs associated with the reheaters was also achieved. Moreover, the sum of the total cost rates of all other system components was reduced. The slight increase in the exergoeconomic factor of the "other components" to 0.46 indicated that the cost reduction mainly results from reduced costs associated with the exergy destruction in the components. As the component cost rates of the majority of cost-intense components are reduced, the specific cost per unit of exergy of the fuel to the subsequent components is reduced, decreasing $\dot{C}_{D,k}$.

5.3. Exergy-based evaluation of CES system integration

In this section, the results from the exergy-based evaluation of several CES system configurations are presented, and the enhancement in the thermodynamic and economic performance of CES systems with integration of heat sources and sinks is quantified. The integration of re-gasifying LNG was considered as a heat sink for CES systems instead of and in combination with cold storage. Waste heat at 350-450 °C and natural gas combustion were considered as heat sources.

5.3.1. Comparative energetic and exergetic analysis

Two adiabatic CES systems and eight systems with integration of external heat and/or cold sources were compared using energetic and exergetic analysis on the system level. The exergy of the fuel E_F, the exergy of the product E_P and the exergetic efficiency ε_{tot} of selected systems are represented in Figure 5.16. The exergy values are given in MWh over the duration of one daily cycle (τ_{char}= 8 h, τ_{dis}= 4 h). The mass flow rate of the inlet air was set to 200 kg/s for all systems. As a result, the compression work W_{CM} of 1,105 MWh is equal for all systems and is indicated in the figure for comparison.

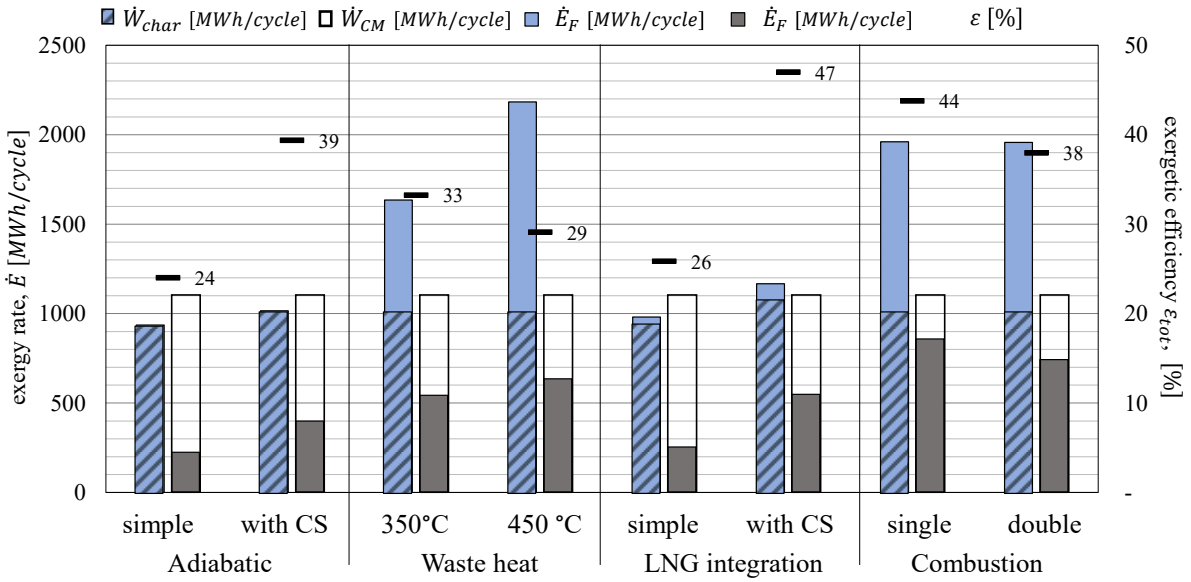

Figure 5.16: Exergetic analysis results for the integrated CES system configurations.

The product of all systems is discharged electricity. The fuel to the systems is the sum of the electricity charged ($W_{CM} - W_{EX}$) and the low-temperature exergy $E_{Q,cold}$ (for LNG integration) and/or the exergy of the supplied fuel E_{NG} (for combustion) and/or the high-temperature exergy $E_{Q,hot}$ (for waste heat integration), Table B.1. The results show that the integration of waste heat does not have a positive effect on the exergetic efficiency despite the desired increase in the specific power output of the discharge unit. The exergy content of the heat that needs to be supplied in order to elevate the TIT to 350 °C and 450 °C, respectively, is more significant than the increase in the discharge power.

The electricity charged to the LNG integrated systems is slightly higher than in the adiabatic CES systems. Due to the additional low-temperature exergy, less air needs to be fed to the cold expander in the liquefaction process, and the electricity generated in the expander is reduced (W_{EX} ↓). The LNG integrated system with CS reaches the highest ε_{tot} of 47 %. Reason for this is that the contribution of the low-temperature exergy $E_{Q,cold}$ to the exergy of the fuel E_F in the systems with LNG integration is relatively small in comparison to its significant improvement of the yield of the liquefaction process.

The roundtrip, energetic, and exergetic efficiency of the ten evaluated systems are given in Table 5.8. The *RTE* gives the ratio between the electricity discharged and the electricity charged (W_{dis}/W_{char}).The values of the *RTE*, consequently, may exceed 1. The values of the *RTE*, the energetic and the exergetic efficiency of the adiabatic systems are the same as no external heat source or sink, needs to be accounted for in the energetic or exergetic evaluation (Table B.1).

Table 5.8: Roundtrip, energetic, and exergetic efficiency of the ten considered system configurations.

System	Abbreviation	RTE	η	ε_{tot}
Adiabatic CES without cold storage	a-CES w/o CS	0.240	0.240	0.240
Adiabatic CES with cold storage	a-CES	0.394	0.394	0.394
Waste heat integration with TIT of 350 °C	WH 350	0.535	0.234	0.332
Waste heat integration with TIT of 450 °C	WH 450	0.625	0.194	0.291
Diabatic CES with a single combustion chamber	d-CES	0.845	0.448	0.438
Diabatic CES with two combustion chambers	d-CES 2	0.732	0.388	0.380
LNG integration without cold storage	LNG w/o CS	0.260	0.251	0.254
LNG integration with cold storage	LNG a-CES	0.506	0.452	0.470
LNG integration and waste heat	LNG + WH	0.804	0.253	0.376
LNG integration and combustion	LNG d-CES	1.084	0.480	0.477

The adiabatic CES system without cold storage (a-CES w/o CS) reaches efficiencies by 40 % lower than the a-CES system. With the integration of LNG, the *RTE* of the a-CES w/o CS increases by only 2 % to 26 % and the ε_{tot} increases by 1.4 %. Even when the mass flow of the LNG is increased, the *RTE* does not increase any further due to the fixed $\Delta T_{MHE1,min}$, while the ε_{tot} is reduced (Figure 4.11). In contrast, the addition of cold storage increases the *RTE* by 64 %. Reason for this is, that the LNG enters the MHE1 at a temperature of - 158 °C while the high-grade cold storage supplies low-temperature exergy at temperatures as low as - 180 °C. As a result, the integration of re-gasifying LNG cannot replace the cold storage.

Integrating waste heat to the a-CES system was found favorable for the *RTE*, increasing from 39.4 % to 62.5 %, while the energetic and the exergetic efficiency of the systems drop by 50 % and 26 %, respectively. The lower energetic and exergetic efficiency can be explained by the excess heat vented after the expansion process. With waste heat integration, the amount and temperature; and accordingly, the exergy content of the vented heat is elevated causing the exergy losses of the system to increase.

The integration of a combustion process augments all three efficiencies. The *RTE* is doubled and the energetic and exergetic efficiency increase by 5.4 and 4.4 percentage points, respectively. The values achieved for the *RTE* of 73-85 % are significantly higher than values stated in literature (55-60 % [15, 43]), which can be explained by a larger mass flow rate of the

fuel, see Figure C.3. The efficiency of the double combustion configuration is slightly lower than the single combustion configuration (d-CES 1). Due to decreased TIT, the *RTE*, energetic and exergetic efficiency drop by approximately 15 % at the same total mass flow rate of the fuel $\dot{m}_{NG}$. The introduction of two smaller sized separate combustion chambers is expected to lower the specific costs due to lower maximum TIT.

The integration of LNG to the a-CES system increases the *RTE* by 28 % and the ε_{tot} by 6 percentage points. Re-gasifying LNG is thus a thermodynamically feasible low-temperature exergy source when cold storage is present. The systems with simple integration of liquefied natural gas (LNG, LNG w/o CS) reach exergetic efficiencies of 25-47 %, similar to the value range proposed in literature of 33-43 % [62, 63, 64]. The *RTE*, in contrast, are lower than anticipated, instead of reaching expected values of 63-70 % [8, 62, 63] the *RTE* of the LNG system reaches only 51 %. With additional waste heat integration, the system reaches a *RTE* of 84 %. While the CES system with integration of LNG and combustion achieves the highest exergetic efficiency of 47.7 % and the highest *RTE* of 108 % under the given conditions.

5.3.2. Comparative economic analysis

The effect of the integration of heat sources and sinks on the bare module costs (BMC) of selected components of the systems can be seen in Figure 5.17. All systems operate with the same mass flow of inlet air and liquefaction pressure. The BMC of the compressors are therefore constant for all considered systems.

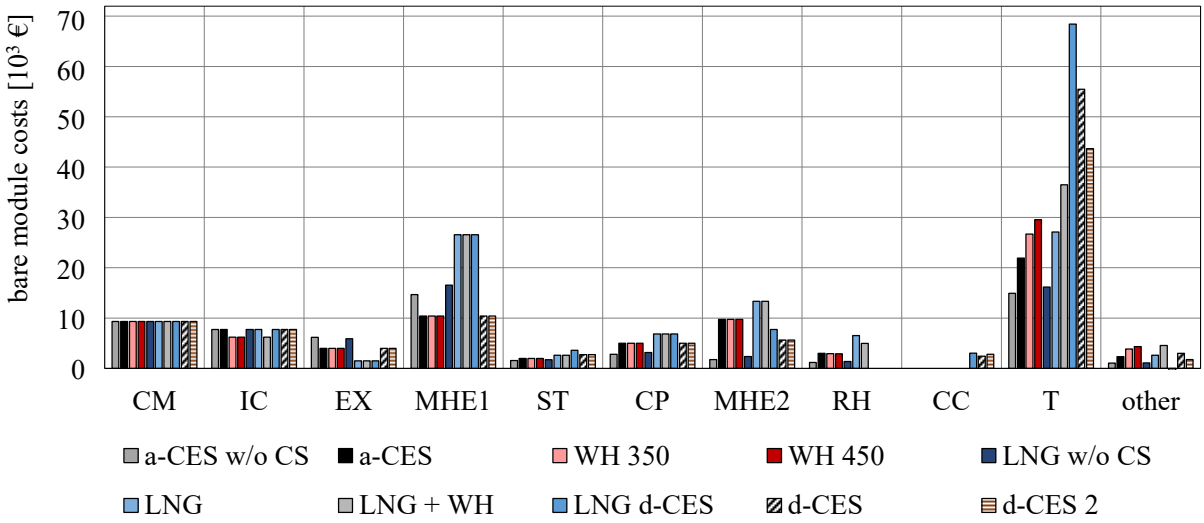

Figure 5.17: Bare module costs of the components of the integrated systems (CM – compressors, IC – intercoolers, EX – expander, MHE – main heat exchanger, ST – storage tank, CP – cryogen pump, RH – reheaters, CC – combustion chamber(s), T – turbines, HS – heat storage, CS – cold storage and other components).

The costs associated with the intercoolers and the reheaters are reduced in the systems with waste heat integration as thermal oil is used as heat transfer and storage medium and a smaller heat exchanger area is necessary. The cost of heat storage increases accordingly.

For the systems that do not contain cold recovery and storage, environmental air is used as a heat source for the evaporation of the liquid air (discharge). The LMTD of the MHE2 is increased significantly, reducing the components BMC to one-third of that of the a-CES system. The LMTD of the MHE1, in contrast, decreases without the low-temperature exergy supplied from cold storage, increasing the needed heat exchanger area and costs by 40% while a significantly smaller share of air is liquefied. Due to the reduced liquid yield, the costs of all components in the discharge unit are reduced in the absence of cold storage in comparison to all other CES systems.

With the integration of LNG to the MHE1 of the CES system, the A_{MHE1} and the BMC increase to more than twice with respect to the a-CES system. As the amount of air liquefied is increased by up to 40%, the investment cost of the components in the discharge unit increase alongside. In order to account for both the effect on the economic and the thermodynamic performance, the levelized costs were calculated in comparative economic analysis.

The TCI, the specific investment costs c_i, and the $LCOE_{dis}$ of the two adiabatic and eight integrated CES system configurations are given in Table 5.9. The assumptions made in the analysis are described in section 3.2. The economic analysis was performed on two system designs:

a) a constant mass flow rate of the inlet air of 200 kg/s, and
b) a discharge capacity of 100 MW.

The discharge capacities are given for the case a), as a reference. The adiabatic CES system with cold storage (a-CES) reaches a discharge capacity of 100 MW at a mass flow at the inlet of the compression process of approximately 200 kg/s. Some systems of the systems reach discharge capacities of two to three times higher than the a-CES system which results in low specific investment costs c_i and $LCOE_{dis}$.

Table 5.9: Results of economic analysis for the ten CES system configurations.

System	$\dot{m}_{air}$ = 200 kg/s				$\dot{W}_{dis}$ = 100 MW	
	TCI, 10^6 €	c_i, €/kW	LCOE, €/MWh	$\dot{W}_{dis}$, MW	c_i, €/kW	LCOE, €/MWh
a-CES w/o CS	61.2	1,835	295	56	1,719	283
a-CES	75.4	1,269	195	100	1,269	195
WH 350	80.1	993	150	136	1,040	154
WH 450	83.4	884	131	159	950	138
d-CES	105.7	830	128	214	977	140
d-CES 2	93.0	843	136	186	954	143
LNG w/o CS	65.4	1,735	274	63	1,647	265
LNG a-CES	104.1	1,278	181	137	1,323	186
LNG + WH	112.3	869	121	218	966	130
LNG d-CES	134.1	770	115	293	959	131

The specific investment costs c_i are determined by the total capital investment (TCI) of the system over the installed discharge capacity. The specific costs of CES systems decrease with size. The scaling factor for the systems was found to be between 0.81-0.92, which refers to a decrease in costs by 10-25 % when the capacity of the system is doubled.

The integration of cold storage reduced the $LCOE_{dis}$ by 32-34 % despite an additional investment of approximately € 15 million. The integration of waste heat reduces the $LCOE_{dis}$ further, by 21-30 % compared to the a-CES. The CES systems with natural gas firing reached the lowest specific investment costs c_i when the mass flow is kept consistent and for an installed discharge capacity of 100 MW. The lowest $LCOE_{dis}$ at the given assumption was achieved by the CES system with both waste heat and waste cold integration of 130 €/MWh, followed by the diabatic CES systems and the CES system with waste heat integration at 450 °C of 131-143 €/MWh. The additional costs associated with the waste heat, combustion and/or waste cold integration are rather low relative to the increase in *RTE*, resulting in a significantly lower $LCOE_{dis}$ of the respective systems.

Despite the similar thermodynamic performance of the two d-CES systems, the levelized costs of the d-CES 2 with two combustion chambers are lower. Reason for this is the temperature at the outlet of the combustion chambers. The material of the TIT is selected according to this temperature. To achieve the same power capacity in the single combustion d-CES system than in the double combustion d-CES 2. The TIT of the d-CEs system will accordingly exceed that of the d-CES 2 system and necessitate more expensive turbine materials while the additional investment associated with the second combustion chamber is rather low in comparison. The sensitivity of the $LCOE_{dis}$ of the d-CES system over the mass flow rate of the fuel to the system is given in Figure D.9 in Appendix D. Despite the lower investment costs of the d-CES 2 system; the d-CES system achieves slightly lower $LCOE_{dis}$. Reason for this is the by 15 % higher *RTE*. The specific investment costs c_i of all systems are represented over the *RTE* in Figure 5.18.

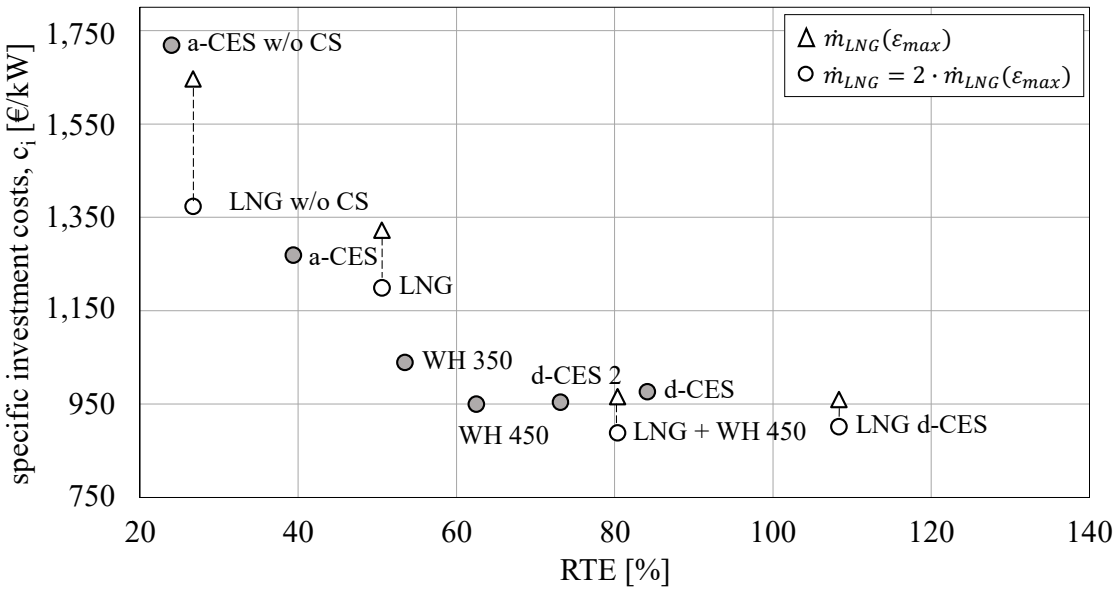

Figure 5.18: Specific investment costs over RTE of the ten CES systems for $\dot{W}_{dis}$ = 100 MW.

The systems with higher *RTE* reach significantly lower specific investment costs and $LCOE_{dis}$. Reason for this is that the charging unit makes up for the highest share in the investment costs and higher *RTE* significantly reduce the size of the charging unit necessary to supply 100 MW of discharge power.

For the systems with LNG integration, a range for the $LCOE_{dis}$ is indicated in Figure 5.18. Reason for this is that specific costs of the systems are a function of the mass flow of the LNG supplied. For exergetic and preliminary economic analysis the mass flow of the LNG was adjusted to the value of highest exergetic efficiency ε_{max} as described in section 4.4.3. The sensitivity of the specific investment costs and the $LCOE_{dis}$ over the mass flow of LNG supplied is shown in Figure 5.19. For small mass flowrates of the LNG (< 9 % of $\dot{m}_{air}$), the splitting ratio is gradually reduced, and the *RTE* increases linearly, Figure 4.11. The $\Delta T_{min,MHE1}$ is thereby fixed but the LMTD changes. When a splitting ratio of r = 0.08 is reached, the splitting ratio cannot be reduced further without violating the constraint for the $\Delta T_{min,MHE1}$. As a result, the *RTE* does not increase further with an amplified mass flow rate of the LNG. Still, the additional low-temperature exergy increases the LMTD, hence, the BMC of the MHE1 are reduced. As the MHE1 is the second most costly component, the reduction in BMC leads to significantly lower specific investment costs. The $LCOE_{dis}$ reaches values lower than 170 €/MWh at doubled mass flow, while the *RTE* stays constant at 51 % and the exergetic efficiency ε_{tot} drops below 38 %. In Figure 5.18, the specific investment costs of the LNG integrated systems are given for the maximum efficiency case ($\dot{m}_{LNG}(\varepsilon_{max})$) and the case of doubled flowrate. For further comparison the results for the systems with twice as large mass flow $\dot{m}_{LNG}$ than necessary to reach ε_{max} are considered.

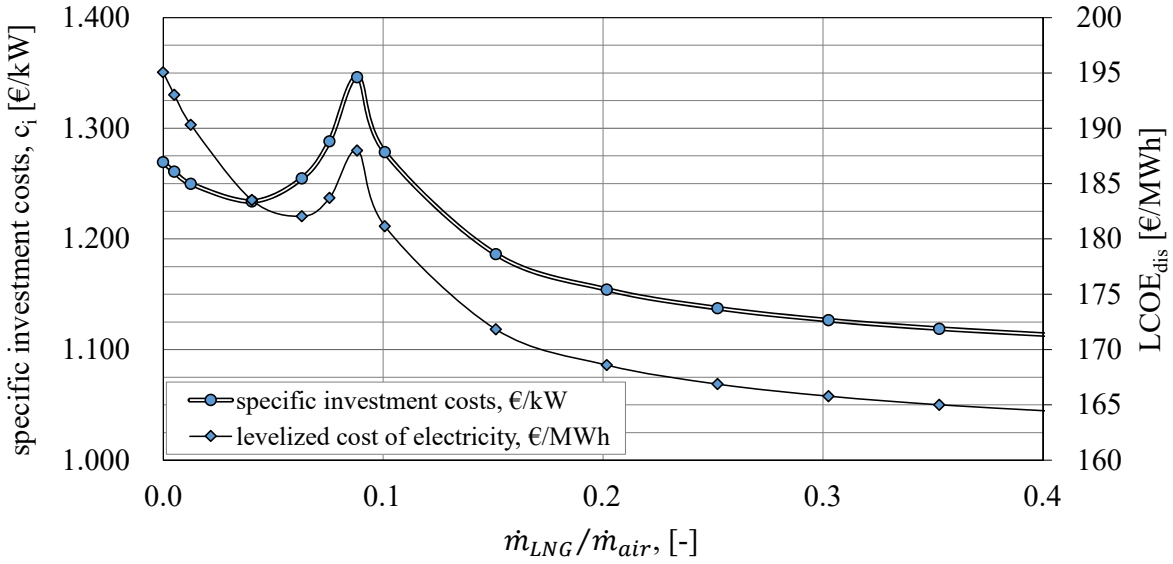

Figure 5.19: Specific investment costs and $LCOE_{dis}$ over the specific mass flow of LNG.

In Figure 5.20, the $LCOE_{dis}$ is broken down into the cost shares associated with the fuel costs, the cost of electricity charged, the operational expenditure (OPEX) and the capital expenditure (CAPEX) related to the charging, the storage, and the discharging unit. The a-CES with waste heat integration reached $LCOE_{dis}$ comparable with the CES system with combustion. Also, their specific costs are competitive despite the lower *RTE*, Figure 5.18. The waste heat integration may become more promising when taking the dependency on fuel prices and the environmental impact of the combustion gases into account.

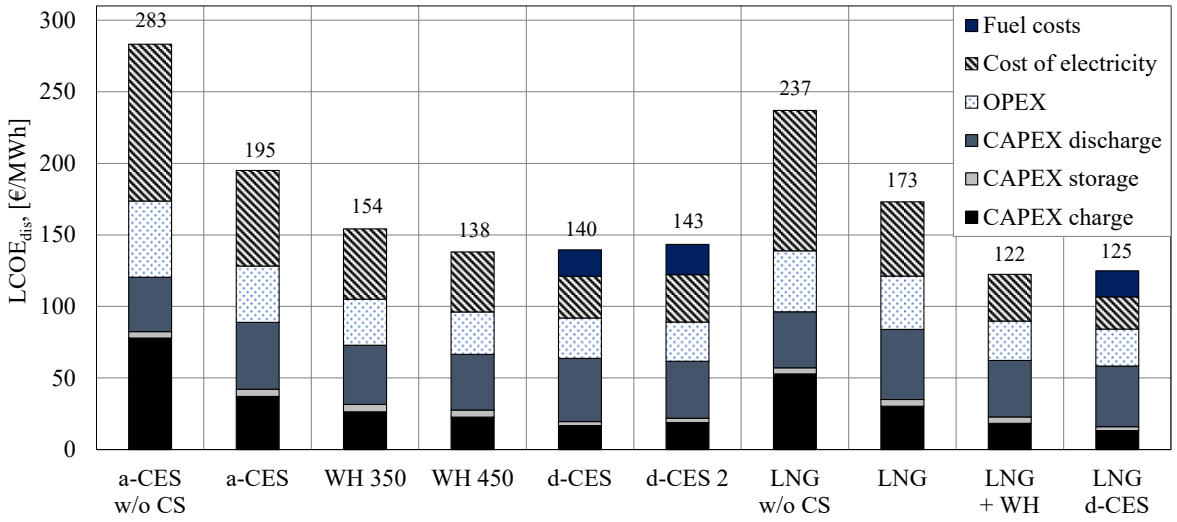

Figure 5.20: The levelized cost of electricity of the ten CES system configuration with indicated shares of the costs associated with the CAPEX, the OPEX, the cost of electricity charged and the fuel costs at $\dot{W}_{dis}$ *= 100 MW and* $\dot{m}_{LNG} = \dot{m}_{LNG}(\varepsilon_{max})$.

With increased $\dot{m}_{LNG}$, the systems with LNG integration became even more competitive. To draw a comparison between the different CES systems at a single electricity price and NG price is misleading. The $LCOE_{dis}$ of the different systems is compared for various electricity prices, FLH_{dis}, natural gas prices and CO_2 emission prices in section 5.4.2. The $LCOE_{dis}$ is highly dependent on the initial assumptions made in the economic analysis. Thus, a sensitivity analysis was performed to evaluate the weighted effect of changes applied to the initial economic parameters. The results from economic sensitivity analysis of the adiabatic CES system are discussed in section 5.4.1. In section 5.4.3, the results for CES economic assessment are compared to values reported in the literature and values proposed for competing technologies.

5.4. Economic viability of CES systems

In this section, the economic viability of CES systems is further assessed. The results from economic sensitivity analysis performed on the adiabatic and the integrated systems are presented. The parameters which affect the economic feasibility of the systems are revealed. The most suitable applications are identified accordingly. The results obtained in economic analysis discussed in section 5.2.2 and section 5.3.2 are compared to values presented in the literature. Finally, CES economic performance is compared to other bulk ES technologies.

5.4.1. Economic sensitivity analysis of the a-CES system

The weighted effect of changes in the economic parameters on the levelized cost of discharged electricity of the adiabatic CES system is shown in Figure 5.21. The $LCOE_{dis}$ changes proportionally to changes in the bare module costs (BMC), the OMC and the price of electricity c_{el}. The annual full-load hours of the discharge unit FLH_{dis}, the *RTE*, the capacity of the discharge unit and the economic life have an inverse and non-linear relationship to the $LCOE_{dis}$. Changes in the FLH_{dis} have the strongest influence on the $LCOE_{dis}$.

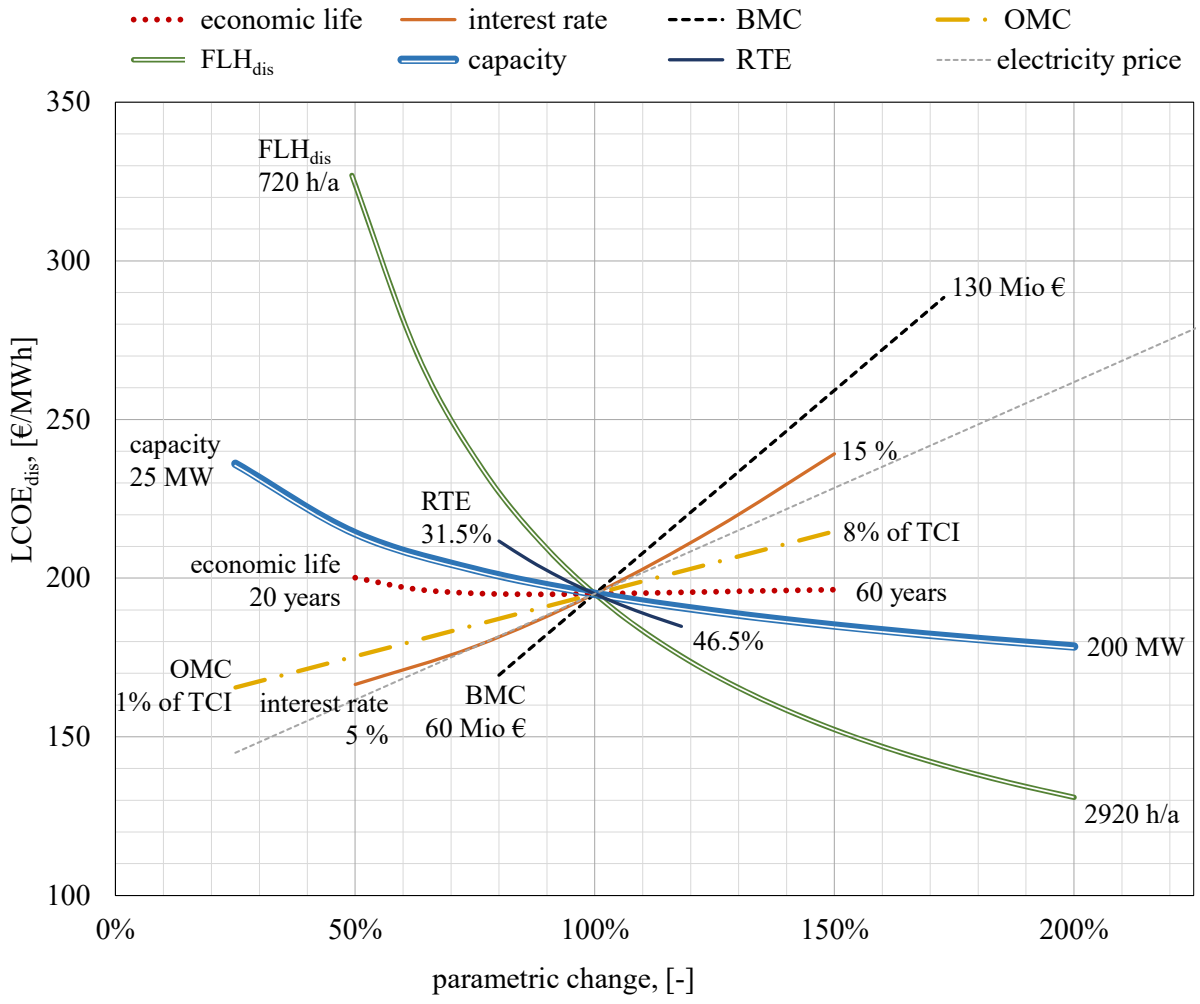

Figure 5.21: Economic sensitivity analysis results of the a-CES system.

In principle, ES systems have significantly lower operation hours than most power plants. The CES systems assessed in this work have a charge-to-discharge ratio of two, which refers to two charging hours for every hour of discharge. Consequently, even if the storage duration is zero (when the discharge process takes place immediately after the charging process), the maximum number of FLH of the discharge unit is 2,920 hours annually.

When the FLH_{dis} are further decreased in relation to the base case assumption (1,460 h/a), the $LCOE_{dis}$ increases significantly, exceeding values of 250 €/MWh. Already a 10 % reduction of the FLH_{dis}, increases the $LCOE_{dis}$ by 8 %. Thus, only applications which comprise a frequent and extensive operation are economically feasible for CES systems. Potential applications were discussed in section 2.5, and the characteristics (cycles per annum and discharge duration) of considered applications are given in Table A.2 through Table A.5. The ES applications which were found to have annual operation hours suitable for CES are; load shedding or shifting (720-3,000 h/a [93]) or peak shaving (up to 2,500 h/a [72, 37, 93]), energy arbitrage or RE time shift (up to 3,000 h/a [103]) and capacity firming (1,200-2,000 h/a [37]), section 2.5. The operation as a reserve in standby, in contrast, is economically not viable for CES systems, despite their low standby losses. Reason for this is not only the low number of operation hours, but also the economic value for reserve capacity and black start application is rather low in comparison to other applications (Table A.7) [97, 106, 107]. The majority of T&D support services are not suitable for CES operation, due to low operation hours and difficult prediction of the revenue streams.

The second strongest weighted change of the $LCOE_{dis}$ is caused by changes in the BMC of the system (Figure 5.21). The bare module costs (BMC) were varied to show the effect of changes in the initial investment costs of the system on the $LCOE_{dis}$. Investment costs commonly tend to be higher than in the initial cost estimation. For this reason, the BMC were varied from 80 % to 180 %. When the BMC are almost twice as large, the $LCOE_{dis}$ reaches values higher than 290 €/MWh. The reduction of investment cost is therefore of great importance to CES economic feasibility. The validation of the cost estimates is of importance to the conclusiveness and significance of economic values presented in this work. The specific investment costs are further discussed in section 5.4.3.

The *RTE* also has a strong influence on the $LCOE_{dis}$, yet not as strong as the investment costs. An improvement of the system efficiency at the expense of an equally high (in percentile) investment is consequently not viable. As an increase in *RTE* commonly is coupled with an increase in the investment costs, the *RTE* was varied only by +/- 20 %. A reduction of the RTE also increases the dependency on the price of electricity charged to the system. The effect on the $LCOE_{dis}$ caused by changes in the electricity price is only indicated with a dotted line in Figure 5.21, as a reference in comparison to the other parameters. The behavior of the $LCOE_{dis}$ of different CES systems with various *RTE* for varying electricity prices and FLH_{dis} is discussed in the following section 5.3.2 and can be seen in Figure 5.22 and Figure 5.23.

The specific costs of CES systems are decreased by approximately 23 % with doubled capacity ($\alpha = 0.82$). The $LCOE_{dis}$ decreases accordingly with increased capacity (Figure 5.21). With the assumptions made, a 200 MW a-CES system reaches a $LCOE_{dis}$ of 180 €/MWh. A change in the interest rate at which the allowance for funds is lent is of similar significance than a change in the *RTE*. When the interest rate is reduced by 20 %, the $LCOE_{dis}$ is reduced by approximately 13 %. At an interest rate of 5 %, the $LCOE_{dis}$ becomes as low as 165 €/MWh.

The OMC of the CES systems are assumed as a share of the TCI. According to literature, OMC for CES systems can be as low as 1.5-3 % of the equipment costs [8] or even lower [20]. When varying the share from 1-8 % of TCI, the $LCOE_{dis}$ changes linearly with an increase/decrease in OMC. OMC as low as 1 % of TCI would allow the $LCOE_{dis}$ to drop below 170 €/MWh. The economic life of the CES system was found to have less influence on the $LCOE_{dis}$, despite its large value range.

5.4.2. Economic sensitivity analysis of the integrated CES systems

Electricity is traded in different markets, and the electricity price changes significantly over time, see Figure B.1a. The number of hours in a year at which electricity is available at a given price is limited. To evaluate the economic performance of the various CES systems presented in section 5.3, the electricity price is given as a function of FLH of discharge.

In Figure 5.22, the $LCOE_{dis}$ of the different systems is compared to increasing FLH_{dis}. The price of electricity is given as a function of the operation hours of the charging system based on the German day-ahead market in 2018 [138]. The systems are assumed to operate in the hours of the lowest electricity prices (see Figure B.1c). For the natural gas price, an average of the Henry Hub natural gas spot prices in the year 2018 was used (c_{NG} = 126 €/ton_{NG} [139]).

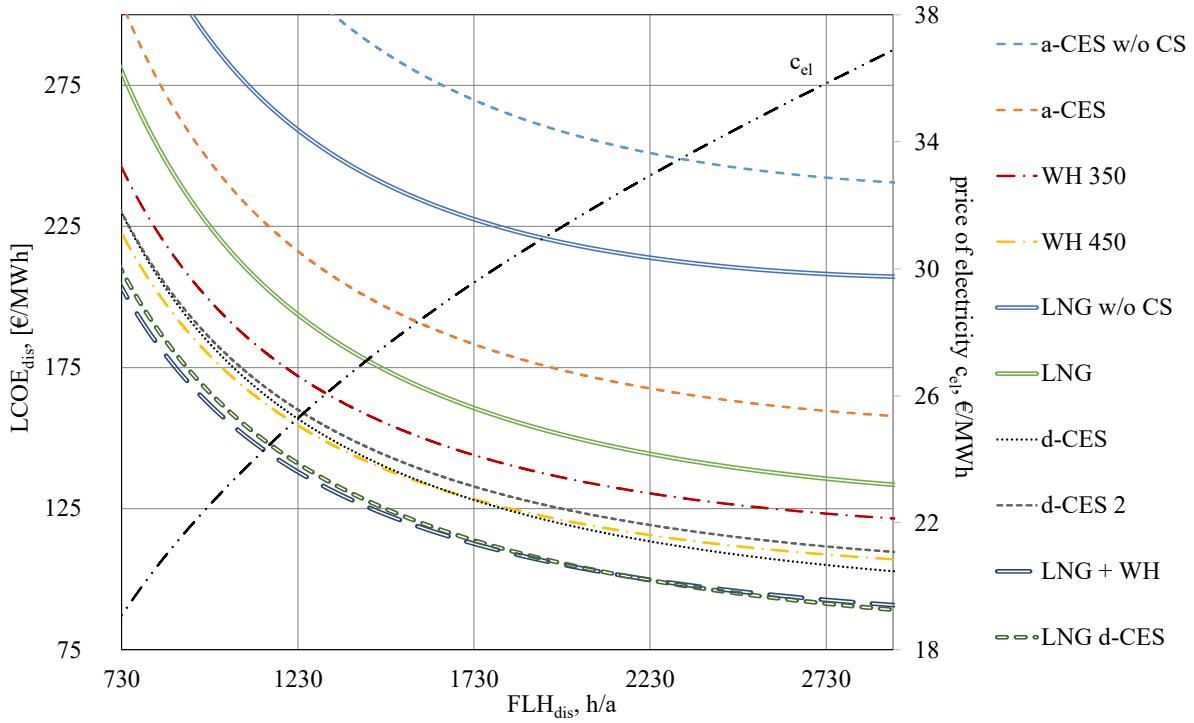

Figure 5.22: $LCOE_{dis}$ over the FLH_{dis} for the ten considered systems.

The higher the operation hours of the storage, the lower the $LCOE_{dis}$ of the system. With increased FLH_{dis}, the average price at which the electricity is charged to the system increases. For this reason, systems with higher *RTE* become more competitive at higher FLH_{dis}, despite higher initial investment costs.

For FLH_{dis} higher than approximately 1,730 h/a, the $LCOE_{dis}$ of the d-CES decrease below the $LCOE_{dis}$ of the a-CES system with waste heat integration at 450°C, the latter of which is more competitive at lower FLH_{dis}. The LNG systems with waste heat integration and with internal combustion also intersect but at higher FLH (2,150 h/a). Despite the small difference in $LCOE_{dis}$ of the two diabatic CES systems, the d-CES 2 system cannot compete due to its inferior *RTE*.

The ten systems were also compared, taking into account CO_2 emission prices of up to 40 €/ton$_{CO2}$, Figure D.10. The CO_2 emissions amount to 0.208 and 0.239 kg$_{CO2}$/kWh$_{dis}$ for the d-CES and the d-CES 2 system, respectively, similar to the CO_2 emissions of natural gas power plants (0.2 kg$_{CO2}$/kWh$_{dis}$ [140]). Already at an emission price of only 2.5 €/ ton$_{CO2}$, the attractiveness of diabatic CES systems decreases significantly as the $LCOE_{dis}$ of the d-CES systems becomes higher than that of the WH 450 system. At higher emission prices of 20-40 €/ton$_{CO2}$, even the WH 350 system becomes more economically feasible than the d-CES system.

Electricity prices and natural gas prices are impossible to predict over 40 years to come. When comparing the systems at fixed daily operation hours (τ_{char}/τ_{dis} = 8h/4h), the natural gas prices and the electricity prices can be varied more strongly. In Figure 5.23 (a) and (b), the LCOE$_{dis}$ of selected systems is compared over the price of the electricity charged to the systems. The price of electricity is only depicted until 80 €/MWh to make the intersections more visible. For higher electricity prices, the trends for the graphs stay consistent. The cost-optimal system (lowest $LCOE_{dis}$) is indicated with a black line for the different electricity price intervals.

For negative electricity prices (< - 15 €/MWh) the LNG integrated CES system without CS is most competitive, see Figure 5.23 (a). For positive electricity prices, only the two LNG integrated systems with either waste heat or combustion compete for the lowest $LCOE_{dis}$. At lower electricity prices, the LNG + WH system is more competitive; the LNG d-CES becomes more economical at higher electricity prices. With a higher natural gas price or CO_2 equivalent emission prices, the intersection of the $LCOE_{dis}$ graphs is shifted towards higher electricity prices. For the given cases of c_{NG}=126 €/ton$_{NG}$ (average 2018) and twice as large costs of c_{NG}= 252 €/ton$_{NG}$ (black dotted line in Figure 5.23), the LNG d-CES system becomes the cost-optimal system for electricity prices higher than c_{el} = 27 €/MWh and c_{el} = 49 €/MWh, respectively.

Both, the potential for integration of LNG and the recovery of waste heat are site dependent. Especially the availability of LNG waste cold is very limited. Only 23 large-scale land-based LNG receiving terminals exist in Europe. As an alternative, only the systems without LNG integration were compared in Figure 5.23 (b).

When only the CES systems without LNG integration are compared, the a-CES without cold storage is the cost-optimal CES system for electricity prices lower than - 23 €/MWh, followed by the waste heat integrated system WH 450 and the d-CES system. Depending on the fuel costs (126-252 €/ton$_{NG}$) the waste heat integration (450°C) is more economically feasible than the d-CES system until the price of electricity exceeds 20-46 €/MWh. The a-CES, in contrast, is in none of the given scenarios as the cost-optimal solution. As a result, the waste heat integration is evaluated as the most suitable option, taking into account increasing CO_2 emission prices and the dependency on fuel prices. Whereas, the d-CES system is the best alternative when a low-cost low-emission fuel becomes available.

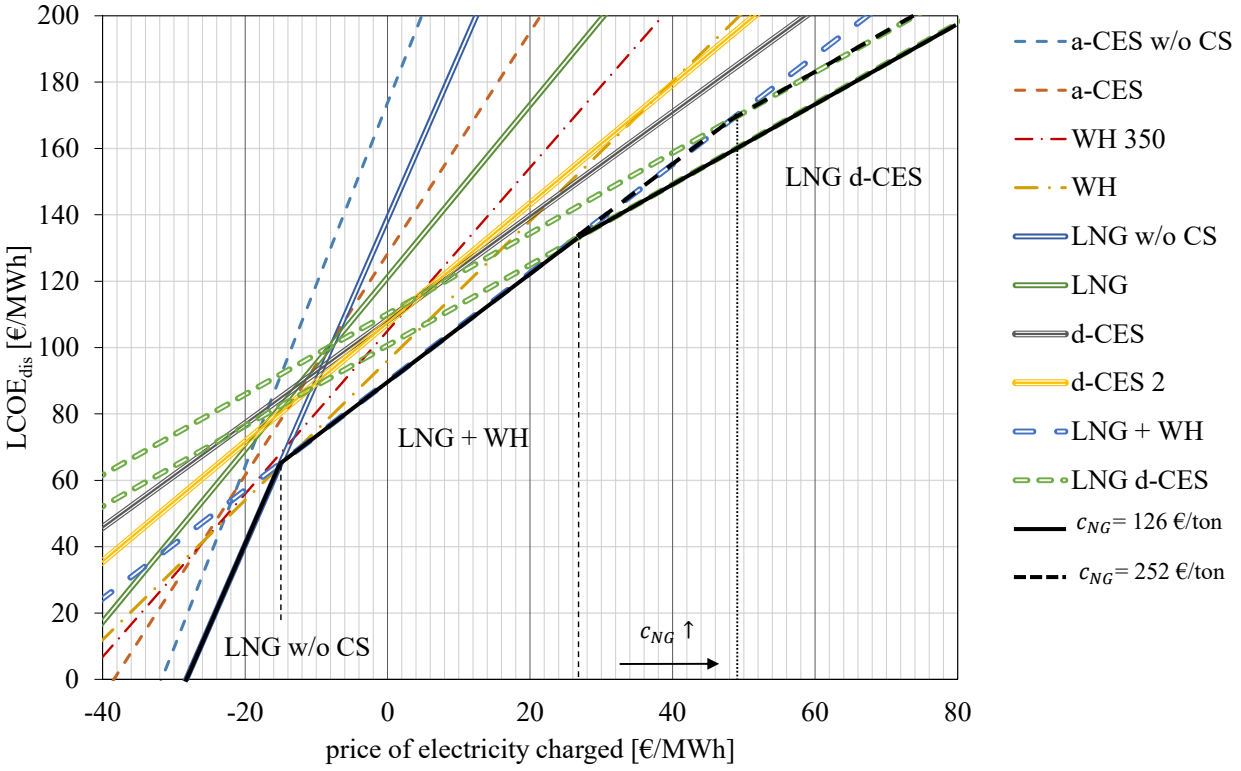

(a)

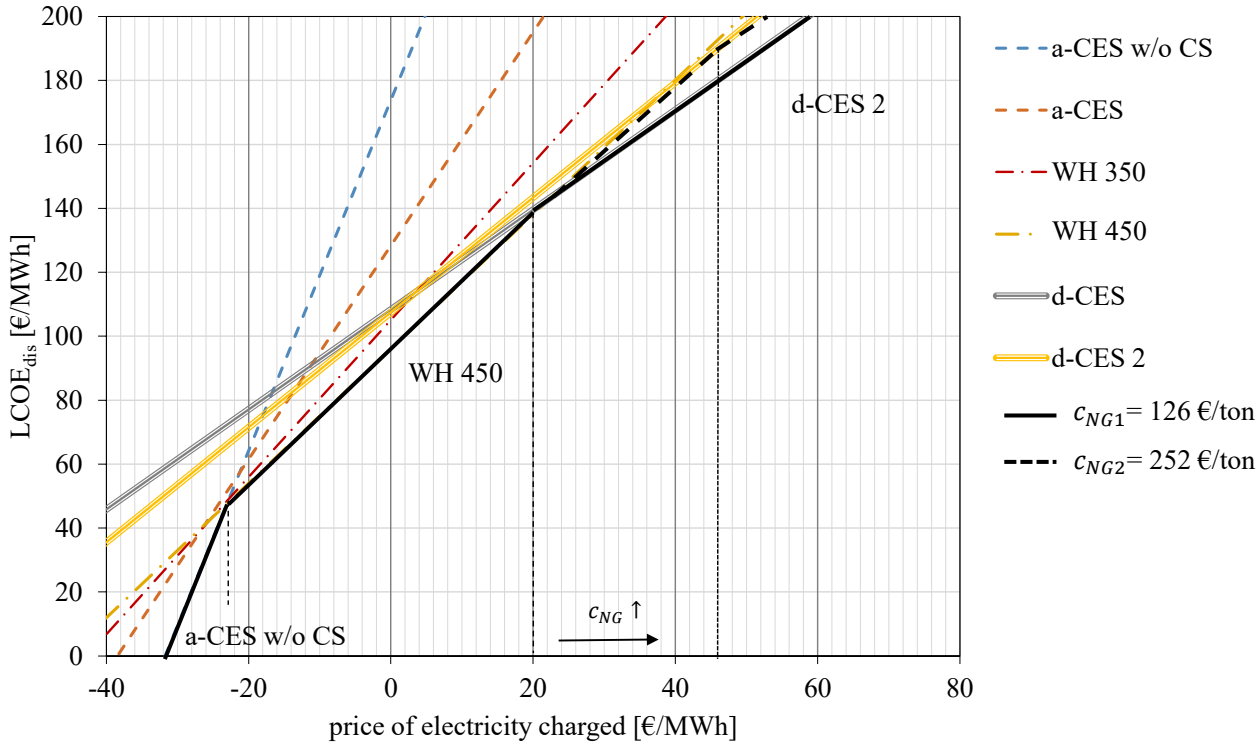

(b)

Figure 5.23: LCOE$_{dis}$ over the price of electricity for (a) all ten analyzed systems, and (b) the systems without LNG integration.

5.4.3. Validation and assessment of results

The $LCOE_{dis}$ of selected CES systems was compared with the $LCOE_{dis}$ of other bulk ES technologies to evaluate the competitiveness of the CES systems presented in this work, see Figure 5.24. The $LCOE_{dis}$ of the pumped hydro storage (PHS) and the adiabatic and the diabatic compressed air energy storage (CAES) are based on the data and the assumptions presented in [87]. The same assumptions were also adopted for the calculation of the levelized costs of the CES systems. Hence, the results slightly differ from the results presented in Figure 5.20. The values from the literature were compared to the a-CES system and the CES systems with the integration of waste heat (WH 450), combustion (d-CES) and re-gasifying LNG discussed in section 5.3.

Costs are very sensitive to the assumptions made in the estimation of the BMC and in the economic analysis (section 5.4.1). When comparing different grid-scale electricity storage technologies, the economic analysis needs to be performed with the same method and assumptions. For the results shown in Figure 5.24, the interest rate was set to 8 %, and daily-cycling operation was anticipated. Natural gas costs of 3.5 €ct/kWh and a CO_2 emission price of 5 €/t_{CO2} were considered for all systems [87].

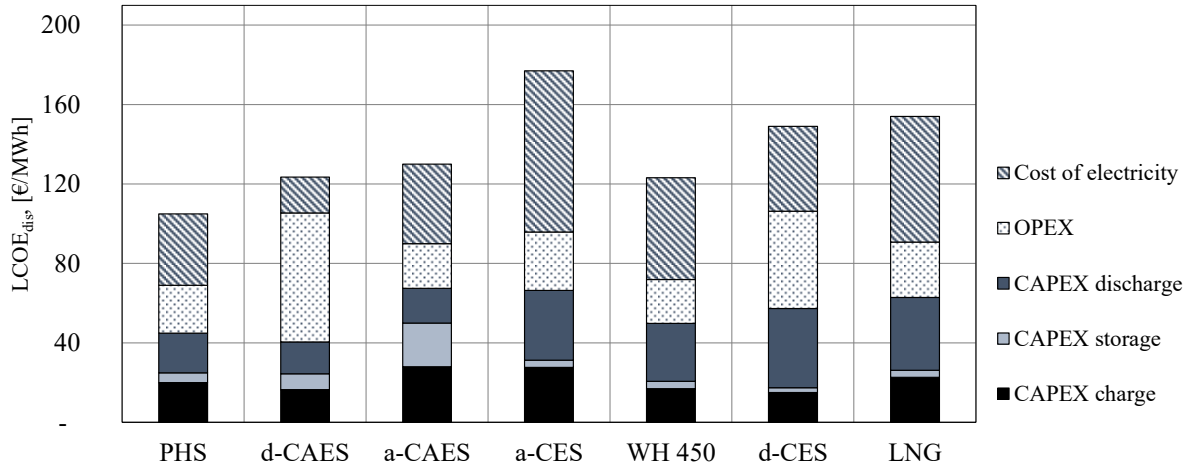

Figure 5.24: $LCOE_{dis}$ of PHS, d-CAES, a-CAES adopted from [87] and selected CES systems presented in this work.

The levelized costs associated with the initial investment (CAPEX) and the operation and maintenance (OPEX) of the adiabatic CES system is comparable to the a-CAES system. However, the $LCOE_{dis}$ of the a-CES is 28% higher due to the low RTE, despite the relatively low price of electricity of 30 €/MWh. As a result, only the integrated systems reach competitive $LCOE_{dis}$ under the given assumptions. In particular, the waste heat integrated system reaches a $LCOE_{dis}$ similar to the d-CAES system.

The initial investment of the CES systems presented in this work are based on cost estimation from various sources, see section 3.3.1. Hence, it is necessary to validate the specific investment costs with the aid of the values for the specific investment costs reported in the literature. In Figure 5.25, the specific investment costs obtained in the economic analysis of the base case systems, the optimized systems and the integrated systems (CES (results)) are compared to the

specific investment costs reported in the literature for PHS and CAES. The data for CES specific investment costs given in the literature (Figure 2.7 in section 2.4.2) is also shown as a reference in Figure 5.25 (CES (literature)).

The data is presented in a box-plot diagram; differentiating the lower, middle, and upper quartile with a box containing 50 % of the data points. The middle quartile or "median" indicates that half of the values are less or equal (and half are higher or equal) to the value. The arithmetic mean value is also indicated in Figure 5.25. The data for the PHS and the CAES are extracted from an extensive independent review on ES technologies [68].

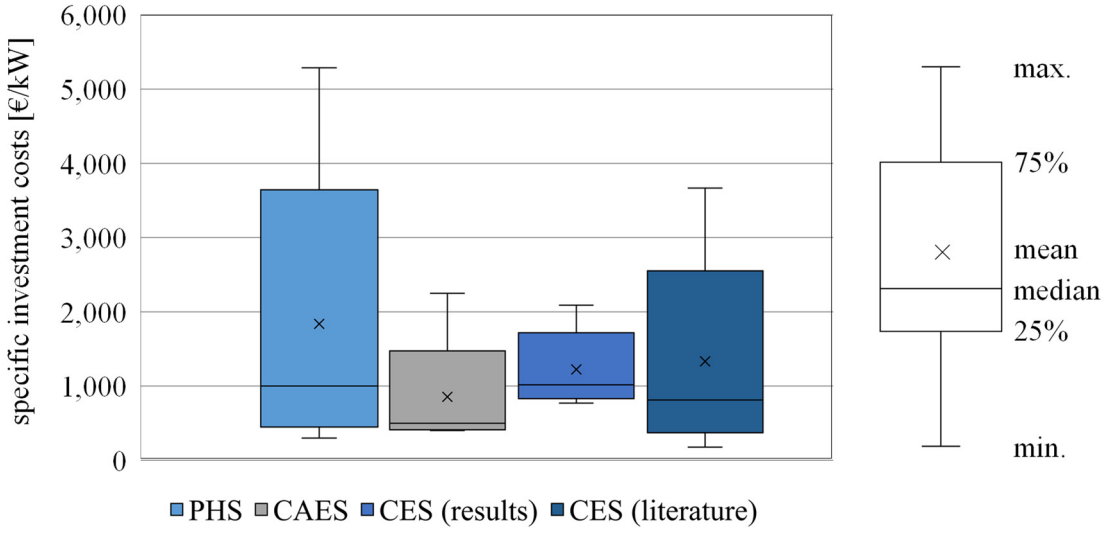

Figure 5.25: Box-plot diagram of the specific costs of PHS, CAES [68], and CES extracted from literature compared to values achieved in the analysis.

The values reported on PHS specific investment costs vary more strongly than for CAES and CES, which can be explained by the large number of PHS projects installed worldwide, ranging in size and economic conditions. Only a few CAES systems exist [76] and the investment costs reported in the literature are rather based on estimates than actual plants.

The values for the specific investment costs of CES systems determined in this thesis are within the cost range reported in the literature [6, 13-14, 16, 30-31, 34-35, 60, 68, 79]. The investment costs evaluated in this work vary less significantly than the values suggested in the literature. The majority of the systems in this thesis were designed for either 200 kg/s or for 100 MW of discharge power, and the specific investment costs of CES systems reduce with increased capacity (economy of scale). Hence, the deviation of the values given in the literature from the specific investment costs computed in this work can be explained by the larger capacity range of CES systems from 10 to 500 MW_{dis} [7, 16, 17, 29, 72]. The approach for the estimation of the BMC and economic assessment of CES systems that has been used is therefore validated.

Despite PHS reaching significantly higher values for the specific investment costs, the median value of PHS specific investment costs is comparable with that of CES (Figure 5.25). Due to the similar characteristics, CES is suitable for similar applications of PHS and CAES.

The specific investment costs of approximately 1,000 €/kW (1,270 €/kW for the a-CES) are comparable with the majority of value propositions introduced in section 2.5.2. However, the identified value propositions do not return the total revenue required, which is necessary to cover also the OMC, and the cost of the charged electricity of the CES systems. The total revenue requirement for the CES systems presented in this work range from 1,900-2,850 €/kW over 10 years while the additive value propositions for the same period reach a maximum of 1,600 €/kW [97, 106, 107, 108, 109].

With regard to the results of the economic sensitivity analysis, the specific investment costs, and the stacked value proposition, two sets ES applications can be identified to have the highest potential for CES:

- load follow together with renewable energy capacity firming, or
- renewable energy capacity firming in parallel with peak shaving (Figure 2.12).

In Figure 5.26, the $LCOE_{dis}$ obtained in the analysis is compared to competing technologies for an installed capacity of 100 MW/ 800MWh. The values presented are adopted from a broad study on energy storage costs [141], which was extended with CES by Highview Ltd. [142]. The comparison shows that battery-based technologies (e.g., Li-Ion, Zinc) cannot compete at large capacities. PHS reaches a higher $LCOE_{dis}$ than in the previous comparison as the economic life was kept to 20 years, while in the previous study 80 years were estimated for the PHS system. The higher value for the $LCOE_{dis}$ of the PHS system in [141] (compared to [87]) can also be explained by the large value range for the specific costs of PHS systems (Figure 5.25).

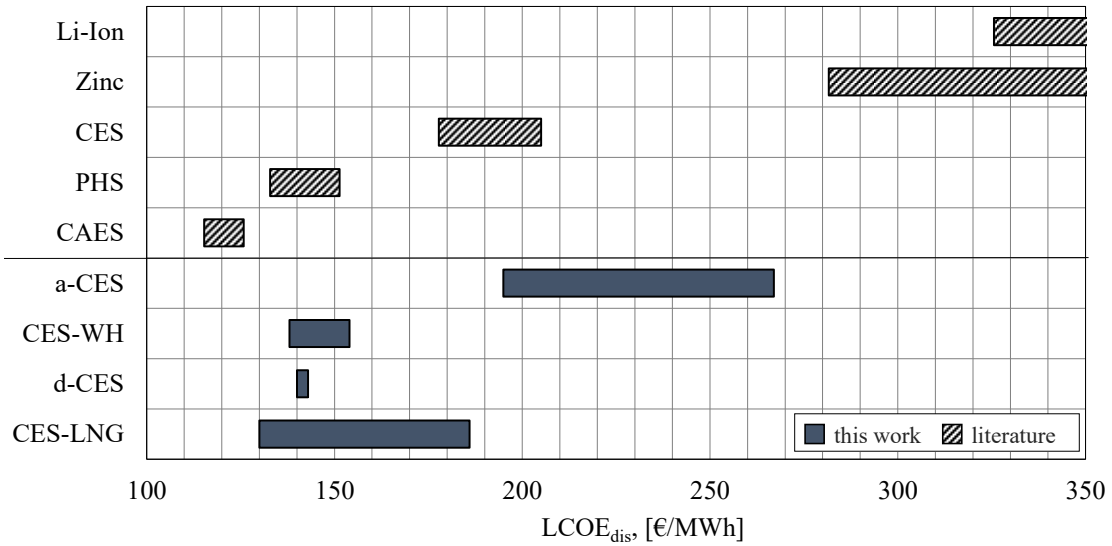

Figure 5.26: $LCOE_{dis}$ of selected CES systems compared to values from the literature [141, 142].

In general, a large number of studies investigating the $LCOE_{dis}$ (or levelized cost of storage LCOS) of different ES technologies have been published lately [87]. Different studies apply different research approaches and various assumptions, e.g., in terms of ES system design, performance, and size, or economic parameters. The $LCOE_{dis}$ reported for PHS range from 120 to 185 €/MWh. $LCOE_{dis}$ value ranges of 100-175 €/MWh are anticipated for CAES and 50-500 €/MWh (or 200-700 €/MWh [143]) for battery technologies [102, 143]. The value ranges

of the $LCOE_{dis}$ of PHS and CAES based on reviewed literature are given in a box diagram in comparison to CES in Figure D.12.

Despite the deviation of the results for the $LCOE_{dis}$ in the diverse studies, general conclusions can be made that were consistent independent of the study performed and can also be observed in Figure 5.26:

- the stand-alone adiabatic CES cannot compete with CAES and PHS in terms of the $LCOE_{dis}$.
- the integrated CES systems achieve $LCOE_{dis}$ values comparable with PHS and CAES,
- battery-based and hydrogen-based ES cannot compete at large scales and reach significantly higher values for the $LCOE_{dis}$ than CES.

Due to the absence of geographical constraints and the specific investment costs being similar to other bulk ES technologies, the CES technology may still be competitive. This is particularly the case when either the investment costs are reduced further or the *RTE* is increased, which can be achieved by the integration of external heat sources and sinks to CES systems.

Thus far, CES systems are expected to be able to compete for the selected frequent ES applications (with high discharge durations and a large number of cycles per annum) and create revenues that cover the initial investment costs.

5.5. Summary of the results and discussion

Evaluation of the charging processes

Three Claude-based and three Linde-based air liquefaction processes are compared in exergy-based analysis, and two charging configurations were identified:

- the most cost-efficient liquefaction process, the Kapitza process, and
- the process with the best thermodynamic performance, the Heylandt process.

The performance enhancement of the six liquefaction processes through the integration of cold storage was quantified: the liquid yield γ was significantly increased by 80-200 %, the specific power requirement w_{char} was reduced by 30-70 % and the exergetic efficiency ε of all liquefaction processes assessed was considerably improved by up to 200 %. The Claude-based systems reached the highest exergetic efficiencies, the lowest specific work requirement and the highest liquid yields. Sensitivity analysis showed that for lower liquefaction pressures (< 95 bar) the Claude and the Kapitza process are superior to the Heylandt process. The minimum work required to liquefy one kg of air in the Heylandt process amounts to 967 kJ/kg at 120 bar, reaching an exergetic efficiency of 81 %. The Claude/Kapitza process required more liquefaction work (w_{min}= 984 kJ/kg, 85 bar), and reached ε_{max} of only 78.5 %. The economic analysis revealed that the Kapitza process-based system has both the lowest specific investment cost and total revenue requirement of all three systems under the given conditions.

Evaluation of the adiabatic CES systems

Two stand-alone adiabatic CES systems (100 MW/400 MWh) based on the cost-optimal liquefaction process (*Base Case A*) and the highest-efficiency liquefaction process (*Base Case B*) were evaluated and optimized with exergy-based methods. The base case systems reached exergetic efficiencies of 44.5 % and 46.8 %. The exergy destruction in the charging process dominated with a share of 64-66 % of the exergy destroyed in the overall system, which puts emphasis on the importance of the selection and performance of the liquefaction process. The discharge system and the storage system made up only 28-30 % and 6 % of the overall exergy destruction, respectively. The exergy losses are caused almost exclusively by the thermal exergy vented from the heat storage to the environment after the discharge process. The effect of cold storage and heat storage were found significant to the performance of the overall system.

The total revenue requirement for the Base Cases A and B amounted to € 37.3 million and € 39.0 million annually, respectively. The heat exchangers were found to cause 62–64 % of the investment costs in both base case systems. The higher costs of the Base Case B were mainly attributed to the cost of MHE1, which is twice expensive if compared to that of Base Case A. Despite the lower exergetic efficiency and *RTE* of the Base Case A, a lower $LCOE_{dis}$ of 255 €/MWh was achieved, compared to 267 €/MWh in the Base Case B. The Base Case A was expected to stay more economically viable than the Base Case B, under the given condition and for electricity prices lower than 100 €/MWh.

In the iterative exergoeconomic analysis, the five sets of components which cause the majority of costs in both systems were identified: *the main heat exchangers*, *the turbines*, *the intercoolers*, *the compressors,* and *the reheater*s. The costs associated with the initial investment and the OMC are significantly higher than the costs associated with the thermodynamic inefficiencies (exergy destruction) in the majority of components. The decision

variables necessary to be changed for cost reduction of the investment costs were identified and applied in four iterations. In each of the iterations, a sensitivity analysis of the *RTE* and the $LCOE_{dis}$ was conducted. In both systems, the interrelation of the components was found to be very strong. Changing parameters with the intention of cost reduction in a single component had a great influence on the performance and costs of other components. The objective of reducing the costs associated with the initial investment $\dot{Z}_k$ was achieved for all of the selected components.

The Optimized Case B achieved lower levelized costs and higher exergetic efficiencies throughout the iterative optimization. The $LCOE_{dis}$ of the Base Case A was reduced from 255 €/MWh to 208 €/MWh at the expense of a reduction in the exergetic efficiency from 44.4 % to 38.1 %. The $LCOE_{dis}$ of the prior less cost-effective Base Case B was reduced to 195 €/MWh (ε_{tot} = 39.6 %).

Evaluation of the integration of heat sources and sinks to CES

Eight systems with integration of external heat and/or cold sources were compared in energetic, exergetic and economic analysis to two adiabatic CES systems. The integration of LNG waste cold as an alternative to cold storage was found thermodynamically infeasible. The low-temperature exergy supplied by the LNG increased ε_{tot} by only 1.4 %, while cold storage increases ε_{tot} by more than 60 %. When introducing LNG in addition to cold storage, the amount of air liquefied increases by another 40 %. Waste heat integration was found to be only beneficial to the *RTE* (39.4 % → 62.5 %). The energetic and exergetic efficiencies decrease by up to 50 %. Despite the additional investment, the integrated systems reach significantly lower specific investment costs and $LCOE_{dis}$ due to the increased *RTE* concerning the a-CES system. The CES system with both waste heat and waste cold integration achieved the lowest $LCOE_{dis}$ of 130 €/MWh. The diabatic CES systems and the system with waste heat integration (450 °C) reached comparably low $LCOE_{dis}$ of 131-143 €/MWh. CO_2 emission prices of only 2.5 €/ton would make the d-CES inferior to the waste heat integrated system. The costs of the LNG integrated systems were found to decrease with an increased mass flow of LNG, despite no further increase in *RTE* (51 %). With an increase of the $\dot{m}_{LNG}$ from 10-20 % of $\dot{m}_{air}$, the $LCOE_{dis}$ is reduced by 10 % and reaches values lower than 122-170 €/MWh.

Economic sensitivity analysis

Changes in the full load hours of the discharge unit were revealed to have the strongest influence on the $LCOE_{dis}$. Therefore only frequent energy applications were evaluated to be economically viable for CES systems, e.g., load shedding, energy time shift or capacity firming. Despite the low storage losses, the operation as a reserve is unsuitable for CES systems. As changes in the investment costs also have a strong influence on the $LCOE_{dis}$, the specific investment cost obtained in economic analysis was validated in comparison to values reported in the literature. CES systems are able to achieve competitive specific investment costs (1,000 €/kW) similar to PHS and can compete for the same applications. The adiabatic CES was found inferior to compressed air energy storage (CAES) and pumped hydro storage (PHS) in terms of the $LCOE_{dis}$ due to the lower *RTE*. The integrated systems, in contrast, achieved competitive values for the $LCOE_{dis}$ but entail site dependency. Potential methods of integrating heat sources and/or sinks to CES systems require a more thorough investigation in terms of availability and costs. None of the stacked value propositions identified in section 2.5.2 based on the reviewed literature cover the total revenue required for the CES systems presented in this work (1,900-2,850 €/kW).

Chapter 6: Conclusion and outlook

Cryogenic energy storage is a grid-scale energy storage concept with promising characteristics such as; being based on mature technology, high volumetric energy density, absence of geographical constraints, long cycle life, and low storage losses. The largest drawback of the technology that limits its commercialization and successful application (e.g., for grid balancing) is the high specific cost relative to its low roundtrip efficiency (40-60 %). The integration of heat sources and sinks have benefits for both CES efficiency and costs. However, so far, no highest-efficiency or cost-optimal system configuration for CES has been identified, nor the effect of the integration on the economic and thermodynamic performance has been thoroughly investigated.

This work aimed to identify measures for cost reduction and thermodynamic performance enhancement of CES systems with the aid of exergy-based methods. Under steady-state operation, various system configurations were designed in Aspen Plus® based on an extensive literature review and sensitivity analysis. Cryogenics-based energy storage state of the art was assessed and benchmarked towards competing technologies. Potential applications and challenges to CES commercialization were assessed. The most competitive charging process configurations with regards to costs and thermodynamic performance were identified. The effect of cold storage on the efficiency and costs was measured. Two base case systems were presented and evaluated in exergetic, economic, and exergoeconomic analysis. In the exergoeconomic analysis, the cost of the thermodynamic inefficiencies in the system was quantified, and measures for cost reduction were identified. In exergoeconomic optimization, two optimized cases were obtained. Eight systems with the integration of waste heat, combustion, and LNG waste cold were designed based on the optimized CES configuration. The integrated systems were further evaluated in comparative exergetic and economic analysis. In an economic sensitivity analysis, the economic viability of CES was assessed and the results from the economic analyses conducted in this work were validated with respect to values reported in literature.

6.1. Summary of the main results

The extended summary of the main results is given in section 5.5. The main findings identified in this thesis are:

- The integration of cold storage significantly increases the thermodynamic performance and reduce the costs of the liquefaction (charging) processes in CES systems.
- The Linde-based liquefaction processes are not suitable for implementation in CES systems.
- The costs associated with the initial investment dominate in the majority of the components of the CES systems, while the costs associated with exergy destruction are minor.
- A cost-optimal adiabatic CES system design was obtained; the $LCOE_{dis}$ of the 100 MW/400 MWh system was reduced from 267 €/MWh to 195 €/MWh at the expense of a reduction in the roundtrip efficiency from 47 to 40 %.
- With the integration of waste heat, combustion and/or re-gasifying LNG, the $LCOE_{dis}$ are reduced to 122-170 €/MWh.
- The integration of CES was found a viable option reaching efficiencies larger than 70 %.
- The $LCOE_{dis}$ when recovering waste heat at 450 °C is competitive with d-CES systems at higher fuel or CO_2 emission prices.
- The integration of LNG is not an alternative to cold storage and is only beneficial to CES thermodynamic performance in combination with cold storage.
- The operation hours of the discharge unit, the specific costs, the response time and the RTE are the limiting factors for CES economic feasibility.
- Only frequent bulk ES applications with long discharge duration are suitable for CES systems.
- CES specific costs reached a median value of approximately 1,000 €/kW, similar to PHS.
- The stacked value proposition when providing multiple ES applications was found to potentially reach values of 1,600 €/kW.
- The combined applications that are most feasible for CES systems are *load follow* with *RE capacity firming* and *RE capacity firming* with *peak shaving* apart from other frequent bulk energy applications.
- The stacked value propositions identified for the combined applications adopted from the reviewed literature do not recover the revenue required for the CES systems under the given assumptions.

6.2. Scope of the present work

The benchmark analysis presented revealed the advantages of CES towards other bulk ES technologies. When assessing potential applications, this work showed that means to reduce the high specific investment costs and increase the RTE need to be implemented before CES becomes competitive. The cost-optimal design configuration for the adiabatic CES system presented in this work as well as the quantified enhancement in the thermodynamic and the economic performance of CES with system integration should be considered for future process design and analysis.

The charging process was shown to cause both the majority of exergy destruction and the majority of the investment costs in the CES systems. The choice of the liquefaction process is therefore of great significance to the economic and the thermodynamic viability of the systems. The Linde-based processes that were presented in various publications and patents [10, 40, 41, 43, 44, 52] are not viable for implementation in CES systems. Instead of the Linde-process, the Heylandt process is recommended as the charging process for CES systems with cold recovery and storage.

Despite the cold storage configuration itself not being subject to this thesis, the necessity for further development of the cold storage was confirmed. The low-temperature exergy recovery is of crucial importance to the *RTE* and the cost-effectiveness of the entire CES system. The liquefaction work and the levelized costs of the liquefied air is shown to be reduced to half, despite the additional investment costs associated with the cold storage. Even when an additional heat sink, e.g. “waste cold” from LNG regasification is available, the cold storage is still necessary to enable reasonable *RTE* and $LCOE_{dis}$. Without the high-grade cold (- 180 °C to - 160 °C) provided by the internal cold recovery and storage, the CES with integration of re-gasifying LNG would reach a *RTE* of only 26 %. Thus, in particular low-cost material that can realize the efficient recovery of the high-grade cold is an important subject for further research and essential for CES commercialization.

In the exergoeconomic analysis, the reduction in efficiency was found to be stronger than expected when changing the parameters of selected components. The operation of selected components was found to have a significant influence on the performance of other components. The strong correlation between the components limits the cost-saving potential of CES systems, which is why the endogenous and exogenous part of the exergy destruction of the components in CES systems should be identified in an advanced exergetic analysis.

CES is based on mature components commonly used in the LNG value chain, for industrial gases and power generation. Due to the worldwide increasing LNG capacity, a reduction in the costs of large-scale cryogenic equipment is plausible, which would have a positive effect on CES commercialization. Also, the further development of gas turbines for low-temperature heat recovery application could be of remarkable benefit to CES systems. After the exergoeconomic optimization was performed, the turbines remained the components with the highest cost-importance. Thus, a cost reduction of the turbines could reduce the $LCOE_{dis}$ of the CES systems notably.

For system integration, several findings were of significance. The specific costs of the CES system were found to be reduced with larger mass flow rates of LNG, despite no further increase in the RTE. Thus, mass flow rates of the LNG higher than necessary to increase the RTE are recommended. The integration of LNG to adiabatic CES systems with cold storage was found

to increase the share of air liquefied by another 27 %. The RTE of 63-70 % as proposed in [8, 62, 63], however, are not achievable with LNG integration alone. Only systems with internal combustion of natural gas or the combination of both waste heat and cold achieve RTE of 70 % and higher. The integration of LNG shows great potential and should be subject to further investigation. In particular, the applicability of integrating LNG to the main heat exchanger in the CES system should be assessed with regards to associated costs and risks.

The recovery of waste heat was claimed a core advantage of CES systems in various publications [8, 10, 14, 74]. The recovery of waste heat was proven beneficial for the *RTE* in this work. The energetic and exergetic efficiency, in contrast, were shown to decrease due to the heat which is not used in the discharge but vented before the intercooling process. In particular, for CES systems with waste heat integration, an additional ORC recovering the surplus heat is strongly recommended. Moreover, further investigation of the availability of waste heat sources with suitable temperatures (> 300 °C) and suitable energy transfer materials is necessary to evaluate the economic feasibility.

The efficiencies proposed in the literature are only achievable at significantly higher costs than suggested or with the integration of external heat sources or sinks. For a 100 MW/400 MWh stand-alone adiabatic CES system, *RTE*s of 40-47 % at specific investment costs of 1,270-2,090 €/kW are realizable, reaching $LCOE_{dis}$ as low as 195 €/MWh.

The $LCOE_{dis}$ of the CES system is only competitive to PHS and CAES with the integration of external heat sources or sinks. With the integration of waste heat or LNG regasification, CES loses the competitive-edge towards PHS and CAES of site-independent storage. Whereas, a waste heat source may be more easily accessible than an underground salt cavern for CAES or an elevated water reservoir with significant scale for PHS. With the integration of combustion, CES loses its advantage of being classified as a “carbon-neutral” or “low-carbon” technology. This work showed that the integration of CES systems is of significance to both costs and thermodynamic performance which is why a thorough assessment of the availability and hidden costs of heat sources and sinks is another potential research field in the context of CES.

The findings of this research are also applicable to other fields. The advances made can be applied to cold power generation cycles integrated in LNG regasification units or in the field of introducing flexible loads, e.g., using LNG terminals or ASU as variable loads.

The slow response time of CES systems was identified to be one of the main limiting factors for CES to provide selected ES applications. This obstacle could be overcome by coupling CES systems with a high power ES technology, e.g., flywheel or battery-based storage. Reducing the response or “ramp up” time of CES would significantly increase the number of applications CES could supply. Moreover, this work showed that for greater revenue, the storage needs to provide multiple applications. With a faster response time, CES would be suitable for more easily combinable ES applications, which would significantly increase the monetary value of the technology.

The identified stacked value propositions for the combined ES applications were found to cover the costs associated with the total capital investment of the CES systems but were unable to recover the total revenue required. Either additional revenue streams need to be identified, and financial incentives for the investment in ES need to be given, or the CES costs need to be significantly reduced, in order for CES to become economically viable.

6.3. Limitations

In this work, the systems were simulated under steady-state conditions. The thermodynamic performance of the system may differ significantly during the start-up, the shut-down or part load operation of the CES system. Not only the constraint of the response time but also the efficiency have a significant effect on CES economic viability. Thus, a dynamic simulation investigating the drop in the efficiency and associated costs should be undertaken.

For the economic evaluation, the bare module costs are estimated based on an existing system design. The cost estimates are always exposed to large uncertainties and can be a strong point of weakness. Whereas in this work the assumptions made and sources accessed are thoroughly unfolded and enable further improvement of the cost estimates. Moreover, the costs were partially based on past purchase orders and costs published by the technologies' manufacturers and developers which reduce uncertainties. Finally, the specific costs were validated with values stated in literature and undertaken sensitivity analysis.

For the monetary evaluation of different ES applications, value propositions given for selected ES applications in literature were assessed. The monetary value proposition of a specific application can only be gained in detailed simulation and analysis (energy system modeling), taking into account the storage configuration and the market conditions.

In this work, CES was benchmarked towards other bulk ES technologies that compete for the same applications. Flexibility could also be supplied to power grids by other means, e.g., grid interconnection, demand-side management, or flexible generation. A comparison should be drawn between the application of bulk ES and other flexibility options for CES feasibility.

6.4. Summary of potential future work

This work addressed several challenges of CES, and many interesting results were obtained. Nonetheless, further investigation is necessary to analyze and optimize CES and facilitate the further development and application of the technology. Based on the main findings, scope, and limitations of this research, the following potential research paths were identified:

- Dynamic simulation of the proposed cost-optimal adiabatic CES system.
- Application of an advanced exergoeconomic analysis on the proposed system.
- Assessment of the market potential of CES systems and monetary value proposition of CES applications through energy system and ES application modeling.
- Feasibility study on the integration of waste heat, ORC, and LNG in regards to availability, risks, costs.
- Assessment of low-cost and high-efficient cold storage material and geometry.
- Evaluation of air separation or liquefaction units and LNG terminals as potential variable loads or ES.
- Experimental studies on components of CES systems to identify technological difficulties in the process design and validate the behavior, e.g., the cryogenic pump, the high-pressure cryogenic HE, cold expander or the cold storage and recovery.

References

[1] T. Kousksou, P. Bruel, A. Jamil, T. ElRhafiki and Y. Zeraouli, "Energy storage: Applications and challenges," *Solar Energy Materials & Solar Cells*, 120:59-80, 2014.

[2] S. Hamdy, T. Morosuk and G. Tsatsaronis, "Cryogenics-based energy storage: Evaluation of cold exergy recovery cycles," *Energy,* 138:1069-1080, 2017.

[3] S. Hamdy, T. Morosuk and G. Tsatsaronis, "Cryogenic Energy Storage: Characteristics, Potential Applications and Economic Benefit," in *Recent Developments in Cryogenics Research*, New York, Nova Science Publishers, Inc., 2019, pp. 277-310.

[4] M. Beaudin, H. Zareipour, A. Schellenberg and W. Rosehart, "Chapter 1 – Energy Storage for Mitigating the Variability of Renewable Electricity Sources," in *Energy Storage for Smart Grids - Planning and Operation for Renewable and Variable Energy Resources (VERs)*, Academic Press Inc, 2015, pp. 1-33.

[5] A. Solomon, D. M. Kammena and D. Callaway, "The role of large-scale energy storage design and dispatch in the power grid: A study of very high grid penetration of variable renewable resources," *Applied Energy,* 134:75-89, 2014.

[6] A. Castillo and D. F. Gayme, "Grid-scale energy storage applications in renewable energy integration: A survey," *Energy Conversion and Management,* 87:885-894, 2014.

[7] D. Akinyele and R. Rayudu, "Review of energy storage technologies for sustainable power networks," *Sustainable Energy Technologies and Assessments,* 8:74-91, 2014.

[8] D. Strahan, M. Akhurst, D. A. Atkins, P. I. Arbon and M. Ayres, "Liquid Air in the energy and transport systems. Opportunities for industry and innovation in the UK," Center For Low Carbon Futures, 2013. URL: https://www.dearman.co.uk/wp-content/uploads/2016/05/Liquid-air-in-the-energy-transport-systems.pdf (last accessed 21.05.2019)

[9] D. Mohler and D. Sowder, "Chapter 23 – Energy Storage and the Need for Flexibility on the Grid," in *Renewable Energy Integration - Practical Management of Variability, Uncertainty and Flexibility in Power Grids*, Academic Press Inc, 2014, pp. 285-292.

[10] B. Ameel, C. T'Joen, K. De Kerpel, P. De Jaeger, H. Huisseune and M. Van Belleghem, "Thermodynamic analysis of energy storage with a liquid air Rankine cycle," *Applied Thermal Engineering,* 53:130-140, 2013.

[11] W.-D. Steinmann, "Thermo-mechanical concepts for bulk energy storage," *Renewable and Sustainable Energy Reviews,* 75:205-219, 2017.

[12] B. Stöver, C. Bergins, A. Aleksee and C. Stiller, "Flüssigluftenergiespeicher (LAES): ein flexibles System für großtechnische Anwendung," in *Kraftwerkstechnik 2014: Strategien, Anlagentechnik und Betrieb*, M. Beckmann and A. Hurtado, Eds., Freiberg,

SAXONIA Standortentwicklungs- und –verwaltungsgesellschaft mbH, 2014, pp. 876-886.

[13] G. Strbac, M. Aunedi, D. Pudjianto, P. Djapic, F. Teng, A. Sturt, D. Jackravut, R. Sansom, V. Yufit and N. Brand, "Strategic Assessment of the Role and Value of Energy Storage Systems in the UK Low Carbon Energy Future," Imperial College, London, 2012. URL: https://www.carbontrust.com/media/129310/energy-storage-systems-role-value-strategic-assessment.pdf (last accessed 20.05.2019)

[14] R. Morgan, S. Nelmes, E. Gibson and G. Brett, "An analysis of a large-scale liquid air energy storage system," in *Proceedings of the Institution of Civil Engineers - Energy*, 168(2):135-144 2015.

[15] B. Stöver, S. Rehfeldt, A. Alekseev and C. Stiller, "Process Engineering and Thermodynamic Evaluation of Concepts for Liquid Air Energy Storage," Duisburg, Pullach, Germany, 2013.
URL: http://pennwell.websds.net/2013/vienna/pge/papers/T7S4O3-paper.pdf (last accessed 10.11.2018)

[16] R. Morgan, S. Nelmes, E. Gibson and G. Brett, "Liquid air energy storage - analysis and first results from pilot scale demonstration plant," *Applied Energy,* 137:845-853, 2015.

[17] L. Chai, J. Jiu, L. Wang, L. Yue, L. Yang, Y. Sheng and H. Chen, "Cryogenic energy storage characteristics of a packed bed at different pressures," *Applied Thermal Engineering,* 63:439-446, 2014.

[18] G. Brett and M. Barnett, "The application of liquid air energy storage for large scale long duration solutions to grid balancing," *EPJ Web of Conferences 79, 03002,* 2014.

[19] D. Strahan, "Liquid Air Technologies - a guide to the potential," Centre for Low Carbon Futures and Liquid Air Energy Network, Birmingham, 2013. URL: http://dearman.co.uk/wp-content/uploads/2016/05/Liquid-air-technologies.pdf (last accessed 20.05.2019).

[20] P. Agrawal, A. Nourai, L. Markel and R. Fioravanti, "Characterization and Assessment of Novel Bulk Storage Technologies - A Study for the DOE Energy Storage Systems Program," Sandia National Laboratories, Carlifornia, SAND2011-3700, 2011. URL: https://prod-ng.sandia.gov/techlib-noauth/access-control.cgi/2011/113700.pdf (last accessed 21.05.2019).

[21] E. Smith, "Storage of Electrical Energy using Supercritical Liquid Air," in *Proceedings of the Institution of Mechanical Engineers June 1977 vol. 191 no. 1*, Newcastle, 1977.

[22] H. Wakana, K. Chino and O. Yokomizo, "Cold heat-reused air liquefaction/vaporization and storage gas turbine electric power system". USA Patent US 20010004830 A1, 2001.

[23] K. Chino and H. Araki, "Evaluation of Energy Storage Method Using Liquid Air," *Heat Transfer - Asian Research,* 29(5):347-357, 2000.

[24] H. Araki, M. Nakabaru and K. Chino, "Simulation of Heat Transfer in the Cool Storage Unit of aLiquid–Air Energy Storage System," *Heat Transfer - Asian Research,* 31(4):284-294, 2002.

[25] K. Chino, Y. Nishiura, Y. Noguchi and O. Yokomizo, "Energy storaging type gas turbine power generating system". Japan Patent JP3460433B2, 2003.

[26] M. Atsumi, "Liquid air storage gas turbine power generation system". Japan Patent JPH08149722A, 1996.

[27] K. Kishimoto, K. Hasegawa and T. Asano, "Development of Generator of Liquid Air Energgy Storage Energy System," *Technical Review - Mitsubishi Heavy Industries*, 35(3):117-120, 1998.

[28] T. Tsuji, "Cryogenic turbine power generation system". Japan Patent JPH11343865A, 1999.

[29] Y. Ding, L. Tong, P. Zhang, Y. Li, J. Radcliffe and L. Wang, "Chapter 9 - Liquid Air Energy Storage," in *Storing Energy* , T. M.Letcher, Ed., Oxford, Elsevier, 2016, pp. 167-181.

[30] Liquid Air Energy Network, "Liquid Air Energy Network," 2013. [Online]. URL: http://www.liquidair.org.uk/about (last accessed 15.12.2017).

[31] Highview Enterprises Ltd, "Highview Power Storage," 2017. [Online]. URL: www.highview-power.com (last accessed 15.05.2019).

[32] Highview Power Storage, "Liquid Air Energy Network," March 2012. [Online]. URL: http://www.liquidair.org.uk/files/appendices/01.pdf. (last accessed 26.10. 2016).

[33] EERA/EASE, "European Association for Storage of Energy," 16 01 2017. [Online]. URL: http://ease-storage.eu/wp-content/uploads/2015/10/EASE-EERA-recommendations-Roadmap-LR.pdf (last accessed 21.05.2019).

[34] J. C. Mankins, "Technology readiness assessments: A retrospective," *Acta Astronautica,* 65(9–10):1216-1223, 2009.

[35] J. C. Mankins, "Technology Readiness Levels," White paper NASA, 1995. [Online]. URL: http://www.artemisinnovation.com/images/TRL_White_Paper_2004-Edited.pdf (last accessed 20.05.2019).

[36] S. Hamdy, T. Morosuk and G. Tsatsaronis, "Exergoeconomic optimization of an adiabatic cryogenics-based energy storage system," *Energy, 183:*812-824, 2019.

[37] H. Chen, T. N. Cong, W. Yang, C. Tan, Y. Li and Y. Ding, "Progress in electrical energy storage system: A crytical review," *Progress in Natural Science ,* 19(3):291-312, 2009.

[38] O. Edberg and C. Naish, "Energy Storage and Management Study," AEA Technology plc, Ayrshire, ED47766 (4), 2010.

[39] Y. Li, "Cryogen Based Energy Storage: Process Modelling and Optimization.," University of Leeds, Dissertation, Leeds, 2011.

[40] H. Peng, X. Shan, Y. Yang and X. Ling, "A study on performance of a liquid air energy storage system with packed bed units," *Applied Energy*, 211:126–135, 2018.

[41] X. She, X. Peng, B. Nie, G. Leng, X. Zhang, L. Weng, L. Tong, L. Zheng, L. Wang and Y. Ding, "Enhancement of round trip efficiency of liquid air energy storage through effective utilization of heat of compression," *Applied Energy*, 206:1632-1642, 2017.

[42] A. Sciacovelli, A. Vecchi and Y. Ding, "Liquid air energy storage (LAES) with packed bed cold thermal storage – From component to system level performance through dynamic modelling," *Applied Energy,* 190:84–98, 2017.

[43] G. L. Guizzi, M. Manno, L. M. Tolomei and R. M. Vitali, "Thermodynamic analysis of a liquid air energy storage system," *Energy,* 93:1639-1647, 2015.

[44] X. Xue, S. X. Wang, X. L. Zhang, C. Cui, L. Chen, Y. Zhou and J. Wang, "Thermodynamic analysis of a novel liquid air energy storage system," *Physics Procedia,* 67:733-738, 2015.

[45] Y. Li, H. Chen and Y. Ding, "Fundamentals and applications of cryogen as a thermal energy carrier: A critical assessment," *International Journal of Thermal Science,* 49(6):941-949, 2010.

[46] S. Hamdy, F. Moser, T. Morosuk and G. Tsatsaronis, "Exergy-Based and Economic Evaluation of Liquefaction Processes for Cryogenics Energy Storage," *Energies,* 493:1-18, 2019.

[47] F. G. Kerry, Industrial gas handbook: gas separation and purification, Boca Raton, Florida, USA: Taylor & Francis Group, LLC, 2007.

[48] R. F. Barron, Cryogenic Systems, Second Edition ed., New York: Oxford University Press, Clarendon Press, Oxford, 1985.

[49] D. M. Herron and R. Agrawal, "Air liquefaction: distillation," in *Encyclopedia of Separation Science*, Air Products and Chemicals, Inc, Allentown, PA, USA, 2000. URL: http://index-of.co.uk/Tutorials-2/AIR%20LIQUEFACTION%20-%20DISTILLATION.pdf (last accessed 20.05.2019)

[50] E. Borri, A. Tafone, A. Romagnoli and G. Comodi, "A preliminary study on the optimal configuration and operating range of a ‘‘microgrid scale” air liquefaction plant for Liquid Air Energy Storage," *Energy Conversion and Management*, 143:275-285 2017.

[51] R. F. Abdo, H. T. Pedro, R. N. Koury, L. Machado, C. F. Coimbra and M. P. Porto, "Performance Evaluation of various cryogenic energy storage systems," *Energy,* 90:1024-1032, 2015.

[52] H. Chen, Y. Ding, T. Peters and F. Berger, "A method of storing energy and a cryogenic energy storage system". USA Patent EP1989400A1, 27 02 2006.

[53] L. Hüttermann and R. Span, "Investigation of storage materials for packed bed cold storages in liquid air energy storage (LAES) systems," *Energy Procedia,* 143:693-698, 2017.

[54] B. Kantharaj, S. Garvey and A. Pimm, "Thermodynamic analysis of a hybrid energy storage system based on compressed air and liquid air," *Sustainable Energy Technologies and Assesments,* 11:159-164, 2015.

[55] X. Weiqing, W. Jia, C. Maolin and S. Yan, "Liquid air fueled open-closed cycle Stirling engine," *Energy Conversion and Management,* 94:210-220, 2015.

[56] C. Ordonez, "Liquid nitrogen fueled closed Brayton cycle cryogenic heat engine," *Energy Conversion & Management,* 41:331-341, 2000.

[57] Y. Li, H. Cao, S. Wang, Y. Jin, D. Li, X. Wang and Y. Ding, "Load shifting of nuclear power plants using cryogenic energy storage technology," *Applied Energy ,* 113:1710-1716, 2014.

[58] J. Szargut and I. Szczygiel, "Utilization of the cryogenic exergy of liquid natural gad (LNG) for the production of electricity," *Energy,* 34(7):827-837, 2009.

[59] S. Hamdy, T. Morosuk and G. Tsatsaronis, "Exergetic and economic assessment of integrated cryogenic energy storage systems, " *Cryogenics,* 99:39–50, 2019.

[60] M. Papapetrou, G. Kosmadakis, A. Cipollina, U. L. Commare and G. Micale, "Industrial waste heat: Estimation of the technically available resource in the EU per industrial sector, temperature level and country," *Applied Thermal Engineering,* 138:207-216, 2018.

[61] Q. Zhang, C. F. Heuberger, I. E. Grossmann, A. Sundaramoorthy and J. M. Pinto, "Optimal Scheduling of Air Separation with Cryogenic Energy Storage," *Computer Aided Chemical Engineering, Elsevier,* 37:2267-2272, 2015.

[62] I. Lee, J. Park and I. Moon, "Conceptual design and exergy analysis of combined cryogenic energy storage and LNG regasification processes: Cold and power integration," *Energy,* 140:106 -115, 2017.

[63] T. Zhang, L. Chen, X. Zhang, S. Mei, X. Xue and Y. Zhou, "Thermodynamic analysis of a novel hybrid liquid air energy storage system based on the utilization of LNG cold energy," *Energy,* 155:641-650, 2018.

[64] J. Kim, Y. Noh and D. Chang, "Storage system for distributed-energy generation using liquid air combined with liquefied natural gas," *Applied Energy,* 212:1417–1432, 2018.

[65] X. Peng, X. She, L. Cong, T. Zhang, C. Li, Y. Li and L. Wang, "- Thermodynamic study on the effect of cold and heat recovery on performance of liquid air energy storage," *Applied Energy,* 221:86-99, 2018.

[66] P. Farres-Antunez, H. Xue and A. J. White, "Thermodynamic analysis and optimisation of a combined liquid air and pumped thermal energy storage cycle," *Journal of Energy Storage,* 18:90-102, 2018.

[67] M. Waterson, "The characteristics of electricity storage, renewables and markets," *Energy Policy,* 104:466-473, 2017.

[68] S. Sabihuddin, A. E. Kiprakis and M. Mueller, "A Numerical and Graphical Review of Energy Storage Technologies," *Energies,* 8:172-216, 2015.

[69] M. S. Guney and Y. Tepe, "Classification and assessment of energy storage systems," *Renewable and Sustainable Energy Reviews,* 75:1187-1197, 2017.

[70] A. K.-Y. Yoon, H. S. N. and Y. S. Yoon, "Analysis of Vanadium Redox Flow Battery Cell with Superconducting Charging System for Solar Energy," *Electrical and Electronic Engineering,* 6(1):1-5, 2016.

[71] B. Robyns, B. François, G. Delille and C. Saudemont, Energy Storage in Electric Power Grids, First Edition ed., ISTE Ltd and Wiley & Sons, 2015.

[72] X. Luo, J. Wang, M. Dooner and J. Clarke, "Overview of current development in electrical energy storage technologies and the application potential in power system operation," *Applied Energy,* 137:511–536, 2015.

[73] M. Aneke and M. Wang, "Energy storage technologies and real life applications – A state of the art review," *Applied Energy,* 179:350–377, 9 July 2016.

[74] Y. Li, H. Chen, X. Zhang, C. Tan and Y. Ding, "Renewable energy carriers: Hydrogen or liquid air/nitrogen?," *International Journal of Thermal Sciences,* 49:941-949, 2010.

[75] H. H. Alyami and R. Williams, "Study and Evaluation of Liquid Air Energy Storage Technology For a Clean and Secure Energy Future Challenges and opportunities for Alberta wind energy industry," *American Journal of Engineering Research (AJER),* 4(8):41-54, 2015.

[76] D. Wolf, *Methods for Design and Application of Adiabatic Compressed Air Energy Storage Based on Dynamic Modeling,* Oberhausen: Verlag Karl Maria Laufen, 2011.

[77] S. Wang, X. Xue, X. Zhang, J. Guo, Y. Zhou and J. Wang, "The application of cryogens in liquid fluid energy storage systems," in *25th International Cryogenic Engineering Conference and the International Cryogenic Materials Conference in 2014, ICEC 25-ICMC 2014*, Enschede, Netherlands, 2014.

[78] F. Díaz-González, A. Sumper and O. Gomis-Bellmunt, Energy Storage in Power Systems, First Edition ed., John Woley&Sons, Ltd., 2016.

[79] H. Ibrahim, A. Ilinca and J. Perron, "Energy storage systems—Characteristics and comparisons," *Renewable and Sustainable Energy Reviews,* 15(2):1221-1250, 2008.

[80] J. K. Kaldellis and D. Zafirakis, "Optimum energy storage techniques for the improvement of renewable energy sources-based electricity generation economic efficiency," *Energy,* 32(12):2295–2305, 2007.

[81] M. Budt, D. Wolf, R. Span and J. Yan, "A review on compressed air energy storage: Basic principles, past milestones and recent developments," *Applied Energy,* 170:250-268, 2016.

[82] L. Welder, P. Stenzel, N. Ebersbach, P. Markewitz, M. Robinius, B. Emonts and D. Stolten, "Design and Evaluation of Hydrogen Electricity Reconversion Pathways in National Energy Systems Using Spatially and Temporally Resolved Energy System Optimization," *International Journal of Hydrogen Energy,* 44(19):9594-9607, 2018.

[83] C. Xie, Y. Hong, Y. Ding, Y. Li and J. Radcliffe, "An economic feasibility assessment of decoupled energy storage in the UK: With liquid air energy storage as a case study," *Applied Energy ,* 225:244-257, 2018.

[84] EPRI and the U.S. Department of Energy , "EPRI-DOE Handbook of Energy Storage for Transmission & Distribution Applications," Electric Power Research Institute, Inc., Palo Alto, California and Washington, DC, 2003. URL: https://www.sandia.gov/ess-ssl/publications/ESHB%201001834%20reduced%20size.pdf (last accessed 20.05.2019)

[85] L. Welder, P. Stenzel, N. Ebersbach, P. Markewitz, M. Robinius, B. Emonts, D. Stolten, "Design and Evaluation of Hydrogen Electricity Reconversion Pathways in National Energy Systems Using Spatially and Temporally Resolved Energy System Optimization," *International Journal of Hydrogen Energy,* 44(19):9594-9607, 2018.

[86] Highview Enterprises Ltd , "Cost Estimator," 2017. [Online]. URL: http://www.highview-power.com/cost-estimator/ (last accessed 16.10.2017).

[87] V. Jülch, "Comparison of electricity storage options using levelized cost of storage (LCOS) method," *Applied Energy,* 183:1594–1606, 2016.

[88] F. Klumpp, "Comparison of pumped hydro, hydrogen storage and compressed air energy storage for integrating high shares of renewable energies—Potential, cost-comparison and ranking," *Journal of Energy Storage,* 8:119–128, 2016.

[89] P. Perazzelli and G. Anagnostou, "Design issues for compressed air energy storage in sealed underground cavities," *Journal of Rock Mechanics and Geotechnical Engineering,* 8(3):314-328, 2016.

[90] M. C. Grubelich, S. J. Bauer and P. W. Cooper, "Potential hazards of Compressed Air Energy Storage in Depleted Natural Gas Reservoirs," Sandia National Laboratories, Albuquerque, New Mexico, September 2011. URL: https://prod-ng.sandia.gov/techlib-noauth/access-control.cgi/2011/115930.pdf (last accessed 21.05.2019).

[91] W. P. Schmidt, K. Winegardner, M. Dennehy and H. Castle-Smith, "Safe Design and Operation of a Cryogenic Air Separation Unit," *Process Safety Progress,* 20(4):269-279, December 2001.

[92] O. Palizban and K. Kauhaniemi, "Energy storage systems in modern grids—Matrix of technologies and applications," *Journal of Energy Storage,* 6:248–259, 2016.

[93] R. Carnegie, D. Gotham, D. Nderitu and P. V. Preckel, *Utility Scale Energy Storage Systems - Benefits, Applications, and Technologies,* USA: State Utility Forecasting Group, 2013. URL: https://www.purdue.edu/discoverypark/sufg/docs/publications/SUFG%20Energy%20Storage%20Report.pdf (last accessed 21.05.2019).

[94] J. Towler, "Energy storage – the missing piece?," 09 2016. [Online]. URL: https://energymanagermagazine.co.uk/energy-storage-the-missing-piece/ (last accessed 18.09.2019).

[95] R. H. Byrne, M. K. Donnelly, V. W. Loose and D. J. Trudnowski, "Methodology to Determine the Technical Performance and Value Proposition for Grid-Scale Energy Storage Systems," Sandia National Laboratories, Livermore, California, 2012. URL: https://www.sandia.gov/ess-ssl/publications/SAND2012-10639.pdf (last accessed 20.05.2019).

[96] M. Katsanevakis, R. A. Stewart and J. Lu, "Aggregated applications and benefits of energy storage systems with application-specific control methods: A review," *Renewable and Sustainable Energy Reviews,* 75:719–741, 2017.

[97] J. Eyer and G. Corey, "Energy Storage for the Electricity Grid: Benefits and Market Potential Assessment Guide," Sandia National Laboratories, New Mexico and Livermore, SAND2010-0815 February 2010. URL: https://www.sandia.gov/ess-ssl/publications/SAND2010-0815.pdf (last accessed 21.05.2019).

[98] N. Günter and A. Marinopoulosc, "Energy storage for grid services and applications: Classification, market review, metrics, and methodology for evaluation of deployment cases," *Journal of Energy Storage,* 8:226–234, 2016.

[99] Deloitte Development LLC., "Deloitte.com," 2015. [Online]. URL: https://www2.deloitte.com/content/dam/Deloitte/us/Documents/energy-resources/us-er-energy-storage-tracking-technologies-transform-power-sector.pdf (last accessed 21.05.2019)

[100] A. Nourai, "Energy in Transition," DNV GL, 29 10 2011. [Online]. Available: https://blogs.dnvgl.com/energy/stacking-the-energy-storage-value-proposition-bundling-energy-storage-grid-applications (last accessed 21.05.2019).

[101] R. Hledik, R. Lueken, C. McIntyre and H. Bishop, "Stacked Benefits: Comprehensively Valuing Battery Storage in Carlifornia," The Brattle Group, Carlifornia, 2017. [Online]. http://files.brattle.com/files/7208_stacked_benefits_-_final_report.pdf (last accessed 21.05.2019).

[102] A. A. Akhil, G. Huff, A. B. Currier, B. C. Kaun, D. M. Rastler, S. B. Chen, A. L. Cotter, D. T. Bradshaw and W. D. Gauntlett, "DOE/EPRI Electricity Storage Handbook in Collaboration with NRECA," Sandia National Laboratories, California, 2015. URL:

https://prod-ng.sandia.gov/techlib-noauth/access-control.cgi/2015/151002.pdf (last accessed 21.05.2019).

[103] D. Rastler, "Electricity Energy Storage Technology Options - A White Paper Primer on Applications, Costs, and Benefits," EPRI Electric Power Research Institute, California, 2010. URL: http://large.stanford.edu/courses/2012/ph240/doshay1/docs/EPRI.pdf (last accessed 20.05.2019)

[104] S. M. Schoenung and W. V. Hassenzah, "Long- vs. Short-Term Energy Storage Technologies Analysis: A Life-Cycle Cost Study," Sandia National Laboratories, SAND2003-2783, Albuquerque, California, 2003. URL: http://citeseerx.ist.psu.edu/viewdoc/download?doi=10.1.1.177.5959&rep=rep1&type=pdf (last accessed 20.05.2019)

[105] P. Denholm, E. Ela, B. Kirby and M. Milligan, "The Role of Energy Storage with Renewable Electricity Generation NREL/TP-6A2-47187," National Renewable Energy Laboratory, Colorado, 2010. https://www.nrel.gov/docs/fy10osti/47187.pdf (last accessed 21.05.2019)

[106] J. Eyer, R. S. Brown and B. Norris, "Guide to estimating benefits and market potential for electricity storage in New York," New York State Energy Research and Development Authority (NYSERDA), New York, 2007. URL: https://www.nyserda.ny.gov/-/media/Files/Publications/Research/Electic-Power-Delivery/Estimating-Benefits-Market-Potential-NYC.pdf (latest accessed 21.05.2019).

[107] A. Berrada, K. Loudiyi and I. Zorkani, "Valuation of energy storage in energy and regulation markets," *Energy,* 115:119-118, 2016.

[108] M. Beaudin, H. Zareipour, A. Schellenberglabe and W. Rosehart, "Energy storage for mitigating the variability of renewable electricity sources: an updated review," *Energy for Sustainable Development,* 14(4):302–314, 2010.

[109] A. Nourai, "Installation of the First Distributed Energy Storage System (DESS) at American Electric Power (AEP)," SAND2007-3580, Sandia National Laboratories, Albuquerque, 2007. URL: https://prod-ng.sandia.gov/techlib-noauth/access-control.cgi/2007/073580.pdf (last accessed 20.05.2019).

[110] M. J. Moran, H. N. Shapiro and D. D. Boettner, Fundamentals of Engineering Thermodynamics, Hoboken, NJ: John Wiley & Sons, Inc., 1987.

[111] G. Tsatsaronis and F. Cziesla, "Thermoeconomics," in *Enccyclopedia of Physical Science and Technology*, Vol. 16, Third Edition, New York, Academic Press, 2002, pp. 659-680.

[112] A. Bejan, G. Tsatsaronis and M. Moran, Thermal Design & Optimization, Canada: John Wiley & Sons Inc., 1996.

[113] G. Tsatsaronis, "Definitions and nomenclature in exergy analysis and exergoeconomics," *Energy,* 32:249–253, 2007.

[114] T. Morosuk and G. Tsatsaronis, "Splitting physical exergy: Theory and application," *Energy,* 167:698-707, 2019.

[115] J. Szargut, "Chemical exergies of the elements," *Applied Energy,* 32(4):269-286, 1989.

[116] R. Smith, "Chemical Process Design and Integration," John Wiley & Sons, Ltd, Manchester, 2014.

[117] Electric Power Research Institute, Technical Assessment Guide (TAG), Palo Alto, CA: EPRI TR-102276-V1R7, 1993.

[118] G. D. Ulrich and P. T. Vasudevan, "Chapter 5 Capital Cost Estimation," in *Chemical Engineering - Process design and economics - A practical guide*, New Hampshire, USA, Process Publishing, 2004, pp. 352-419.

[119] M. S. Peters, K. D. Timmerhaus and R. E. West, "Chapter 12 Materials-Handling Equipment - Design and Costs," in *Plant Design and Economics of Chemical Engineers*, New York, USA, McGraw-Hill Companies, Inc., 2003, pp. 485-589.

[120] G. Xu, F. Liang, Y. Yang, Y. Hu, K. Zhang and W. Liu, "An Improved CO_2 Separation and Purification System Based on Cryogenic Separation and Distillation Theory," *Energies,* 7(5):3484-3502, 2014.

[121] G. Towler and R. Sinnott, Chemical Engineering Design: Principles, Practice and Economics of Plant and Process Design, Oxford, UK: Elsevier Inc., 2008.

[122] A. Lazzarettoa and G. Tsatsaronis, "SPECO: A systematic and general methodology for calculating efficiencies and costs in thermal systems," *Energy,* 31(8-9):1257-1289, 2006.

[123] Aspen Technology, Inc., "aspentech," 2019. [Online]. URL: http://www.aspentech.com (latest accessed 29.01.2019).

[124] F-Chart Software, LLC, "EES Engineering Equation Solver," 2019. [Online]. URL: http://www.fchart.com/ees/ (latest accessed 29.01.2019).

[125] International Organization for Standardization, "Standard Atmosphere ISO 2533:1975," ISO, 1975. [Online]. URL: https://www.iso.org/standard/7472.html (latest accessed 30.01.2019).

[126] M. Kanoglu, I. Dincer and M. A. Rosen, "Performance analysis of gas liquefaction cycles," *International Journal of Energy Research,* 32(1):35-43, 2008.

[127] M. Sorgenfrei, "Analysis of IGCC-Based Plants with Carbon Capture for an Efficient and Flexible Electric Power Generation," Technische Universität Berlin, Dissertation, Berlin, 2016.

[128] Air separation plants, "linde-engineering.com," [Online]. URL: https://www.linde-engineering.com/en/images/Air_separation_plants_History_and_progress_in_the_course_of_time_tcm19-457349.pdf (latest accessed 17.01.2019).

[129] M. Aneke and M. Wang, "Potential for improving the energy efficiency of cryogenic air separation unit (ASU) using binary heat recovery cycles," *Applied Thermal Engineering,* 81:223-231, 2015.

[130] A. J. Pimm, S. D. Garvey and B. Kantharaj, "Economic analysis of a hybrid energy storage system based on liquid air and compressed air," *Journal of Energy Storage,* vol. 4:24-35, 2015.

[131] C. Day, "Basics and applications of cryopumps,", Forschungszentrum Karlsruhe, Eggenstein-Leopoldshafen, 2007.
URL: https://cds.cern.ch/record/1047069/files/p241.pdf (latest accessed 21.05.2019).

[132] C. Forman, I. K. Muritala, R. Pardemann and B. Meyer, "Estimating the global waste heat potential," *Renewable and Sustainable Energy Reviews,* 57:1568-1579, 2016.

[133] L. Miró, S. Brückner and L. F.Cabeza, "Mapping and discussing Industrial Waste Heat (IWH) potentials for different countries," *Renewable and Sustainable Energy Reviews,* 51:847-855, 2015.

[134] P. Krawczyk, Ł. Szabłowski, S. Karellas, E. Kakaras and K. Badyda, "Comparative thermodynamic analysis of compressed air and liquid air energy storage systems," *Energy,* 142:46-54, 2018.

[135] S. Kumar, H.-T. Kwon, K.-H. Choi, W. Lim, J. H. Cho, K. Tak and I. Moon, "LNG: An eco-friendly cryogenic fuel for sustainable development," *Applied Energy,* 88(12):4264-4273, 2011.

[136] B. B. Kanbura, L. Xiang, S. Dubey, F. H. Choo and F. Duan, "Cold utilization systems of LNG: A review," *Renewable and Sustainable Energy Reviews,* 79:1171–1188, 2017.

[137] R. Agarwal, T. J. Rainey, S. M. A. Rahman, T. Steinberg, R. K. Perrons and R. J. Brown, "LNG Regasification Terminals: The Role of Geography and Meteorology on Technology Choices," *Energies,* 10(2152):1-19, 2017.

[138] Bundesnetzagentur, "Smard Strommarktdaten," Bundesnetzagentur, 2018. [Online]. URL: https://www.smard.de/home c

[139] U.S. Energy Information Administration, "eia - natural gas," 2019. [Online]. URL: https://www.eia.gov/dnav/ng/hist/rngwhhdM.htm (latest accessed 17.04.2019).

[140] V. Quaschning, Regenerative Energiesysteme, München: Carl Hanser Verlag , 2015.

[141] Lazard, "Lazard's levelized cost of storage - version 2.0," New York, 2016. URL: https://www.lazard.com/media/438042/lazard-levelized-cost-of-storage-v20.pdf (latest accessed 20.05.2019).

[142] S. Nelmes, "Liquid air energy storage (LAES)," presentation, Highview Enterprises Lmtd., London, 2017. URL: https://warwick.ac.uk/fac/sci/eng/research/grouplist/electricalpower/images/newsnevents/hies2017/presentations/hies2017_highview.pdf (latest accessed 20.05.2019).

[143] B. Zakerin and S. Syri, "Electrical energy storage systems: A comparative life cycle cost analysis," *Renewable and Sustainable Energy Reviews,* 42:569-596, 2015.

[144] C. Bussarcd, M. Moosa, R. Alvarezbd, P. Wolfcd, T. Thiencd, H. Chenbd, Z. Caicd, M. Leutholdacd, D. Saueracd and A. Moserbd, "Optimal allocation and capacity of energy storage systems in a future European power system with 100% renewable energy generation," *Energy Procedia,* 46:40-47, 2014.

[145] International Energy Agency, "Technology Roadmap: Hydrogen and Fuel Cells," OECD/IEA, Paris, 2015. URL: https://www.iea.org/publications/freepublications/publication/TechnologyRoadmapHydrogenandFuelCells.pdf (latest accessed 21.05.2019).

[146] E. Barbour, "Energy Storage Sense," [Online]. URL: http://energystoragesense.com/. (latest accessed 31.07.2018).

[147] A. Sternberg and A. Bardow, "Power-to-What? – Environmental assessment of energy storage systems," *Energy & Environmental Science,* 2:389-400, 2015.

[148] F. Dıaz-Gonzalez, A. Sumper and O. Gomis-Bellmunt, "Short-Term Applications of Energy Storage Installations in the Power System," in *Energy Storage in Power Systems*, John Wiley & Sons, Ltd., 2016, pp. 209-267.

[149] J. McDowall, "Integrating energy storage with wind power in weak electricity grids," *Journal of Power Sources,* 162(2):959–964, 2006.

[150] Chemical Engineering, "Plant Cost Index," Access Intelligence, LLC, 2019. [Online]. URL: https://www.chemengonline.com/site/plant-cost-index/ (latest accessed 05.02.2019).

[151] Fusion Media Limited, "investing.com," 2007-2019. [Online]. URL: https://de.investing.com/currencies/eur-usd-historical-data (latest accessed 26.04.2019).

[152] Highview, "Technology and performance review," March 2012. [Online]. URL: http://www.liquidair.org.uk/files/appendices/01.pdf (latest accessed 14.02.2018).

[153] James Chater, "Stainless Steel World," KCI Publishing, September 2017. [Online]. URL: http://www.stainless-steel-world.net/webarticles/2018/01/16/lift-off-energy-storage-brings-renewable-energy-to-the-mainstream.html (latest accessed 17.02.2019).

Appendix A

Table A.1: Comparison of CES characteristics to other bulk energy storage technologies

	CES	PHS	CAES	H2
RTE [%]	40 – 50 [37, 38] 63 – 70 with integration [8, 62, 63]	75-85 [79] [80] 65 – 87 [68] 70 – 80 [78, 33] 79.2 [88] 76 [87]	40 – 75 [33] 57 – 89 [68] 38 – 54 [81] 68.8 [88] 55 [87]	30 – 50 [74] [85] 62 – 80 [144] 26.6 [88] 41 [87] 29 – 33 [145]
Power capacity [MW]	20-500+ [8] 10 – 500 [16, 7, 72, 29, 17]	50 – 3,000 [146], 100– 5,000 [37] 10 – 8,000 [68]	5–300 [37] 0.01 – 3,000 [68] 0.005 – 1,000 [81]	0–50 [37] (modular) 300 [88]
Energy density [Wh/l]	120-200 [37] 90 [73] [18] 160-200 [10, 37, 17]	0.5 - 1.5 [37] 0.5 – 1.33 [68]	3-6 [37] 0.4 – 20 [68] 0.5 – 25 [81]	133-785 [74] 500+ [37]
Response time	<150 s (dis) [75], 20 min (char) [18]	sec-min's [146]	10-15 min [76], < 1-15 min [81]	Seconds [37]
Storage duration	Hours – day [7, 37, 11]	Hours – days [146] Hours–months [37]	Hours – days [146] Hours–months [37]	Hours–months [37]
Cost [€/kWh]	3 – 32 [37]	14-29 [80], 5-104 [37], 337-580 [84] 0.95-275 [68], 20 [144], 10-20 [87]	2-52 [37] 0.95-132 [68] 20-30 [87]	0.3 [144] 0.3-0.6 [87] 0.95 [145]
Cost [€/kW]	526 – 2,526 [29]	623 – 2,076 [37] 2,021 – 5,794 [84] 368 – 1,579 [33] 284 – 5,004 [68] 633 [144], 513 [88]	415 – 830 [37] 526 – 2,315 [33] 379 – 2,129 [68] 957 [88]	> 2,000 [85] 297 – 693 [144] 2,737 [88] 1,798 – 5,962 [145]
Lifespan [years]	25-60 [29] [37] [38] [20]	40–60 [37] 20 - 80 [68] 80 [88] [87]	20–40 [37] [68] 40 [88] 35 [87]	5 – 15 [37] 30 [88] [87] 2 - 7 [145]
Maturity of technology	Developing/demo [20]	Mature [146] Fully commercialized [68]	Demo/early Commercialized [20] [81] Proven [68]	Developing/demo [20] Demo [145]
Specific energy [Wh/kg]	150 – 250 [37], 100 – 200 [17, 20], 100 –143 [18], 150 [16], 400 [32]	0.3 – 1.33 [68]	3.2 – 60 [68]	-
Self-discharge rate (%/day)	0.2 [16, 12]	0 [68]	0 [68]	0 [147] [144]
Discharge time	Minutes to hours [7, 37, 11]	Hours to days [78]	Hours to days [81]	Hours [145]
Construction time [years]	1 – 2 [15] [76]	5 – 10 [15] [76]	5 – 10 [15] [76]	<1 [148]

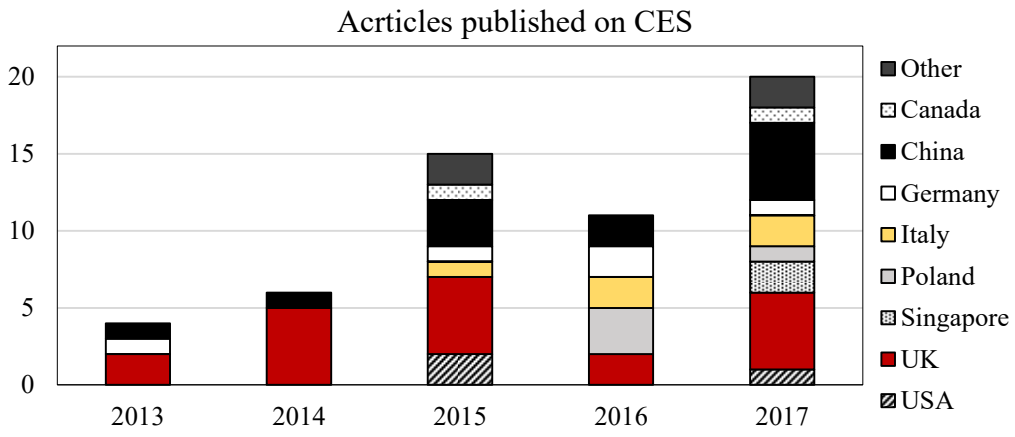

(a)

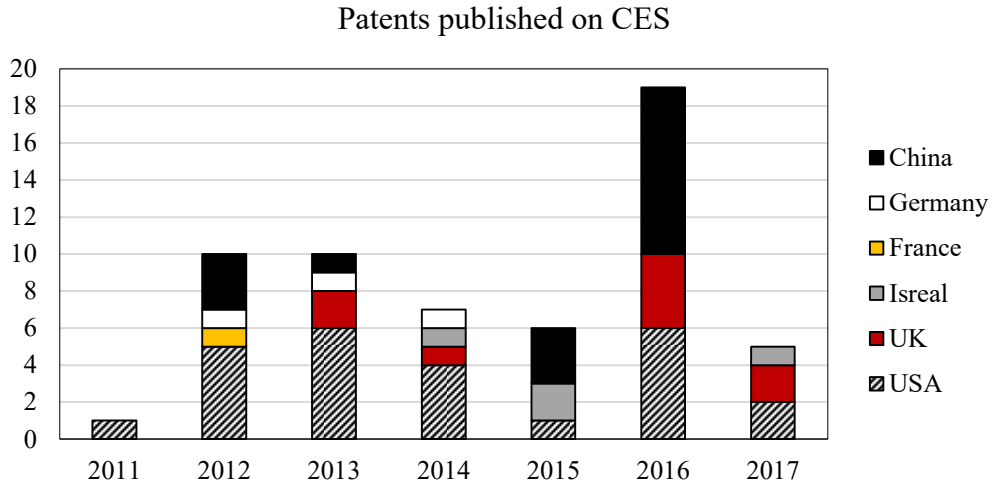

(b)

Figure A.1: Number and country of origine of (a) research articles and (b) patents published from 2013 to 2017

Table A.2: Bulk energy applications compatible with CES characteristics [3].

Application	Storage power, MW	Response time	Discharge time	Cycles per anum
Energy arbitrage	10's to 100's [37, 92, 93] [84] [102] [104] [103]	min's-hrs [37] [105]	hrs-day [37, 92, 93] [78] [84] [102] [104] [103]	300–400 [37] [102] [103] 60–250 [84]
Peak shaving	≤500 [37] 0.1–100+ [72]	min [72]	1-10h [72, 37, 93]	50–250 [37]

Table A.3: Ancillary services compatible with CES characteristics [3].

Application	Storage power, MW	Response time	Discharge time	Cycles per anum
Load following	≤100 [92] [102], 100's [37] [104]	several min [102] mins-hrs [105]	hrs-day [37, 92] [104] mins–1 h [102], 1–5 h [78]	NA
Non-spinning reserve	≤100 [92] [104] [103] > 100 [37] 2–200 [84]	≤10 min [84] [102] [104] [61]	hrs-day [37] 1–5 h [78] [84] [103]	5–20 [84]
Black start	≤50 [37] [102] ≥10 [84]	≤2 h [37] mins - 1h [84] [105]	15 mins–1 h [102], 1–5h [78] [84], ≤16 h [92]	10–20 [37] [102] rare [84]
Load shedding (load shift)	1-200 [93] 10–100+ [72]	10 min [93] <10min [72]	3-10h [93] 12 + h [72]	60-250 [93]

Table A.4: Frequency regulation services compatible with CES characteristics [3].

Application	Storage power, MW	Response time	Discharge time
Tertiary reserve	≤100 [37]	15 ≤ t ≤ 60 min [37] [84] [102] [105]	≥1h [37] 1–5h [78] [84]

Table A.5: Renewable energy integration applications compatible with CES [3].

Application	Storage power, MW	Response time	Discharge time	Cycles per anum
Time shift	1–100's [25] [30] [53] [103]	≤30 min [37] <10min[25] [93]	≤5 h [37] 3 ≤ t ≤ 12h [25] [93] [103]	≤ 4,000 [37] acc. ref. profile [93] 300-500 [103]
Capacity firming	≤500 [37] [102]	≤30 min [92]	≤4h [37] 2–6h [78] [84] [102]	300–500 [37] 5–100 [102]

Table A.6: T&D support applications compatible with CES characteristics [3].

Application	Storage power, MW	Response time	Discharge time	Cycles per year
Transmission curtailment	10–100+ [72, 93] [102] [103]	Min [72, 93] mins-hrs [105]	2 ≤ t ≤ 12 h [93] [78] [84] [102] [103]	10–50 [102]
Distribution upgrade deferral	0.5–10 [102] 1-100 [103]	mins-hrs [105]	1–6h [78] [84] [103] [102]	50–100 [102], 300-500 [103]
Congestion relief	1–100 [102]	NA	1–6h [78] [84] [102]	50–100 [102]
Load shedding (load shift)	1-200 [93] 10–100+ [72]	10 min [93] <10min [72]	3-10h [93] 12 + h [72]	60-250 [93]

Table A.7: Results of the literature review on the economic value of potential CES applications [3] based on [97] [106] [107] [108] [109].

Applications		Value proposition, €/kW
Bulk energy	Energy arbitrage	300 [107], 400-700 [97]
	Peak shaving	600 [109], 832 [106], 850 [107]
Ancillary service	Load following	215 [109], 600-1,000 [97], 753 [106], 770 [107]
	Spinning reserve	258 [106], 57-225 [97]
	Black start	NA
Frequency regulation	Tertiary reserve	72 [106], 104 [107]
RE integration	Time shift	655 [149], 233-389 [97]
	Capacity firming	330 [107] , 323 [106], 709-915 [97]
T&D support	Transmission curtailment	1,200 [106] [107], 481-1,079 [97]
	Distribution upgrade deferral	666-1,067 [109], 1,060 [107], 481-1,079 [97]
	Congestion relief	72 [106], 60 [107], 481-1,079 [97]
	Load shedding& shift	NA

Application compatibility		High energy applications		High power applications	
		Occasional use	Frequent use	Occasional use	Frequent use
High energy applications	Occasional use				Medium
	Frequent use		High		
High power applications	Occasional use				
	Frequent use	Medium			Low

Figure A.2: Classification of compatibility of occasional and frequent use energy storage applications [3] adopted from [100] based on [97].

Appendix B

Exergetic analysis

Table B.1: Definition of the exergetic and energetic efficiencies for CES systems [59].

System	Energetic efficiency, η_{CES}	Exergetic efficiency, ε_{CES}
Adiabatic	$\frac{\dot{W}_{dis}}{\dot{W}_{char} \cdot \frac{\tau_{char}}{\tau_{dis}}}$	$\frac{\dot{W}_{dis}}{\dot{W}_{char} \cdot \frac{\tau_{char}}{\tau_{dis}}}$
Waste heat	$\frac{\dot{W}_{dis}}{\dot{W}_{char} \cdot \frac{\tau_{char}}{\tau_{dis}} + \dot{Q}_{\mathrm{hot}}}$	$\frac{\dot{W}_{dis}}{\dot{W}_{char} \cdot \frac{\tau_{char}}{\tau_{dis}} + \dot{E}_{\mathrm{heat}}}$
Waste cold	$\frac{\dot{W}_{dis}}{(\dot{W}_{char} + \lvert\dot{Q}_{\mathrm{cold}}\rvert) \cdot \frac{\tau_{char}}{\tau_{dis}}}$	$\frac{\dot{W}_{dis}}{(\dot{W}_{char} + \dot{E}_{\mathrm{cold}}) \cdot \frac{\tau_{char}}{\tau_{dis}}}$
Combustion	$\frac{\dot{W}_{dis}}{\dot{W}_{char} \cdot \frac{\tau_{char}}{\tau_{dis}} + \dot{m}_{\mathrm{CH4}} \cdot LHV_{CH4}}$	$\frac{\dot{W}_{dis}}{\dot{W}_{char} \cdot \frac{\tau_{char}}{\tau_{dis}} + \dot{E}_{\mathrm{CH4}}}$

Exergy balance of the a-CES system:

$$\underbrace{\tau_{char} \cdot \left(\dot{E}_1 + \sum \dot{W}_{CM} - \dot{W}_{EX}\right)}_{E_{F,tot}} = \underbrace{\tau_{dis} \cdot \left(\sum \dot{W}_T - \dot{W}_{CP}\right)}_{E_{P,tot}} + E_{L,tot} + E_{D,tot} \tag{6.1}$$

Exergy losses of the a-CES system:

$$E_{L,tot} = \tau_{char} \cdot \left(\dot{E}_{17} + \dot{E}_{19}\right) + \tau_{dis} \cdot \dot{E}_{32} + \tau_{stor} \cdot \dot{E}_{q,heat} \tag{6.2}$$

The exergy of the losses accounts the exergy losses associated with all streams exiting the system and all heat losses over the system boundaries. The heat losses of the heat storage $\dot{E}_{q,heat}$ are multiplied with the storage time (τ_{stor}).

Table B.2: Definition of exergy of fuel and exergy of product of pumps and turbines for different cases of the entering and the exiting temperature (T_1, T_2).

Component	Below ambient temp.	Crossing ambient temp.	Above ambient temp.
Cryogen pump	$T_1, T_2 < T_{\mathrm{amb}}$ $\dot{E}_F = \dot{W}_{p1} + \left(\dot{E}_1^T - \dot{E}_2^T\right)$ $\dot{E}_P = \dot{E}_2^M - \dot{E}_1^M$	$T_1 < T_{\mathrm{amb}} < T_2$ $\dot{E}_F = \dot{W}_{p1} + \dot{E}_1^T$ $\dot{E}_P = \dot{E}_2^M - \dot{E}_1^M + \dot{E}_2^T$	$T_{\mathrm{amb}} < T_1, T_2$ $\dot{E}_F = \dot{W}_{p1}$ $\dot{E}_P = \dot{E}_2 - \dot{E}_1$
Turbine	$T_3, T_4 < T_{\mathrm{amb}}$ $\dot{E}_F = \left(\dot{E}_3^M - \dot{E}_4^M\right)$ $\dot{E}_P = \dot{W}_{t1} + \left(\dot{E}_4^T - \dot{E}_3^T\right)$	$T_{\mathrm{amb}} < T_3, T_4 < T_{\mathrm{amb}}$ $\dot{E}_F = \left(\dot{E}_3^M - \dot{E}_4^M\right) + \dot{E}_3^T$ $\dot{E}_P = \dot{W}_{t1} + \dot{E}_4^T$	$T_{\mathrm{amb}} < T_3, T_4$ $\dot{E}_F = \dot{E}_3 - \dot{E}_4$ $\dot{E}_P = \dot{W}_{t1}$

Exergy balances for selected CES components:

Table B.3: Definition of exergy of fuel and exergy of product for each component type used [2].

Component	Stream temperatures	Exergy of fuel $\dot{E}_F$	Exergy of product $\dot{E}_P$
Compressor CM1-4	$T_{amb} < T_{in}, T_{out}$	$\dot{E}_{in} - \dot{E}_{out}$	$\dot{W}_{CM}$
Two-flow heat exchanger HE1-4, HE6-9	$T_{amb} < T_{hot,out}, T_{cold,in}$	$\dot{E}_{hot,in} - \dot{E}_{hot,out}$	$\dot{E}_{cold,in} - \dot{E}_{cold,out}$
Two-flow heat exchanger HE10	$T_{cold,out}, T_{hot,out} < T_{amb} < T_{hot,in}$	$\dot{E}_{cold,in} - \dot{E}_{cold,out} + \dot{E}_{hot,in} - \dot{E}^M_{hot,out}$	$\dot{E}^T_{hot,out}$
Main heat exchanger 1 System 1	$T_{33}, T_{34}, T_{35}, T_{36}, T_{13}, T_{16} < T_{amb} < T_{12}, T_{17}$	$\dot{E}_{16} - \dot{E}^M_{17} + \dot{E}_{33} - \dot{E}_{34} + \dot{E}_{35} - \dot{E}_{36}$	$\dot{E}_{13} - \dot{E}_{12} + \dot{E}^T_{17}$
Main heat exchanger 2 System 1	$T_{33}, T_{34}, T_{35}, T_{36}, T_{21}, T_{22} < T_{amb}$	$\dot{E}_{21} - \dot{E}_{22}$	$\dot{E}_{34} - \dot{E}_{32} + \dot{E}_{36} + \dot{E}_{35}$
Cryogen pump P1, P2	$T_{in}, T_{out} < T_{amb}$	$\dot{W}_P + \dot{E}^T_{in} - \dot{E}^T_{out}$	$\dot{E}^M_{out} - \dot{E}^M_{in}$
Turbine T1-4	$T_{amb} < T_{in}, T_{out}$	$\dot{E}_{in} - \dot{E}_{out}$	$\dot{W}_T$
Expander EX	$T_{out} < T_{amb} < T_{in}$	$\dot{E}^M_{in} - \dot{E}^M_{out} + \dot{E}^T_{in}$	$\dot{W}_T + \dot{E}^T_{out}$
Throttling valve TV	$T_{in}, T_{out} < T_{amb}$	$\dot{E}^M_{in} - \dot{E}^M_{out}$	$\dot{E}^T_{in} + \dot{E}^T_{out}$
Flash tank, Storage tank FT, ST	$T_{in}, T_{out} < T_{amb}$	$\dot{E}_{in} - \dot{E}_{out,loss}$	$\dot{E}_{out,product}$
Main heat exchanger 1 System 2	$T_{13}, T_{18} < T_{amb} < T_{12}, T_{19}$	$\dot{E}_{18} - \dot{E}^M_{19}$	$\dot{E}_{13} - \dot{E}_{12} + \dot{E}^T_{19}$
Main heat exchanger 2 System 2	$T_{33}, T_{34}, T_{35}, T_{36}, T_{21}, T_{22} < T_{amb}$	$\dot{E}_{21} - \dot{E}_{22}$	$\dot{E}_{34} - \dot{E}_{32} + \dot{E}_{36} + \dot{E}_{35}$
Two-flow heat exchanger HE Rankine	$T_{cold,in}, T_{hot,out} < T_{amb} < T_{cold,out}, T_{hot,in}$	$\dot{E}_{cold,in} + \dot{E}_{hot,in} - \dot{E}^M_{cold,out} - \dot{E}^M_{hot,out}$	$\dot{E}^T_{hot,out} + \dot{E}^T_{cold,out}$

Exergetic efficiency of the liquefaction processes:

$$\varepsilon = \frac{\dot{E}_{liquid\ air} + \dot{E}_{q,hot}}{\dot{W}_{char} + \dot{E}_{q,cold}} \tag{6.3}$$

The fuel supplied to the liquefaction system is the charging power $\dot{W}_{Char}$ and the exergy of the low-temperature exergy supplied by the cold storage $\dot{E}_{q,\mathrm{cold}}$:

$$\dot{W}_{Char} = \sum \dot{W}_{CM} - \dot{W}_{EX} \tag{6.4}$$

$$\dot{E}_{q,cold} = \left|(1 - T_{cold}/T_0) \cdot \dot{Q}_{\mathrm{cold}}\right| = \dot{m}_{liquid} \cdot \Delta e_{R218} + \dot{m}_{methanol} \cdot \Delta e_{methanol} \tag{6.5}$$

T_{cold} (or T_{hot}) denote the thermodynamic mean temperatures at which the low-temperature energy (or the heat) is supplied. Both the exergy of the liquefied air $\dot{E}_{liquid\ air}$ and the exergy of the heat supplied to the heat storage $\dot{E}_{q,hot}$ are products of the liquefaction process:

$$\dot{E}_{liquid\ air} = \dot{m}_{liquid} \cdot e_{liquid\ air} \tag{6.6}$$

$$\dot{E}_{Q,hot} = (1 - T_0/T_{hot}) \cdot \dot{Q}_{heat} \tag{6.7}$$

The definitions of fuel and product for CES system components can be found in Table B.3. The specific work needed to liquefy one kg of air :

$$w = \frac{\dot{W}_{char}}{\dot{m}_{liquid\ air}} \left[kJ/kg_{liquid\ air}\right] \tag{6.8}$$

Exergetic and energetic efficiencies for different CES systems:

$$\dot{E}_{\mathrm{heat}} = (1 - T_0/T_{hot}) \cdot \dot{Q}_{\mathrm{heat}} \tag{6.9}$$

$$\dot{E}_{\mathrm{cold}} = \left|(1 - T_0/T_{cold}) \cdot \dot{Q}_{\mathrm{cold}}\right| \tag{6.10}$$

T_{hot} and T_{cold} are the thermodynamic average temperatures at which the heat and cold energy are supplied, respectively.

The cold exergy supplied by the regasifying LNG is the difference between the physical exergy of the LNG entering the MHE2 and the thermal exergy of the exiting stream: $\dot{E}_{\mathrm{cold}} = \dot{E}^{T}_{\mathrm{LNG1}} - \dot{E}^{T}_{\mathrm{LNG2}}$, also see [46].

Economic analysis

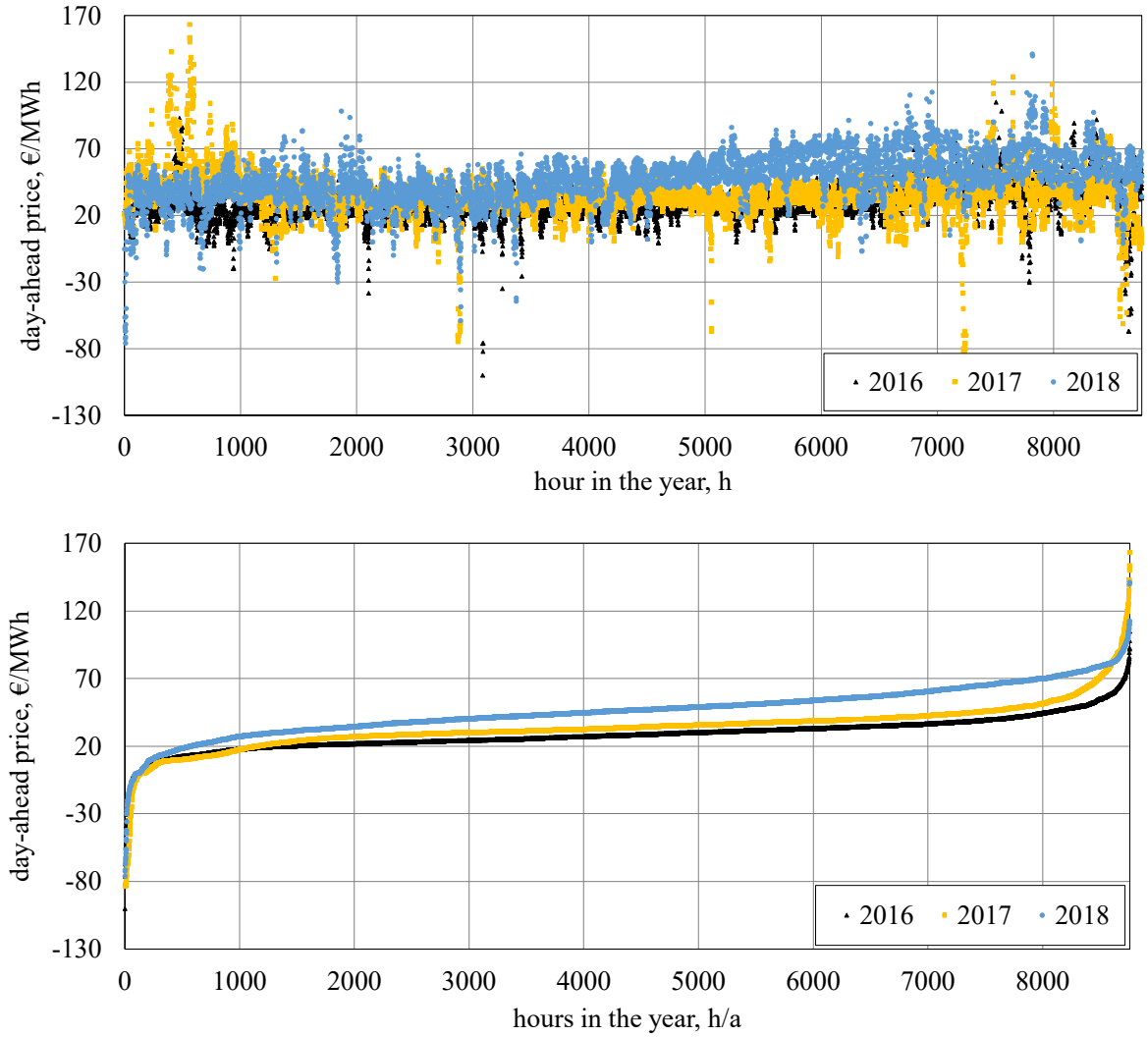

Figure B.1: (Average) Day-ahead market clearing price over the hours in the year in Germany for the years 2016-2018, starting with the lowest prices in the year.

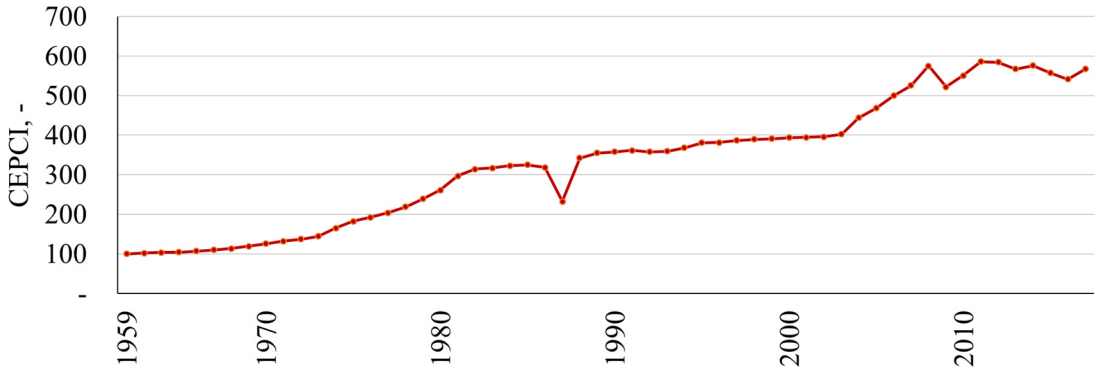

Figure B.2: Historical development of the annual average value of the CEPCI [150]

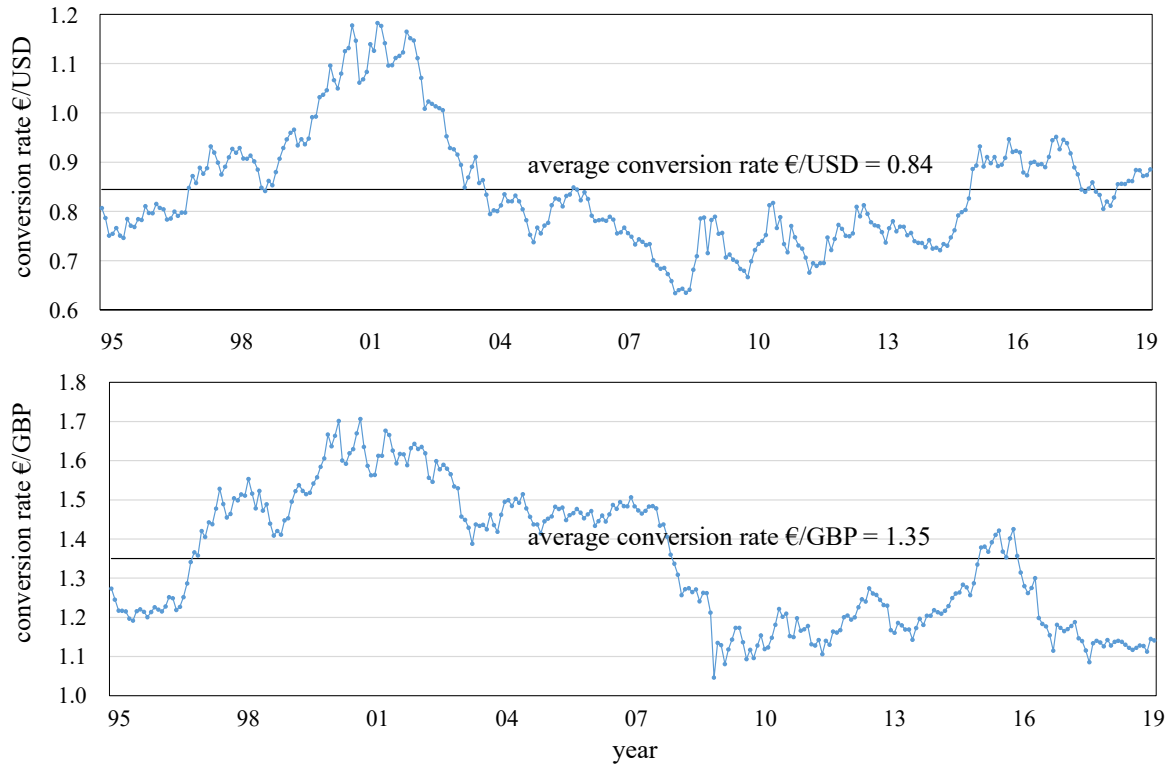

Figure B.3: Historical data for the conversion rate of €/USD and €/GBP [151]

Cost estimation

Compressors

- design: centrifugal type
- range of operation: 40-45 MW, flow rate 150+ m³/s
- construction materials: aluminum, stainless/carbon steel, copper windings in motor [8]
- Cost estimate based on commercial 10 MW plant (η = 0.6, charge/discharge = 2) by Highview [152], cost exponent extracted from [121]
- Reference year and currency: £2012

Design variable	Cost function [′000 €$_{2017}$]	Based on
capacity, $\dot{W}_{CM}$[MW] max 30 MW	$917 \cdot \left(\frac{\dot{W}_{CM}}{8\ MW}\right)^{0.60}$	[20], [119]

Cold Expander

- design: radial gas and liquid expander [118], centrifugal, [8]
- range of operation: 8-10 MW
- Construction material: carbon steel (> -196°C), stainless steel or Aluminum (> -255 °C) [119]
- subject to application: multistage and compressor loaded [8]
- Reference year and currency: $2004

Design variable	Cost function [′000 €$_{2017}$]	factor	Based on
capacity, $\dot{W}_{EX}$[MW] max 5.5 MW	$f_m \cdot 1{,}587 \cdot \left(\frac{\dot{W}_{EX}}{0.001\ \text{MW}}\right)^{0.70}$	$f_{m,ss}$= 5.0, $f_{m,cs}$= 3.0,	[118]

Cryogenic Feed Pump

- design: multi-stage reciprocating pump [152] or centrifugal pump out of aluminum and stainless steel with copper windings in the motor [8]
- range of operation: 200+ kg/s, 5 MW
- construction material: stainless steel or Aluminum (> -255 °C) [119]
- cryogenic pumps available from LNG industry: single pump up to 50 kg/s, > 100 bar (200 bar target) [18].
- subject to application: 200 bar [18] and 300 kg/s [8]
- Reference year and currency: £2012

Design variable	Cost function [′000 €$_{2017}$]	Based on
Flow rate, $\dot{m}_P$[kg/s] max 50 kg/s [18]	$743 \cdot \left(\frac{\dot{m}_P}{23\ \text{kg/s}}\right)^{0.6}$	[152]

Turbines

- design: multi-stage radial or for larger-scale axial gas turbines [18]
- range of operation: 200+ kg/s, 25+ MW
- construction material:
- carbon steel (cs) for TIT < 425 °C, >450°C
  - stainless steel (ss) for TIT < 650 °C, and
  - some stainless steels for TIT e.g. ss304 < 870 °C
  - metal alloys (ma) for TIT < 1100 °C [118].
- availability: single turbine up to 45 MW [8]
- reference year and currency: \$2004

Design variable	Cost function ['000 €$_{2017}$]	factor	Based on
capacity, $\dot{W}_T$[MW] max 45 MW [8]	$f_m \cdot 3{,}945 \cdot \left(\frac{\dot{W}_T}{0.0001}\right)^{0.588}$	$f_{m,cs}$= 3.5, $f_{m,ss}$= 6.0-7.0, $f_{m,ma}$= 8.0	[118]

Combustion chamber

- Reference year and currency: \$mid1994

Design variable	Cost function ['000 €$_{2017}$]	Based on
Outlet temperature T_{CC}[K], mass flow $\dot{m}_{air}$[kg/s]	$\left(\frac{59.67}{0.995 - \frac{p_{ex}}{p_{in}}}\right) \cdot \dot{m}_{air} \cdot \left(1 + \exp(0.018 \cdot T_{CC} - 26.4)\right)$	[112]

Cryogenic heat exchangers

- design: multi-stream plate-fin heat exchangers [116, 8] or printed circuit heat exchangers [153]
- range of operation: 70 – 120 m²
- assumption: k = 70 [W/(m² K)] high-pressure evaporation/liquefaction of gas
- construction material: aluminum or stainless steel for > - 255 °C [119]
- reference year and currency: \$2004

Design variable	Cost function ['000 €$_{2017}$]	Assumptions	Adopted from
HE area, A_{MHE}[m^2]	$\left(91.28 + 45.64\left(f_m + f_p\right)\right) \cdot \frac{A_{MHE}}{2{,}000}$	flat-plate, k= 70 W/(m²K), $f_{m,ss}$ =2.3, $f_p = 0.0016 \cdot p\,[bar] + 1.0203 \approx$ 1.2 ... 1.3 (plate-fin)	[118]

Figure B.4: Printed circuit heat exchanger by Heatric used by Highview Ltd. in the Demonstration plant [153]

Heat exchangers:

In order to estimate cost of heat exchangers, the logarithmic mean temperature needs to be calculated, in equation ((6.11) the logarithmic mean temperature difference $LMTD$ for a two stream heat-exchanger is given.

$$LMTD = \frac{\Delta T_1 - \Delta T_2}{ln\left(\frac{\Delta T_1}{\Delta T_2}\right)} = \frac{(T_{Hot,in} - T_{Cold,out}) - (T_{Hot,out} - T_{Cold,in})}{ln\frac{(T_{Hot,in} - T_{Cold,out})}{(T_{Hot,out} - T_{Cold,in})}} \tag{6.11}$$

$$A_{HE} = \frac{\dot{Q}[W]}{LMTD[K] \cdot k[\mathrm{W/m^2K}]} \tag{6.12}$$

After assumption of the overall heat transfer coefficient k the heat exchanger area is calculated over equation (6.12, the heat duty $\dot{Q}[W]$ is calculated in Aspen Plus Software.

Intercoolers and reheaters

- design: multi-stage reciprocating pump [152] or centrifugal pump out of aluminum and stainless steel with copper windings in the motor [8]
- range of operation: 5,000 – 20,000 m²
- assumption: k = 300 [W/(m² K)] high-pressure gas inside tube and liquid outside
- construction material: carbon steel [119]
- Reference year and currency: $2004

Design variable	Cost function ['000 €$_{2017}$]	Assumptions	Adopted from
HE area, $A_{HE}[\mathrm{m^2}]$	$\left(f_p \cdot 1.3 + 1.88\right) \cdot\ 57.64 \cdot \frac{A_{HE}}{1{,}000}$	$f_p = 0.0016 \cdot p\ [bar]\ +$ 1.0203 ≈1…1.3, gas/liquid, shell/tube, cs/cs	[118]

Storage tanks

- design: double-wall flat-bottom tank [15], field erected flat bottom tank [119]
- range of operation:
  - liquid air: 3,000 tons, 12,540 m³ of liquid air (f_d= 1.0, $f_{m,ss\ 316}$ = 3.0)
  - cold storage:
    - approximately 2,000 m³ of Methanol (f_d= 2.0, $f_{m,ss}$ = 2.0)
    - approximately 4,000 m³ of R218 (f_d= 2.0, $f_{m,ss}$ = 2.0)
  - heat storage:
    - approximately 4,000 m³ (f_d= 2.0, $f_{m,cs}$ = 1.0)
- construction material: stainless steel 316 for liquid air, stainless steel 304 for R218 and carbon steel for Methanol, water and thermal oil.
- Reference year and currency: \$2004

Design variable	Cost function ['000 €$_{2017}$]		Based on
capacity, $\dot{v}_{char} \cdot \tau_{char}$[m³] max 1, 200 tons [20]	$f_d \cdot f_m \cdot (0.0458 \cdot \dot{v}_{char} \cdot \tau_{char} + 117.80)$	$f_{m,ss}$ = 2.0…3.0 $f_{m,cs}$ = 1.0	[119]

Exergoeconomic analysis

Compressors

Cost balance $$\dot{Z}_{CM1} + \dot{C}_1^T + \dot{C}_1^M + c_{el,char} \cdot \dot{W}_{CM1} = \dot{C}_2^T + \dot{C}_2^M \quad (6.13)$$

Ancillary equation "P-rule" $$\frac{\dot{C}_2^T - \dot{C}_1^T}{\dot{E}_2^T - \dot{E}_1^T} = \frac{\dot{C}_2^M - \dot{C}_1^M}{\dot{E}_2^M - \dot{E}_1^M} \quad (6.14)$$

Fuel $$\dot{C}_{P,CM1} = \dot{C}_2 - \dot{C}_1 \quad (6.15)$$

Product $$\dot{C}_{F,CM1} = c_{el,char} \cdot \dot{W}_{CM1} \quad (6.16)$$

Intercoolers – recovery of compression heat ($T_{cold,in} \geq T_0$)

Cost balance $$\dot{Z}_{HE1} + \dot{C}_{hot,in} + \dot{C}_{cold,in} = \dot{C}_{hot,out} + \dot{C}_{cold,out} \quad (6.17)$$

Ancillary equations "F-rule" $$c_2^T = c_3^T \quad (6.18)$$

$$c_2^M = c_3^M \quad (6.19)$$

$$c_{48}^M = c_{47}^M \quad (6.20)$$

Fuel $$\dot{C}_{F,HE1} = \dot{C}_{hot,in} - \dot{C}_{hot,out} \quad (6.21)$$

Product $$\dot{C}_{P,HE1} = \dot{C}_{cold,out} - \dot{C}_{cold,in} \quad (6.22)$$

Splitter

Cost balance $$\dot{Z}_{SP} + \dot{C}_{in} = \dot{C}_{out,1} + \dot{C}_{out,2} \quad (6.23)$$

Ancillary equations "F-rule" $$c_{in}^T = c_{out,1}^T \quad (6.24)$$

$$c_{in}^M = c_{out,1}^M \quad (6.25)$$

$$c_{in}^M = c_{out,2}^M \quad (6.26)$$

Fuel $$\dot{C}_{F,SP} = \dot{C}_{in} \quad (6.27)$$

Product $$\dot{C}_{P,SP} = \dot{C}_{out,1} + \dot{C}_{out,2} \quad (6.28)$$

Expander

Cost balance $$\dot{Z}_{EX} + \dot{C}_{in} = \dot{C}_{out} + c_{el,char,2} \cdot \dot{W}_{EX} \quad (6.29)$$

Ancillary equations $$c_{in}^{M} = c_{out}^{M} \quad (6.30)$$

"F-rule" $$\frac{\dot{C}_{out}^{T} - \dot{C}_{in}^{T}}{\dot{E}_{out}^{T} - \dot{E}_{in}^{T}} = c_{el,char,2}$$

Fuel $$\dot{C}_{F,EX} = \dot{C}_{in}^{M} - \dot{C}_{out}^{M} \quad (6.31)$$

Product $$\dot{C}_{P,EX} = c_{el,2} \cdot \dot{W}_{EX} + \dot{C}_{out}^{T} - \dot{C}_{in}^{T} \quad (6.32)$$

Mixer

Cost balance $$\dot{Z}_{Mix} + \dot{C}_{in,1} + \dot{C}_{in,2} = \dot{C}_{out} \quad (6.33)$$

Ancillary equations $$c_{in,1}^{M} = c_{out}^{M} \quad (6.34)$$

Fuel $$\dot{C}_{F,EX} = \dot{C}_{in,1} + \dot{C}_{in,2} \quad (6.35)$$

Product $$\dot{C}_{P,EX} = \dot{C}_{out} \quad (6.36)$$

Main heat exchanger 1

Cost balance $$\dot{Z}_{MHE1} + \dot{C}_{16} + \dot{C}_{10} + \dot{C}_{Methanol,in} + \dot{C}_{R218,in} = \dot{C}_{17} + \dot{C}_{11} + \dot{C}_{Methanol,out} + \dot{C}_{R218,out} \quad (6.37)$$

Ancillary equations $$c_{16}^{T} = c_{17}^{T} \quad (6.38)$$

"F-rule" $$c_{16}^{M} = c_{17}^{M} \quad (6.39)$$

$$c_{Methanol,in}^{M} = c_{Methanol,out}^{M} \quad (6.40)$$

$$c_{Methanol,in}^{T} = c_{Methanol,out}^{T} \quad (6.41)$$

$$c_{R218,out}^{M} = c_{R218,out}^{M} \quad (6.42)$$

$$c_{R218,out}^{T} = c_{R218,out}^{T} \quad (6.43)$$

$$c_{10}^{M} = c_{11}^{M} \quad (6.44)$$

Fuel $$\dot{C}_{F,MHE1} = \dot{C}_{16} - \dot{C}_{17} + \dot{C}_{R218,in} - \dot{C}_{R218,out} + \dot{C}_{Methanol,in} - \dot{C}_{Methanol,out} + \dot{C}_{10}^{M} - \dot{C}_{11}^{M} \quad (6.45)$$

Product $$\dot{C}_{P,MHE1} = \dot{C}_{11}^{T} - \dot{C}_{10}^{T} \quad (6.46)$$

Throttling valve

Cost balance $$\dot{Z}_{TV} + \dot{C}_{in} = \dot{C}_{out} \quad (6.47)$$

Ancillary equations $$c_{in}^{M} = c_{out}^{M} \quad (6.48)$$

"F-rule"

Fuel $$\dot{C}_{F,TV} = \dot{C}_{in}^{M} - \dot{C}_{out}^{M} \quad (6.49)$$

Product $$\dot{C}_{P,TV} = \dot{C}_{out}^{T} - \dot{C}_{in}^{T} \quad (6.50)$$

Flash tank

Cost balance $$\dot{Z}_{FL} + \dot{C}_{in} = \dot{C}_{out,liquid} + \dot{C}_{out,gas} \quad (6.51)$$

Ancillary equations $$c_{in}^{M} = c_{out,gas}^{M} \quad (6.52)$$

"F-rule" $$c_{in}^{T} = c_{out,gas}^{T} \quad (6.53)$$

$$c_{in}^{M} = c_{out,liquid}^{M} \quad (6.54)$$

Fuel $$\dot{C}_{F,FL} = \dot{C}_{in}^{M} - \dot{C}_{\mathrm{out,gas}} \quad (6.55)$$

Product $$\dot{C}_{P,FL} = \dot{C}_{\mathrm{out,liquid}} \quad (6.56)$$

Cryogen pump

Cost balance $$\dot{Z}_{CP} + \dot{C}_{in} + c_{el,dis} \cdot \dot{W}_{EX} = \dot{C}_{out} \quad (6.57)$$

Ancillary equations $$c_{in}^{T} = c_{out}^{T} \quad (6.58)$$

"F-rule"

Fuel $$\dot{C}_{F,CP} = c_{el,dis} \cdot \dot{W}_{EX} + \dot{C}_{in}^{T} - \dot{C}_{out}^{T} \quad (6.59)$$

Product $$\dot{C}_{P,CP} = \dot{C}_{out}^{M} - \dot{C}_{in}^{M} \quad (6.60)$$

Main heat exchanger 2 – evaporation of liquid air

Cost balance $$\dot{Z}_{MHE2} + \dot{C}_{20} + \dot{C}_{Methanol,in} + \dot{C}_{R218,in} = \dot{C}_{21} + \dot{C}_{Methanol,out} + \dot{C}_{R218,out} \quad (6.61)$$

Ancillary equations

$$c_{20}^{T} = c_{21}^{T} \tag{6.62}$$

"F-rule"

$$c_{20}^{M} = c_{21}^{M} \tag{6.63}$$

$$c_{Methanol,in}^{M} = c_{Methanol,out}^{M} \tag{6.64}$$

$$c_{R218,out}^{M} = c_{R218,out}^{M} \tag{6.65}$$

"P-rule"

$$\frac{\dot{C}_{Methanol,out}^{T} - \dot{C}_{Methanol,in}^{T}}{\dot{E}_{Methanol,out}^{T} - \dot{E}_{Methanol,in}^{T}} = \frac{\dot{C}_{R218,out}^{T} - \dot{C}_{R218,in}^{T}}{\dot{E}_{R218,out}^{T} - \dot{E}_{R218,in}^{T}} \tag{6.66}$$

Fuel

$$\dot{C}_{F,MHE2} = \dot{C}_{20} - \dot{C}_{21} \tag{6.67}$$

Product

$$\dot{C}_{P,MHE2} = \dot{C}_{R218,out} - \dot{C}_{R218,in} + \dot{C}_{Methanol,out} - \dot{C}_{Methanol,in} \tag{6.68}$$

Reheaters + HE5

Cost balance

$$\dot{Z}_{RH} + \dot{C}_{cold,in} + \dot{C}_{hot,in} = \dot{C}_{cold,out} + \dot{C}_{hot,out} \tag{6.69}$$

Ancillary equations

$$c_{hot,in}^{T} = c_{hot,out}^{T} \tag{6.70}$$

"F-rule"

$$c_{hot,in}^{M} = c_{hot,out}^{M} \tag{6.71}$$

$$c_{cold,in}^{M} = c_{cold,out}^{M} \tag{6.72}$$

Fuel

$$\dot{C}_{F,HE1} = \dot{C}_{hot,in} - \dot{C}_{hot,out} \tag{6.73}$$

Product

$$\dot{C}_{P,HE1} = \dot{C}_{cold,out} - \dot{C}_{cold,in} \tag{6.74}$$

Turbines

Cost balance

$$\dot{Z}_{T,i} + \dot{C}_{in} = \dot{C}_{out} + c_{el,dis,i} \cdot \dot{W}_{T,i} \tag{6.75}$$

Ancillary equations

$$c_{in}^{M} = c_{out}^{M} \tag{6.76}$$

"F-rule"

$$c_{in}^{T} = c_{out}^{T} \tag{6.77}$$

$$c_{el,dis} = \frac{\sum c_{el,dis,i} \cdot \dot{W}_{T,i}}{\sum \dot{W}_{T,i}} \tag{6.78}$$

Fuel

$$\dot{C}_{F,T} = \dot{C}_{in} - \dot{C}_{out} \tag{6.79}$$

Product $$\dot{C}_{P,T} = c_{el,dis} \cdot \dot{W}_T \quad (6.80)$$

Storage tanks

Cost balance $$\dot{Z}_{ST} + \dot{C}_{in} = \dot{C}_{out} + c_q \cdot \dot{E}_{Q,loss,ST} \quad (6.81)$$

Ancillary equations $$c_{in}^M = c_{out}^M \quad (6.82)$$

"F-rule" $$\mathrm{c_q} = 0 \quad (6.83)$$

Fuel $$\dot{C}_{F,ST} = \dot{C}_{in} \quad (6.84)$$

Product $$\dot{C}_{P,ST} = \dot{C}_{out} \quad (6.85)$$

Overall system

Cost balance $$\dot{Z}_{ST} + \dot{C}_{in} = \dot{C}_{out} + c_q \cdot \dot{E}_{Q,loss,ST} \quad (6.86)$$

Ancillary equations $$c_{in}^M = c_{out}^M \quad (6.87)$$

"F-rule" $$\mathrm{c_q} = 0 \quad (6.88)$$

Fuel $$\dot{C}_{F,ST} = \dot{C}_{in} \quad (6.89)$$

Product $$\dot{C}_{P,ST} = \dot{C}_{out} \quad (6.90)$$

Appendix C

Table C.1: Stream values of the Base Case A for the states indicated in the flowsheet in Figure 4.2.

stream no.		m_dot [kg/s]	p [bar]	T [°C]	h [kJ/kg]	s [kJ/kgK]	e_M [kJ/kg]	e_T [kJ/kg]
1	air	214	1	15	-10	0	0	0
2	air	214	5	198	176	0	127	42
3	air	214	4	18	-8	0	122	0
4	air	214	20	203	181	0	249	45
5	air	214	19	18	-12	-1	245	0
6	air	214	89	203	181	-1	372	48
7	air	214	87	18	-25	-1	370	0
8a	air	214	85	-41	-98	-1	368	8
8b	air	83	85	-41	-98	-1	368	8
9	air	83	1	-191	-222	-1	6	164
10	air	131	85	-41	-98	-1	368	8
11	air	131	80	-177	-391	-3	363	284
12	air	131	1	-193	-391	-3	11	594
13	air	107	1	-193	-428	-4	7	691
14	air	0	1	-193	-428	-4	7	691
15	air	24	1	-193	-227	-1	7	169
16	air	106	1	-191	-223	-1	6	165
17	air	106	1	17	-8	0	0	0
18	air	107	1	-193	-428	-4	7	691
19	air	214	1	-193	-428	-4	7	691
20	air	214	161	-186	-403	-4	420	280
21	air	214	155	-23	-92	-2	417	4
22	air	214	155	28	-24	-1	417	0
23	air	214	150	188	164	-1	414	43
24	air	214	45	68	37	-1	313	5
25	air	214	43	188	165	0	309	40
26	air	214	13	68	41	0	209	4
27	air	214	12	188	165	0	206	39
28	air	214	4	68	43	0	106	4
29	air	214	4	188	165	0	103	38
30	air	214	1	68	43	0	2	4
31	air	214	1	0	-25	0	0	0
32	methanol	98	5	-21	-7743	-9	1	9
33	methanol	98	5	-56	-7871	-9	1	39
34	methanol	48	5	-54	-7864	-9	1	36
35	methanol	48	5	-23	-7750	-9	1	10
36	R218	498	2	-60	-9668	-3	8	25
37	R218	498	2	-180	-9776	-4	8	132
38	R218	244	2	-178	-9775	-4	8	128
39	R218	244	2	-62	-9670	-3	8	26

Table C.2: Stream values of the Base Case B for the states indicated in the flowsheet in Figure 4.2.

stream no.		m_dot [kg/s]	p [bar]	T [°C]	h [kJ/kg]	s [kJ/kgK]	e_M [kJ/kg]	e_T [kJ/kg]
1	air	186	1	15	-10	0	0	0
2	air	186	5	214	193	0	136	49
3	air	186	5	18	-8	0	131	0
4	air	186	25	219	198	0	267	52
5	air	186	24	18	-13	-1	263	0
6	air	186	123	218	198	-1	399	56
7	air	186	120	18	-31	-1	397	0
8	air	58	120	18	-31	-1	397	0
9	air	58	1	-172	-200	-1	6	116
10	air	128	120	18	-31	-1	397	0
11	air	128	111	-177	-390	-3	390	265
12	air	128	1	-193	-390	-3	11	590
13	air	104	1	-193	-428	-4	7	690
14	air	0	1	-193	-428	-4	7	690
15	air	24	1	-193	-227	-1	7	169
16	air	82	1	-178	-208	-1	6	130
17	air	82	1	11	-15	0	0	0
18	air	104	1	-193	-428	-4	7	690
19	air	208	1	-193	-428	-4	7	690
20	air	208	161	-186	-403	-4	420	280
21	air	208	155	-23	-92	-2	417	4
22	air	208	155	36	-14	-1	417	1
23	air	208	150	201	179	-1	414	49
24	air	208	45	78	47	-1	313	6
25	air	208	43	201	178	0	309	45
26	air	208	13	77	51	0	209	6
27	air	208	12	201	179	0	206	44
28	air	208	4	77	52	0	106	6
29	air	208	4	201	179	0	103	43
30	air	208	1	78	53	0	2	6
31	air	208	1	0	-25	0	0	0
32	methanol	96	5	-21	-7743	-9	1	9
33	methanol	96	5	-56	-7871	-9	1	39
34	methanol	47	5	-54	-7864	-9	1	36
35	methanol	47	5	-23	-7750	-9	1	10
36	R218	484	2	-60	-9668	-3	8	25
37	R218	484	2	-180	-9776	-4	8	132
38	R218	237	2	-178	-9775	-4	8	128
39	R218	237	2	-62	-9670	-3	8	26

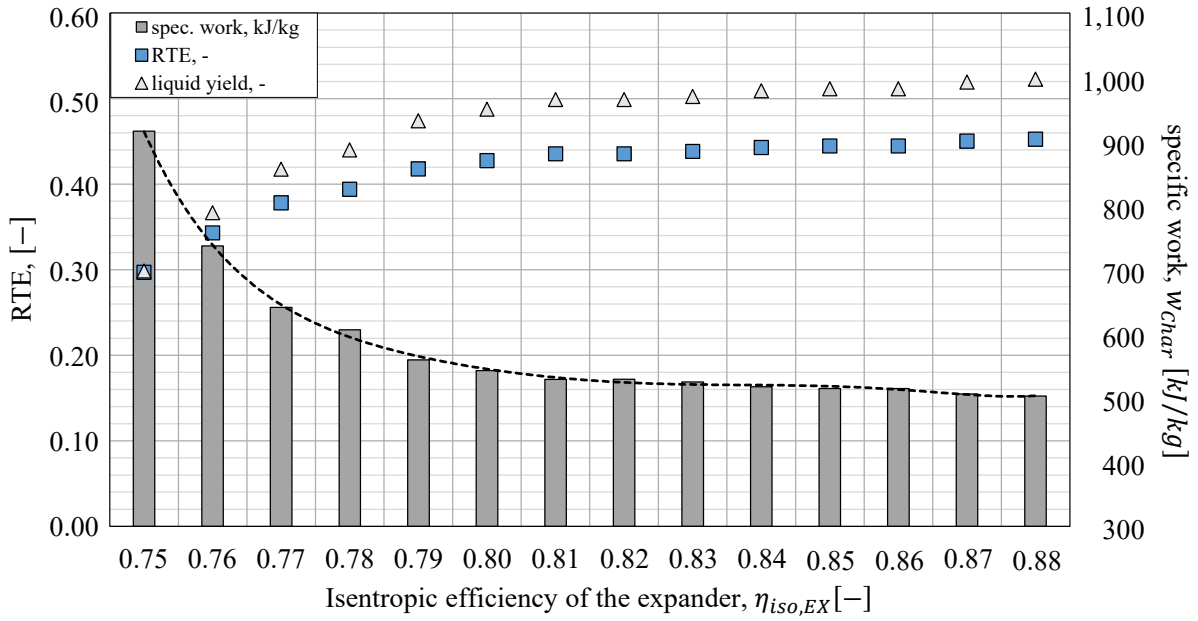

Figure C.1: Roundtrip efficiency, liquid yield and specific liquefaction work over the isentropic efficiency of the expander (Kapitza, p_{CM}=85 bar)

Table C.3: Stream values for the states indicated in the flowsheets in Figure 4.6

Stream	Variable, unit		Claude		Kapitza		Heylandt	
				+ storage		+ storage		+ storage
1	$\dot{m}$	kg/h	100.0	100.0	100.0	100.0	100.0	100.0
	T	°C	25.0	25.0	25.0	25.0	25.0	25.0
	p	bar	200.0	200.0	200.0	200.0	200.0	200.0
2	$\dot{m}$	kg/h	100.0	100.0	100.0	100.0	36.0	76.1
	T	°C	-4.0	-2.0	-4.0	-2.0	25.0	25.0
	p	bar	200.0	200.0	200.0	200.0	200.0	200.0
3	$\dot{m}$	kg/h	34.3	73.2	34.3	73.3	36.0	76.1
	T	°C	-4.0	-2.0	-4.0	-2.0	-177.6	-180.5
	p	bar	200.0	200.0	200.0	200.0	200.0	200.0
4	$\dot{m}$	kg/h	34.3	73.2	34.3	73.3	36.0	76.1
	T	°C	-190.8	-182.8	-190.6	-182.8	-193.9	-194.0
	p	bar	200.0	200.0	200.0	200.0	1.01	1.01
5	$\dot{m}$	kg/h	34.3	73.2	34.3	73.3	28.6	62.3
	T	°C	-194.1	-194.0	-194.1	-194.0	-193.9	-194.0
	p	bar	1.03	200.0	1.03	1.03	1.03	1.03
6	$\dot{m}$	kg/h	31.2	61.5	31.1	61.5	7.4	13.7
	T	°C	-194.1	-194.0	-194.1	-194.0	-176.5	-179.0
	p	bar	1.03	1.03	1.03	1.03	1.03	1.03
7	$\dot{m}$	kg/h	3.1	11.8	3.2	11.8	71.4	37.7
	T	°C	-194.1	-194.0	-194.1	-194.0	-176.4	-177.4
	p	bar	1.03	1.03	1.03	1.03	1.03	1.03
8	$\dot{m}$	kg/h	3.1	11.8	68.9	38.5	71.4	37.7
	T	°C	-192.0	-191.0	-191.7	-192.1	-7.3	24.0
	p	bar	1.03	1.03	1.03	1.03	1.03	1.03
9	$\dot{m}$	kg/h	65.7	26.8	65.7	26.7	64.0	24.0
	T	°C	-4.0	-2.0	-4.0	-2.0	25.0	25.0
	p	bar	200.0	200.0	200.0	200.0	200.0	200.0
10	$\dot{m}$	kg/h	65.7	26.8	65.66	26.7	64	24.0
	T	°C	-191.6	-191.2	-191.6	-191.2	-176.4	-176.4
	p	bar	1.03	1.03	1.03	1.03	1.03	1.03
11	$\dot{m}$	kg/h	68.8	73.0	-	-	-	-
	T	°C	-191.7	-182.8	-	-	-	-
	p	bar	1.03	200.0	-	-	-	-
12	$\dot{m}$	kg/h	68.8	38.6	68.9	73.3	-	-
	T	°C	24.0	23.4	24.0	24.0	-	-
	p	bar	1.03	1.03	1.03	1.03	-	-

Table C.4: Stream values for the states indicated in the flowsheets in Figure 4.5

Stream	Variable, unit	Simple Linde + storage		Precooled Linde + storage		Dual-pressure Linde + storage	
1	$\dot{m}$ kg/h	100.0	100.0	100.0	100.0	100.0	100.0
	T °C	25.0	25.0	25.0	25.0	25.0	25.0
	p bar	200.0	200.0	200.0	200.0	33.4	33.4
2	$\dot{m}$ kg/h	100.0	100.0	100.0	100.0	547.3	137.3
	T °C	-102.4	-125.3	-113.6	-138.7	24.1	24.2
	p bar	200.0	1.03	200.0	200.0	30.4	30.4
3	$\dot{m}$ kg/h	100.0	100	100	100	547.3	137.3
	T °C	-191.8	-191.7	-192.3	-193.1	25.0	25.0
	p bar	1.03	1.03	1.03	1.03	200.0	200.0
4	$\dot{m}$ kg/h	9.0	31.2	19.8	44.1	547.3	137.3
	T °C	-191.8	-192.7	-192.3	-193.1	-105.0	-124.5
	p bar	1.03	1.03	1.03	1.03	200.0	200.0
5	$\dot{m}$ kg/h	91.0	68.8	80.2	55.9	547.3	137.3
	T °C	-191.8	-192.7	-192.3	-193.1	-146.2	-146.2
	p bar	1.03	1.03	1.03	1.03	30.4	30.4
6	$\dot{m}$ kg/h	91.0	68.8	80.2	55.9	100.0	100.0
	T °C	24.0	24.0	24.0	-95.8	-146.2	-146.2
	p bar	1.03	1.03	1.03	1.03	30.4	30.4
7	$\dot{m}$ kg/h	-	-	-	-	100.0	100.0
	T °C	-	-	-	-	-192.9	-192.9
	p bar	-	-	-	-	1.03	1.03
8	$\dot{m}$ kg/h	-	-	-	-	40.0	40.0
	T °C	-	-	-	-	-193.0	-193.0
	p bar	-	-	-	-	1.03	1.03
9	$\dot{m}$ kg/h	-	-	-	-	60.0	60.0
	T °C	-	-	-	-	-193.0	-193.0
	p bar	-	-	-	-	1.03	1.03
10	$\dot{m}$ kg/h	-	-	-	-	60.0	60.0
	T °C	-	-	-	-	24.0	24.0
	p bar	-	-	-	-	1.03	1.03
11	$\dot{m}$ kg/h	-	-	-	-	447.3	37.3
	T °C	-	-	-	-	-146.2	-146.2
	p bar	-	-	-	-	30.4	30.4
12	$\dot{m}$ kg/h	-	-	-	-	447.3	37.3
	T °C	-	-	-	-	24.0	24.0
	p bar	-	-	-	-	30.4	30.4

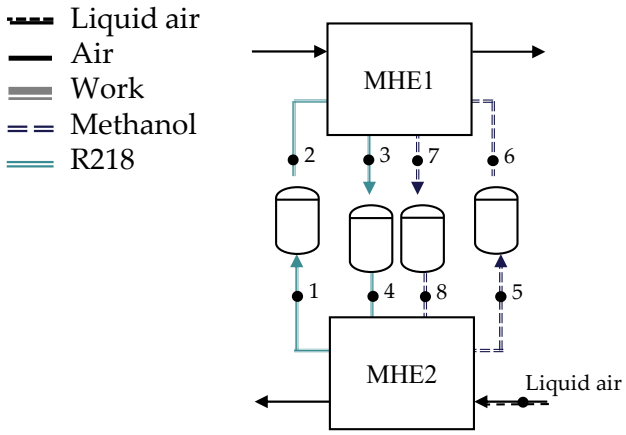

Figure C.2: Flowsheet of the cold storage integration into the CES system.

Table C.5: Stream values for states indicated in the flowsheets (a) in Figure 4.10 for the adiabatic CES systems with and without cold storage and with waste heat integration.

Stream	Variable		Adiabatic		Waste heat	
			w/o CS	w/ CS	350 °C	450 °C
a1	$\dot{m}$	kg/s	198.3	198.3	198.3	198.3
	T	°C	15.0	15.0	15.0	15.0
	p	bar	1.0	1.0	1.0	1.0
a2	$\dot{m}$	kg/s	198.3	198.3	198.3	198.3
	T	°C	18.0	18.0	18.0	18.0
	p	bar	180.0	180.0	180.0	180.0
a3	$\dot{m}$	kg/s	123.8	65.5	65.5	65.5
	T	°C	18.0	18.0	18.0	18.0
	p	bar	180.0	180.0	180.0	180.0
a4	$\dot{m}$	kg/s	59.4	105.7	105.7	105.7
	T	°C	-193.2	-193.2	-193.2	-193.2
	p	bar	1.1	1.1	1.1	1.1
a5	$\dot{m}$	kg/s	1187	211.4	211.4	211.4
	T	°C	194	194	350	450
	p	bar	150	150	151	151
a6	$\dot{m}$	kg/s	118.7	211.4	211.4	211.4
	T	°C	194	194	350	450
	p	bar	12.2	12.2	12.2	12.2
LNG1	$\dot{m}$	kg/s	-	-	-	-
	T	°C	-	-	-	-
	p	bar	-	-	-	-
LNG2	$\dot{m}$	kg/s	-	-	-	-
	T	°C	-	-	-	-
	p	bar	-	-	-	-
NG1	$\dot{m}$	kg/s	-	-	-	-
	T	°C	-	-	-	-
	p	bar	-	-	-	-
NG2	$\dot{m}$	kg/s	-	-	-	-
	T	°C	-	-	-	-
	p	bar	-	-	-	-

Table C.6: Stream values for states indicated in the flowsheets (a) in Figure 4.10 for the adiabatic CES systems with and without cold storage and with single and double combustion.

Stream		Adiabatic		Combustion	
		w/o CS	w/ CS	single	double
a1	$\dot{m}$	198.3	198.3	198.3	198.3
	T	15.0	15.0	15.0	15.0
	p	1.0	1.0	1.0	1.0
a2	$\dot{m}$	198.3	198.3	198.3	198.3
	T	18.0	18.0	18.0	18.0
	p	180.0	180.0	180.0	180.0
a3	$\dot{m}$	123.8	65.5	65.5	65.5
	T	18.0	18.0	18.0	18.0
	p	180.0	180.0	180.0	180.0
a4	$\dot{m}$	59.4	105.7	105.7	105.7
	T	-193.2	-193.2	-193.2	-193.2
	p	1.1	1.1	1.1	1.1
a5	$\dot{m}$	1187	211.4	211.4	211.4
	T	194	194	1100	733.6
	p	150	150	80	80
a6	$\dot{m}$	118.7	211.4	211.4	211.4
	T	194	194	594.2	718.2
	p	12.2	12.2	9.0	8.8
NG1	$\dot{m}$	-	-	4.5	3
	T	-	-	15	15
	p	-	-	80	80
NG2	$\dot{m}$	-	-	-	2
	T	-	-	-	15
	p	-	-	-	8

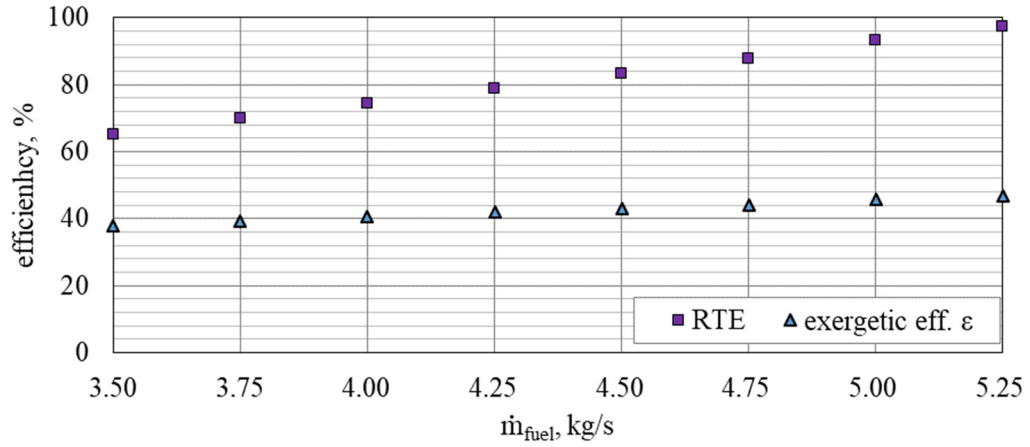

Figure C.3: Roundtrip efficiency and exergetic efficiency over mass flow rate of the fuel for the d-CES system

Table C.7: Stream values for the states indicated in the flowsheets (a) and (b) in Figure 4.10, for the CES systems with and without integration of LNG.

Stream	Variable		Adiabatic		LNG integration			
			w/o CS	w/ CS	w/o CS	w/ CS	450 °C	combustion
a1	$\dot{m}$	kg/s	198.3	198.3	198.3	198.3	198.3	198.3
	T	°C	15.0	15.0	15.0	15.0	15.0	15.0
	p	bar	1.0	1.0	1.0	1.0	1.0	1.0
a2	$\dot{m}$	kg/s	198.3	198.3	198.3	198.3	198.3	198.3
	T	°C	18.0	18.0	18.0	18.0	18.0	18.0
	p	bar	180.0	180.0	180.0	180.0	180.0	180.0
a3	$\dot{m}$	kg/s	123.8	65.5	123.8	16.3	16.3	16.3
	T	°C	18.0	18.0	18.0	18.0	18.0	18.0
	p	bar	180.0	180.0	180.0	180.0	180.0	180.0
a4	$\dot{m}$	kg/s	59.4	105.7	64.9	144.9	144.9	144.9
	T	°C	-193.2	-193.2	-193.2	-193.2	-193.2	-193.2
	p	bar	1.1	1.1	1.1	1.1	1.1	1.1
a5	$\dot{m}$	kg/s	1187	211.4	129.8	289.7	289.7	289.7
	T	°C	194	194	194	200	450	1098
	p	bar	150	150	150	150	150	80
a6	$\dot{m}$	kg/s	118.7	211.4	129.8	289.7	289.7	289.7
	T	°C	194	194	194	200	450	404.5
	p	bar	12.2	12.2	12.2	12	12	9.0
LNG1	$\dot{m}$	kg/s	-	-	5.5	20.0	20.0	20.0
	T	°C	-	-	-158	-158	-158	-158
	p	bar	-	-	32	32	32	32
LNG2	$\dot{m}$	kg/s	-	-	5.5	20.0	20.0	20.0
	T	°C	-	-	-9.3	-4.3	-4.3	-4.3
	p	bar	-	-	30	30	30	30
NG1	$\dot{m}$	kg/s	-	-	-	-	-	6.2
	T	°C	-	-	-	-	-	15
	p	bar	-	-	-	-	-	80
NG2	$\dot{m}$	kg/s	-	-	-	-	-	-
	T	°C	-	-	-	-	-	-
	p	bar	-	-	-	-	-	-

Appendix D

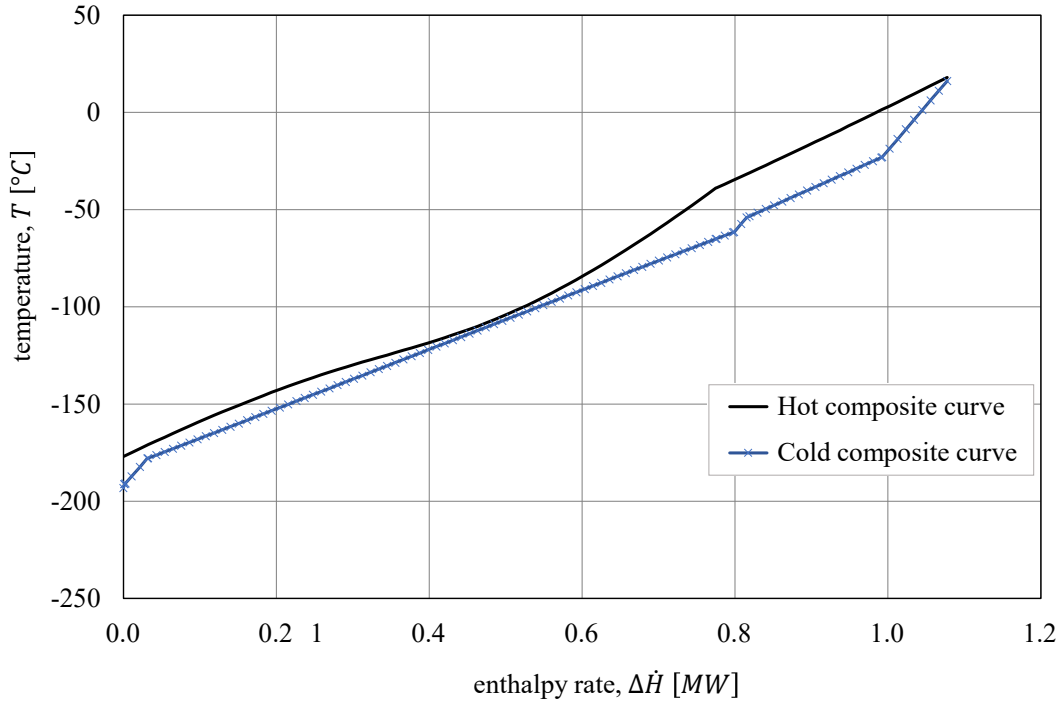

Figure D.1a): T,$\Delta\dot{H}$-diagrams of the heat exchange in the MHE1 of the Claude liquefaction process.

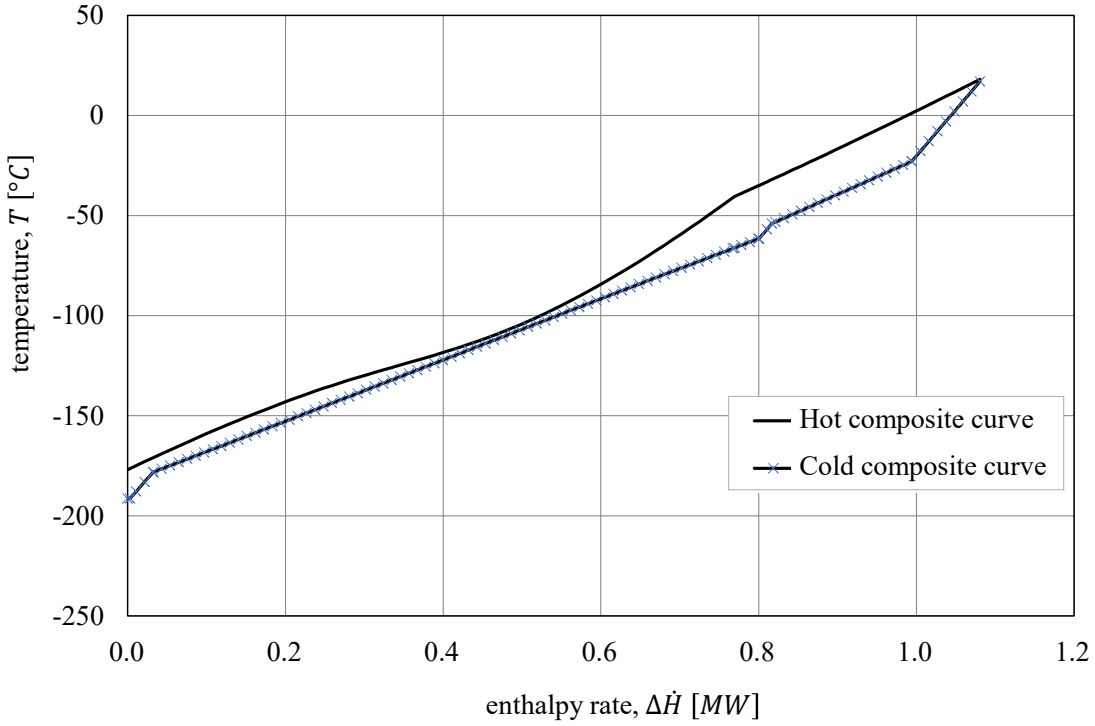

Figure D.1b): T,$\Delta\dot{H}$-diagrams of the heat exchange in the MHE1 of the Kapitza liquefaction process.

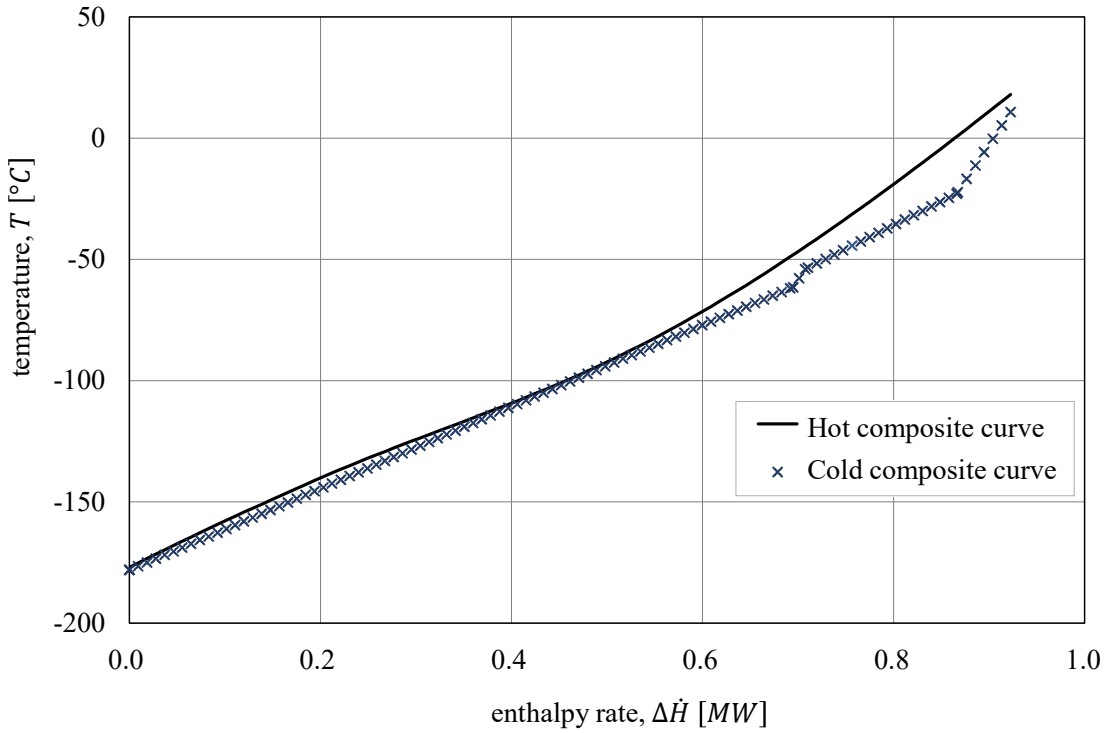

Figure D.1c): T,$\Delta\dot{H}$-diagrams of the heat exchange in the MHE1 of the Heylandt liquefaction process.

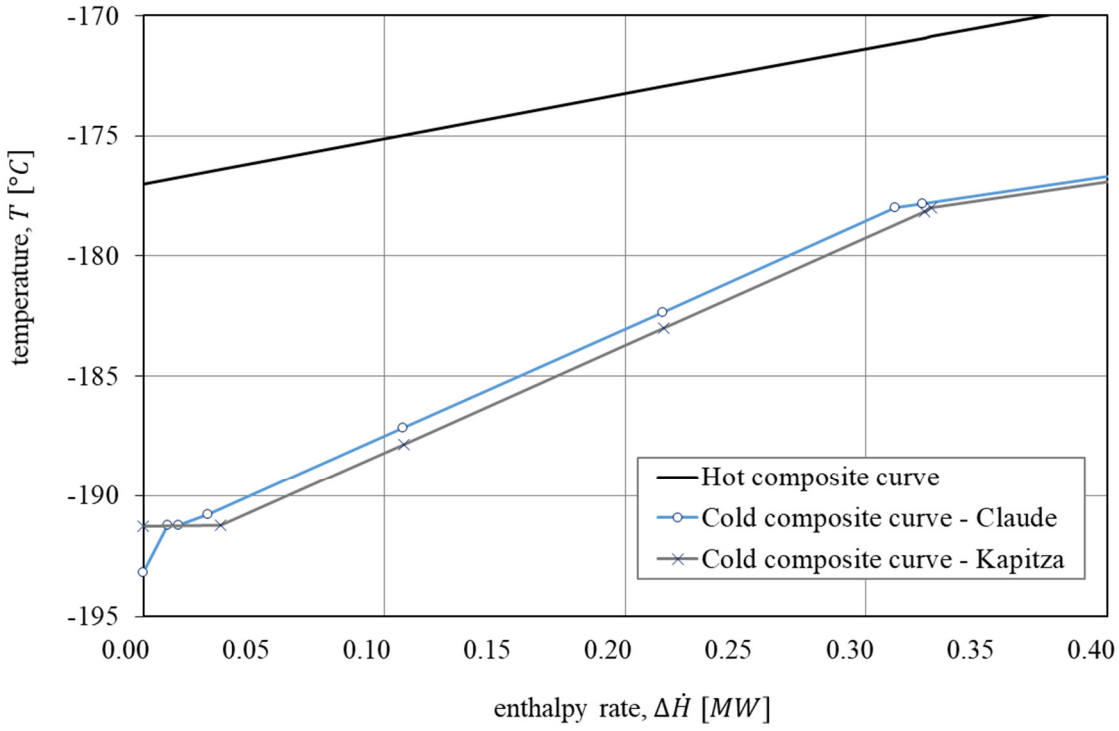

Figure D.2: Comparison of the composite curves of the MHE1 for the Claude and the Kapitza process.

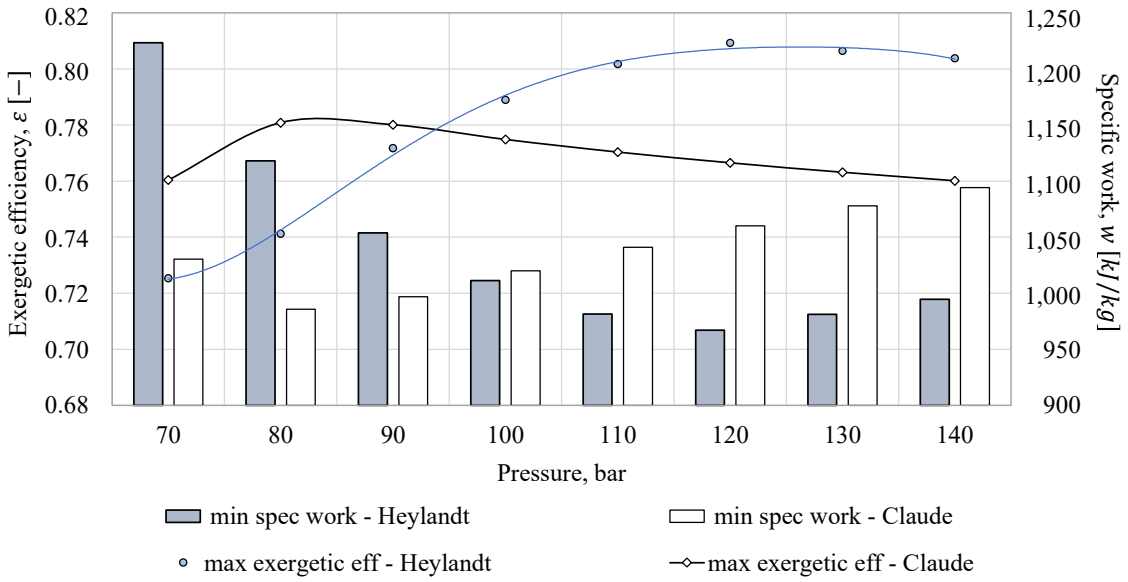

Figure D.3: Maximum exergetic efficiency ε and minimum specific work required for liquefaction w over liquefaction pressures from 70 bar to 140 bar for the Claude process and the Heylandt process.

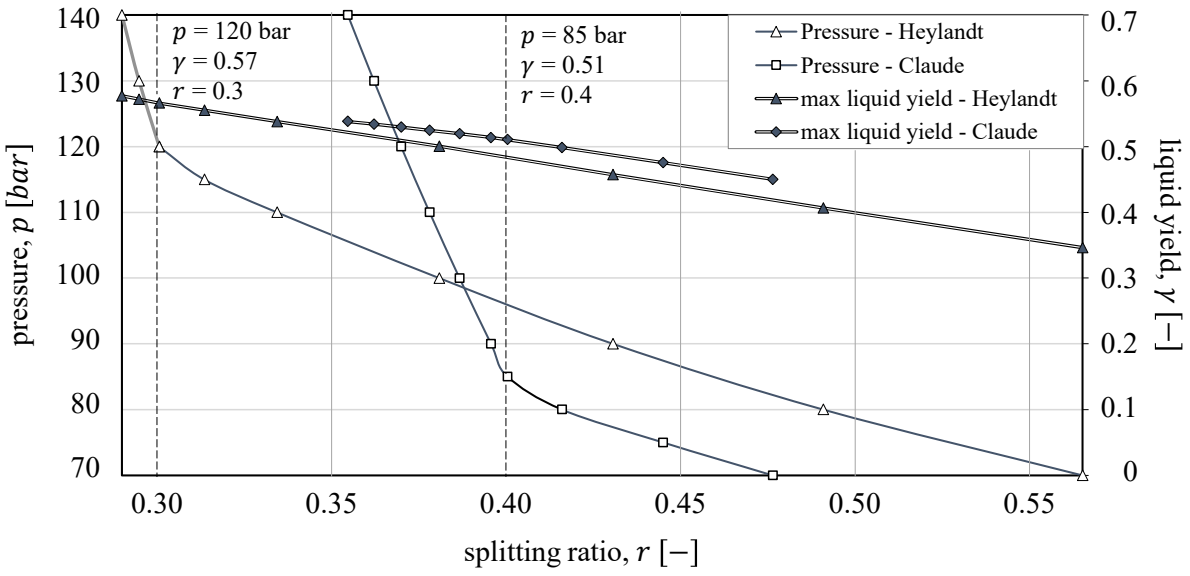

Figure D.4: Maximum liquid yield and liquefaction pressure over the splitting ratio for a) the Heylandt and b) the Claude and the Kapitza process – the maximum efficiency points are indicated with a dashed line

Table D.1: Exergy analysis results on component level for Base Case A (Kapitza, 95 bar)

Component	E_F [MWh]	E_P [MWh]	E_D [MWh]	Epsilon [%]
AC1	322	289	33	0.897
HE1	80	71	9	0.884
AC2	327	293	34	0.897
HE2	83	75	8	0.908
AC3	332	298	34	0.898
HE3	85	79	7	0.923
SP1	643	643	0	-
EXP1	240	184	55	0.769
Mix1	146	146	0,1	0.999
MHE1	364	302	62	0.831
TV	369	325	44	0.880
ST	898	896	2	0.997
SP2	299	299	0	-
P	373	354	19	0.950
MHE2	239	224	15	0.936
HE5	366	357	9	0.976
HE6	51	37	14	0.720
T1	120	108	12	0.903
HE7	37	30	7	0.809
T2	116	105	11	0.903
HE8	36	29	7	0.804
T3	115	104	11	0.903
HE9	38	29	9	0.766
T4	115	104	11	0.903
HS	225	213	12	0.947
CS	224	210	14	0.935

Table D.2: Exergy analysis results on component level for Base Case B (Heylandt, 120 bar)

Component	E_F [MWh]	E_P [MWh]	E_D [MWh]	epsilon[%]
AC1	305	275	31	0.899
HE1	80	71	8	0.895
AC2	310	279	31	0.900
HE2	83	76	7	0.915
AC3	317	286	32	0.900
HE3	86	80	7	0.922
SP1	591	591	0	-
EXP1	181	131	50	0.725
Mix1	91	89	1	0.986
MHE1	300	271	28	0.906
TV	389	334	56	0.857
ST	326	324	2	0.943
SP2	290	290	0	-
P	362	344	18	0.950
MHE2	232	218	15	0.936
HE5	356	348	9	0.975
HE6	53	40	13	0.756
T1	119	108	11	0.906
HE7	39	32	7	0.817
T2	116	105	11	0.906
HE8	39	31	7	0.813
T3	115	104	11	0.906
HE9	37	31	6	0.849
T4	114	104	11	0.906
HS	224	215	9	0.958
CS	224	210	14	0.935

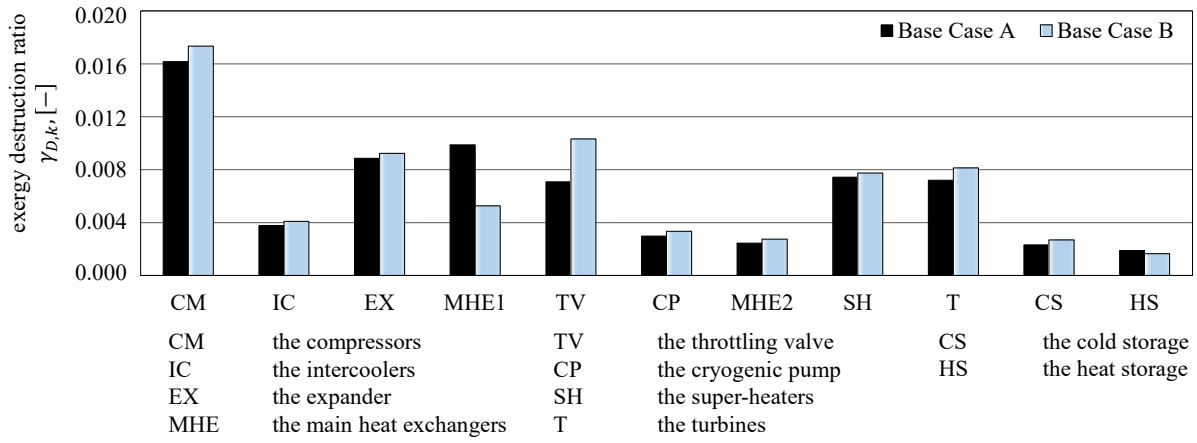

Figure D.5: Exergy destruction ratio of selected components for the base case systems

Table D.3: Economic analysis results for Base Cases A and B

Parameter		Unit	Base Case A	Base Case B
Fixed Capita Investment	FCI	10^6 €	167,283	179,909
Total Capital Investment	TCI	10^6 €	194,215	208,874
Levelized Carrying Charges	CCL	10^6 €/a	19,860	21,359
Levelized Fuel Costs	FCL	10^6 €/a	8,645	8,207
Levelized O&M Costs	OMCL	10^6 €/a	8,797	9,461
Total Revenue Requirement	TRRL	10^6 €/a	37,302	39,027
Levelized cost of discharged electricity	LCOE	€/MWh	255,50	267,31

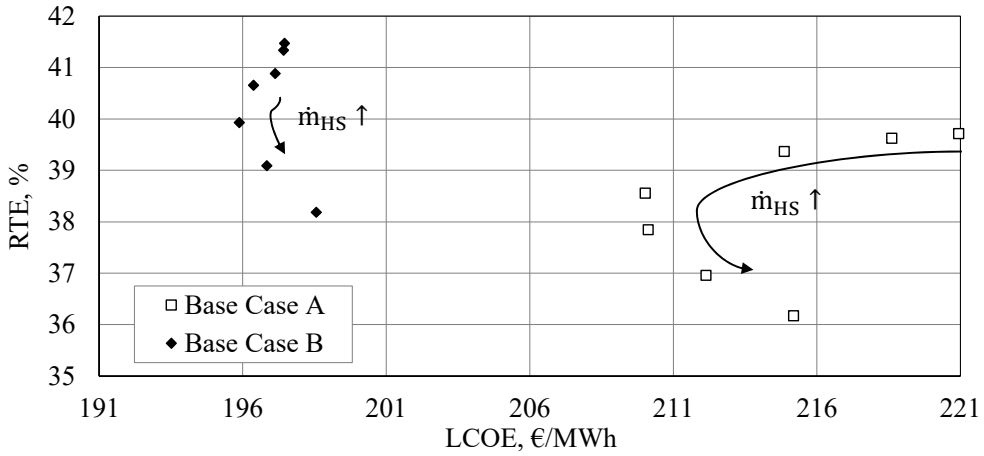

Figure D.6: Effect of the increased mass flow rate of the heat storage media on the RTE over the $LCOE_{dis}$ for both base cases

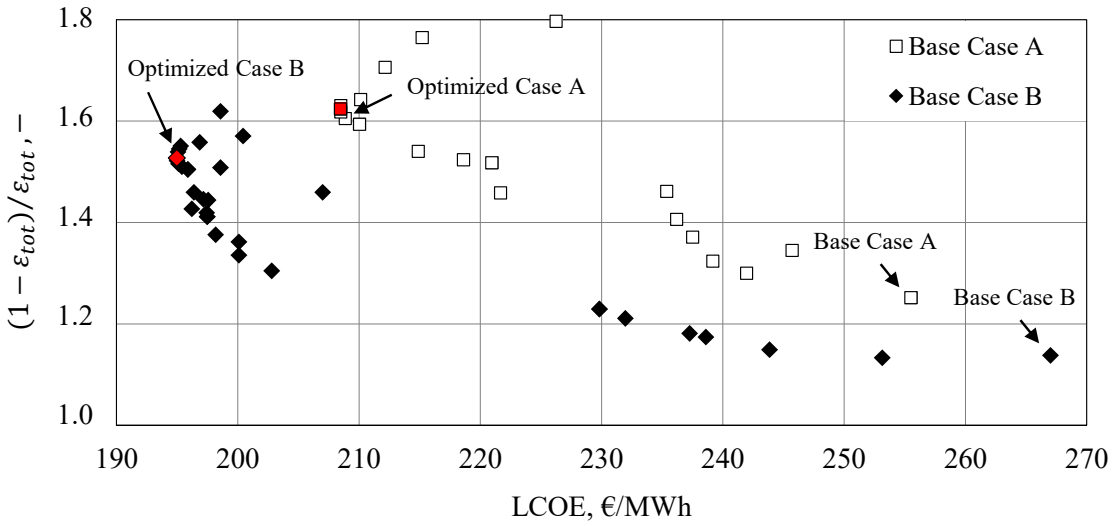

Figure D.7: Specific exergy destruction and losses over the cost of the final product for the optimized cases after parametric changes on Base Cases A and B.

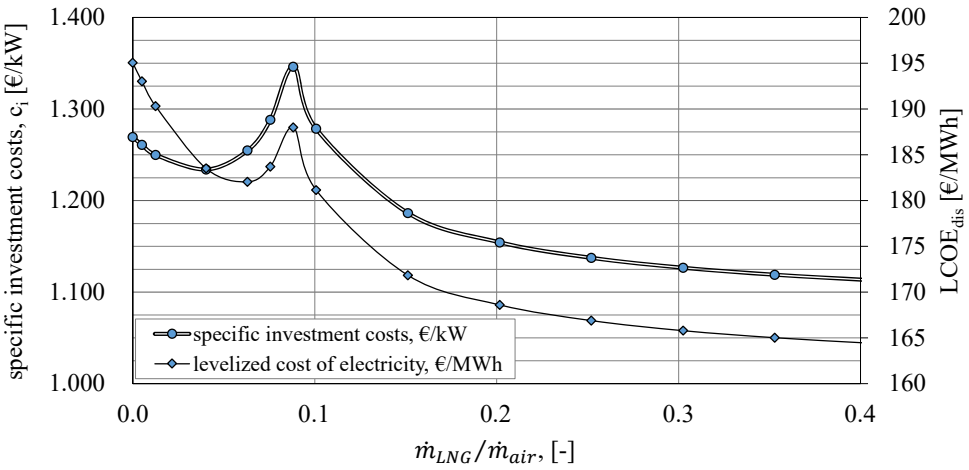

Figure D.8: $LCOE_{dis}$ over mass flow of LNG supplied to the a-CES system with LNG integration and $\dot{m}_{air}$ = 200 kg/s

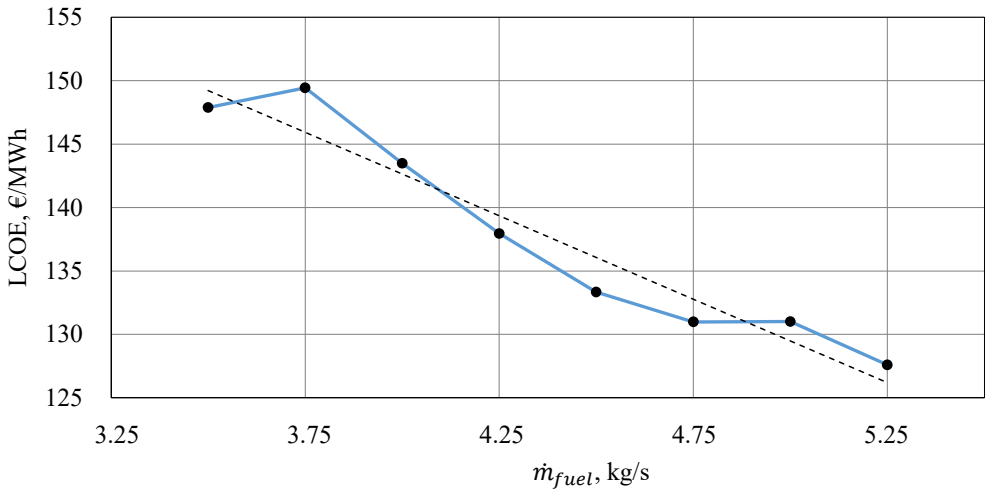

Figure D.9: $LCOE_{dis}$ over the mass flow of fuel supplied to the d-CES system with $\dot{m}_{air}$ = 200 kg/s

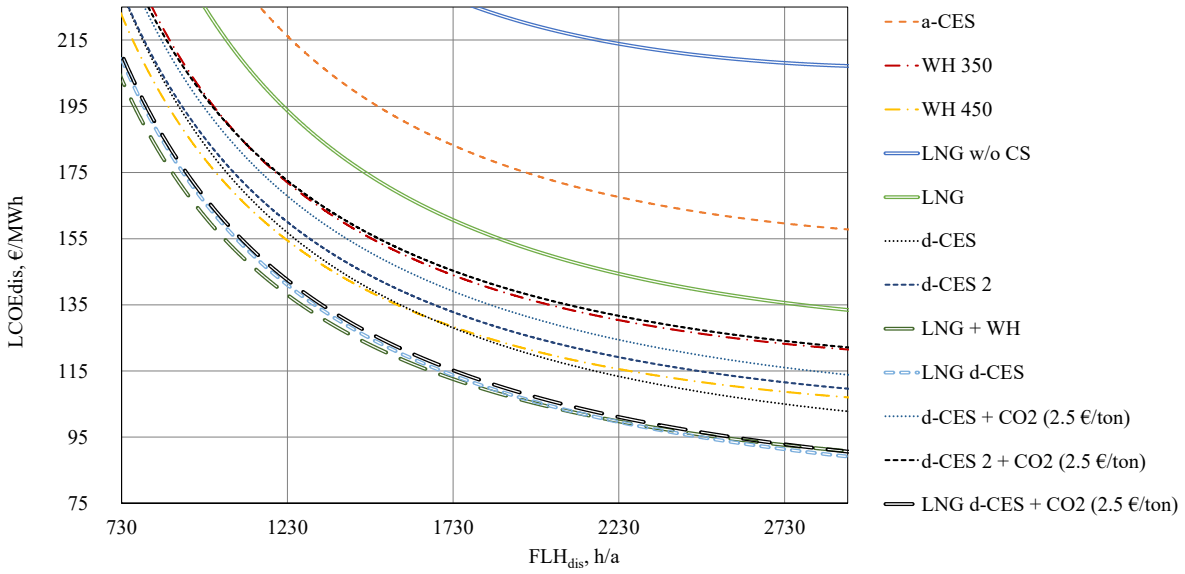

Figure D.10 a): $LCOE_{dis}$ over FLH for all considered systems with/without consideration of a CO_2 emission price of 2.5 €/ton $\dot{W}_{dis}$ = 100 MW

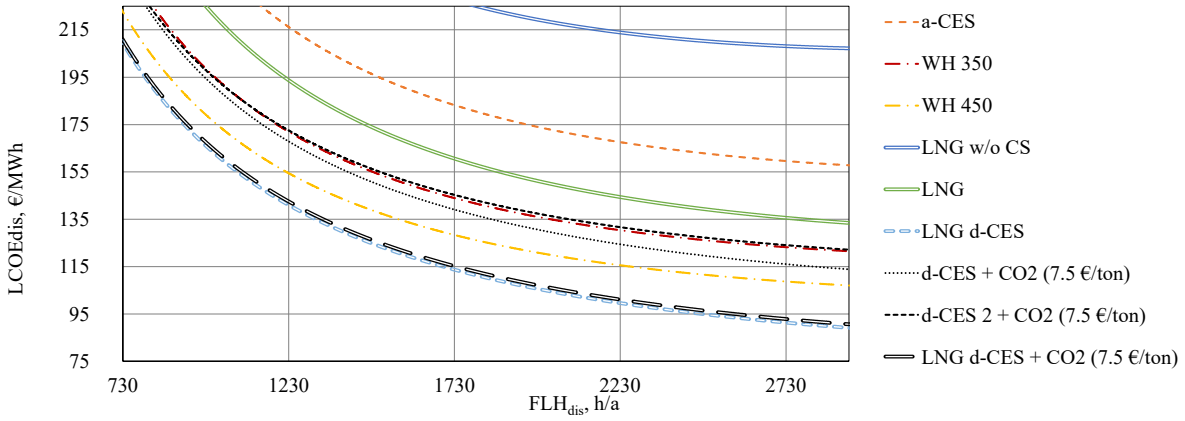

Figure D.10 b): $LCOE_{dis}$ over FLH for all considered systems with/without consideration of a CO_2 emission price of 7.5 €/ton $\dot{W}_{dis}$ = 100 MW

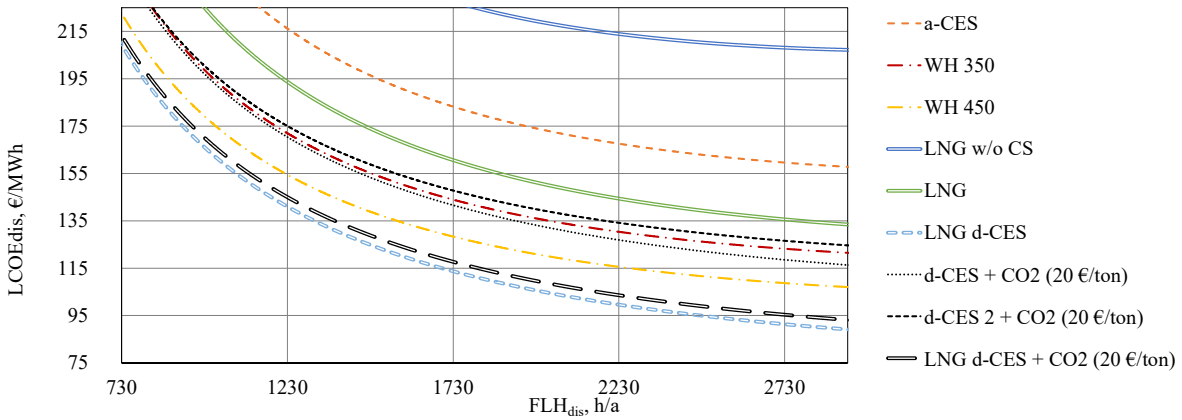

Figure D.10 c): $LCOE_{dis}$ over FLH for all considered systems with/without consideration of a CO_2 emission price of 20 €/ton $\dot{W}_{dis}$ = 100 MW

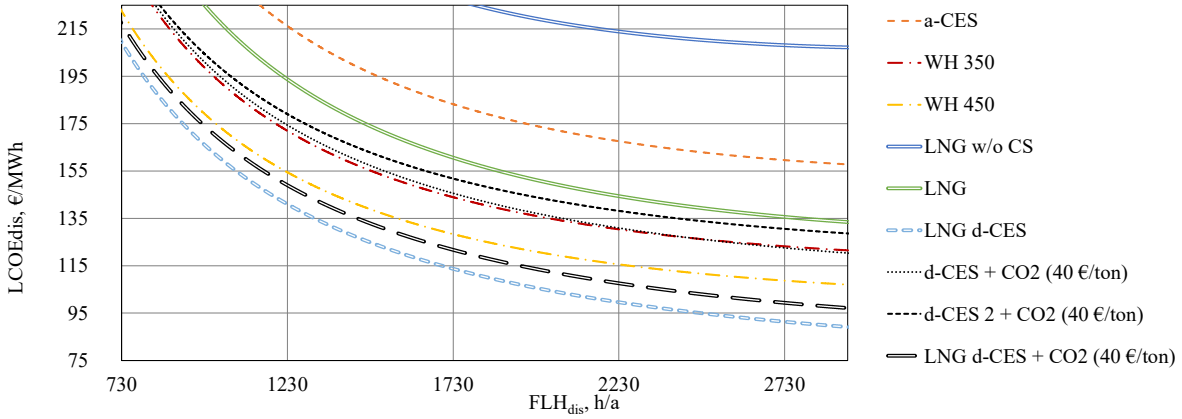

Figure D.10 d): $LCOE_{dis}$ over FLH for all considered systems with/without consideration of a CO_2 emission price of 40 €/ton $\dot{W}_{dis}$ = 100 MW

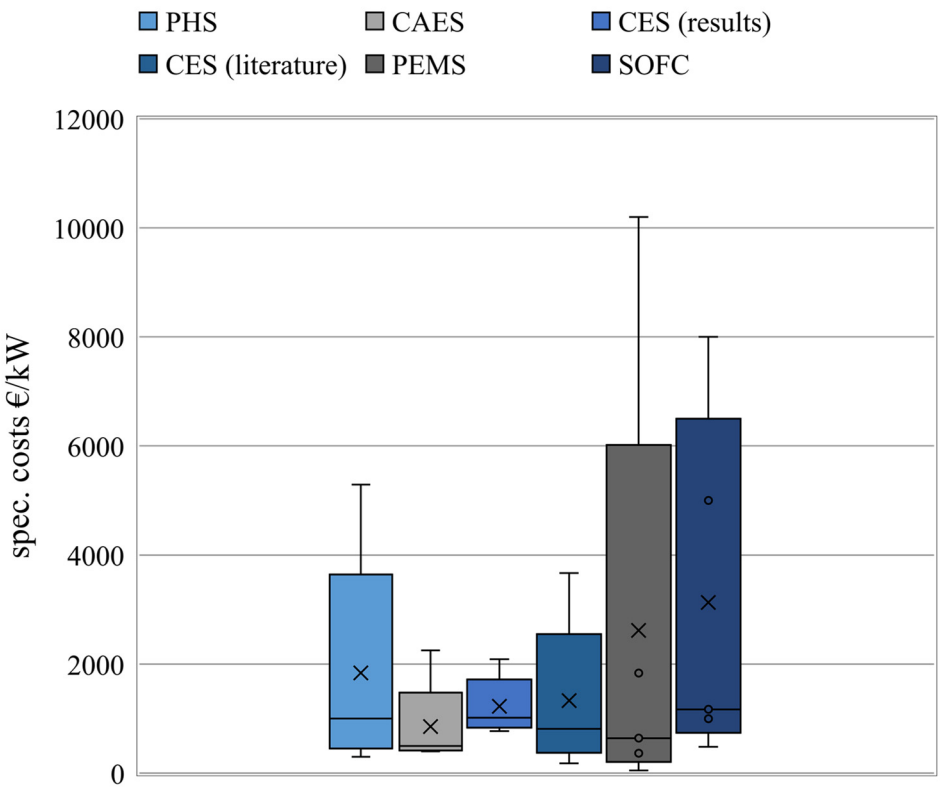

Figure D.11: Box-plot diagram of the specific costs of different bulk ES technologies and CES.

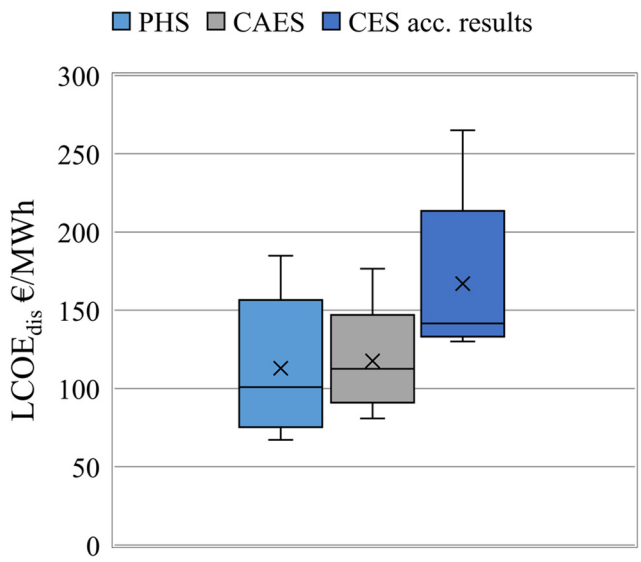

Figure D.12: Box-plot diagram of the LCOE$_{dis}$ of PHS and CAES adopted from [102, 143] [87] [142] and CES computed in this work.